Joel J. Alpízar-Castillo

Residential Multi-Carrier Energy Storage Systems As Potential Flexibility Providers In Low-Voltage Networks

RESIDENTIAL MULTI-CARRIER ENERGY STORAGE SYSTEMS AS POTENTIAL FLEXIBILITY PROVIDERS IN LOW-VOLTAGE NETWORKS

A NEW PLAYER HAS JOINED THE GAME

RESIDENTIAL MULTI-CARRIER ENERGY STORAGE SYSTEMS AS POTENTIAL FLEXIBILITY PROVIDERS IN LOW-VOLTAGE NETWORKS

A NEW PLAYER HAS JOINED THE GAME

Dissertation

for the purpose of obtaining the degree of doctor
at Delft University of Technology
by the authority of the Rector Magnificus prof. dr. ir. T.H.J.J. van der Hagen,
chair of the Board of Doctorates,
To be defended publicly on
Friday 13 of June, 2025, at 15:00 o'clock

by

Joel Jesus ALPIZAR CASTILLO

Master of Science in Senior International Management,
Complutense University of Madrid, Spain,
born in San Jose, Costa Rica.

This dissertation has been approved by the promotors

Composition of the doctoral committee:

Rector Magnificus	Chairperson
Prof. dr. ir. P. Bauer	Delft University of Technology, promotor
Dr. ir. L. M. Ramírez Elizondo	Delft University of Technology, promotor

Independent members:	
Em. prof. dr. ir. M. Zeman,	Delft University of Technology
Prof. dr. ir. J.A. La Poutré,	Delft University of Technology
Prof. dr. L. Bertling Tjernberg	KTH Royal Institute of Technology, Sweden
Dr. S. H. Tindemans,	Delft University of Technology
Dr. M. Cucuzella	University of Groningen

The FLEXINet project was carried out with a Top Sector Energy subsidy from the Ministry of Economic Affairs and Climate, carried out by the Netherlands Enterprise Agency (RVO). The specific subsidy for this project concerns the MOOI subsidy round 2020.

Keywords: Aggregated Control, Energy Hub, Energy Management, Energy Storage, Low-Voltage Distribution Network, Multi-Carrier Energy System

Printed by: ProefschriftMaken

Cover design by: Chiini Lin

ISBN/EAN (Hardcopy): 978-94-6384-773-5
ISBN/EAN (Digital): 978-94-6518-042-7

An electronic version of this dissertation is available at
https://repository.tudelft.nl/record/uuid:76075049-7656-4c49-b206-e742a65b6062

To all those who,
before convincing others,
have to start the day
with the burden of convincing themselves
of what they are truly capable of.

CONTENTS

LIST OF FIGURES

List of Tables

SUMMARY

The integration of renewable energy sources and heating electrification strategies in households is an unavoidable component of the energy transition. Unfortunately, the pace at which such integration occurs has proven challenging for the distribution system operators. On the one hand, system operators design low-voltage networks for low, unidirectional power flows at the connection points with the consumers, with expected lifetimes of several decades. On the other, the decreasing prices, together with the economic and environmental incentives to install (mainly) rooftop PV systems and heat pumps, create highly stochastic, bidirectional and potentially high-power power flows at the connection points of the former consumers, transforming them into prosumers. This thesis studies the misalignment between the interests of system operators and prosumers, proposing realistic alternatives that are achievable in the short term. This thesis hypothesizes that the aggregation of residential multi-carrier energy storage systems would be capable of bridging the interests between prosumers and distribution system operators. To validate the hypothesis, this thesis is comprised of five research topics.

Distribution system operators commonly address the grid congestion through infrastructure reinforcements, which is slow and expensive. Chapter 2 studies how energy storage systems with different carriers can provide a collaborative solution involving prosumers as ancillary services providers at the distribution level. Specifically for the European urban context, this chapter analyzed renewable energy sources, batteries, supercapacitors, hydrogen fuel cells, thermal energy storage, and electric vehicles through a thorough review of successful implementations. The correlations found between individual energy storage technologies and ancillary services provided insight into the flexibility opportunities each technology can provide to the grid. It was concluded that multi-carrier systems would provide the most robust yet flexible solution.

Based on the previous premise, Chapter 3 evaluated four multi-carrier energy system configurations for a Dutch household. The chapter also provides analytical models for every component (including the thermal losses from the thermal storage to the ground) and the space heating and electrical demands. The results suggest that using a heat pump combined with a photovoltaic system and a battery provides the best trade-off for the prosumer. The photovoltaic-thermal system alone could not supply the thermal demand required for comfortable space heating nor reach temperatures high enough to charge the thermal storage. Combining the thermal storage with the heat pump allows a certain degree of flexibility for the heat pump activation at the cost of COPs between 0.8 and 1.38 when used to charge the thermal storage, thus increasing energy consumption and equivalent emissions considerably.

Chapter 4 then elaborates on different energy management strategies to control the multi-carrier systems as proposed above. Two adaptable energy management system strategies were proposed for any system architecture with a reduced number of constraints. The first strategy uses genetic algorithms with a discrete-continuous approach

for the power setpoints, maximizing thermal comfort and minimizing energy cost and CO_2 equivalent emissions. The EMS employs random forests for short-term predictions of the PV generation and electric and thermal demand. The results demonstrate that the strategy can solve the power allocation problem in the order of 1 s, including forecasting 60 minutes. This strategy, however, is too computationally demanding for complex distribution systems with multiple houses. Therefore, the second strategy uses a policy-based heuristic method to control the multi-carrier system, minimizing energy costs and maximizing thermal comfort. Also, this strategy allows the EMS to follow, or not, an external power setpoint from an aggregator, resulting in control decisions in the order of 30 ms. In addition, an ageing-aware EMS was briefly introduced, demonstrating the importance of ageing the BESS during operation.

Chapter 5 investigates, from a cost perspective, what conditions can make it attractive for individual prosumers to participate in a low-voltage ancillary service market, specifically power curtailment and peak shaving. For the former, it was shown that there are conditions where curtailing power does not significantly reduce the system's revenue but greatly reduces the peak power injected into the grid. However, it was also shown that curtailing might affect the power electronic components of the solar converter, potentially reducing its expected lifetime compared to a normal operation without curtailment. Similarly, an estimation of the degradation of the batteries for the cases with and without providing peak shaving was done using a semi-empirical ageing model, concluding that doing peak shaving to ensure a fixed power exchange with the grid will drastically reduce the life of the battery. Therefore, following an external setpoint to reduce occasional peaks would extend the battery's life. The results suggest that power curtailment and peak shaving can be attractive for prosumers, thus creating opportunities for ancillary services business models at the residential scale.

Chapter 6 incorporated households with single- and multi-carrier energy storage in a low-voltage distribution network to quantify the benefit of aggregation for the prosumers and system operators. The aggregator is generally assumed to have full observability and controllability of the assets, which is unrealistic in many cases. For this reason, this chapter considered separate controllers for the prosumers and the aggregator. Using a real 301-node low-voltage residential distribution network in the Netherlands, it was demonstrated that aggregated multi-carrier energy storage can ensure the voltage conditions established in EN50160 for penetrations of PV systems coupled with heat pumps up to 80 %. In contrast, aggregated single-carrier storage can reach 60 % and centralized storage only 40 %. Despite generating an economic benefit while supporting the grid, the high investment costs for both single- and multi-carrier storage result in unattractive conditions for prosumers compared to a case with only PV and heat pumps, requiring compensations for around half of the energy purchase costs for the single-carrier storage and higher than the total energy costs for the multi-carrier.

In summary, it was proved that, from a technical perspective, aggregated residential multi-carrier energy systems are a robust yet flexible solution for the voltage problems caused by the energy transition in residential low-voltage distribution networks. However, the current state of thermal storage makes the technology too expensive to be economically attractive.

SAMENVATTING

De integratie van hernieuwbare energiebronnen en elektrificatiestrategieën voor verwarming in huishoudens is een onvermijdelijk onderdeel van de energietransitie. Helaas blijkt het tempo waarin deze integratie plaatsvindt een uitdaging te zijn voor de netbeheerders. Enerzijds, ontwerpen netbeheerders laagspanningsnetwerken voor lage, unidirectionele krachtstroom bij de aansluitpunten met de consumenten, met verwachte levensduren van enkele decennia. Anderzijds zorgen de dalende prijzen, samen met de economische en milieustimuli om (voornamelijk) PV-systemen op daken en warmtepompen te installeren, voor zeer stochastische, bidirectionele en potentieel hoogvermogen krachtstroom bij de aansluitpunten van de voormalige consumenten, waardoor ze prosumenten worden. Deze scriptie bestudeert de verschillen tussen de belangen van netbeheerders en prosumenten en stelt realistische alternatieven voor die op korte termijn haalbaar zijn. Deze scriptie stelt de hypothese dat de aggregatie van residentiële multi-carrier energieopslagsystemen in staat zou zijn om de belangen van prosumenten en netbeheerders te overbruggen. Om de hypothese te valideren, bestaat deze scriptie uit vijf onderzoeksonderwerpen.

Netbeheerders pakken netcongestie doorgaans aan door infrastructuurversterkingen, wat traag en duur is. Hoofdstuk 2 bestudeert hoe energieopslagsystemen met verschillende carriers een gezamenlijke oplossing kunnen bieden waarbij prosumenten als aanbieders van ondersteunende diensten op distributieniveau worden betrokken. Specifiek voor de Europese stedelijke context analyseerde dit hoofdstuk hernieuwbare energiebronnen, batterijen, supercondensatoren, brandstofcellen, thermische energieopslag en elektrische voertuigen door middel van een grondige review van succesvolle implementaties. De correlaties die werden gevonden tussen individuele energieopslagtechnologieën en ondersteunende diensten gaven inzicht in de flexibiliteitsmogelijkheden die elke technologie aan het net kan bieden. Er werd geconcludeerd dat multi-carrier systemen de meest robuuste, maar flexibele oplossing zouden bieden.

Op basis van de vorige premisse evalueerde Hoofdstuk 3 vier configuraties van multi-carrier energiesystemen voor een Nederlands huishouden. Het hoofdstuk biedt ook analytische modellen voor elk onderdeel (inclusief de thermische verliezen van de thermische opslag naar de grond) en de ruimteverwarming en elektrische vraag. De resultaten suggereren dat het gebruik van een warmtepomp in combinatie met een fotovoltaïsch systeem en een batterij de beste afweging biedt voor de prosument. Het fotovoltaïsch-thermische systeem alleen kon niet voldoen aan de thermische vraag die nodig is voor comfortabele ruimteverwarming, noch temperaturen bereiken die hoog genoeg zijn om de thermische opslag op te laden. Het combineren van de thermische opslag met de warmtepomp biedt een zekere mate van flexibiliteit voor de activering van de warmtepomp, maar tegen de kosten van COP's tussen 0,8 en 1,38 wanneer deze wordt gebruikt om de thermische opslag op te laden, waardoor het energieverbruik en de equivalente emissies aanzienlijk toenemen.

Hoofdstuk 4 werkt vervolgens verschillende energiebeheerstrategieën uit om de voorgestelde multi-carrier systemen te controleren. Twee aanpasbare energiebeheersystemen werden voorgesteld voor elke systeemarchitectuur met een beperkt aantal beperkingen. De eerste strategie maakt gebruik van genetische algoritmen met een discrete-continue benadering voor de vermogenssetpoints, waarbij thermisch comfort wordt gemaximaliseerd en energiekosten en CO_2-equivalente emissies worden geminimaliseerd. Het EMS maakt gebruik van random forests voor kortetermijnvoorspellingen van de PV-opwekking en de elektrische en thermische vraag. De resultaten tonen aan dat de strategie het vermogensallocatieprobleem kan oplossen in de orde van 1 s, inclusief voorspellingen van 60 minuten. Deze strategie is echter te computationeel veeleisend voor complexe distributiesystemen met meerdere huizen. Daarom maakt de tweede strategie gebruik van een op beleid gebaseerde heuristische methode om het multi-carrier systeem te controleren, waarbij energiekosten worden geminimaliseerd en thermisch comfort wordt gemaximaliseerd. Bovendien stelt deze strategie het EMS in staat om al dan niet een extern vermogenssetpoint van een aggregator te volgen, wat resulteert in controlebeslissingen in de orde van 30 ms. Daarnaast werd kort een verouderingsbewuste EMS geïntroduceerd, waarbij het belang van veroudering van de BESS tijdens de werking werd aangetoond.

Hoofdstuk 5 onderzoekt vanuit kostenperspectief onder welke voorwaarden het aantrekkelijk kan zijn voor individuele prosumenten om deel te nemen aan een laagspanningsmarkt voor ondersteunende diensten, specifiek vermogensinperking en piekafvlakking. Voor het eerste werd aangetoond dat er omstandigheden zijn waarin het beperken van vermogen de inkomsten van het systeem niet significant vermindert, maar de piekvermogen die in het net wordt geïnjecteerd aanzienlijk vermindert. Er werd echter ook aangetoond dat inperking invloed kan hebben op de vermogenselektronica van de zonne-omvormer, waardoor de verwachte levensduur ervan mogelijk wordt verkort in vergelijking met normaal gebruik zonder inperking. Evenzo, werd een schatting gemaakt van de degradatie van de batterijen voor de gevallen met en zonder piekafvlakking, waarbij gebruik werd gemaakt van een semi-empirisch verouderingsmodel, en geconcludeerd dat het uitvoeren van piekafvlakking om een vast vermogen uit te wisselen met het net de levensduur van de batterij drastisch zal verkorten. Daarom zou het volgen van een extern setpoint om incidentele pieken te verminderen de levensduur van de batterij verlengen. De resultaten suggereren dat vermogensinperking en piekafvlakking aantrekkelijk kunnen zijn voor prosumenten, waardoor kansen ontstaan voor bedrijfsmodellen voor ondersteunende diensten op residentiële schaal.

Hoofdstuk 6 integreerde huishoudens met enkel- en multi-carrier energieopslag in een laagspanningsdistributienetwerk om het voordeel van aggregatie voor de prosumenten en netbeheerders te kwantificeren. De aggregator wordt over het algemeen ervan verondersteld volledige observatie- en controleerbaarheid van de activa te hebben, wat in veel gevallen onrealistisch is. Om deze reden beschouwde dit hoofdstuk afzonderlijke controllers voor de prosumenten en de aggregator. Met behulp van een echt 301-node laagspanningsresidentieel distributienetwerk in Nederland werd aangetoond dat geaggregeerde multi-carrier energieopslag de spanningscondities kan waarborgen die zijn vastgesteld in EN50160 voor penetraties van PV-systemen in combinatie met warmtepompen tot 80 %. Daarentegen kan geaggregeerde enkel-carrier opslag 60 % bereiken

en gecentraliseerde opslag slechts 40 %. Ondanks het genereren van een economisch voordeel terwijl het net wordt ondersteund, resulteren de hoge investeringskosten voor zowel enkel- als multi-carrier opslag in onaantrekkelijke voorwaarden voor prosumenten in vergelijking met een geval met alleen PV en warmtepompen, waarbij compensaties nodig zijn voor ongeveer de helft van de energiekosten voor de enkel-carrier opslag en hoger dan de totale energiekosten voor de multi-carrier.

Samenvattend werd aangetoond dat, vanuit technisch perspectief, geaggregeerde residentiële multi-carrier energiesystemen een robuuste, maar flexibele oplossing, zijn voor de spanningsproblemen veroorzaakt door de energietransitie in residentiële laagspanningsdistributienetwerken. De huidige staat van thermische opslag maakt de technologie echter te duur om economisch aantrekkelijk te zijn.

PREFACE

The existing energy matrix has a severe case of addiction to fossil fuels. As such, one cannot bluntly remove them because of the implications it would have, both for the energy infrastructure and us who depend on it, but also due to the influence of the suppliers of the drug. Instead, as in any rehabilitation treatment, small steps must be made carefully as part of a detoxification. This thesis aims to study and propose short-term, realistic solutions for the traditional end of the energy chain –residential heating– and the implications it entails in the electric network. Yet, it shall be noted that these efforts, albeit valuable, will not make a significant change in the impact fossil fuels have on the world. However, they at least transfer back the responsibility to those who should have it, instead of delegating it to the consumers who do not have any other real option.

Joel Jesus Alpizar Castillo
Delft, February 2025

1

INTRODUCTION

"Dedication is a talent on its own"

Alphonse Elric, Fullmetal Alchemist: Brotherhood, Episode 7, by Hiromu Arakawa.

1

1.1. BACKGROUND AND MOTIVATION

Traditionally, medium- and high-voltage networks have been the centre of attention of system operators, as high-power systems are normally connected to such systems. Such connections require detailed planning, and system operators usually demand some degree of flexibility from asset owners, either consumers or generators. In such a scheme, residential low-voltage distribution networks were considered to be less risky, as they only consume energy, and their loads were relatively low power, as the most energy-intensive activities (transportation and heating) relied on fossil fuels. Therefore, unlike the larger consumers who can participate in the ancillary service markets, residential prosumers were only expected to consume energy using low-power loads which do not cause major challenges in the low-voltage distribution infrastructure. Nevertheless, the energy transition dramatically shifted the paradigm for residential consumers.

In the energy transition scheme, residential prosumers are encouraged to install distributed generators based on renewable energy sources (RES), typically PV systems, as most of the energy generated at the beginning of the energy supply chain comes from fossil fuels [1]. In addition, many existing households are replacing their gas boilers with heat pumps (HP), which are also becoming the norm for new buildings [2]. Similarly, the electrification of transportation has reached a point where the purchase of electric vehicles (EVs) now competes with internal combustion, and the number houses installing chargers soared [3]. This way, distribution system operators (DSOs) have seen a drastic change in the power exchange behaviour from residential consumers in a short time, challenging their traditional reinforcement-based system management strategies.

The responses from DSOs can be categorized into regulatory and policy, and technical. The first includes administrative actions requested by the DSO to the regulatory authorities to minimize the effect of the energy transition in the electrical network. For example, in Germany and the United Kingdom, there is a limit to how much power a residential system can inject into the grid, based on its nominal power [4], [5]. Also, some authors have demonstrated that flat energy and variable demand tariffs are less risky while still being attractive for prosumers [6]. The second category includes technical actions so that the cyber-physical distribution system can manage the new power flow conditions. Among those actions are grid reinforcement and restructuration and more robust power flow control mechanisms [7]. Those categories, despite fundamentally different, share one common bottleneck, both require long realization times; the former due to regulatory, social acceptance and institutional barriers, and the second due to required technological development, engineering design and commissioning [8] and, more recently, a shortage in workforce [9]. This way, effective solutions require using available technologies and the current regulatory frameworks as much as possible.

This thesis aims to comprehensively study residential prosumers' effect on the low-voltage distribution networks caused by the energy transition. Following the current – and envisioning future– technology trends, multi-carrier energy systems, comprised of electric and thermal components, are evaluated as both the cause and solution for the congestion on the distribution network. Thereby, this work intends to propose realistic, collaborative-based solutions for the current and near-future challenges faced by distribution system operators at the low-voltage residential distribution level. Such solutions are based on techno-economic analyses and could be deployed in the short term.

1.2. THE FLEXINET PROJECT: KEY CHALLENGES AND RESEARCH GAPS

This dissertation has been carried out as part of the FLEXINet project. A research project funded by a Top Sector Energy subsidy from the Ministry of Economic Affairs and Climate, carried out by the Netherlands Enterprise Agency (RVO). The aim of this project is to demonstrate the potential benefits of energy storage in different carriers and how such a combination can accelerate the energy transition. In addition, this thesis also included electric and thermal power generation devices, i.e., a PV, a photovoltaic-thermal system (PVT) and a heat pump. The project was comprised of a consortium of eight companies, three research institutions and two living labs, who worked together to design, integrate, install and test a multi-carrier energy system at the facilities of The Green Village at the Delft University of Technology's campus.

The FLEXINet project aims for an end-to-end analysis of residential multi-carrier energy storage to provide flexibility to the low-voltage distribution network. As such, a number of challenges arise, including hardware development, communications interoperability, local system modelling and control, aggregated system modelling and control, energy market analysis and social acceptance, to mention some. This thesis focuses on the research gaps related to local system modelling and control, aggregated system modelling and control and energy market analysis. The remaining challenges will be addressed by other researchers within the project.

1.2.1. LOCAL SYSTEM MODELLING AND CONTROL

Industry and academia have focus mostly on the coupling of electric systems, such as PV and BESS, as pivotal point towards the energy transition. However, thermal systems are as critical, given the amount of energy required for space heating alone, yet, little attention has been given to study them working together with the electrical system. Among the reasons, studies suggest the difference in time constants (very fast electric systems against slow thermal systems), software incompatibility, model and simulation complexity, and few case scenarios available given the early technology readiness of some technologies (e.g., PVT and thermal storage). More punctually, the research gaps found, which are addressed in this thesis, are:

- the inclusion of PVT and TESS as part of the main thermal network of a residential building and not as support devices,
- the effects of locating a thermal energy storage system underground outside the house due to space constraints,
- the quantification of equivalent CO_2 emissions associated with heating electrification in residential buildings through heat pumps, and
- the lack of plug-and-play frameworks for modelling and control of residential multi-carrier energy systems with low computational cost.

To address those research gaps, this thesis provides a detailed analytical framework to model the components that comprise a residential multi-carrier system, both individu-

ally and coupled with one or more. Similarly, different control strategies are proposed and compared, so that future researchers could use them, based on their needs.

1.2.2. AGGREGATED SYSTEM MODELLING AND CONTROL

The energy transition impulses the electrification of fossil fuel-dependent systems, such as transportation and heating. In countries such as the Netherlands, with mild to low temperatures, heating is a crucial factor to consider in every household, while the charging of electric vehicles can be done either at the household level or through the public charging infrastructure. Still, both increase considerably the energy consumed per household and the peak demand causing congestion in the grid. Typically, DSOs face congestion by the network infrastructure. Nevertheless, this approach has been proven ineffective due to the time, cost and logistics it requires. Using energy storage has been proposed as an alternative, but most of the literature has focused on centralized single-carrier systems, resulting in the following research gaps:

- many works focus on optimal sizing and placing of energy storage systems instead of using available resources; however, most DSOs cannot own energy storage assets due to regulation limitations,
- most of the business models proposed suggest a single owner of all storage assets in the network, instead of considering storage assets owned by individual prosumers who could collaborate with the DSO,
- most of the aggregation strategies found focus on medium and high voltage networks; nevertheless, low-voltage networks are particularly critical for the energy transition, as they do not have ancillary services providers to support the DSO, and the demand increase caused by the heating electrification and electric mobility can potentially cause major voltage challenges,
- the control techniques for single-carrier systems focus on mid- to large-scale assets in medium voltage distribution networks, leaving aside multi-carrier systems and low-voltage residential distribution networks,
- dependency on test networks with a small number of connections (either DRES and BESS assets, or loads) for case scenarios, instead of using data from existing distribution networks,
- the aggregators are assumed to have full observability and controllability over the assets, potentially causing privacy challenges for residential prosumers who would own assets connected to the network, and would require complex communication infrastructure, and
- the control is usually either consumer-centred or DSO-centred, instead of balancing between their interests.

The previous research gaps are addressed in this thesis by proposing different aggregation control strategies for single- and multi-carrier residential systems. Those strategies will be compared so that the advantages and disadvantages of both the control strategy and the system architecture (single- or multi-carrier) are clearly defined.

1.2.3. ENERGY MARKET ANALYSIS

Although a solution is technically feasible, it does not necessarily mean it can be implemented. For that reason, an understanding of the current state-of-the-art on ancillary services would provide insight into how to support the DSOs. Then, based on this, it would be possible to propose participation mechanisms for residential prosumers that require little to no change in the current policy framework in the Netherlands. Thus, the research gaps found are

- the lack of studies on ancillary services at the low-voltage networks from multiple energy storage systems, considering other carriers than electric (e.g., thermal storage),
- the quantification of the effects of deploying energy storage systems in distribution networks,
- the available energy storage systems are considered as assets of the DSO or TSO while most frameworks forbid them from owning energy storage assets,
- unclear correlation between different energy storage systems capabilities and the needs of the DSOs,
- the lack of studies on real distribution systems,
- the quantification of the degradation effects on residential battery energy storage systems and power electronic converters while providing ancillary services,
- a study on the technical and economic feasibility of implementing ancillary services at the low-voltage distribution networks in the short term,

The analysis done to fill those research gaps consisted of a thorough literature review on ancillary services implementation, so a correlation of the opportunities each component of the multi-carrier energy system has towards providing ancillary services becomes clear. Then, based on that information, the ancillary services with fewer policy bottlenecks will be selected and simulated to determine their technical and financial feasibility.

1.3. RESEARCH OBJECTIVE

To address the challenges and research gaps pointed out in Section 1.2, the main objective of this thesis is as follows.

"To demonstrate whether aggregated multi-carrier energy systems, composed of single-carrier energy devices coupled together, can provide additional flexibility to the residential low-voltage network, when considering the optimal energy flows, through the quantification of the economic impact when installing the system in a household building."

The following research questions were raised to achieve the aforementioned objective, and specific objectives were proposed to fill the research gaps identified.

1

Q1. *What is the behaviour of a thermal energy storage system when coupled together with a battery energy storage system, a heat pump and a photo-voltaic thermal system as a multi-carrier energy system to supply electric and thermal load requirements at the household level?*

- Identify the behaviour changes of a thermal energy storage system when coupled together with a battery energy storage system, a heat pump and a photo-voltaic thermal system, as a multi-carrier energy storage system to supply electrical and thermal loads simultaneously at the household level **Chapters 2 and 3**.

Q2 *What are the advantages multi-carrier energy systems have over single-carrier energy systems when aggregated, considering the cost/benefit of providing simultaneous ancillary services to the electrical network?*

- Determine the individual and combined contributions of single-carrier energy storage devices within a multi-carrier energy storage system towards providing flexibility to the network **Chapter 2**.
- Compare the effect aggregated distributed generators with thermal and battery energy storage systems coupled as a multi-carrier energy storage system have on the electrical network against non-coordinated distributed generators without storage systems and non-coordinated distributed generators with single-carrier battery energy storage systems **Chapter 6**.

Q3 *How to determine the optimal combination of ancillary services a multi-carrier energy system comprised of a PV, a BESS, a HP and a TESS can provide, which satisfies the local demand at the household level while minimizing the adverse effects on the grid and the environment when aggregated at the community level, and maximizing the advantage for the prosumer?*

- Propose an optimization strategy for the energy flow in the multi-carrier energy system that maximizes the profit at the household level **Chapter 4**, while minimizes the impact on the energy network at the aggregated level, considering the $CO_{2,eq}$ emissions during the operation of the system **Chapter 6**.
- Propose a business model that evaluates the economic feasibility of implementing a multi-carrier energy system at the household level to provide voltage support to the low-voltage distribution network through peak-shaving and power curtailment **Chapter 5**.

1.4. CONTRIBUTIONS

Having answered the previous research questions, the contributions of this dissertation are listed as follows:

- A comparative analysis of the correlation between ESSs in different energy carriers with the ancillary services they can provide to identify, based on the literature, the potential benefits of using multi-carrier energy systems (**Chapter 2**).

- A comparative analysis of different combinations of a PVT, a HP, a TESS, and a BESS coupled as a multi-carrier energy system for household applications, based on electrical consumption from the grid, thermal power generation for space heating, and equivalent $CO_{2,eq}$ emissions **(Chapter 3)**.
- A multi-objective genetic algorithm energy management system for short-term predictions in a residential multi-carrier energy system that accounts for energy costs, equivalent $CO_{2,eq}$ emissions and thermal comfort **(Chapter 4)**.
- An estimation of the technical and economic conditions that would make it attractive for prosumers, given six case scenarios, to participate as flexibility providers through peak-shaving and power curtailment in low-voltage residential networks **(Chapter 5)**.
- A quantitative comparison of the economic benefit for the prosumer and voltage-control capabilities for the DSO, of a centralized BESS and aggregated single- and multi-carrier residential storage systems while providing voltage support in a low-voltage distribution network **(Chapter 6).**

Aside from the previous contributions, numerous open-access models were developed in Python and made available throughout this thesis. Such models are listed below.

- A modular library to simulate a house with a multi-carrier energy system comprised of a combination of space heating and electric elements **(Chapter 3)** [10].
- An analytical model for an underground water tank thermal energy storage system considering the soil's temperature gradient **(Chapter 3)** [10].
- A modular genetic algorithm energy management system for short-term multi-objective predictive control of a residential multi-carrier energy system **(Chapter 4)** [11].
- A modular heuristic energy management system for residential multi-carrier energy system considering thermal comfort, energy cost and a power setpoint from an aggregator **(Chapter 4)** [12].
- A model to estimate the degradation of the switches that comprise a converter during power curtailment **(Chapter 5)** [13].
- A voltage-based model to estimate the voltage throughout a low-voltage distribution network, considering prosumers with an independant energy management system (EMS) that can or not follow a setpoint from an aggregator **(Chapter 6)** [12].

1.5. THESIS OUTLINE

This thesis is comprised of five chapters dedicated to answer the research questions proposed in Section 1.3. Figure 1.1 provides schematic with the main topic per chapter, and their correlation. First, Chapter 2 provides an overview on the main ancillary services

1

available to support the electric system operators and their relationship between single- and multi-carrier systems. Chapter 3 establishes the mathematical background to model the individual components of a residential multi-carrier energy system and their interaction. Chapter 4 then compares different home energy management systems, including a novel short-term predictive control based on genetic algorithms. Chapter 5 elaborates on the techno-economic analysis required to establish the market mechanisms that would allow a feasible participation of residential prosumers to support the low-voltage distribution network. Chapter 6 provides an aggregation strategy to coordinate multiple residential multi-carrier energy systems and support the low-voltage distribution network through voltage control services. Finally, Chapter 7 summarizes the conclusions of this thesis and proposes new research lines based on this work.

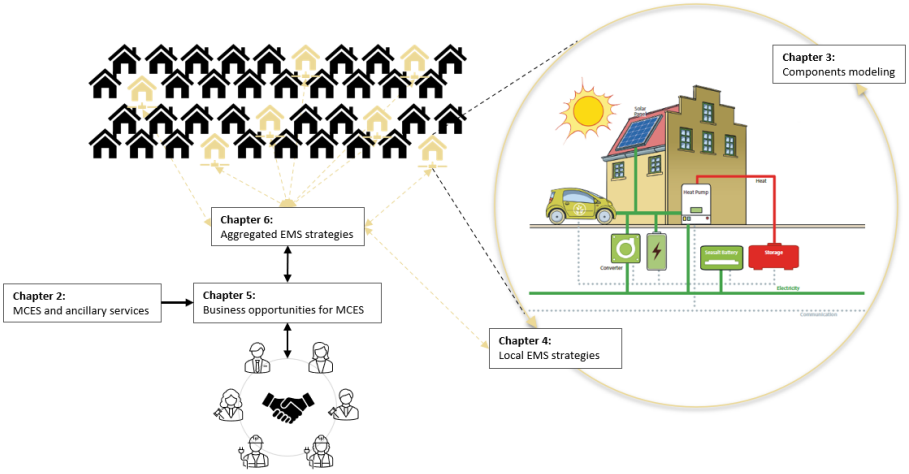

Figure 1.1: Outline of this thesis and correlation of chapters (adapted from [14]).

BIBLIOGRAPHY

[1] "Electricity 2024: Analysis and forecast to 2026", International Energy Agency, Tech. Rep., 2024. [Online]. Available: https://www.iea.org/reports/electricity-2024.

[2] "Net zero roadmap: A global pathway to keep the 1.5 °c goal in reach", in International Energy Agency, 2023, ch. Space heating. [Online]. Available: https://www.iea.org/reports/space-heating.

[3] "Global ev outlook 2024", International Energy Agency, Tech. Rep., 2024. [Online]. Available: https://www.iea.org/reports/global-ev-outlook-2024.

[4] "Export limitation", SolarEdge, Application Note Version 2.8, Mar. 2022. [Online]. Available: https://knowledge-center.solaredge.com/sites/kc/files/feed-in_limitation_application_note.pdf.

[5] "Technical requirements for customers' export and import limitation schemes", Energy Networks Association, Engineering Recommendation G100 Issue 2 2022 Amendment 2, Apr. 2023. [Online]. Available: https://www.energynetworks.org/assets/images/ENA_EREC_G100_Issue_2_Amendment_2_(2023).pdf.

[6] D. Azuatalam, A. C. Chapman, and G. Verbič, "Probabilistic assessment of impact of flexible loads under network tariffs in low-voltage distribution networks", *Journal of Modern Power Systems and Clean Energy*, vol. 9, no. 4, pp. 951–962, 2021. DOI: 10.35833/MPCE.2019.000136.

[7] "2030-2050 integrated infrastructure outlook", Netbeheer Nederland, Tech. Rep., Oct. 2024. [Online]. Available: https://www.energiekompas2050.nl/wp-content/uploads/2024/01/II3050-Main-Report-20240118-1.pdf.

[8] F. Norouzi, T. Hoppe, L. R. Elizondo, and P. Bauer, "A review of socio-technical barriers to smart microgrid development", *Renewable and Sustainable Energy Reviews*, vol. 167, p. 112 674, 2022, ISSN: 1364-0321. DOI: https://doi.org/10.1016/j.rser.2022.112674. [Online]. Available: https://www.sciencedirect.com/science/article/pii/S1364032122005640.

[9] G. Hovnanian, A. Kumar, and R. Luby, "Will a labor crunch derail plans to upgrade us infrastructure?", 2022. [Online]. Available: https://www.mckinsey.com/industries/public-sector/our-insights/will-a-labor-crunch-derail-plans-to-upgrade-us-infrastructure#/.

[10] J. Alpízar-Castillo, *MCES Library*, https://github.com/jjac13/MCES_Library, 2024.

[11] J. Alpízar-Castillo, *GA HEMS*, https://github.com/jjac13/GA_HEMS, 2023.

[12] J. Alpízar-Castillo, *LV network simulator public*, https://github.com/jjac13/LV_network_simulator_public, 2025.

[13] J. Alpízar-Castillo and C. Engstrom, *BESS PEC degradation*, https://github.com/jjac13/BESS_PEC_degradation, 2025.

[14] FLEXINet, *Hybrid energy storage systems as multi-carrier flexibility providers — tudelft.nl*, 2021. [Online]. Available: https://www.tudelft.nl/ewi/over-de-faculteit/afdelingen/electrical-sustainable-energy/dces/research/hybrid-energy-storage-systems-as-multi-carrier-flexibility-providers.

2

Multi-Carrier Energy and Ancillary Services: A Review on the Challenges, Opportunities and Case Studies in Distribution Systems

"You should enjoy the little detours. To the fullest. Because that's where you'll find the things more important than what you want"

Ging Freecss, Hunter x Hunter (2011), Episode 148, by Yoshihiro Togashi.

This Chapter is based on:

- J. Alpízar-Castillo, L. Ramirez-Elizondo, and P. Bauer, "Assessing the Role of Energy Storage in Multiple Energy Carriers toward Providing Ancillary Services: A Review," Energies, vol. 16, no. 1, p. 379, Dec. 2022.

2.1. Introduction

As the global trend in energy is to displace fossil fuels as the primary source of electricity, transport, and heat production, alternatives such as renewable energy sources (RESs), electric vehicles (EVs), and heat pumps (HPs) are playing a significant role in the energy transition. Following the Renewable Energy Directive (2018/2001/EU), the power generation in the European Union has to achieve 32 % from RESs by 2030 [1] (or eventually 40 % if the proposal in [2] is approved), under the Regulations on the Internal Market for Electricity (2019/943/EU) [3]. However, a massive deployment of renewable energy sources distributed generators (DGs) without the integral participation of the stakeholders in the energy supply chain (see Figure 2.1) can cause a series of problems in the grid. Those problems are described in Section 2.2.

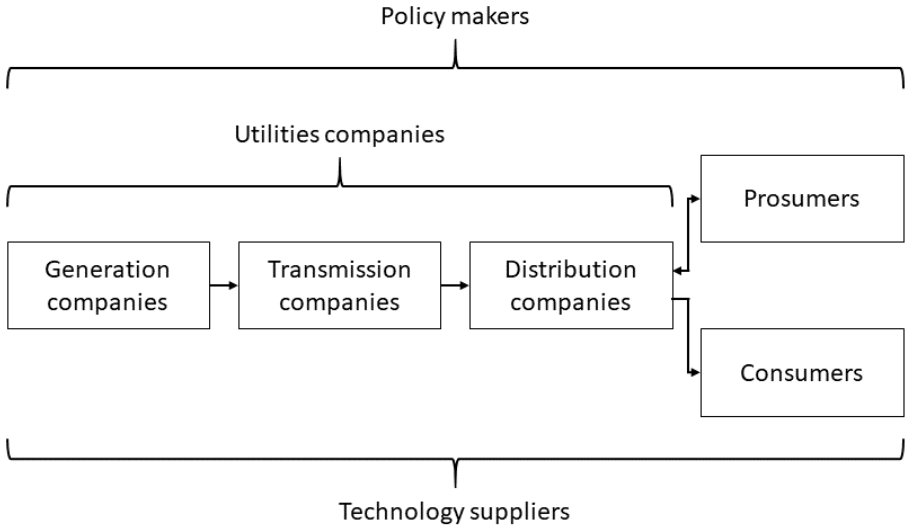

Figure 2.1: Energy market supply chain and stakeholders.

With the scheme presented in Figure 2.1, when installing RESs, the users are not only mere consumers but become prosumers actively participating in the energy exchange with the grid. This transition causes unprecedented alterations in the energy flux, as the effects of the DG are nonlinear concerning the penetration level [4], [5]. Owing to the improvements in batteries' efficiency and reductions in price [6], electric vehicle sales are increasing and battery energy storage systems (BESSs) are more commonly installed together with RESs. The effects of energy storage systems (ESSs) on the grid still need to be investigated [7]; however, an appropriate deployment, combined with RES and EV in distribution networks, can improve the grid's performance, as well reduce the adverse effects of DGs on them [6]–[9].

Numerous projects studies been conducted to combine different assets such as RESs, BESSs, and EVs in various configurations, creating microgrids [10]. It is considered a smart grid when those microgrids react to the needs of the electrical network. A business

case is needed to evaluate the feasibility of microgrids, as the conditions are different among countries or even cities within the same country. In [11], key performance indicators were proposed to validate the feasibility of deploying a smart grid in Greece under the context of the One Network for Europe (OneNet) project. Although the smart grids studied by [10] presented encouraging results, extrapolating them to different scales is not straightforward. Scalability, replicability, and interoperability are the main challenges to generalizing the results from a local experiment [12]. Therefore, researchers are working toward understanding the behaviour of smart grids under different conditions to forecast their scaled outcomes [12].

Complementary to the electrical energy exchange, systems can participate in heat exchange and regulation [13]. This kind of multi-carrier energy system (MCES) involves a transversal approach, considering the production and storage of electricity and heat, allowing the bidirectional energy flow, and is open to including different technologies associated with each system component. As expected, the energy management systems (EMSs) face challenges regarding the control strategies, as they need to consider communication infrastructure [6], [9], energy management algorithms [6], [9], weather conditions forecast [9], and demand response predictions [14], to mention some.

Despite the challenges mentioned above, there is consensus in the literature that adding thermal energy storage systems (TESSs) provides a more integral approach to smart grids and cities. In this scenario, the prosumers collaborate with the distribution system operators (DSOs) through ancillary services to keep the grid operating in the most favorable conditions [15]–[20]. Therefore, the motivation of the present study was to investigate, through an exhaustive review, the ancillary services that a multi-carrier energy storage systems (MCESSs) can provide to reduce the effect of DGs on the distribution grids. A selection of relevant reviews is presented in Table 2.1. As can be seen, previous reviews did not describe a correlation between MCES and ancillary services, and a comprehensive study on the implementation of MCESSs as ancillary services providers has not been reported in the literature; therefore, this Chapter:

- determines the correlation between ESSs in different energy carriers with the ancillary services they can provide, and
- identifies potential benefits of using multi-carrier energy systems.

This Chapter is organized as follows: the main problem is analyzed in Section 2.2. Section 2.2.1 lists the main strategies to displace fossil fuels as the primary energy source; Section 2.2.2 details the main effects those strategies are having on the grid. The emerging solutions to address those effects are mentioned in Section 2.2.3. Section 2.3 explores the ancillary services prosumers can provide to the grid. As sources of integral solutions, multi-carrier energy storage systems are detailed in Section 2.4. The results are discussed in Section 2.5, and Section 2.6 presents the main conclusions.

Table 2.1: Findings and research gaps of recent review papers.

Main topic	Major findings	Research gaps	Ref.
Challenges associated with smart grid implementations.	Identification of the main challenges to transforming the existing power network into a smart grid. ESS can balance the supply and demand mismatch through ancillary services.	Aggregation of multiple ESS in the low-voltage network. The effect of combined ESS.	[21]
Capacity sizing methods, power converter topologies to interface multiple ESS, architectures, control, and EMS to couple two or more ESS.	When multiple ESS are coupled, the trend is to couple a high-power storage system to meet transient power behaviour and a high-energy storage system to supply energy in the long term. The most common combination of ESS is BESS with supercapacitors (SC). Time delays between control layers affect the overall operation and stability.	Aggregation of multiple microgrids. Consider ancillary services. Inclusion of thermal energy systems. Multi-objective sizing methods for several ESS coupled.	[22]
How EV chargers can provide ancillary services to system operators.	Classification of the ancillary services available. Identification of the ancillary services EV can provide to the DSO and TSO theoretically and which are on a commercial stage. Identification of the actors involved.	Ancillary services from other ESS than EV. Smart charging infrastructure to diversify the commercial stage ancillary services available.	[23]
The techno-economic and regulatory status of energy storage and power quality services at the distribution level.	Including RES causes reluctance by the DSO, as it changes their business models, generally seen as profit loss instead of new business opportunities. BESS distributed in the grid will play a significant role in the implementation of RES, but their deployment has to consider the BESS total life cycle. BESS can address grid challenges through ancillary services as long as such services are appropriately recognized and rewarded by the DSO.	Quantification of the effects of deploying ESS. The impact of combined ESS. Aggregation of multiple ESS in the low-voltage network.	[24]

Analysis of potential ancillary services for transmission level and distribution level networks.	Voltage control, congestion management, and peak shaving are the most suitable ancillary services at the distribution level. Primary frequency control, reactive power control, and peak shaving are more effective for the transmission level. Centralized and distributed ESS are reliable alternatives for ensuring grid stability.	Considers the ESS as assets of the DSO or TSO. Aggregation of multiple ESS. Network equivalent models.	[25]
Coordination strategies of multiple microgrids in the distribution network.	Identification of aggregation strategies to provide ancillary services and market participation. Aggregated microgrids have the potential to facilitate the inclusion of RES into the grid. Standardization for interconnection and interoperability to participate in the energy market. Standardization in cyber-security.	Considers the microgrids as assets of the DSO or TSO. Inclusion of thermal energy systems.	[26]
Planning and deployment of DG and ESS, including their barriers and technologies available for implementation.	Identification of recent planning and allocation strategies for DG and ESS. Identification of uncertainty modeling methods for DG and ESS planning.	Correlation of the ESS and the needs of the system operators. Considers the microgrids as assets of the DSO or TSO. Inclusion of thermal energy systems. Grid failure studies on the distribution level. Multi-objective sizing methods for ESS.	[27]

2.2. PROBLEM DESCRIPTION

The CO_2 level in the atmosphere, among other greenhouse gases, has dramatically increased since the Industrial Revolution. Despite being hard to define, a point of no return is an already discussed threat [28]. In response, authorities worldwide have proposed strategies and policies toward the transition to RES, electric mobility, and, more recently, the electrification of heating systems to displace fossil fuels as the primary energy source, for instance, the Paris Agreement and Sustainable Development Goals 7

2

and 13 at the international level; most countries have set their own environmental goals [29]. Despite those efforts, by 2020, only 11.4 % of global energy consumption was produced by renewable energies (6.4 % hydro, 2.2 % wind, and 1.1 % solar) [30], [31] (Individual metrics by country can also be found.). Unavoidably, some obstacles have appeared in the process, especially in urban areas due to reduced space, as shown in Figure 2.2, necessitating new solutions. multi-carrier energy storage systems were investigated as possible sources of flexibility by supporting grid operators in urban areas through ancillary services.

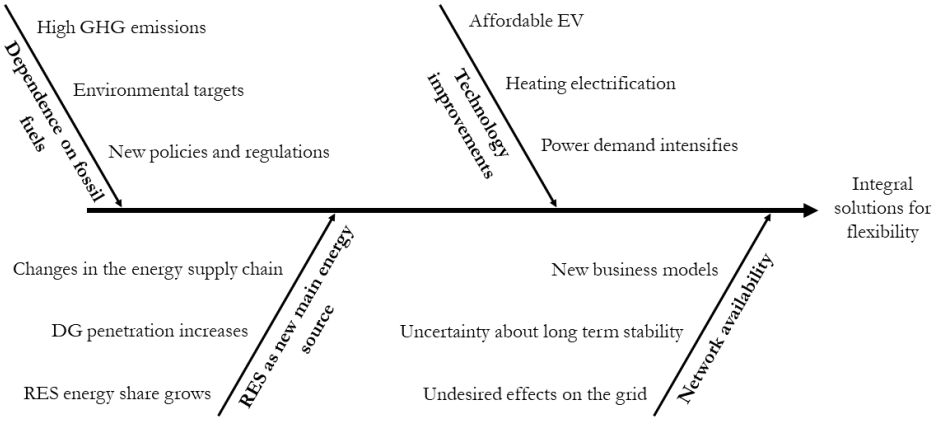

Figure 2.2: Causes and effects of the transition to RESs, resulting in the need for integral solutions.

2.2.1. Traditional Solutions to Displace Fossil Fuels

From the energy perspective, several strategies have been considered to mitigate the anthropogenic contribution to the greenhouse effect in the atmosphere. In 2018, the distribution of the global total energy consumption by final use was 51 % thermal, 32 % transport, and 17 % power, whereas renewable energy supplied only 10.9 % (5.2 % thermal, 1.1 % transport, and 4.6 % power) [29]. Specific measures are considered per sector, highlighting RESs in power generation, electric mobility in transport, and heating electrification in heat production. This section presents the status and goals of the solutions implemented to displace fossil fuels as the primary energy source per sector.

Renewable Energy Sources

In the last two decades, the share of renewable energy sources has consistently increased yearly. Wind and solar installed power have increased notably when analyzing each source individually during the last decade. However, their contribution is still not comparable with other RES, such as hydropower or biomass. Nonetheless, this increasing trend might not be enough to accomplish Sustainable Development Goal 7 [32]. Cost-wise, PV and wind systems' deployment capital and operational expenses have decreased due to technological improvements, manufacturing processes, and incentives from tax authorities in multiple countries [33].

Both centralized plants and distributed generation have caused many challenges as RESs gained ground in the energy mix, which can be addressed with different energy storage strategies [34]–[36], but more studies are required. A significant challenge is that both PV and wind depend on mid- and long-term weather predictions, the variability in which is enhanced due to global warming. Furthermore, the datasets used to estimate the generation potential from renewable sources use historical measurements and different numerical models, which do not necessarily converge when compared [37]. This mismatch causes a proportional behaviour between the increase in weather-dependent RESs and their deployment and integration complexity on the existing network.

ELECTRIC MOBILITY

In 2020, the transport sector consumed around 60 % of the global oil demand [32]. However, electric vehicle (EV) sales are consistently rising as a measure to change the primary energy source for the sector from fossil fuels to electricity [38]. Three critical mitigation responses were proposed in [39] to reduce the transport $CO_{2,eq}$ emissions: avoid and reduce the need for motorized travel, shift to more environmentally friendly transport modes, and improve the efficiency of transport modes, where electric mobility plays a key role. Regarding the last point, smart charging devices for EVs are constantly being developed by research groups worldwide, with approaches such as charging profiles [40], wireless charging [41], increasing the process efficiency [42], or decreasing the charging time [43], for instance, in the attempt to reduce the effects on the grid. The requirements for electrical mobility exceed the vehicles and their charging stations: urban planning must be considered and electric systems reinforced, as the demand will increase to meet the power requirements [44], [45].

HEATING ELECTRIFICATION

Given that more than half of the total final energy consumption is dedicated to heat-related processes, being only 10.2 % from renewable sources [29], heating electrification is expected to play a significant role in the energy transition. Multiple authors agree on the potential of heat pumps (HPs) [46]–[48]; other technologies, such as heat pipes, are other promising alternatives to fossil fuel-based heating systems [49]. Three major techno-economical obstacles were analyzed in [50]. First, electricity is more expensive than fossil fuels, resulting in a less profitable solution unless distribution companies implement new utility tariffs or business models. Second, the nature of the local energy mix, i.e., If the primary energy source of the mix is already fossil-fuel-based, increasing the power demand will likely result in more greenhouse gas emissions, requiring more high-level solutions. Third, heat pumps consume more energy under very low temperatures due to the larger compression ratios, low heat production, and frosting, resulting in less attractiveness compared with conventional heating systems. Hence, integral solutions involving new products, optimization, and energy management and exchange systems are required.

2.2.2. UNDESIRED EFFECTS OF DISTRIBUTED GENERATION ON THE GRID

Grid managers need to be able to control the production and flow of energy among the transmission and distribution networks to ensure their stability. When energy sources

are transitioned from controllable fossil fuel plants to RESs, numerous nonlinear phenomena manifest on the grid, as they were not designed for RESs or DGs. This section briefly presents the counterproductive effects DGs (mainly PV) cause on the network. Table 2.2 presents a list of reported challenges.

Grid Congestion

A fundamental disadvantage of PV and wind power as energy sources compared with fossil fuels is their inherent dependency on weather conditions (e.g., solar irradiance, temperature, and wind speed), causing stochastic behaviour of the instantaneous output power. Due to their non-controllable nature, the bigger the share of PV or wind in the energy mix, the less inertia the network will have, as inertia comes from the kinetic energy of rotating generators [51]. Sudden variations in local weather conditions can cause disturbances in energy production, increasing the probabilities of power swings due to the weakened frequency response and reducing the reliability of the power supply quality. At the same time, the seasonal variability in the PV systems is significant (especially in higher latitudes): a property that can intensify the mismatch between the demand profile and the PV generation curve, even under clear-sky conditions.

Overvoltage

The traditional electrical grid infrastructure was designed to have a central power injection point, which the grid operator can regulate. However, distributed generation can lead to excessive power flowing through the low-voltage lines, causing reverse flow, thus increasing the system voltage [52], [53]. Unbalances between the lines can also cause overvoltage [52], [54]. In [55], it was found that low-power (6 kW) single-phase PV inverters could cause voltage variations of up to 2 % in low-voltage networks (higher values are unlikely, yet not impossible). In [56] was concluded that overvoltage is the dominant effect when defining the PV penetration limit on low-voltage systems. DSOs rely on thermal generators to address overvoltage; however, as thermal generators will deprecate due to environmental goals; DSOs need to find alternatives to compensate for the power imbalances [57].

Underused Capacity Due to Power Curtailment

Increasing the RES share in the energy mix is intended to reduce $CO_{2,eq}$ emissions; however, [58] evidenced that it is a misconception that maximizing RESs without considering their effect on the whole energy system always lowers $CO_{2,eq}$ emissions. PV and wind power plants usually need to be overdimensioned to counteract the weather variability [59]; thus, power needs to be curtailed, resulting in lost energy and frequency shifts. Multiple research groups have studied this effect and proposed strategies to exploit the curtailed power, including coordinated power compensation algorithms [60], battery storage [61], EV charge coordination [62], and introducing electric heaters and thermal energy storage [63]. Nevertheless, the energy is either lost or traded with neighbouring countries in most cases, requiring transmission network improvements [64].

Uncertainty in Long-Term Effects on Grid Stability

The stability of the grid is one of the biggest concerns for grid managers. They require information on how the demand changes over time and how they can control the production in real time to address sudden power fluctuations and avoid causing problems

for the prosumers, consumers, and the network. With environmental targets, such as the Paris Agreement or Sustainable Development Goal 7, renewable energy distributed generation incorporates stochastic energy production and distribution behaviours. Additionally, the electrification of heating and the consistent growth in EV penetration make the production vs. demand comparison forecasts more complex. According to [29], between 2017 and 2018, there was a 63 % increase in the global number of electric passenger cars; moreover, the usage of RESs in heating, ventilation, and air conditioning (HVAC) supplied around 10 % of the energy; yet, there has been slow progress in policy support.

UTILITY RATE VARIATION

Distributed energy resources also consistently affect the profile of electricity prices [5]. As explained by [65], the current trend is transitioning from dependent customers to more independent prosumers. To cover the energy purchase reduction and premature grid reinforcements, the rates will increase, encouraging consumers to transition and urging new utility business models compatible with the distributed generation scheme. At the same time, current regulations are required to establish the framework for those new business models. These regulations are designed to minimize the risk instead of creating synergies between the parts of the energy supply chain [66], [67]. The current policies are mostly net metering and feed-in tariffs, which successfully stimulate decentralized generation but might cause mid- and long-term problems, as they need to consider the effects of DGs on the grid [68]. For that reason, new policies should focus on establishing energy-sharing guidelines and allow full participation of disadvantaged and vulnerable communities [69].

2.2.3. EMERGING SOLUTIONS

Multiple strategies have been proposed to overcome the energy transition challenges produced by RESs and DGs in electrical networks, as shown in Table 2.2. This Chapter focuses on how energy storage systems from different carriers can provide flexibility through ancillary services in urban areas, as discussed in Sections 2.3 and 2.4. Although the focus is on the technical perspective, regulatory solutions are also required to modernize policy frameworks.

From the technical perspective, the solutions found in the literature can be classified into two different yet mutually dependent groups. The first is energy modeling and control strategies for energy management systems (EMSs). These strategies aim to maximize the usage of the network's infrastructure while minimizing losses and adverse effects. A comparison of different optimization strategies used in microgrids worldwide is presented in [70], classifying the methods as deterministic, metaheuristic, artificial intelligence, or others, providing insights into their best applications. The second strategy involves developing or upgrading existing devices to execute the energy management algorithms, such as ESSs, converters, and other novel devices, which is equally important.

Table 2.2: Reported unexpected outcomes on the grid due unplanned DG deployment.

Phenomenon	Detail	Proposed solution	Ref.
Loss of inertia and frequency shifts	The effect of different levels of PV and wind in Jordan's national grid is analyzed, resulting in a penetration of over 40 % that would compromise the frequency stability of the system due to a reduction in its inertia.	As a neighbouring country, the interconnection with Egypt can support the system.	[71]
Voltage limit violations	Circuits operate at, or near, their limits to connect any further DG in South-West England.	High-voltage network reinforcement.	[72]
Voltage limit violations	Overvoltages surpass the 110 % limit in the rural low-voltage grid in Portugal, given the low load required near the injection point, forcing an intermittent connection of the inverter to the grid.		[73]
Voltage limit violations	Voltage fluctuation due to grid congestion produced by generator start-ups to supply the demand planned to be met by wind farms in Germany.	Export of excess power to neighbouring countries.	[74]
Power curtailment and grid congestion	Increment in installed PV and wind systems in Italy caused grid congestion and power curtailment.	Development of a smart grid and use of dynamic line rating to reduce the power curtailment levels from 1 % to 2 %.	[74]
Power curtailment and grid congestion	The German regulations give DG priority access to the grid infrastructure, which, added to the single price zone electric market, created severe grid congestion, resulting in 4.7 TWh curtailed due to feed-in management in 2015.	Development and implementation of a congestion management strategy on the distribution level to provide flexibility as an alternative to power curtailment.	[75]
Power curtailment	Power curtailment in China of 17.1 % in the wind and 10 % in solar during 2016.	Enhance consumption near the injection point, implement subsidies and feed-in tariffs, and ultra-high-voltage transmission.	[76]

Uncertainty on long-term effects	Islanded systems, such as Crete and Cyprus, would be more affected by the massive deployment of RES due to their stochasticity.	The interconnection of Greece (Attica Crete), Cyprus and Israel allows high penetration of RES while providing a secure match between demand and supply, reducing the need of fossil fuel-based plants.	[77]
Uncertainty on long-term effects	By 2011, The Netherlands implemented several policies to ensure the network infrastructure could support the incoming power plants to supply the increasing demand, creating uncertainty for the transmission system operators regarding the grid's costs and the market's behaviour.		[78]
Utilities rates variation	A study about the reaction of the electrical utility market related to the massification of DG in Brazil demonstrated that utility companies need a solid framework to regulate the DG, as their advantages still need to be fully understood.	Implement strategies and models to understand the effect of DG at the micro and mini level, to implement more efficient utilities.	[79]

A progressive regulatory framework is also required for a successful transition. Such frameworks include policies designed for more dynamic energy flow and consider all the parts in the value chain, avoiding governance barriers to adequate RES project deployment [69], [80]. In this context, multiple strategies have constantly been proposed, including new utility models more suitable for the new generation scheme [81] and incentives that encourage prosumers to participate in energy exchange [68]. From the policymakers' perspective, [57] mentioned the most relevant codes for electricity markets in Europe, referred to as the Target Model, which includes: the EU Directives 2009/72/EC, 2019/944, and 2019/943, and the EU Commission Regulations 2017/2195, 2017/1485, 2015/1222, and 2016/1719. Additionally, technical standards are continuously being developed and adjusted worldwide, aiming to establish the operating parameters to be used in the regulations intended to minimize adverse effects on the network, such as UL 1741 [82], IEEE 519 [83], IEC 61727 [84], and EN 50160 [85]. From boh the policy and technical perspectives, the responsibility of stability control is assigned to the transmission system operators.

Despite previous efforts to establish working frameworks, they tended to be monodisciplinary. For example, the Smart Grids Architecture Model framework, developed by the

European Telecommunications Standards Institute, the European Committee for Electrotechnical Standardization, and the European Committee for Standardization, exclusively addresses the technical components, ignoring the social aspects [86]. What is more, the energy market has barriers related to uncertainty about the performance of the RESs, the effect of DGs and ESSs on electrical networks, privacy policies, and the lack of incentives for prosumers, among others [57], [87], [88]. Consequently, numerous smart grid projects prematurely fail [89]. Some authors, such as [11], [90], mentioned that the new business models should compensate storage system owners based on the imbalances they can cover, either individually or aggregated, as well as the eventually accelerated aging caused by supporting the grid. For instance, the results in [90] showed a return on investment between 9.5 and 19.1 years when BESSs are deployed to provide frequency balancing in the Italian wholesale market, which might not be attractive to investors, as the expected life of a BESS is between 5 and 15 years.

2.3. Ancillary Services

As early as 2008, [91] recommended a proactive DG transition, allowing grid operators to take advantage of the systems to increase the network's performance. However, as pointed out in [92], and following what is presented in Table 2.2, most of the challenges are currently solved by reinforcing the infrastructure to handle the new power sources or exporting the energy to neighbouring countries (which usually requires infrastructure improvement). Instead, actively including the DG system assets in energy exchange, especially as BESSs and EVs are more commonly included within DG systems, can also be a solution. Multiple authors [92]–[96] recommended more flexible electric systems oriented toward cooperative energy exchange business models, exploiting the DG systems as ancillary services providers. This section details the primary ancillary services of distributed systems with electric energy storage systems that can be provided to the grid (Note that the inclusion of BESSs with RESs in DGs is not dependent on all of the studied ancillary services, meaning that some of them do not require BESSs, RESs, or both). It is assumed that higher power and energy costs imply a higher operational cost. Therefore, grid operators desire that some consumers purchase power in a cheaper, lower-demand timeframe so the power demand is more evenly distributed throughout the day.

A summary of successful implementations and proofs of concept is shown in Table 2.3. The results demonstrate an increase in the power quality of the grid due to reductions in the rate of the change in frequency and voltage fluctuations, thus, in power losses. Nonetheless, new utility models are required to increase the profitability of ESS implementation. Likewise, some ancillary services can provide support when thermal systems are implemented. For instance, using TESS to reduce the heat load at the community level (peak shaving) or controlling the head demand either controlled by an intelligent thermostat or through the direct control of heat pumps (demand response), reducing the fluctuation in temperature in both cases.

Table 2.3: Representative cases of reported outcomes of ancillary services through DG systems.

Ancillary service	Detail	Results	Ref.
Reactive power control	Simulation using the IEEE 9-bus system, considering synchronous generators and a cluster of coherent grid-following DG under different control strategies.	Controlled power converters enhanced the network performance, reducing the rate of change of frequency.	[97]
Reactive power control	Simulation of a Newcastle, Australia, rural network using a 33-node network with 11 loads on a medium voltage, with collected data of PV generation, loads, and network voltage from trial sites.	Reduction of curtailment losses and overvoltages.	[98]
Energy arbitrage	Multiple scenarios were studied in the Belfast City Hospital, Northern Ireland, using different BESS and PV combinations and dimensions to provide grid services and energy arbitrage.	BESS is not economically viable for arbitrage alone, but it is if income from other ancillary services is included. Revenue increases with the increase of the BESS power.	[99]
Peak shaving	A peak shaving strategy with different BESS sizes was implemented on a test house, representative of a typical house in Northern Ireland, without considering the heating consumption in the measurements.	The peaks were reduced to less than 5 %of their initial magnitude and duration and avoided between 70 % and 90 % of the energy exports. The system is hardly viable with flat tariffs, but incentive tariffs would result in profit.	[100]
Peak shaving	The economic feasibility of a water tank thermal energy storage system connected to district heating and a heat recovery system in Trondheim, Norway, was tested after implementing a thermal peak shaving strategy.	The system was able to shave up to 39 % of the thermal load and increasing waste heat self-utilization 27 %, resulting in 9 % savings on the annual heating costs.	[101]

Frequency balancing	A combination of BESS and supercapacitor is proposed to provide enhanced frequency response in the UK market, considering the minimum required capacity for each ESS and proposing a power management strategy based on allocating the power so that the state-of-charge (SoC) of the BESS remains near a reference value.	Incorporating the supercapacitor reduced about20 % the usage of the BESS, and the power management strategy reduced the variation in the SoC of the BESS.	[102]
Frequency balancing	Simulation using the IEEE 33-bus system and historical data from the Australian Energy Market Operator, considering BESS provides frequency control services with a per-use-share rental strategy.	The strategy was proven as economically viable and reliable.	[103]
Voltage control	A 21-node system within a 3.09 km line was simulated, including households, an office building, a school, and a store, studying the effect of BESS, EV, and home energy storage systems.	An adequate combination of EV, BESS, and home energy storage systems consistently reduced the voltage fluctuation at the end of the line.	[104]
Voltage control	The North Cyprus power system (132 kV on transmission and 66 kV sub-transmission, 49 busbars, 60 transmission lines, a Y-connected capacitive filter, 432 MW of power plants, and 2.27 MW of DG) is studied to analyze if DG can improve the voltage profile in the network.	If the DG locations are chosen correctly, the system can operate within safe limits with a penetration level of 50 %, achieving a 36.5 % reduction in active power loss.	[105]

Congestion management	A congestion management algorithm was tested in the H2020 InterFlex demonstrator in The Netherlands (26 EV charging points of 22 kW, a 250 kW/315 kWh BESS, and a 260 kWp PV system that supplies 350 apartments through two 630 kVA transformers), based on the loss of life of a transformer and the DSO's financial risk of a blackout due to overloading.	The algorithm successfully predicts the load pattern, allowing a decision-making model to monetize the required flexibility.	[106]
Demand response	Three villages in Portugal clustered the consumers with similar consumption patterns and implemented a demand response strategy.	Reduction in the household energy bill.	[107]
Demand response	A home energy management system was combined with a smart thermostat to control household power-shiftable loads, including BESS and EV, under Turkey's time-of-use and feed-in tariff rates.	A reduction of 53.2 % on the daily costs is achieved under Turkey's time-of-use and feed-in tariff rates.	[108]
Demand response	A TESS was implemented to reduce the required cycles of an air source heat pump.	The fluctuation in the outlet water temperature was reduced, while the unit decreased the number of on-off operations.	[109]
Direct load management	A home energy management system (HEMS) was implemented in a single-family villas category in Riyadh, Saudi Arabia, aiming to achieve a net zero energy home.	Reduction in the household energy consumption by 37 % when compared against the energy use index in ASHRAE 100-2015, modifying the luminance level and the HVAC load.	[110]

2.3.1. REACTIVE POWER CONTROL

Section 2.2.2 mentioned that the uncontrolled injection of active power in the grid causes voltage increases, leading to undesired overvoltage. The DSO is responsible for ensuring voltage stability. Currently, network operators use thermal generators to compensate for power fluctuations; however, due to environmental goals, such plants will be decommissioned in the short and mid term, requiring for new sources of reactive power con-

trol [57]. Reactive power handling can balance this effect. Modern inverters can independently control active and reactive power under the inverter-allowed apparent power, increasing the RES hosting capacity of the local network [111], [112]. Reactive power control can more than merely compensate for the effect of RES active power injection on the grid. DSOs may use the reactive power supply from distributed generators to ensure voltage quality of the network at lower voltages than thermal generators, typically used at high voltage levels [112]. Nevertheless, the IEEE Standard 1547, widely used for manufactures and used as reference for grid codes such as ENTSO-E RfG [113], does not allow any inverter interconnected with the grid to adjust its voltage using reactive power compensation [114]. Therefore, DG cannot provide reactive power compensation, thus, forcing the DSO to invest in alternatives instead of considering collaborative solutions.

2.3.2. ENERGY ARBITRAGE

The power demand on the grid is not constant over time; yet, it usually has a periodic pattern during the day, with expected peaks that depend on the circuit needs [115]. For that reason, DSOs usually have dynamic tariffs, where power and energy are more expensive during high-demand or peak hours [116]. From a financial approach, consuming energy when it is cheaper would result in a cost reduction opportunity. However, consumption mostly depends on activities; thus, moving the consumption periods outside the peak hours is only sometimes an option. Given that, BESSs can provide a profitable solution. The energy can be purchased when it is cheaper and used when it is more expensive without affecting daily activities, as demonstrated by [117]. From the grid perspective, it also reduces the grid's congestion because the demand increases in low-consumption periods and decreases during high-consumption periods, decreasing the demand gap during the day.

2.3.3. PEAK SHAVING

Similar to the energy arbitrage modus operandi, peak shaving can reduce the building's power peaks consumed from the grid during high-demand intervals. Under this scheme, however, the intention is to reduce the costs related to power instead of energy (which would eventually occur, depending on the utility model) [118]. From the grid perspective, the effects are similar. However, as the intention is to flatten the power consumed from the grid, it reduces its variability. Peak shaving allows a smoother energy exchange, preventing reverse current flow and voltage rise [118]. Multiple approaches have been applied in the literature to achieve this effect, considering the power source and implementation scale. A summary of the state-of-the-art methods can be found in [119].

2.3.4. FREQUENCY BALANCING

Traditionally, electric systems were designed for bulk-power plants with synchronous generators. On the other hand, RESs, more specifically variable renewable generation (e.g., wind or PV), are primarily inverter-based nonsynchronous energy sources. For that reason, increasing their share in the energy mix can lead to a more significant rate of change in the frequency and frequency deviations [120]. Nevertheless, modern inverters have frequency management functions that, when combined with a BESS, contribute to the network to reduce frequency deviations even further than conventional generation,

due to their faster power response [121], building the concept of virtual inertia [122].

2.3.5. VOLTAGE CONTROL

Erratic voltage behaviour caused by an unevenly distributed high penetration of RESs on the grid is a significant challenge. Grid administrators have developed and implemented different control strategies to mitigate this effect to fulfill interconnection and power quality standards [123], such as IEEE 1547 [114] or ANSI C84.1 [124], respectively. However, the inclusion of BESSs can mitigate the volatility in the power flow, as demonstrated by [125]. The energy produced by power peaks can be stored, consumed, or injected back into the grid. Hence, DGs with BESSs can provide stability to the grid regarding voltage variations if coordinated.

2.3.6. CONGESTION MANAGEMENT

When multiple distributed energy sources are included in the network, uncertainty in the energy flow is included in the system, creating congestion at the transmission level [126]. BESSs can manage the congestion in transmission lines to inject, store, or consume energy based on local or global network requirements, conducting the power flow [25], [126]. Thus, if RESs and BESSs are coordinated in a smart grid, energy can be managed following local demand, reducing the congestion in the power lines at higher levels.

2.3.7. DEMAND RESPONSE MANAGEMENT

If the utility tariffs are known beforehand, the end-users can adapt their consumption as a response according to changes in the power and energy costs; this behaviour is defined as demand response management [127]. In this context, demand response algorithms commonly choose the heating and air conditioning loads. HVAC systems and heat pumps are often controllable loads that can be manipulated due to the rooms' thermal inertia and flexible temperature setpoints. As long as comfort is not compromised, especially in high-latitude countries, they represent a significant share of urban energy consumption [128], [129]. Furthermore, demand management can be beneficial not only for the consumers from the economic perspective but for DSOs from a technical perspective; the power demand during peak hours decreases, and the load behaviour supports the grid in maintaining the frequency after power swings [127], [130].

2.3.8. DIRECT LOAD MANAGEMENT

As shown in [127], some authors considered direct load management as a category of demand response management. The difference is that direct load management algorithms modify the load in real time to meet the smart grid requirements, optimizing the energy consumed by specific loads as much as possible, and not only responding as pricing changes in energy. Consequently, the loads to be managed should be flexible enough, and some studies recommend HVAC, heat pumps, and EV as preferred considering their impact on the instantaneous power consumption [131], [132]. Likewise, the Internet of things and smart meters were also considered as part of the solution [133].

2.4. Multi-carrier Energy Storage Systems

In Section 2.3, electric ancillary services were studied; however, heating systems can provide similar services under specific energy system architectures. Multi-carrier energy systems are multiple-input, multiple-output systems that combine different energy types, such as thermal and electrical, as shown in Figure 2.3. An optimized MCES obtains better performance than when each system works individually. Considering the complexity of the MCES, only the storage elements were analyzed, as the contribution focuses on the ancillary services that multi-carrier energy storage systems can provide as part of an MCES. Therefore, Section 2.4.1 mentions the main strategies to model MCESs. In Section 2.4.2, multiple ESSs are proposed as possible elements of a multi-carrier energy storage system. Section 2.4.3 provides an overview of the state of the art of combined storage systems as part of MCESs.

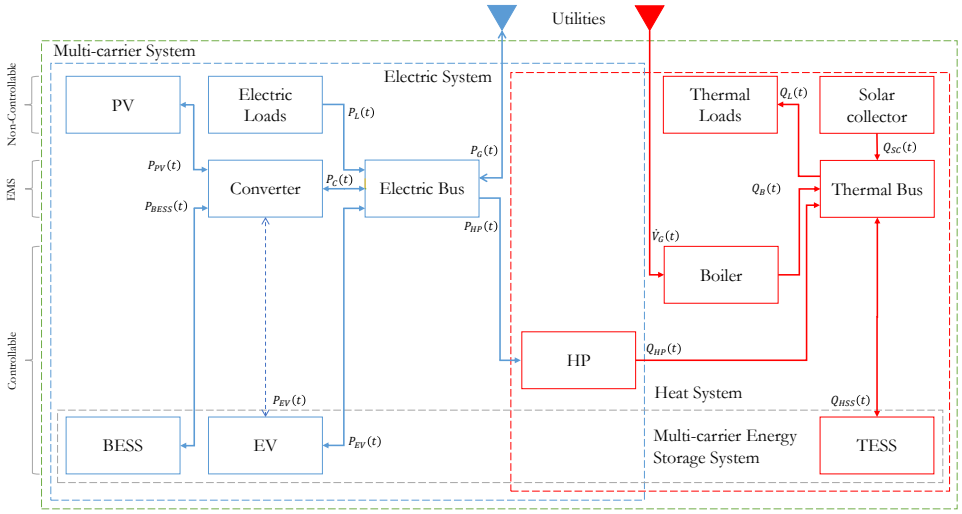

Figure 2.3: Schematic of the energy flow of a multi-carrier energy storage system

2.4.1. Mathematical Modeling of Multi-carrier Energy Systems

Describing the behaviour of multi-carrier energy systems depends on the correlation between each energy system considered in the designed topology and its components. For instance, a simplified schematic is presented in Figure 2.3, where the energy flows among the chosen devices are indicated. MCESs can provide suitable frameworks to combine electrical and thermal ancillary services if adequately implemented. Additional elements can be added to achieve the desired topology, e.g., wind systems, biofuel systems, cooling systems, supercapacitors, or hydrogen fuel cells. Because of the complexity, multiple modelling approaches have been proposed in the literature to overcome the challenge of simulating complex MCESs, including graph-based [134], port-Hamiltonian [135], probabilistic [136], stochastic [137], and information gap decision

theory [138]. Chapter 3 elaborates on the mathematical description of the individual components of a residential MCES and their interaction. Then, Chapter 4 compares different EMS strategies to control de power flow within the MCES.

2.4.2. ELEMENTS IN MULTI-CARRIER ENERGY STORAGE SYSTEMS

Considering the different requirements, a synergic combination of various ESSs would provide a more extensive range of possible ancillary services, as each ESS has individual applications. ESSs provide crucial support to the transmission system operators (TSOs) and distribution system operators during blackouts. This section considers electric, thermal, and chemical storage devices and electric vehicles (note that electric vehicles can behave as both a storage device and a controllable electrical load, according to the EMS algorithm).

Mechanical energy storage systems, particularly pumped storage hydropower (PSH), are promising solutions. As a mature technology, PSH has the highest installed capacity worldwide. Its most common applications are short- and long-term energy management, back-up, and black start [24]. Nevertheless, it is geographically limited and requires extensive environmental studies and permits, making it challenging to locally implement PSH in urban areas [139]. As the focus is on the European urban environments, such methods are excluded from the review; however, the advantages of mechanical energy storage are described in [24], [139].

Multiple key performance indicators are available to compare different ESS technologies. To compare technologies independent of the application, the most common indicators are: the cost per unit of energy, the number of cycles (life), power range, energy density, and efficiency. For specific applications, one can use the levelized cost of storage (LCOS), as it depends on the number of cycles per year, the depth of discharge, and the discharge duration. Figure 2.4 shows a comparison summary of the studied elements, where the performance ranges for the main attributes are presented. Figure 2.5 depicts the energy availability, response times, and power ranges for the ESSs considered within the scope of this work. Although PSH was not extensively covered in this work, it was included in Figure 2.5 as a comparison point for the other ESSs, given its relevance and suitability to provide ancillary services when incorporated into the grid. For both figures, the literature survey was performed using general searching terms. The references were selected based on citation metrics (number of citations of the paper and rank of the journal), date of publication, and consistency with other publications).

BATTERY ENERGY STORAGE SYSTEMS

Battery energy systems store energy based on an electrochemical process. Multiple technologies have been developed to enhance their performance, increasing energy density and decreasing costs, including lead-acid, nickel-metal hydrate, and lithium-based [147]. Traditionally, lead-acid batteries were used as a backup in electrical systems. However, in the last decade, the prices of lithium-based batteries have dramatically decreased, which, added to their superior performance, has allowed more complex and reliable uses for the batteries [148]. A comprehensive review on the integration of BESSs into distribution systems was conducted by [6], including a comparison of the three main technologies of Li-ion BESSs. Table 2.4 presents a comparison of the best and worst per-

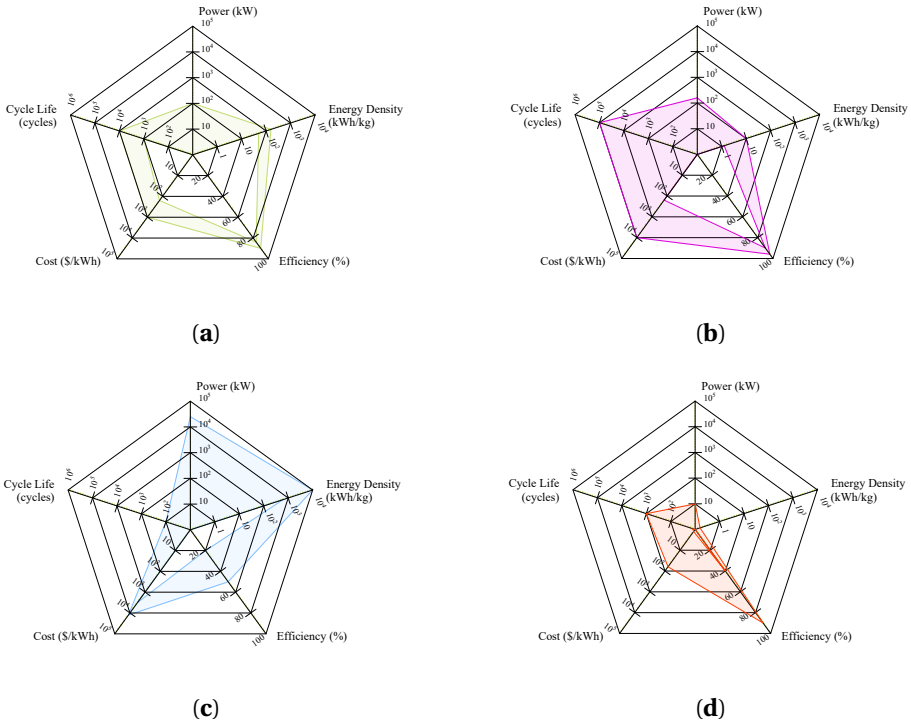

Figure 2.4: Comparison of the reported performance of the main attributes of different energy storage systems. The colored area represents the range between the best- and worst-case scenario reported in the literature per attribute. Note that the increases in the graphs are on a logarithmic scale in all attributes but the efficiency. (**a**) Reported performance of Li-ion batteries [127], [140], [141]. (**b**) Reported performance of supercapacitors [127], [140], [141]. (**c**) Reported performance of hydrogen fuel cells [127], [140], [141]. (**d**) Reported performance of thermal energy storage [141]–[145]. The power on this graph represents the heat transfer rate.

formance found for different metrics per technology

The energy storage market includes other technologies, such as flow batteries (highlighting chemistries based on vanadium [149], but also zinc, iron, copper, and halides [150]), and salt batteries (e.g., sodium-sulfur [151], sodium-nickel-chloride [152], and sea-salt [153]). However, some of those batteries are still in early stages or development (e.g., flow batteries not based on vanadium and the sea-salt battery). On the other hand, some mature technologies are incompatible with the urban requirements despite having advantages over the lithium-based BESSs that can be used in other contexts. For instance, vanadium-based flow battery cost per energy unit is about one-third of that of lithium technologies [154], but its energy density is almost one order of magnitude lower [155], making it unsuitable for applications where high energy densities are required. Molten-salts batteries, such as sodium-sulfur and sodium-nickel-chloride, have energy densities similar to those of lithium-based technologies but operate at temperatures above 100 °C and up to 400 °C, which raises hazards and risk concerns [156].

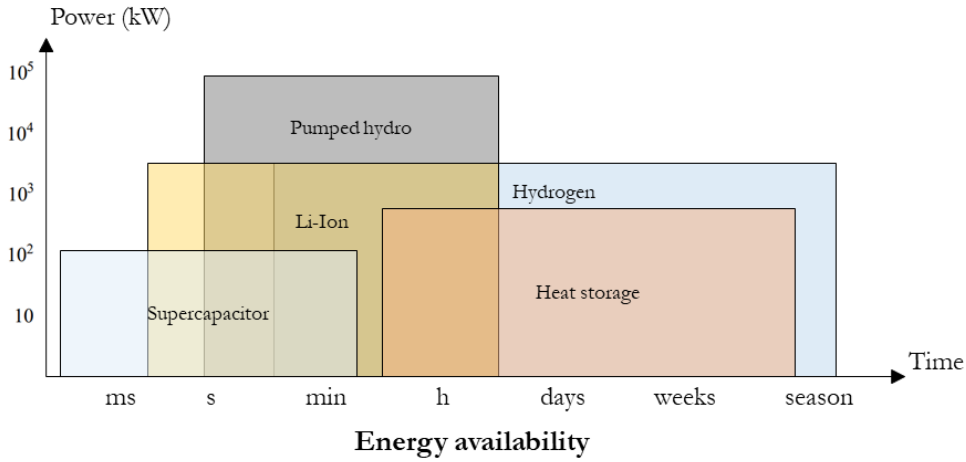

Figure 2.5: Comparison of the reported available power and energy, starting from the reaction time, of different energy storage systems [139], [140], [146].

Although some advances in such technologies working at room temperature have been achieved, there are challenges associated with lifetime and capacity fading [157].

Table 2.4: Performance ranges for lithium iron phosphate (LFP), lithium nickel manganese cobalt (NMC), and lithium nickel aluminium cobalt (NCA) BESSs [6], [158].

	LFP	**NMC**	**NCA**
Energy density (Wh/kg)	75–190	120–200	140–240
Power density (W/kg)	200–1600	600–2400	600–700
Cell efficiency (%)	88–90	94–95	94–95
Cost (USD/Wh)	300–600	300–600	300–600
Lifetime (cycles)	5000–10,000	500–4000	500–3000

SUPERCAPACITORS

Capacitors are well-known devices that store energy through electric fields, reacting as a low-pass filter with short reaction times. Despite having low energy density, supercapacitors have high power density, short charge/discharge cycles, and long life [159], [160]. Given those characteristics, supercapacitors are suitable for high-power, low-energy peaks, providing availability during voltage dips or short interruptions [140].

THERMAL ENERGY STORAGE SYSTEMS

In Section 2.2, it was mentioned that a significant share of energy in the mix is dedicated to producing heat, primarily from fossil fuels. Modern alternatives are under con-

stant development to produce heat from electricity (building the concept of power-to-heat) or based on the thermal properties of different materials [161]. On the other hand, heat sources have long transient responses, leading to slow reaction times and energy loss. To overcome this challenge, authors [162], [163] have mentioned the need for thermal energy storage to optimize the cycles of the heat energy source. Hence, [163] highlighted the importance of thermal energy storage when flexibility is considered. In [142], thermal energy storage systems were categorized as: active, when the system stores energy through a fluid that can flow between reservoirs; passive, when the energy storage medium is solid.

HYDROGEN FUEL CELLS

A hydrogen fuel cell (HFC) is a device that transforms the chemical energy from the reduction-oxidation reaction of a constant inflow of hydrogen and oxygen into electrical energy. This process occurs in an electrolyte, according to which the fuel cell can be categorized as alkaline, proton exchange membrane, phosphoric acid, molten carbonate, or solid oxide [164]. HFCs are combined with electrolyzers to produce and store hydrogen. However, the expected lifetime of an HFC is around 5 to 15 years [141], and its roundtrip efficiency is around 20–35 %, both of which are lower than those of other ESS technologies [165]. The reason is that the overall efficiency includes the fuel cell efficiency (40–60 %) [166] and the electrolyzer efficiency (40–60 %) [167]. Efficiencies near 45 % were reported but under specific conditions [168]. Additionally, the EMS requires robust control strategies to coordinate the HFC and electrolyzer [169], especially if the goal is to minimize the grid's impact or provide ancillary services. At the same time, the heat produced by the fuel cell can be transferred to a thermal load or storage, but further research is still required [170], [171].

ELECTRIC VEHICLES

In Section 2.2.1, electric mobility was mentioned as a suitable alternative for fossil fuels in transport. In this context, multiple approaches regarding the relationship between the electrical grid and electric vehicles have been proposed to minimize the effect of the increasing power demand to supply the energy required to charge the batteries in the EV. The EV chargers' power depends on the charging level (power for levels 3 and 4 depends on the chargers' characteristics, but can easily surpass 100 kW [172], [173]): between 3.7 kW (16 A per phase) for level 1 to 22 kW (32 A per phase) for level 2 [174]. When connected to the charger, the energy between the grid and the EV can flow from the grid to the EV (G2V) or from the EV to the grid (V2G) [175], following the EMS instructions. However, estimating the optimal power to whether charge or discharge the battery is a difficult task if the goal is to simultaneously minimize the charging time and the effect of the charger on the grid, as not enough data are currently available to make informed decisions in real time [176]–[178]. Another critical point to consider is the batteries' life cycle as an inherent consequence of the electrification of transport based on batteries. The potential of a second life for those batteries can be considered for stationary uses, as studied in [179].

2.4.3. CURRENT STATUS ON COMBINED ENERGY STORAGE SYSTEMS

In Section 2.4.2, energy storage systems were presented, and numerous combinations can be obtained to face different challenges, as reported in Table 2.5. This section analyzes the results of combining two or more of the previous systems, indicating the advantages and individual contributions to the overall result.

The combination of BESSs and supercapacitors connected to a PV installation was studied by [180]–[182], where their compatibility was demonstrated regarding reaction times, power, and energy supply. The supercapacitor smooths the short, high-power peaks in this arrangement, whereas the battery supplies power during longer intervals. This effect has multiple advantages in electrical systems that can be obtained through different topologies. An individual converter for the supercapacitor and the BESS produced better results, as the voltage in the DC line does not directly affect each storage device's voltages [181], [182].

Supercapacitors were also studied with hydrogen fuel cells (including electrolyzers), commonly using the supercapacitor as an auxiliary source to compensate transient events [183]–[185], using different topologies, according to the application. For instance, [184] utilized supercapacitors as a secondary power source in a fuel cell system to protect it against sudden variations in current, increasing the life of the fuel cell. A hybrid converter for electric vehicles, using a proton exchange membrane fuel cell and supercapacitor, was proposed by [185]. Fuel cells and supercapacitors were also combined with wind energy [186] and PV [187] to supply fast variations in the load power that the fuel cell cannot.

To minimize the curtailments of RESs, [188] developed a deep learning algorithm to optimally size and operate an alkaline water electrolyzer and a BESS. The results showed a decrease of 97 % in the curtailed power, with a return on investment shorter than five years. In [189], multiple microgrids (with an HFC, electrolyzer, BESS, and PV) were studied while working in parallel in a low-voltage AC system, using a constant reference inverse droop control method to solve the problem of the impedance differences. Their results showed an improvement in the power distribution and the response speed when the load suddenly changed.

Electric vehicles actively participate in energy exchange; therefore, the chargers' operation must be optimized to avoid significant effects on the grid. Including a BESS provides a solution, creating a demand response scheme, which controls the chargers' high load, as proposed in [190] and demonstrated in [191], where a 138 % reduction in transformer overloading was achieved owing to an appropriate BESS size. Likewise, including an EV in a system can decrease the required size of the BESS to provide services to the grid [192], even when an HFC is also included as part of a hybrid energy storage system [193].

Thermal energy storage systems can also work alongside other energy storage systems. As demonstrated [194], an electric, thermal, and gas coupling was tested using the IEEE 18-bus distribution system, resulting in an energy-sharing scenario that allowed saving energy by sharing with other participants. In [195], BESS and TESS were simulated together to simplify the management of micro-grids and enhance the BESS lifetime, increasing the BESS lifetime by 74 % compared with that of a model that did not consider its aging. A more complex MCES was studied [196], where a combined heat and

power microgrid was controlled through a mixed-integer linear programming-based energy management model on an MPC framework. The microgrid included a natural gas fuel cell, a boiler, a TESS, wind turbines, PV generators, and a BESS. The results showed an economic improvement regarding the system behaviour when supplying electric and thermal loads; however, the thermal system was fossil-fuel-based.

Most of the literature is related to the behaviour of electrical systems coupled together, with few implementations of TESS in comparison. The most common couple at the multi-carrier level (electric and thermal systems) is through heat pumps. Based on the tolerance levels of the habitants of the studied buildings, heat pumps can provide flexibility to the network through ancillary services such as demand response and direct load control [197]–[199], without relying on thermal energy storage. Moreover, the TESs are primarily implemented at the community level [200]–[202]. Therefore, research on how multiple electrical and thermal storage devices couple would provide valuable insights into the energy transition, particularly at a lower level than communal systems.

2.5. Role of Multi-Carrier Energy Systems to Provide Ancillary services

Investments in RESs are growing worldwide to meet sustainability targets. Additionally, RES's versatility in the power range, increasing efficiency and reliability, and substantial cost reduction encourage those investments. Despite this, grid operators are not prepared for their large-scale effects. Large deployments result in adverse phenomena on the electrical network, creating uncertainties in voltage, frequency, and stability, as explained in Section 2.2.2 and summarized in Table 2.2. To address these challenges, the typical solutions require significant upgrades of the electrical systems' infrastructure, highlighting network reinforcements or energy trade, increasing costs, and reducing the revenue in the mid and long terms. Instead, cooperative schemes with the prosumers, who actively participate in the energy exchange, may add value if considered.

Simultaneously, the energy regulations were not initially designed to consider distributed generation, but the emerging policies encourage the usage of RESs. This misalignment results in governance barriers to the adequate deployment of RES projects, regardless of the power scale, because RES penetration is growing faster than the regulatory framework is developing. Especially at the distribution level, DG intensifies the technical challenges, given the stochasticity of the energy flow, and the energy market is affected. The price is updated almost in real time, urging new, progressive, and more flexible business models in the supply chain. Furthermore, strategies promote the electrification of heating and transport, increasing the power demand but decreasing the predictability of its behaviour. The result is an even more complex power flow in an already congested network.

Energy storage can become the core of the energy transition if prosumers and DSOs collaborate through ancillary services. Numerous successful implementations of ancillary services can be found in the literature. Table 2.3 provides a representative list. After analyzing those cases, it was found that including ESSs within the distributed generators reduces the voltage and frequency effects caused on the grid by the RESs, therefore enhancing the outcome of DG, as the ESSs provide the inertia RES undersupply to the

grid (voltage control and frequency balancing). Furthermore, when ESSs are included in the DG systems, it is possible to provide support if an EMS controls the power flow according to the network requirements. There are three ways the DG system can support the grid: it can control its power factor to control the reactive power consumed or injected (reactive power control), reduce the power demanded from the grid at a particular moment (peak shaving, congestion management, demand response, and direct load management), as well as bidirectionally regulate the energy exchange with the grid (energy arbitrage). Depending on their nature, different energy storage devices can provide different services to the grid. However, combining their advantages into a more robust system is possible when working together in a multi-carrier energy storage system. Nonetheless, increasing the number of ESSs in MCESSs involves more complex requirements for modeling and simulation, especially if multiple energy carriers are considered.

At the multi-carrier level, the state-of-the-art literature highlights MCESSs as a promising alternative for prosumers to become ancillary services providers [203]. Although more studies on the behaviour of electrical and thermal storage systems interaction are still required to fully understand their joint operation, the results shown in Table 2.5 support the hypothesis that the coupling between them would allow better control of the system's overall behaviour. Considering that heating systems are required, it is safe to assume that the system is affected by seasonal variations. The time frames with a more significant need for heat coincide with the months with less PV availability. Therefore, under those conditions, options such as TESS and HFC can support the electrical system to provide heat without considerably increasing the power demand during cold seasons (it is considered an electrical source of heat, such as a heat pump.). According to the EMS, when the generation surpasses the consumption, energy can be stored in a BESS if required in the short term or used to produce thermal energy and hydrogen for long-term storage [169]. At the same time, if the surplus power produced by the DG is locally consumed through an electrolyzer, through a heat pump, or stored in a BESS, there will be less congestion on the network, as the energy injected into the grid can be coordinated according with the grid requirements.

It is compelling to analyze how MCESS can provide ancillary services and, therefore, flexibility to the grid. In this regard, Table 2.5 presents a summary of recent studies of how multi-carrier energy storage systems can contribute to diminishing the impact of DGs on electrical networks. The results suggest that energy arbitrage can be combined with demand response management or direct load control. The charge of BESSs or TESSs can be scheduled to purchase the energy during cheaper timeframes as an energy arbitrage strategy. At the same time, the power used to charge the ESSs during those timeframes can vary, in response to the congestion with demand response and direct load control strategies, to reduce their contribution to the grid congestion. Peak shaving can also be used with energy arbitrage or congestion management. Unlike demand response control or direct load control, peak shaving uses ESSs to smooth the peak without translating it to another moment. Thus, if the energy is purchased during a cheap timeframe and adequately scheduled for peak shaving, the amount of energy might not change, but its costs will be reduced as will power demand costs.

Table 2.5: Examples of reported implementations of ancillary services through multi-carrier energy storage systems.

System architecture	Detail	Results	Ref.
PV + BESS + TESS	Three load-shifting strategies were proposed to control an islanded multi-carrier microgrid in Abu Dhabi, UAE, including demand response management.	The coordination of charge and discharge of the different ESS, combined with the PV regulation, allowed the implementation of a demand response management, whid cooling loads shifted thanks to the TESS and curtailed, if needed, to supply the power demand within the network.	[204]
PV + BESS + TESS + EV + CHP	A multi-carrier energy system was tested with heat and electrical load data from a hospital in Okinawa, Japan, to minimize the annual costs while increasing the system's resilience.	The system successfully reduced the costs while providing a more resilient system against grid blackouts, regardless of the seasonal variability, and with an acceptable life cycle performance, also showing compatibility with demand response management.	[205]
PV + wind + concentrating solar power + BESS + TESS	The optimal capacities of BESS and TESS for a multi-carrier energy system in North China were determined, considering curtailment and operative constraints.	The obtained capacities of BESS and TESS showed annual profits of $4.95 million, considering a generation price of 0.094 $/kWh, with an annual curtailment rate lower than 5 %.	[206]
PV + BESS + TESS	A study of BESS and TESS as sources of flexibility was performed in Victoria, Australia, considering cost minimization and electric self-sufficiency. The influence of electricity price signals was also taken into account.	The multi-carrier energy system showed optimal results when the objective was cost reduction. Most of the revenue came from the PV + BESS coupling, given the thermal load considered, as it allowed energy arbitrage and demand response management. On the other hand, self-sufficiency does not show economic benefits or flexibility options.	[207]

PV + wind + diesel generation + BESS + TESS	To size the optimal BESS and TESS, data from a greenhouse with a microgrid in Iran was used to simulate an islanded condition in case of disconnection from the grid.	Once the microgrid is islanded, the BESS supports the frequency shifts. Moreover, the combination of BESS and TESS resulted in a reduction of 19 % of the costs than when only the BESS is implemented.	[208]
BESS + TESS + CHP + chiller + boiler + spinning reserve	An artificial neural network fed with data from a shopping mall in Bangkok, Thailand, was used to create a load forecast strategy that reduces the operative costs when implemented in a multi-carrier energy system.	The numerical results showed a reduction of 12.52 % in the total operating cost compared to a similar EMS without BESS and spinning reserve when implementing the direct load management strategy.	[209]
PV + BESS + solar heat exchanger + boiler	A residential area with centralized PV and solar heat exchangers was simulated using electrical, cooling and thermal load data to study the effect of combining electrical and thermal storage to minimize the energy purchase costs. Constraints included energy balance, electricity price, capacity, and charge and discharge power of the BESS.	The results show a 15 % reduction in the total energy costs bought from the utilities thanks to the PV generation and energy arbitrage, without compromising the demand.	[210]
Photovoltaic-thermal + TESS	A centralized photovoltaic-thermal system combined with a community-level TESS was simulated for an energy network in The Netherlands to determine the optimal size of the TESS to reduce cost and $CO_{2,eq}$ emissions when considering thermal, cooling, and electrical loads.	The results showed reductions in annual costs between 10.5 % and 31.9 %, and in $CO_{2,eq}$ emissions between 14.9 % and 47.8 %, depending on the demand analyzed: heating, heating, and cooling, or heating cooling and electrical.	[211]

Table 2.6: Role of the elements in a multi-carrier energy system when providing ancillary services.

Challenge	**RES**	**Energy storage systems**				**EV**	**HP**
		BESS	**Supercapacitors**	**HFC**[1]	**TESS**		
Voltage limit compliance	Reactive power control, voltage control	Congestion management					
Power curtailment	Energy arbitrage	Energy arbitrage		Energy arbitrage		Energy arbitrage	
Loss of inertia	Frequency balancing	Frequency balancing, congestion management		Frequency balancing, congestion management			
Rates variation		Energy arbitrage, demand response management, peak shaving	Peak shaving	Energy arbitrage, demand response management, direct load control, peak shaving	Demand response management, peak shaving	Energy arbitrage, demand response management, direct load control, peak shaving	Demand response management, direct load control
Grid congestion		Congestion management, demand response management, peak shaving	Peak shaving	Congestion management, demand response management, direct load control, peak shaving	Demand response management, peak shaving	Demand response management, direct load control, peak shaving	Demand response management, direct load control

The main components of an MCESS are described in Table 2.6 with the ancillary services described in Section 2.3. The categorization is based on the successful implementations reported in the literature, considering the power and energy requirements and the energy management required to provide each ancillary service.

As expected, the ancillary services with common operation goals share the required subsystem on the MCES. Reactive power control, frequency balancing, and voltage control take advantage of the inverter's adjustable power factor and power output, allowing it to provide power during a shortage or inject reactive power in case of unbalances between phases [51], explaining why the RESs are required. Energy storage devices such as BESSs or HFCs can also achieve these functions, but it is less likely that their capacity would be big enough to create an impact. On the other hand, peak shaving and energy arbitrage are intended to regulate the power and energy purchased from the grid, respectively, requiring the store of energy. Thus, BESSs play a significant role, as their energy density–price ratio and reaction time makes them more affordable than HFCs, and as the energy is stored, it does not depend on weather conditions, as it does in RESs. Supercapacitors can also considerably contribute to peak shaving due to their power density. However, their lower energy density makes them unsuitable for operation beyond minutes. EVs can also provide support. Nevertheless, transportation is the primary goal of the energy stored in their batteries; therefore, a robust EMS strategy is required to ensure they will be reasonably charged when the user unplugs them from their charging stations without creating disturbances in the system.

From the thermal perspective, TESS is indispensable in assisting the heating system. TESSs can be used to reduce the energy purchased at a particular moment to generate heat (peak shaving) or to displace the purchase to more convenient timeframes (demand response management), independent of the heat source (e.g., boiler or heat pump). Due to the growing interest in electrifying heat production, energy conversion devices, such as heat pumps, must be considered part of the ancillary services. Such devices also must be included at the individual level, as most energy networks do not allow sharing of heat between buildings [211]. HFCs can also generate heat, but this is a side effect of the process needing improvement to be fully deployed. Furthermore, the implementation costs are a restriction for now.

Controlling the loads can also be beneficial for the grid, whether the control is based on the current state of the grid (direct load control) or trends (demand response management). The EMS orchestrates the power distribution and flows from the grid, loads, and ESSs. It is crucial to considering that the energy stored can be obtained from the grid. This consumption needs to be appropriately addressed, as the grid considers it a load. Charging EVs is also a task that should be coordinated, as mentioned before, due to the high power the charger can demand, making it a critical load to manage by the EMS if there is any EV connected to the system at a particular moment.

When considering the interaction of EVs and the grid, both G2V and V2G scenarios can provide flexibility. G2V can occur either at a constant rate or following a profile determined by the grid state in a smart grid behaving as a demand response [175]. Moreover, EV batteries can also be used as BESSs regarding ancillary services, as previously discussed, assuming the EMS is robust enough. For that reason, EVs can be a solution to reduce the size of BESSs in the scenario of reactive activity of the BESS (only works

when there is energy consumption), as it is likely that the EV is at home at the same time the energy is consumed in a household. On the other hand, a more complex sizing methodology must be followed under more proactive activity.

Most of the literature reflects the main barriers described by [86]. Because there is uncertainty in both the amount of energy and power an MCESS can provide to the network and how the energy network will behave, new regulations are moving slowly. At the same time, this causes a reaction in the market, as the lack of regulations stops the DSO and TSO from proposing new business models to include DGs in the energy market as ancillary services providers, so it is attractive for prosumers to participate. In this regard, more research is needed to understand how the combined reaction of distributed MCESSs will affect the energy exchange between the DSO and the prosumers, as proposed by several authors [12], [57], [90], and the aging of the BESS [88]. In this way, innovative business models can be proposed to accelerate a collaborative energy transition.

Accurate models to predict DG power production are crucial for their adequate inclusion on the distribution grid to provide ancillary services. Multiple challenges must be faced to obtain a reliable estimation of the RES potential [212] and to optimally allocate the power when including storage [213], [214]. Different approaches can be considered to forecast the meteorological resources used by RESs. For instance, [215] classified the forecasting models as meteorological, statistical, AI-based, and hybrid (combination of multiple models). The first two were traditionally used before more robust AI-based models were computationally possible. It was found that individual AI models had accuracies of around 10 %, whereas hybrid models achieved accuracies near 5 % of error in exchange for more computational resources and more extensive datasets. When considering storage also, the computational cost substantially increases for both the sizing of the components [216] and control of the energy flow [213], [214], especially if the system considers more than one type of storage [217], [218].

It is noteworthy that accurate models to predict DG power production are crucial for their adequate inclusion in the distribution grid to provide ancillary services. Multiple challenges must be faced to obtain a reliable estimation of the RES potential and to allocate the power when including storage optimally. Different approaches can be considered to forecast the meteorological resources used by RESs.

2.6. CONCLUSIONS

This Chapter investigated how energy storage systems can minimize the adverse phenomena caused by DGs on the grid. Energy storage systems from different carriers were analyzed, identifying the ancillary services they can provide. The documented outcomes suggest that when ESSs provide ancillary services, the result is a more flexible and cooperative network. Finally, the state-of-the-art multi-carrier energy storage systems were presented as a more robust solution to combine multiple ancillary services, maximizing their advantages.

It was highlighted that an increase in noninertial, weather-dependent RESs (such as PV and wind) alone would not be enough to keep track of the upcoming demand trend, especially as EVs and heating electrification become more common in households. However, adding multi-carrier storage systems to the network (centralized, lo-

cal, or distributed) is a promising solution to increase the flexibility the system requires to counteract their variability. Numerous cases of implementation of ancillary services using energy storage systems were mentioned and analyzed. It was found that HFCs and BESSs can provide more ancillary services among the ESSs studied. Implementation costs and efficiency limit the first, whereas the second is limited to electric carriers. From the thermal perspective, TESSs and HPs can be combined to optimally produce and store thermal energy. In this sense, as the heat pump acts as an energy conversion device, it couples the thermal and electrical systems, thus expanding the opportunities to provide ancillary services. Chapter 3 elaborates on the interaction between the components of a multi-carrier energy system at the household level.

Hence, flexibility is the core of successful DG deployments. A cooperative scheme where prosumers offer ancillary services to the DSOs may contribute to controlling the effects of DGs on the grid and achieving a more robust and resilient network. This scheme creates a win-win scenario for DSOs and prosumers, incentivizing the prosumers to support the grid in exchange for rates that allow them to recover their investments. Chapter 5 elaborates on the requirements from a prosumer perspective that would make it attractive to participate in such collaborative schemes. The literature proves that implementing ancillary services with a single carrier can reduce costs. Furthermore, combining different carriers also allows more efficient energy usage, as it can conveniently be converted from one carrier to another.

Distribution system operators can use distributed generation and storage to address stability challenges. Distributed systems owners would find such collaboration attractive if ancillary services were included in the regulatory framework and new tariffs were proposed for them to use their assets to support the grid. Among those services are reactive power control, frequency balancing, voltage control, and congestion management, as their effect is at the distribution lines level. On the other hand, energy arbitrage, peak shaving, demand response management, and direct load control focus on the amount and manner in which the user consumes power and energy. Their implementation can lead to economic advantages. However, it requires robust control algorithms for the EMS, especially when the number of elements increases, creating opportunities for further work to determine if the same system can provide multiple ancillary services or if there are mutually exclusive combinations. For this reason, Chapter 4 investigates how different EMS strategies can be used by the prosumers to maximize their revenue, while minimizing their impact on the grid. Then, Chapter 6 determines the impact of aggregating multiple residential multi-carrier energy systems in a low-voltage network to minimize the impacts of RES penetration and heating electrification.

BIBLIOGRAPHY

[1] *DIRECTIVES DIRECTIVE (EU) 2018/2001 OF THE EUROPEAN PARLIAMENT AND OF THE COUNCIL of 11 December 2018 on the promotion of the use of energy from renewable sources.*

[2] *Proposal for a DIRECTIVE OF THE EUROPEAN PARLIAMENT AND OF THE COUNCIL amending Directive (EU) 2018/2001 of the European Parliament and of the Council, Regulation (EU) 2018/1999 of the European Parliament and of the Council and Directive 98/70/EC of the European Parliament and of the Council as regards the promotion of energy from renewable sources, and repealing Council Directive (EU) 2015/652, 14 July 2021.*

[3] *REGULATION (EU) 2019/ 943 OF THE EUROPEAN PARLIAMENT AND OF THE COUNCIL - of 5 June 2019 - on the internal market for electricity.*

[4] W. Meesenburg, T. Ommen, and B. Elmegaard, "Dynamic exergoeconomic analysis of a heat pump system used for ancillary services in an integrated energy system", *Energy*, vol. 152, pp. 154–165, Jun. 2018, ISSN: 03605442. DOI: 10.1016/j.energy.2018.03.093.

[5] L. Schibuola, M. Scarpa, and C. Tambani, "Demand response management by means of heat pumps controlled via real time pricing", *Energy and Buildings*, vol. 90, pp. 15–28, Mar. 2015, ISSN: 03787788. DOI: 10.1016/j.enbuild.2014.12.047.

[6] M. Stecca, L. R. Elizondo, T. B. Soeiro, P. Bauer, and P. Palensky, "A comprehensive review of the integration of battery energy storage systems into distribution networks", *IEEE Open Journal of the Industrial Electronics Society*, vol. 1, pp. 46–65, 1 2020, ISSN: 26441284. DOI: 10.1109/OJIES.2020.2981832.

[7] C. K. Das, O. Bass, G. Kothapalli, T. S. Mahmoud, and D. Habibi, "Overview of energy storage systems in distribution networks: Placement, sizing, operation, and power quality", *Renewable and Sustainable Energy Reviews*, vol. 91, pp. 1205–1230, Aug. 2018, ISSN: 18790690. DOI: 10.1016/j.rser.2018.03.068.

[8] J. Hennessy, H. Li, F. Wallin, and E. Thorin, "Flexibility in thermal grids: A review of short-term storage in district heating distribution networks", vol. 158, Elsevier Ltd, 2019, pp. 2430–2434. DOI: 10.1016/j.egypro.2019.01.302.

[9] S. Chapaloglou, A. Nesiadis, K. Atsonios, *et al.*, "Microgrid energy management strategies assessment through coupled thermal-electric considerations", *Energy Conversion and Management*, vol. 228, Jan. 2021, ISSN: 01968904. DOI: 10.1016/j.enconman.2020.113711.

[10] M. Jiménez, I. Onyeji, A. Colta, *et al.*, *Smart Grid Projects in Europe: Lessons Learned and Current Developments;* JRC, 2012. [Online]. Available: https://ses.jrc.ec.europa.eu/sites/ses/files/documents/smart_grid_projects_in_europe_lessons_learned_and_current_developments.pdf.

[11] N. Sijakovic, A. Terzic, G. Fotis, *et al.*, "Active system management approach for flexibility services to the greek transmission and distribution system", *Energies*, vol. 15, no. 17, 2022, ISSN: 1996-1073. DOI: 10.3390/en15176134. [Online]. Available: https://www.mdpi.com/1996-1073/15/17/6134.

[12] G. Fotis, C. Dikeakos, E. Zafeiropoulos, S. Pappas, and V. Vita, "Scalability and replicability for smart grid innovation projects and the improvement of renewable energy sources exploitation: The flexitranstore case", *Energies*, vol. 15, no. 13, 2022, ISSN: 1996-1073. DOI: 10.3390/en15134519. [Online]. Available: https://www.mdpi.com/1996-1073/15/13/4519.

[13] M. Mansoor, M. Stadler, M. Zellinger, K. Lichtenegger, H. Auer, and A. Cosic, "Optimal planning of thermal energy systems in a microgrid with seasonal storage and piecewise affine cost functions", *Energy*, vol. 215, Jan. 2021, ISSN: 03605442. DOI: 10.1016/j.energy.2020.119095.

[14] S. Baldi, A. Karagevrekis, I. T. Michailidis, and E. B. Kosmatopoulos, "Joint energy demand and thermal comfort optimization in photovoltaic-equipped interconnected microgrids", *Energy Conversion and Management*, vol. 101, pp. 352–363, Jun. 2015, ISSN: 01968904. DOI: 10.1016/j.enconman.2015.05.049.

[15] J. Antonio, A. Robles, C. F. Nava, and L. G. Corona, *Los servicios auxiliares en redes de distribución eléctrica en presencia de gran cantidad de generación fotovoltaica de baja potencia*. 2018, vol. 40, p. 2448. [Online]. Available: http://itcelaya.edu.mx/ojs/index.php/pistas.

[16] P. Kohlhepp, H. Harb, H. Wolisz, S. Waczowicz, D. Müller, and V. Hagenmeyer, "Large-scale grid integration of residential thermal energy storages as demand-side flexibility resource: A review of international field studies", *Renewable and Sustainable Energy Reviews*, vol. 101, pp. 527–547, Mar. 2019, ISSN: 18790690. DOI: 10.1016/j.rser.2018.09.045.

[17] A. T. Hoang, V. V. Pham, and X. P. Nguyen, "Integrating renewable sources into energy system for smart city as a sagacious strategy towards clean and sustainable process", *Journal of Cleaner Production*, vol. 305, Jul. 2021, ISSN: 09596526. DOI: 10.1016/j.jclepro.2021.127161.

[18] M. Richter, "German utilities and distributed pv: How to overcome barriers to business model innovation", *Renewable Energy*, vol. 55, pp. 456–466, Jul. 2013, ISSN: 09601481. DOI: 10.1016/j.renene.2012.12.052.

[19] P. Nillesen, M. Pollitt, and E. Witteler, *New Utility Business Model: A Global View*. Elsevier Inc., Jun. 2014, pp. 33–47, ISBN: 9780128003800. DOI: 10.1016/B978-0-12-800240-7.00002-3.

[20] J. R. Agüero and A. Khodaei, "Roadmaps for the utility of the future", vol. 28, Elsevier Inc., Dec. 2015, pp. 7–17. DOI: 10.1016/j.tej.2015.11.002.

[21] M. Jayachandran, K. P. Rao, R. K. Gatla, C. Kalaivani, C. Kalaiarasy, and C. Logasabarirajan, "Operational concerns and solutions in smart electricity distribution systems", *Utilities Policy*, vol. 74, p. 101 329, 2022, ISSN: 0957-1787. DOI: https://doi.org/10.1016/j.jup.2021.101329. [Online]. Available: https://www.sciencedirect.com/science/article/pii/S0957178721001624.

[22] S. Hajiaghasi, A. Salemnia, and M. Hamzeh, "Hybrid energy storage system for microgrids applications: A review", *Journal of Energy Storage*, vol. 21, pp. 543–570, 2019, ISSN: 2352-152X. DOI: https://doi.org/10.1016/j.est.2018.12.017. [Online]. Available: https://www.sciencedirect.com/science/article/pii/S2352152X18305188.

[23] K. Sevdari, L. Calearo, P. B. Andersen, and M. Marinelli, "Ancillary services and electric vehicles: An overview from charging clusters and chargers technology perspectives", *Renewable and Sustainable Energy Reviews*, vol. 167, p. 112 666, 2022, ISSN: 1364-0321. DOI: https://doi.org/10.1016/j.rser.2022.112666. [Online]. Available: https://www.sciencedirect.com/science/article/pii/S1364032122005585.

[24] N. McIlwaine, A. M. Foley, D. J. Morrow, *et al.*, "A state-of-the-art techno-economic review of distributed and embedded energy storage for energy systems", *Energy*, vol. 229, Aug. 2021, ISSN: 03605442. DOI: 10.1016/j.energy.2021.120461.

[25] G. C. Kryonidis, E. O. Kontis, T. A. Papadopoulos, *et al.*, "Ancillary services in active distribution networks: A review of technological trends from operational and online analysis perspective", *Renewable and Sustainable Energy Reviews*, vol. 147, Sep. 2021, ISSN: 18790690. DOI: 10.1016/j.rser.2021.111198.

[26] J. A. Villanueva-Rosario, F. Santos-García, M. E. Aybar-Mejía, P. Mendoza-Araya, and A. Molina-García, "Coordinated ancillary services, market participation and communication of multi-microgrids: A review", *Applied Energy*, vol. 308, p. 118 332, 2022, ISSN: 0306-2619. DOI: https://doi.org/10.1016/j.apenergy.2021.118332. [Online]. Available: https://www.sciencedirect.com/science/article/pii/S030626192101583X.

[27] D. Zhang, G. Shafiullah, C. K. Das, and K. W. Wong, "A systematic review of optimal planning and deployment of distributed generation and energy storage systems in power networks", *Journal of Energy Storage*, vol. 56, p. 105 937, 2022, ISSN: 2352-152X. DOI: https://doi.org/10.1016/j.est.2022.105937. [Online]. Available: https://www.sciencedirect.com/science/article/pii/S2352152X22019259.

[28] J. Hansen, M. Sato, P. Kharecha, *et al.*, "Target atmospheric co2: Where should humanity aim?", *The Open Atmospheric Science Journa*, vol. 2, pp. 217–231, 2008.

[29] *Renewables 2021 Global Status Report*. 2021. [Online]. Available: https://www.ren21.net/reports/global-status-report/.

[30] H. Ritchie and M. Roser, *Our World in Data*. [Online]. Available: www.ourworldindata.org/renewable-energy.

[31] *The World Bank Indicators*. 2021. [Online]. Available: https://data.worldbank.org/indicator.

[32] *Tracking SDG7 A joint report of the custodian agencies*. 2021. [Online]. Available: https://www.irena.org/publications/2021/Jun/Tracking-SDG-7-2021.

[33] S. Henni, P. Staudt, and C. Weinhardt, "A sharing economy for residential communities with pv-coupled battery storage: Benefits, pricing and participant matching", *Applied Energy*, vol. 301, Nov. 2021, ISSN: 03062619. DOI: 10.1016/j.apenergy.2021.117351.

[34] S. Bandyopadhyay, Z. Qin, L. Ramirez-Elizondo, and P. Bauer, "Comparison of battery technologies for dc microgrids with integrated pv", Institute of Electrical and Electronics Engineers (IEEE), Nov. 2020, pp. 1–9. DOI: 10.1109/icdcm45535.2019.9232746.

[35] S. Wagh, Y. Yu, A. Shekhar, G. R. C. Mouli, and P. Bauer, "Aggregated impact of ev charger type and ev penetration level in improving pv integration in distribution grids", in *2021 IEEE Transportation Electrification Conference Expo (ITEC)*, 2021, pp. 595–600. DOI: 10.1109/ITEC51675.2021.9490054.

[36] R. Jacob, M. Belusko, M. Liu, W. Saman, and F. Bruno, "Using renewables coupled with thermal energy storage to reduce natural gas consumption in higher temperature commercial/industrial applications", *Renewable Energy*, vol. 131, pp. 1035–1046, 2019, ISSN: 0960-1481. DOI: https://doi.org/10.1016/j.renene.2018.07.085. [Online]. Available: https://www.sciencedirect.com/science/article/pii/S0960148118308826.

[37] A. Kies, B. U. Schyska, M. Bilousova, O. E. Sayed, J. Jurasz, and H. Stoecker, "Critical review of renewable generation datasets and their implications for european power system models", *Renewable and Sustainable Energy Reviews*, vol. 152, Dec. 2021, ISSN: 18790690. DOI: 10.1016/j.rser.2021.111614.

[38] I. E. Agency, *Global EV Outlook 2021 Accelerating ambitions despite the pandemic*. 2021. [Online]. Available: www.iea.org/t&c/.

[39] K. Peet, S. Gota, C. Huizenga, *et al.*, *Transport and Climate Change Global Status Report 2018 Partnership on Sustainable, Low Carbon Transport (SLoCaT) SLoCaT Secretariat Team*. [Online]. Available: http://slocat.net/tcc-gsr.

[40] D. Lyu, T. B. Soeiro, and P. Bauer, "Impacts of different charging strategies on the electric vehicle battery charger circuit using phase-shift full-bridge converter", Institute of Electrical and Electronics Engineers Inc., Apr. 2021, pp. 256–263, ISBN: 9781728156606. DOI: 10.1109/PEMC48073.2021.9432497.

[41] F. Grazian, W. Shi, T. B. Soeiro, J. Dong, and P. Bauer, "Electric vehicle charging based on inductive power transfer employing variable compensation capacitance for optimum load matching", vol. 2020-October, IEEE Computer Society, Oct. 2020, pp. 5262–5267, ISBN: 9781728154145. DOI: 10.1109/IECON43393.2020.9254920.

[42] T. M. Al, D. Lyu, T. B. Soeiro, and P. Bauer, "Design of a wide output voltage dual active bridge converter as power electronics building block for the fast charging of electric vehicles", Institute of Electrical and Electronics Engineers Inc., Apr. 2021, pp. 89–96, ISBN: 9781728156606. DOI: 10.1109/PEMC48073.2021.9432516.

[43] C. Riekerk, F. Grazian, T. B. Soeiro, J. Dong, and P. Bauer, "Study on soft start-up and shut-down methods for wireless power transfer systems for the charging of electric vehicles", Institute of Electrical and Electronics Engineers Inc., Jun. 2021, ISBN: 9781728195483. DOI: 10.1109/WoW51332.2021.9462867.

[44] Y. Yu, A. Shekhar, G. C. R. Mouli, P. Bauer, N. Refa, and R. Bernards, "Impact of uncontrolled charging with mass deployment of electric vehicles on low voltage distribution networks", in *2020 IEEE Transportation Electrification Conference Expo (ITEC)*, 2020, pp. 766–772. DOI: 10.1109/ITEC48692.2020.9161574.

[45] L. Wang, Z. Qin, T. Slangen, P. Bauer, and T. van Wijk, "Grid impact of electric vehicle fast charging stations: Trends, standards, issues and mitigation measures - an overview", *IEEE Open Journal of Power Electronics*, vol. 2, pp. 56–74, Jan. 2021. DOI: 10.1109/ojpel.2021.3054601.

[46] R. D. Souza, M. Casisi, D. Micheli, and M. Reini, "A review of small–medium combined heat and power (chp) technologies and their role within the 100% renewable energy systems scenario", *Energies*, vol. 14, 17 Sep. 2021, ISSN: 19961073. DOI: 10.3390/en14175338.

[47] F. Calise, M. D. D'Accadia, C. Barletta, V. Battaglia, A. Pfeifer, and N. Duic, "Detailed modelling of the deep decarbonisation scenarios with demand response technologies in the heating and cooling sector: A case study for italy", *Energies*, vol. 10, 10 Oct. 2017, ISSN: 19961073. DOI: 10.3390/en10101535.

[48] W. Stanek, T. Simla, and W. Gazda, "Exergetic and thermo-ecological assessment of heat pump supported by electricity from renewable sources", *Renewable Energy*, vol. 131, pp. 404–412, 2019, ISSN: 0960-1481. DOI: https://doi.org/10.1016/j.renene.2018.07.084. [Online]. Available: https://www.sciencedirect.com/science/article/pii/S0960148118308814.

[49] B. Kılkış, M. Çağlar, and M. Şengül, "Energy benefits of heat pipe technology for achieving 100% renewable heating and cooling for fifth-generation, low-temperature district heating systems", *Energies*, vol. 14, no. 17, 2021, ISSN: 1996-1073. DOI: 10.3390/en14175398. [Online]. Available: https://www.mdpi.com/1996-1073/14/17/5398.

[50] O. Eguiarte, A. Garrido-Marijuán, P. de Agustín-Camacho, L. del Portillo, and A. Romero-Amorrortu, "Energy, environmental and economic analysis of air-to-air heat pumps as an alternative to heating electrification in europe", *Energies*, vol. 13, 15 Aug. 2020, ISSN: 19961073. DOI: 10.3390/en13153939.

[51] O. Gandhi, D. S. Kumar, C. D. Rodríguez-Gallegos, and D. Srinivasan, "Review of power system impacts at high pv penetration part i: Factors limiting pv penetration", *Solar Energy*, vol. 210, pp. 181–201, Nov. 2020, ISSN: 0038092X. DOI: 10.1016/j.solener.2020.06.097.

[52] L. Wang, R. Yan, and T. K. Saha, "Voltage regulation challenges with unbalanced pv integration in low voltage distribution systems and the corresponding solution", *Applied Energy*, vol. 256, Dec. 2019, ISSN: 03062619. DOI: 10.1016/j.apenergy.2019.113927.

[53] D. Q. Hung and Y. Mishra, "Impacts of single-phase pv injection on voltage quality in 3-phase 4-wire distribution systems", in *2018 IEEE Power Energy Society General Meeting (PESGM)*, 2018, pp. 1–5. DOI: 10.1109/PESGM.2018.8585530.

[54] J. Yaghoobi, M. Islam, and N. Mithulananthan, "Analytical approach to assess the loadability of unbalanced distribution grid with rooftop pv units", *Applied Energy*, vol. 211, pp. 358–367, Feb. 2018, ISSN: 03062619. DOI: 10.1016/j.apenergy.2017.11.030.

[55] D. Schwanz, F. Moller, S. K. Ronnberg, J. Meyer, and M. H. Bollen, "Stochastic assessment of voltage unbalance due to single-phase-connected solar power", *IEEE Transactions on Power Delivery*, vol. 32, pp. 852–861, 2 Apr. 2017, ISSN: 08858977. DOI: 10.1109/TPWRD.2016.2579680.

[56] R. Torquato, D. Salles, C. O. Pereira, P. C. M. Meira, and W. Freitas, "A comprehensive assessment of pv hosting capacity on low-voltage distribution systems", *IEEE Transactions on Power Delivery*, vol. 33, pp. 1002–1012, 2 Apr. 2018, ISSN: 08858977. DOI: 10.1109/TPWRD.2018.2798707.

[57] M. Zafeiropoulou, I. Mentis, N. Sijakovic, *et al.*, "Forecasting transmission and distribution system flexibility needs for severe weather condition resilience and outage management", *Applied Sciences*, vol. 12, no. 14, 2022, ISSN: 2076-3417. DOI: 10.3390/app12147334. [Online]. Available: https://www.mdpi.com/2076-3417/12/14/7334.

[58] G. Morales-España, E. Nycander, and J. Sijm, "Reducing co2 emissions by curtailing renewables: Examples from optimal power system operation", *Energy Economics*, vol. 99, Jul. 2021, ISSN: 01409883. DOI: 10.1016/j.eneco.2021.105277.

[59] S. Vonsien and R. Madlener, "Economic modeling of the economic efficiency of li-ion battery storage with a special focus on residential pv systems", vol. 158, Elsevier Ltd, 2019, pp. 3964–3975. DOI: 10.1016/j.egypro.2019.01.845.

[60] Z. Zhang, C. Dou, D. Yue, B. Zhang, and P. Zhao, "High-economic pv power compensation algorithm to mitigate voltage rise with minimal curtailment", *International Journal of Electrical Power and Energy Systems*, vol. 125, Feb. 2021, ISSN: 01420615. DOI: 10.1016/j.ijepes.2020.106401.

[61] B. Frew, B. Sergi, P. Denholm, *et al.*, "The curtailment paradox in the transition to high solar power systems", *Joule*, vol. 5, pp. 1143–1167, 5 May 2021, ISSN: 25424351. DOI: 10.1016/j.joule.2021.03.021.

[62] A. F. C. Borray, J. Merino, E. Torres, A. Garcés, and J. Mazón, "Centralised coordination of evs charging and pv active power curtailment over multiple aggregators in low voltage networks", *Sustainable Energy, Grids and Networks*, vol. 27, Sep. 2021, ISSN: 23524677. DOI: 10.1016/j.segan.2021.100470.

[63] X. Gou, Q. Chen, K. Hu, *et al.*, "Optimal planning of capacities and distribution of electric heater and heat storage for reduction of wind power curtailment in power systems", *Energy*, vol. 160, pp. 763–773, Oct. 2018, ISSN: 03605442. DOI: 10.1016/j.energy.2018.07.027.

[64] E. Nycander, L. Söder, J. Olauson, and R. Eriksson, "Curtailment analysis for the nordic power system considering transmission capacity, inertia limits and generation flexibility", *Renewable Energy*, vol. 152, pp. 942–960, Jun. 2020, ISSN: 18790682. DOI: 10.1016/j.renene.2020.01.059.

[65] C. Rochlin, "Distributed renewable resources and the utility business model", *Electricity Journal*, vol. 29, pp. 7–12, 1 Jan. 2016, ISSN: 10406190. DOI: 10.1016/j.tej.2015.12.001.

[66] D. E. Dismukes and M. W. Deupree, "The challenges of the regulatory review of diversification mergers", *Electricity Journal*, vol. 29, pp. 8–14, 4 May 2016, ISSN: 10406190. DOI: 10.1016/j.tej.2016.04.009.

[67] A. Satchwell, A. Mills, and G. Barbose, "Regulatory and ratemaking approaches to mitigate financial impacts of net-metered pv on utilities and ratepayers", *Energy Policy*, vol. 85, pp. 115–125, Oct. 2015, ISSN: 03014215. DOI: 10.1016/j.enpol.2015.05.019.

[68] M. Mihaylov, R. Rădulescu, I. Razo-Zapata, *et al.*, "Comparing stakeholder incentives across state-of-the-art renewable support mechanisms", *Renewable Energy*, vol. 131, pp. 689–699, Feb. 2019, ISSN: 18790682. DOI: 10.1016/j.renene.2018.07.069.

[69] C. E. Hoicka, J. Lowitzsch, M. C. Brisbois, A. Kumar, and L. Ramirez Camargo, "Implementing a just renewable energy transition: Policy advice for transposing the new european rules for renewable energy communities", *Energy Policy*, vol. 156, p. 112 435, 2021, ISSN: 0301-4215. DOI: https://doi.org/10.1016/j.enpol.2021.112435. [Online]. Available: https://www.sciencedirect.com/science/article/pii/S0301421521003050.

[70] H. A. Muqeet, H. M. Munir, H. Javed, M. Shahzad, M. Jamil, and J. M. Guerrero, "An energy management system of campus microgrids: State-of-the-art and future challenges", *Energies*, vol. 14, 20 Oct. 2021, ISSN: 19961073. DOI: 10.3390/en14206525.

[71] E. A. Feilat, S. Azzam, and A. Al-Salaymeh, "Impact of large pv and wind power plants on voltage and frequency stability of jordan's national grid", *Sustainable Cities and Society*, vol. 36, pp. 257–271, Jan. 2018, ISSN: 22106707. DOI: 10.1016/j.scs.2017.10.035.

[72] Western, Power, and Distribution, *Distributed generation EHV constraint maps*. 2021. [Online]. Available: https://www.westernpower.co.uk/connections/generation/distributed-generation-ehv-constraint-maps.aspx.

[73] R. J. C. Pinto, S. J. P. S. Mariano, and M. D. R. A. Calado, "Power quality experimental analysis on rural home grid-connected pv systems", *International Journal of Photoenergy*, vol. 2015, 2015, ISSN: 1687529X. DOI: 10.1155/2015/791680.

[74] F. Boshell, R. Miranda, and S. Ratka, *Solutions to Integrate High Shares of Variable Renewable Energy (Report to the G20 Energy Transitions Working Group (ETWG))*. 2019, ISBN: 978-92-9260-135-5.

[75] H. Schermeyer, C. Vergara, and W. Fichtner, "Renewable energy curtailment: A case study on today's and tomorrow's congestion management", *Energy Policy*, vol. 112, pp. 427–436, 2018, ISSN: 0301-4215. DOI: https://doi.org/10.1016/j.enpol.2017.10.037. [Online]. Available: https://www.sciencedirect.com/science/article/pii/S0301421517307115.

[76] X. Zhang, J. X. Wang, Z. Cao, S. Shen, S. Meng, and J. L. Fan, "What is driving the remarkable decline of wind and solar power curtailment in china? evidence from china and four typical provinces", *Renewable Energy*, vol. 174, pp. 31–42, Aug. 2021, ISSN: 18790682. DOI: 10.1016/j.renene.2021.04.043.

[77] M. Brinkerink, B. Ó. Gallachóir, and P. Deane, "A comprehensive review on the benefits and challenges of global power grids and intercontinental interconnectors", *Renewable and Sustainable Energy Reviews*, vol. 107, pp. 274–287, 2019, ISSN: 1364-0321. DOI: https://doi.org/10.1016/j.rser.2019.03.003. [Online]. Available: https://www.sciencedirect.com/science/article/pii/S1364032119301364.

[78] M. J. van Blijswijk and L. J. de Vries, "Evaluating congestion management in the dutch electricity transmission grid", *Energy Policy*, vol. 51, pp. 916–926, Dec. 2012, ISSN: 03014215. DOI: 10.1016/j.enpol.2012.09.051.

[79] C. B. Rosa, P. D. Rigo, G. Rediske, A. P. Moccellin, J. C. Mairesse Siluk, and L. Michels, "How to measure organizational performance of distributed generation in electric utilities? the brazilian case", *Renewable Energy*, vol. 169, pp. 191–203, 2021, ISSN: 0960-1481. DOI: https://doi.org/10.1016/j.renene.2021.01.027. [Online]. Available: https://www.sciencedirect.com/science/article/pii/S0960148121000331.

[80] S. Strunz, P. Lehmann, and E. Gawel, "Analyzing the ambitions of renewable energy policy in the eu and its member states", *Energy Policy*, vol. 156, p. 112 447, 2021, ISSN: 0301-4215. DOI: https://doi.org/10.1016/j.enpol.2021.112447. [Online]. Available: https://www.sciencedirect.com/science/article/pii/S0301421521003177.

[81] T. Yunusov and J. Torriti, "Distributional effects of time of use tariffs based on electricity demand and time use", *Energy Policy*, vol. 156, Sep. 2021, ISSN: 03014215. DOI: 10.1016/j.enpol.2021.112412.

[82] *UL Standard 1741 - Inverters, Converters, Controllers and Interconnection System Equipment for Use With Distributed Energy Resources*. UL, 2021.

[83] *IEEE Standard 519 - Recommended Practice and Requirements for Harmonic Control in Electric Power Systems*. 2014. DOI: 10.1109/IEEESTD.2014.6826459.

[84] *IEC Standard 61727 - Photovoltaic (PV) Systems - Characteristics of the Utility Interface*. IEC, 2004.

[85] *EN Standard 50160 - Voltage characteristics of electricity supplied by public electricity networks*. EN, 2010.

[86] F. Norouzi, T. Hoppe, L. R. Elizondo, and P. Bauer, "A review of socio-technical barriers to smart microgrid development", *Renewable and Sustainable Energy Reviews*, vol. 167, p. 112 674, 2022, ISSN: 1364-0321. DOI: https://doi.org/10.1016/j.rser.2022.112674. [Online]. Available: https://www.sciencedirect.com/science/article/pii/S1364032122005640.

[87] C. Cambini, A. Meletiou, E. Bompard, and M. Masera, "Market and regulatory factors influencing smart-grid investment in europe: Evidence from pilot projects and implications for reform", *Utilities Policy*, vol. 40, pp. 36–47, 2016, ISSN: 0957-1787. DOI: https://doi.org/10.1016/j.jup.2016.03.003. [Online]. Available: https://www.sciencedirect.com/science/article/pii/S095717871630073X.

[88] G. Mohy-ud-din, K. M. Muttaqi, and D. Sutanto, "Frequency control ancillary services using energy storage in the co-optimized energy markets under price uncertainty", in *2021 IEEE Industry Applications Society Annual Meeting (IAS)*, 2021, pp. 1–6. DOI: 10.1109/IAS48185.2021.9677307.

[89] M. Derks and H. Romijn, "Sustainable performance challenges of rural microgrids: Analysis of incentives and policy framework in indonesia", *Energy for Sustainable Development*, vol. 53, pp. 57–70, 2019, ISSN: 0973-0826. DOI: https://doi.org/10.1016/j.esd.2019.08.003. [Online]. Available: https://www.sciencedirect.com/science/article/pii/S0973082619301632.

[90] M. Benini, S. Canevese, D. Cirio, and A. Gatti, "Battery energy storage systems for the provision of primary and secondary frequency regulation in italy", in *2016 IEEE 16th International Conference on Environment and Electrical Engineering (EEEIC)*, 2016, pp. 1–6. DOI: 10.1109/EEEIC.2016.7555748.

[91] Y. Liu, J. Bebic, B. Kroposki, J. D. Bedout, and W. Ren, "Distribution system voltage performance analysis for high-penetration pv", 2008, ISBN: 9781424428502. DOI: 10.1109/ENERGY.2008.4781069.

[92] K. Spiliotis, A. I. R. Gutierrez, and R. Belmans, "Demand flexibility versus physical network expansions in distribution grids", *Applied Energy*, vol. 182, pp. 613–624, Nov. 2016, ISSN: 03062619. DOI: 10.1016/j.apenergy.2016.08.145.

[93] D. Saygin, O. B. Tör, M. E. Cebeci, S. Teimourzadeh, and P. Godron, "Increasing turkey's power system flexibility for grid integration of 50% renewable energy share", *Energy Strategy Reviews*, vol. 34, Mar. 2021, ISSN: 2211467X. DOI: 10.1016/j.esr.2021.100625.

[94] C. D. Iweh, S. Gyamfi, E. Tanyi, and E. Effah-Donyina, "Distributed generation and renewable energy integration into the grid: Prerequisites, push factors, practical options, issues and merits", *Energies*, vol. 14, 17 Sep. 2021, ISSN: 19961073. DOI: 10.3390/en14175375.

[95] S. Goutte and P. Vassilopoulos, "The value of flexibility in power markets", *Energy Policy*, vol. 125, pp. 347–357, Feb. 2019, ISSN: 03014215. DOI: 10.1016/j.enpol.2018.10.024.

[96] M. I. Alizadeh, M. P. Moghaddam, N. Amjady, P. Siano, and M. K. Sheikh-El-Eslami, "Flexibility in future power systems with high renewable penetration: A review", *Renewable and Sustainable Energy Reviews*, vol. 57, pp. 1186–1193, May 2016, ISSN: 18790690. DOI: 10.1016/j.rser.2015.12.200.

[97] H. Bevrani, M. Imanaka, and T. Kato, "Grid dynamics shaping using flexible controlled power converters", *Energy Reports*, vol. 6, pp. 1490–1495, Dec. 2020, ISSN: 23524847. DOI: 10.1016/j.egyr.2020.10.065.

[98] L. Collins and J. K. Ward, "Real and reactive power control of distributed pv inverters for overvoltage prevention and increased renewable generation hosting capacity", *Renewable Energy*, vol. 81, pp. 464–471, Sep. 2015, ISSN: 18790682. DOI: 10.1016/j.renene.2015.03.012.

[99] M. B. Mustafa, P. Keatley, Y. Huang, O. Agbonaye, O. O. Ademulegun, and N. Hewitt, "Evaluation of a battery energy storage system in hospitals for arbitrage and ancillary services", *Journal of Energy Storage*, vol. 43, Nov. 2021, ISSN: 2352152X. DOI: 10.1016/j.est.2021.103183.

[100] C. Jankowiak, A. Zacharopoulos, C. Brandoni, P. Keatley, P. MacArtain, and N. Hewitt, "Assessing the benefits of decentralised residential batteries for load peak shaving", *Journal of Energy Storage*, vol. 32, Dec. 2020, ISSN: 2352152X. DOI: 10.1016/j.est.2020.101779.

[101] H. Li, J. Hou, Z. Tian, T. Hong, N. Nord, and D. Rohde, "Optimize heat prosumers' economic performance under current heating price models by using water tank thermal energy storage", *Energy*, vol. 239, Jan. 2022, ISSN: 03605442. DOI: 10.1016/j.energy.2021.122103.

[102] M. Bahloul and S. K. Khadem, "Design and control of energy storage system for enhanced frequency response grid service", in *2018 IEEE International Conference on Industrial Technology (ICIT)*, 2018, pp. 1189–1194. DOI: 10.1109/ICIT.2018.8352347.

[103] L. Sun, J. Qiu, X. Han, X. Yin, and Z. Dong, "Per-use-share rental strategy of distributed bess in joint energy and frequency control ancillary services markets", *Applied Energy*, vol. 277, Nov. 2020, ISSN: 03062619. DOI: 10.1016/j.apenergy.2020.115589.

[104] Y. Qingyuan and M. Aoki, "Suppression of voltage fluctuation by utilizing consumer-side energy storage devices in pv connected distribution system", vol. 51, Elsevier B.V., Jan. 2018, pp. 432–437. DOI: 10.1016/j.ifacol.2018.11.741.

[105] M. Abujubbeh, M. Fahrioglu, and F. Al-Turjman, "Power loss reduction and voltage enhancement via distributed photovoltaic generation: Case study in north cyprus", *Computers and Electrical Engineering*, vol. 95, Oct. 2021, ISSN: 00457906. DOI: 10.1016/j.compeleceng.2021.107432.

[106] R. Fonteijn, P. H. Nguyen, J. Morren, and J. G. Slootweg, "Demonstrating a generic four-step approach for applying flexibility for congestion management in daily operation", *Sustainable Energy, Grids and Networks*, vol. 23, Sep. 2020, ISSN: 23524677. DOI: 10.1016/j.segan.2020.100378.

[107] R. Barreto, P. Faria, C. Silva, and Z. Vale, "Clustering direct load control appliances in the context of demand response programs in energy communities", vol. 53, Elsevier B.V., 2020, pp. 12 608–12 613. DOI: 10.1016/j.ifacol.2020.12.1827.

[108] A. C. Duman, H. S. Erden, Ö. Gönül, and Ö. Güler, "A home energy management system with an integrated smart thermostat for demand response in smart grids", *Sustainable Cities and Society*, vol. 65, Feb. 2021, ISSN: 22106707. DOI: 10.1016/j.scs.2020.102639.

[109] Q. Meng, X. Ren, W. Wang, *et al.*, "Reduction in on-off operations of an air source heat pump with active thermal storage and demand response: An experimental case study", *Journal of Energy Storage*, vol. 36, Apr. 2021, ISSN: 2352152X. DOI: 10.1016/j.est.2021.102401.

[110] F. AlFaris, A. Juaidi, and F. Manzano-Agugliaro, "Intelligent homes' technologies to optimize the energy performance for the net zero energy home", *Energy and Buildings*, vol. 153, pp. 262–274, Oct. 2017, ISSN: 03787788. DOI: 10.1016/j.enbuild.2017.07.089.

[111] Z. Layate, T. Bahi, I. Abadlia, H. Bouzeria, and S. Lekhchine, "Reactive power compensation control for three phase grid-connected photovoltaic generator", *International Journal of Hydrogen Energy*, vol. 40, pp. 12 619–12 626, 37 Oct. 2015, ISSN: 03603199. DOI: 10.1016/j.ijhydene.2015.07.087.

[112] B. Bayer and A. Marian, "Innovative measures for integrating renewable energy in the german medium-voltage grids", *Energy Reports*, vol. 6, pp. 336–342, Nov. 2020, ISSN: 23524847. DOI: 10.1016/j.egyr.2019.12.028.

[113] IRENA, *Grid codes for renewable powered systems*. International Renewable Energy Agency, 2022, ISBN: 978-92-9260-427-1. [Online]. Available: https://www.irena.org/-/media/Files/IRENA/Agency/Publication/2022/Apr/IRENA_Grid_Codes_Renewable_Systems_2022.pdf.

[114] *IEEE Standard 1547-2018 - For Interconnection and Interoperability of Distributed Energy Resources with Associated Electric Power Systems Interfaces*. IEEE, 2018, ISBN: 9781504446396.

[115] S. Sayeef, S. Heslop, D. Cornforth, *et al.*, *Solar intermittency: Australia's clean energy challenge Characterising the effect of high penetration solar intermittency on Australian electricity networks*. 2012. [Online]. Available: https://publications.csiro.au/publications/publication/PIcsiro:EP121914.

[116] S. D. Braithwait, "Retail pricing responses to the challenge of distributed energy resources", *Electricity Journal*, vol. 31, pp. 38–43, 8 Oct. 2018, ISSN: 10406190. DOI: 10.1016/j.tej.2018.09.001.

[117] E. Pusceddu, B. Zakeri, and G. C. Gissey, "Synergies between energy arbitrage and fast frequency response for battery energy storage systems", *Applied Energy*, vol. 283, Feb. 2021, ISSN: 03062619. DOI: 10.1016/j.apenergy.2020.116274.

[118] M. M. Rana, M. F. Romlie, M. F. Abdullah, M. Uddin, and M. R. Sarkar, "A novel peak load shaving algorithm for isolated microgrid using hybrid pv-bess system", *Energy*, vol. 234, Nov. 2021, ISSN: 03605442. DOI: 10.1016/j.energy.2021.121157.

[119] B. Ceran, J. Jurasz, A. Mielcarek, and P. E. Campana, "Pv systems integrated with commercial buildings for local and national peak load shaving in poland", *Journal of Cleaner Production*, vol. 322, Nov. 2021, ISSN: 09596526. DOI: 10.1016/j.jclepro.2021.129076.

[120] D. S. Kumar, O. Gandhi, C. D. Rodríguez-Gallegos, and D. Srinivasan, "Review of power system impacts at high pv penetration part ii: Potential solutions and the way forward", *Solar Energy*, vol. 210, pp. 202–221, Nov. 2020, ISSN: 0038092X. DOI: 10.1016/j.solener.2020.08.047.

[121] D. Fernández-Muñoz, J. I. Pérez-Díaz, I. Guisández, M. Chazarra, and Á. Fernández-Espina, "Fast frequency control ancillary services: An international review", *Renewable and Sustainable Energy Reviews*, vol. 120, Mar. 2020, ISSN: 18790690. DOI: 10.1016/j.rser.2019.109662.

[122] U. Tamrakar, D. Shrestha, M. Maharjan, B. P. Bhattarai, T. M. Hansen, and R. Tonkoski, "Virtual inertia: Current trends and future directions", *Applied Sciences (Switzerland)*, vol. 7, 7 Jun. 2017, ISSN: 20763417. DOI: 10.3390/app7070654.

[123] M. Rathbun, Y. Xu, R. Roofegari, Z. Qu, and W. Sun, "Impact studies and cooperative voltage control for high pv penetration", *IFAC PapersOnLine*, vol. 51, 28 2018.

[124] *ANSI Standard C841 - American National Standard for Electric Power Systems and Equipment—Voltage Ratings (60 Hz)*. ANSI, 2020.

[125] P. Chaudhary and M. Rizwan, "Voltage regulation mitigation techniques in distribution system with high pv penetration: A review", *Renewable and Sustainable Energy Reviews*, vol. 82, pp. 3279–3287, Feb. 2018, ISSN: 18790690. DOI: 10.1016/j.rser.2017.10.017.

[126] R. Hemmati, H. Saboori, and M. A. Jirdehi, "Stochastic planning and scheduling of energy storage systems for congestion management in electric power systems including renewable energy resources", *Energy*, vol. 133, pp. 380–387, 2017, ISSN: 03605442. DOI: 10.1016/j.energy.2017.05.167.

[127] I. Alotaibi, M. A. Abido, M. Khalid, and A. V. Savkin, "A comprehensive review of recent advances in smart grids: A sustainable future with renewable energy resources", *Energies*, vol. 13, 23 Dec. 2020, ISSN: 19961073. DOI: 10.3390/en13236269.

[128] H. Xu, L. Cheng, N. Qi, and X. Zhou, "Peak shaving potential analysis of distributed load virtual power plants", *Energy Reports*, vol. 6, pp. 515–525, Dec. 2020, ISSN: 23524847. DOI: 10.1016/j.egyr.2020.11.204.

[129] N. Qi, L. Cheng, H. Xu, Z. Wang, and X. Zhou, "Practical demand response potential evaluation of air-conditioning loads for aggregated customers", *Energy Reports*, vol. 6, pp. 71–81, Dec. 2020, ISSN: 23524847. DOI: 10.1016/j.egyr.2020.12.019.

[130] N. Rezaei and M. Kalantar, "Smart microgrid hierarchical frequency control ancillary service provision based on virtual inertia concept: An integrated demand response and droop controlled distributed generation framework", *Energy Conversion and Management*, vol. 92, pp. 287–301, 2015, ISSN: 0196-8904. DOI: https://doi.org/10.1016/j.enconman.2014.12.049. [Online]. Available: https://www.sciencedirect.com/science/article/pii/S0196890414010887.

[131] S. Yilmaz, P. Cuony, and C. Chanez, "Prioritize your heat pump or electric vehicle? analysing design preferences for direct load control programmes in swiss households", *Energy Research and Social Science*, vol. 82, Dec. 2021, ISSN: 22146296. DOI: 10.1016/j.erss.2021.102319.

[132] R. Tang, S. Wang, and C. Yan, "A direct load control strategy of centralized air-conditioning systems for building fast demand response to urgent requests of smart grids", *Automation in Construction*, vol. 87, pp. 74–83, Mar. 2018, ISSN: 09265805. DOI: 10.1016/j.autcon.2017.12.012.

[133] S. V. Oprea and A. Bâra, "Edge and fog computing using iot for direct load optimization and control with flexibility services for citizen energy communities", *Knowledge-Based Systems*, vol. 228, Sep. 2021, ISSN: 09507051. DOI: 10.1016/j.knosys.2021.107293.

[134] A. S. Markensteijn, J. E. Romate, and C. Vuik, "A graph-based model framework for steady-state load flow problems of general multi-carrier energy systems", *Applied Energy*, vol. 280, Dec. 2020, ISSN: 03062619. DOI: 10.1016/j.apenergy.2020.115286.

[135] F. Strehle, M. Pfeifer, L. Kölsch, *et al.*, "Towards port-hamiltonian modeling of multi-carrier energy systems: A case study for a coupled electricity and gas distribution system", vol. 51, Elsevier B.V., Jan. 2018, pp. 463–468. DOI: 10.1016/j.ifacol.2018.03.078.

[136] H. Khorsand and A. R. Seifi, "Probabilistic energy flow for multi-carrier energy systems", *Renewable and Sustainable Energy Reviews*, vol. 94, pp. 989–997, Oct. 2018, ISSN: 18790690. DOI: 10.1016/j.rser.2018.07.008.

[137] A. Kazemdehdashti, M. Mohammadi, A. R. Seifi, and M. Rastegar, "Stochastic energy management in multi-carrier residential energy systems", *Energy*, vol. 202, Jul. 2020, ISSN: 03605442. DOI: 10.1016/j.energy.2020.117790.

[138] S. Rahmani and N. Amjady, "Optimal operation strategy for multi-carrier energy systems including various energy converters by multi-objective information gap decision theory and enhanced directed search domain method", *Energy Conversion and Management*, vol. 198, Oct. 2019, ISSN: 01968904. DOI: 10.1016/j.enconman.2019.111804.

[139] E. E. Michaelides, "Thermodynamics, energy dissipation, and figures of merit of energy storage systems—a critical review", *Energies*, vol. 14, 19 Oct. 2021, ISSN: 19961073. DOI: 10.3390/en14196121.

[140] A. M. Othman and H. A. Gabbar, *Energy storage integration within interconnected micro energy grids*. Elsevier Inc., 2017, pp. 207–220, ISBN: 9780128092323. DOI: 10.1016/B978-0-12-805343-0.00009-7.

[141] A. K. Rohit, K. P. Devi, and S. Rangnekar, "An overview of energy storage and its importance in indian renewable energy sector: Part i – technologies and comparison", *Journal of Energy Storage*, vol. 13, pp. 10–23, Oct. 2017, ISSN: 2352152X. DOI: 10.1016/j.est.2017.06.005.

[142] S. Kuravi, J. Trahan, D. Y. Goswami, M. M. Rahman, and E. K. Stefanakos, "Thermal energy storage technologies and systems for concentrating solar power plants", *Progress in Energy and Combustion Science*, vol. 39, pp. 285–319, 4 Aug. 2013, ISSN: 03601285. DOI: 10.1016/j.pecs.2013.02.001.

[143] H. Mahon, D. O'Connor, D. Friedrich, and B. Hughes, "A review of thermal energy storage technologies for seasonal loops", *Energy*, vol. 239, Jan. 2022, ISSN: 03605442. DOI: 10.1016/j.energy.2021.122207.

[144] P. McKenna, W. J. Turner, and D. P. Finn, "Thermal energy storage using phase change material: Analysis of partial tank charging and discharging on system performance in a building cooling application", *Applied Thermal Engineering*, vol. 198, Nov. 2021, ISSN: 13594311. DOI: 10.1016/j.applthermaleng.2021.117437.

[145] D. Fernandes, F. Pitié, G. Cáceres, and J. Baeyens, "Thermal energy storage: "how previous findings determine current research priorities"", *Energy*, vol. 39, pp. 246–257, 1 2012, ISSN: 03605442. DOI: 10.1016/j.energy.2012.01.024.

[146] K. Mongird, V. V. Viswanathan, P. J. Balducci, *et al.*, "Energy storage technology and cost characterization report", Jul. 2019. DOI: 10.2172/1573487. [Online]. Available: https://www.osti.gov/biblio/1573487.

[147] M. A. Hannan, S. B. Wali, P. J. Ker, *et al.*, "Battery energy-storage system: A review of technologies, optimization objectives, constraints, approaches, and outstanding issues", *Journal of Energy Storage*, vol. 42, Oct. 2021, ISSN: 2352152X. DOI: 10.1016/j.est.2021.103023.

[148] Y. Yang, E. G. Okonkwo, G. Huang, S. Xu, W. Sun, and Y. He, "On the sustainability of lithium ion battery industry – a review and perspective", *Energy Storage Materials*, vol. 36, pp. 186–212, Apr. 2021, ISSN: 24058297. DOI: 10.1016/j.ensm.2020.12.019.

[149] K. Lourenssen, J. Williams, F. Ahmadpour, R. Clemmer, and S. Tasnim, "Vanadium redox flow batteries: A comprehensive review", *Journal of Energy Storage*, vol. 25, Oct. 2019, ISSN: 2352152X. DOI: 10.1016/j.est.2019.100844.

[150] R. K. Emmett and M. E. Roberts, "Recent developments in alternative aqueous redox flow batteries for grid-scale energy storage", *Journal of Power Sources*, vol. 506, Sep. 2021, ISSN: 03787753. DOI: 10.1016/j.jpowsour.2021.230087.

[151] M. Alqarni, "Sodium sulfur batteries allocation in high renewable penetration microgrids using coronavirus herd immunity optimization", *Ain Shams Engineering Journal*, vol. 13, 2 Mar. 2022, ISSN: 20904479. DOI: 10.1016/j.asej.2021.09.017.

[152] Y. Li, L. Shi, X. Gao, *et al.*, "Constructing a charged-state na-nicl2 battery with nicl2/graphene aerogel composite as cathode", *Chemical Engineering Journal*, vol. 421, Oct. 2021, ISSN: 13858947. DOI: 10.1016/j.cej.2020.127853.

[153] D. F. Quintero-Pulido, G. Hoogsteen, M. V. T. Kortenaar, J. L. Hurink, R. E. Hebner, and G. J. Smit, "Characterization of storage sizing for an off-grid house in the us and the netherlands", *Energies*, vol. 11, 2 Feb. 2018, ISSN: 19961073. DOI: 10.3390/en11020265.

[154] R. K. Sankaralingam, S. Seshadri, J. Sunarso, A. I. Bhatt, and A. Kapoor, "Overview of the factors affecting the performance of vanadium redox flow batteries", *Journal of Energy Storage*, vol. 41, p. 102 857, 2021, ISSN: 2352-152X. DOI: https://doi.org/10.1016/j.est.2021.102857. [Online]. Available: https://www.sciencedirect.com/science/article/pii/S2352152X21005806.

[155] L. Briot, M. Petit, Q. Cacciuttolo, and M.-C. Pera, "Aging phenomena and their modelling in aqueous organic redox flow batteries: A review", *Journal of Power Sources*, vol. 536, p. 231 427, 2022, ISSN: 0378-7753. DOI: https://doi.org/10.1016/j.jpowsour.2022.231427. [Online]. Available: https://www.sciencedirect.com/science/article/pii/S0378775322004372.

[156] D. Kumar, S. K. Rajouria, S. B. Kuhar, and D. Kanchan, "Progress and prospects of sodium-sulfur batteries: A review", *Solid State Ionics*, vol. 312, pp. 8–16, 2017, ISSN: 0167-2738. DOI: https://doi.org/10.1016/j.ssi.2017.10.004. [Online]. Available: https://www.sciencedirect.com/science/article/pii/S0167273817306501.

[157] D. Kumar, S. B. Kuhar, and D. Kanchan, "Room temperature sodium-sulfur batteries as emerging energy source", *Journal of Energy Storage*, vol. 18, pp. 133–148, 2018, ISSN: 2352-152X. DOI: https://doi.org/10.1016/j.est.2018.04.021. [Online]. Available: https://www.sciencedirect.com/science/article/pii/S2352152X1730614X.

[158] E. Chemali, M. Preindl, P. Malysz, and A. Emadi, "Electrochemical and electrostatic energy storage and management systems for electric drive vehicles: State-of-the-art review and future trends", *IEEE Journal of Emerging and Selected Topics in Power Electronics*, vol. 4, no. 3, pp. 1117–1134, 2016. DOI: 10.1109/JESTPE.2016.2566583.

[159] C. M. Krishna, "Managing battery and supercapacitor resources for real-time sporadic workloads", *IEEE Embedded Systems Letters*, vol. 3, pp. 32–36, 1 Mar. 2011, ISSN: 19430663. DOI: 10.1109/LES.2010.2098847.

[160] Y. Abdul Wahab, M. N. Naseer, A. A. Zaidi, *et al.*, "Super capacitors in various dimensionalities: Applications and recent advancements", in *Encyclopedia of Energy Storage*, L. F. Cabeza, Ed., Oxford: Elsevier, 2022, pp. 682–691, ISBN: 978-0-12-819730-1. DOI: https://doi.org/10.1016/B978-0-12-819723-3.00020-2. [Online]. Available: https://www.sciencedirect.com/science/article/pii/B9780128197233000202.

[161] H. Behi, M. Behi, A. Ghanbarpour, *et al.*, "Enhancement of the thermal energy storage using heat-pipe-assisted phase change material", *Energies*, vol. 14, 19 Oct. 2021, ISSN: 19961073. DOI: 10.3390/en14196176.

[162] G. Mor, J. Cipriano, B. Grillone, *et al.*, "Operation and energy flexibility evaluation of direct load controlled buildings equipped with heat pumps", *Energy and Buildings*, vol. 253, Dec. 2021, ISSN: 03787788. DOI: 10.1016/j.enbuild.2021.111484.

[163] Y. Dai, L. Chen, Y. Min, *et al.*, "A general model for thermal energy storage in combined heat and power dispatch considering heat transfer constraints", *IEEE Transactions on Sustainable Energy*, vol. 9, pp. 1518–1528, 4 Oct. 2018, ISSN: 19493029. DOI: 10.1109/TSTE.2018.2793360.

[164] L. Fan, Z. Tu, and S. H. Chan, "Recent development of hydrogen and fuel cell technologies: A review", *Energy Reports*, vol. 7, pp. 8421–8446, Nov. 2021, ISSN: 23524847. DOI: 10.1016/j.egyr.2021.08.003.

[165] H. Ishaq, I. Dincer, and G. F. Naterer, "Performance investigation of an integrated wind energy system for co-generation of power and hydrogen", *International Journal of Hydrogen Energy*, vol. 43, no. 19, pp. 9153–9164, 2018, ISSN: 0360-3199. DOI: https://doi.org/10.1016/j.ijhydene.2018.03.139. [Online]. Available: https://www.sciencedirect.com/science/article/pii/S0360319918309303.

[166] M. İnci, "Future vision of hydrogen fuel cells: A statistical review and research on applications, socio-economic impacts and forecasting prospects", *Sustainable Energy Technologies and Assessments*, vol. 53, p. 102 739, 2022, ISSN: 2213-1388. DOI: https://doi.org/10.1016/j.seta.2022.102739. [Online]. Available: https://www.sciencedirect.com/science/article/pii/S2213138822007871.

[167] A. Yilanci, I. Dincer, and H. Ozturk, "A review on solar-hydrogen/fuel cell hybrid energy systems for stationary applications", *Progress in Energy and Combustion Science*, vol. 35, no. 3, pp. 231–244, 2009, ISSN: 0360-1285. DOI: https://doi.org/10.1016/j.pecs.2008.07.004. [Online]. Available: https://www.sciencedirect.com/science/article/pii/S0360128508000439.

[168] D. K. Kim, K. H. Rho, Y. Na, and M. Kim, "Evaluation of energy storage technologies for efficient usage of wind power in the far-eastern region: A techno-economic analysis", *Journal of Energy Storage*, vol. 39, p. 102 595, 2021, ISSN: 2352-152X. DOI: https://doi.org/10.1016/j.est.2021.102595. [Online]. Available: https://www.sciencedirect.com/science/article/pii/S2352152X21003388.

[169] K. Kumar, M. Alam, and V. Dutta, "Energy management strategy for integration of fuel cell-electrolyzer technologies in microgrid", *International Journal of Hydrogen Energy*, vol. 46, pp. 33 738–33 755, 68 Oct. 2021, ISSN: 03603199. DOI: 10.1016/j.ijhydene.2021.07.203.

[170] L. Zhang and J. Xiang, "The performance of a grid-tied microgrid with hydrogen storage and a hydrogen fuel cell stack", *Energy Conversion and Management*, vol. 87, pp. 421–427, 2014, ISSN: 01968904. DOI: 10.1016/j.enconman.2014.07.045.

[171] M. M. Kinnon, G. Razeghi, and S. Samuelsen, "The role of fuel cells in port microgrids to support sustainable goods movement", *Renewable and Sustainable Energy Reviews*, vol. 147, Sep. 2021, ISSN: 18790690. DOI: 10.1016/j.rser.2021.111226.

[172] *SAE Standard J1772 - Electric Vehicle and Plug in Hybrid Electric Vehicle Conductive Charge Coupler*. SAE, 2017.

[173] *INTECO Standard N121:2020 - Infraestructura de centros de recarga para Vehículos Eléctricos (VE). Requisitos*. INTECO, 2020.

[174] *IEC Standard 61851-1 - Electric vehicle conductive charging system - Part 1: General requirements*. IEC, 2017.

[175] A. Colmenar-Santos, A. M. Muñoz-Gómez, E. Rosales-Asensio, and Á. López-Rey, "Electric vehicle charging strategy to support renewable energy sources in europe 2050 low-carbon scenario", *Energy*, vol. 183, pp. 61–74, Sep. 2019, ISSN: 03605442. DOI: 10.1016/j.energy.2019.06.118.

[176] C. Zheng, W. Li, and Q. Liang, "An energy management strategy of hybrid energy storage systems for electric vehicle applications", *IEEE Transactions on Sustainable Energy*, vol. 9, pp. 1880–1888, 4 Oct. 2018, ISSN: 19493029. DOI: 10.1109/TSTE.2018.2818259.

[177] M. Gilanifar and M. Parvania, "Clustered multi-node learning of electric vehicle charging flexibility", *Applied Energy*, vol. 282, Jan. 2021, ISSN: 03062619. DOI: 10.1016/j.apenergy.2020.116125.

[178] Y. Zhao, Z. Wang, Z. J. M. Shen, and F. Sun, "Data-driven framework for large-scale prediction of charging energy in electric vehicles", *Applied Energy*, vol. 282, Jan. 2021, ISSN: 03062619. DOI: 10.1016/j.apenergy.2020.116175.

[179] J. W. Lee, M. H. S. M. Haram, G. Ramasamy, S. P. Thiagarajah, E. E. Ngu, and Y. H. Lee, "Technical feasibility and economics of repurposed electric vehicles batteries for power peak shaving", *Journal of Energy Storage*, vol. 40, Aug. 2021, ISSN: 2352152X. DOI: 10.1016/j.est.2021.102752.

[180] M. E. Glavin and W. G. Hurley, "Optimisation of a photovoltaic battery ultracapacitor hybrid energy storage system", *Solar Energy*, vol. 86, pp. 3009–3020, 10 Oct. 2012, ISSN: 0038092X. DOI: 10.1016/j.solener.2012.07.005.

[181] H. Jung, H. Wang, and T. Hu, "Control design for robust tracking and smooth transition in power systems with battery/supercapacitor hybrid energy storage devices", *Journal of Power Sources*, vol. 267, pp. 566–575, Dec. 2014, ISSN: 03787753. DOI: 10.1016/j.jpowsour.2014.05.061.

[182] Z. Cabrane, M. Ouassaid, and M. Maaroufi, "Analysis and evaluation of battery-supercapacitor hybrid energy storage system for photovoltaic installation", *International Journal of Hydrogen Energy*, vol. 41, pp. 20 897–20 907, 45 Dec. 2016, ISSN: 03603199. DOI: 10.1016/j.ijhydene.2016.06.141.

[183] Y. Zhu, H. Wang, and Z. Zhu, "Improved vsg control strategy based on the combined power generation system with hydrogen fuel cells and super capacitors", *Energy Reports*, vol. 7, pp. 6820–6832, Nov. 2021, ISSN: 23524847. DOI: 10.1016/j.egyr.2021.10.056.

[184] D. Rezzak and N. Boudjerda, "Robust energy management strategy based on nonlinear cascade control of fuel cells-super capacitors hybrid power system", *International Journal of Hydrogen Energy*, vol. 45, pp. 23 254–23 274, 43 Sep. 2020, ISSN: 03603199. DOI: 10.1016/j.ijhydene.2020.05.250.

[185] Y. Zhou, H. Obeid, S. Laghrouche, M. Hilairet, and A. Djerdir, "A novel second-order sliding mode control of hybrid fuel cell/super capacitors power system considering the degradation of the fuel cell", *Energy Conversion and Management*, vol. 229, Feb. 2021, ISSN: 01968904. DOI: 10.1016/j.enconman.2020.113766.

[186] A. Kadri, H. Marzougui, A. Aouiti, and F. Bacha, "Energy management and control strategy for a dfig wind turbine/fuel cell hybrid system with super capacitor storage system", *Energy*, vol. 192, Feb. 2020, ISSN: 03605442. DOI: 10.1016/j.energy.2019.116518.

[187] M. Jami, Q. Shafiee, M. Gholami, and H. Bevrani, "Control of a super-capacitor energy storage system to mimic inertia and transient response improvement of a direct current micro-grid", *Journal of Energy Storage*, vol. 32, Dec. 2020, ISSN: 2352152X. DOI: 10.1016/j.est.2020.101788.

[188] M. H. Shams, H. Niaz, J. Na, A. Anvari-Moghaddam, and J. J. Liu, "Machine learning-based utilization of renewable power curtailments under uncertainty by planning of hydrogen systems and battery storages", *Journal of Energy Storage*, vol. 41, Sep. 2021, ISSN: 2352152X. DOI: 10.1016/j.est.2021.103010.

[189] Q. Li, R. Li, Y. Pu, S. Li, C. Sun, and W. Chen, "Coordinated control of electric-hydrogen hybrid energy storage for multi-microgrid with fuel cell/ electrolyzer/ pv/ battery", *Journal of Energy Storage*, vol. 42, Oct. 2021, ISSN: 2352152X. DOI: 10.1016/j.est.2021.103110.

[190] B. S. K. Patnam and N. M. Pindoriya, "Demand response in consumer-centric electricity market: Mathematical models and optimization problems", *Electric Power Systems Research*, vol. 193, Apr. 2021, ISSN: 03787796. DOI: 10.1016/j.epsr.2020.106923.

[191] U. Datta, A. Kalam, and J. Shi, "Smart control of bess in pv integrated ev charging station for reducing transformer overloading and providing battery-to-grid service", *Journal of Energy Storage*, vol. 28, Apr. 2020, ISSN: 2352152X. DOI: 10.1016/j.est.2020.101224.

[192] M. H. Khooban, T. Niknam, F. Blaabjerg, P. Davari, and T. Dragicevic, "A robust adaptive load frequency control for micro-grids", *ISA Transactions*, vol. 65, pp. 220–229, Nov. 2016, ISSN: 00190578. DOI: 10.1016/j.isatra.2016.07.002.

[193] P. R. Mendes, L. V. Isorna, C. Bordons, and J. E. Normey-Rico, "Energy management of an experimental microgrid coupled to a v2g system", *Journal of Power Sources*, vol. 327, pp. 702–713, Sep. 2016, ISSN: 03787753. DOI: 10.1016/j.jpowsour.2016.07.076.

[194] L. Sun, J. Qiu, X. Han, X. Yin, and Z. Y. Dong, "Capacity and energy sharing platform with hybrid energy storage system: An example of hospitality industry", *Applied Energy*, vol. 280, Dec. 2020, ISSN: 03062619. DOI: 10.1016/j.apenergy.2020.115897.

[195] T. Weitzel, M. Schneider, C. H. Glock, F. Löber, and S. Rinderknecht, "Operating a storage-augmented hybrid microgrid considering battery aging costs", *Journal of Cleaner Production*, vol. 188, pp. 638–654, Jul. 2018, ISSN: 09596526. DOI: 10.1016/j.jclepro.2018.03.296.

[196] Y. Zhang, F. Meng, R. Wang, B. Kazemtabrizi, and J. Shi, "Uncertainty-resistant stochastic mpc approach for optimal operation of chp microgrid", *Energy*, vol. 179, pp. 1265–1278, Jul. 2019, ISSN: 03605442. DOI: 10.1016/j.energy.2019.04.151.

[197] Z. Pan, J. Wu, H. Sun, and M. Abeysekera, "Quantification of operational flexibility from a heating network", vol. 145, Elsevier Ltd, 2018, pp. 516–521. DOI: 10.1016/j.egypro.2018.04.075.

[198] A. Alahäivälä, J. Corbishley, J. Ekström, J. Jokisalo, and M. Lehtonen, "A control framework for the utilization of heating load flexibility in a day-ahead market", *Electric Power Systems Research*, vol. 145, pp. 44–54, 2017, ISSN: 0378-7796. DOI: https://doi.org/10.1016/j.epsr.2016.12.019. [Online]. Available: https://www.sciencedirect.com/science/article/pii/S0378779616305314.

[199] J. Salpakari, J. Mikkola, and P. D. Lund, "Improved flexibility with large-scale variable renewable power in cities through optimal demand side management and power-to-heat conversion", *Energy Conversion and Management*, vol. 126, pp. 649–661, Oct. 2016, ISSN: 01968904. DOI: 10.1016/j.enconman.2016.08.041.

[200] A. Arabkoohsar, "Non-uniform temperature district heating system with decentralized heat pumps and standalone storage tanks", *Energy*, vol. 170, pp. 931–941, Mar. 2019, ISSN: 03605442. DOI: 10.1016/j.energy.2018.12.209.

[201] H. Pieper, T. Ommen, B. Elmegaard, and W. B. Markussen, "Assessment of a combination of three heat sources for heat pumps to supply district heating", *Energy*, vol. 176, pp. 156–170, Jun. 2019, ISSN: 03605442. DOI: 10.1016/j.energy.2019.03.165.

[202] P. Li, N. Nord, I. S. Ertesvåg, Z. Ge, Z. Yang, and Y. Yang, "Integrated multiscale simulation of combined heat and power based district heating system", *Energy Conversion and Management*, vol. 106, pp. 337–354, Dec. 2015, ISSN: 01968904. DOI: 10.1016/j.enconman.2015.08.077.

[203] A. A. M. Aljabery, H. Mehrjerdi, S. Mahdavi, and R. Hemmati, "Multi carrier energy systems and energy hubs: Comprehensive review, survey and recommendations", *International Journal of Hydrogen Energy*, vol. 46, pp. 23 795–23 814, 46 Jul. 2021, ISSN: 03603199. DOI: 10.1016/j.ijhydene.2021.04.178.

[204] B. Mohandes, S. Acharya, M. S. E. Moursi, A. S. Al-Sumaiti, H. Doukas, and S. Sgouridis, "Optimal design of an islanded microgrid with load shifting mechanism between electrical and thermal energy storage systems", *IEEE Transactions on Power Systems*, vol. 35, no. 4, pp. 2642–2657, 2020. DOI: 10.1109/TPWRS.2020.2969575.

[205] H. Masrur, M. Shafie-Khah, M. J. Hossain, and T. Senjyu, "Multi-energy microgrids incorporating ev integration: Optimal design and resilient operation", *IEEE Transactions on Smart Grid*, vol. 13, no. 5, pp. 3508–3518, 2022. DOI: 10.1109/TSG.2022.3168687.

[206] P. Li, Y. Huang, W. Qi, and J. Gan, "Capacity co-optimization of thermal and battery energy storage system in multi-energy complementary system", in *2019 IEEE Innovative Smart Grid Technologies - Asia (ISGT Asia)*, 2019, pp. 3815–3819. DOI: 10.1109/ISGT-Asia.2019.8881407.

[207] H. Wang, N. Good, and P. Mancarella, "Modelling and valuing multi-energy flexibility from community energy systems", in *2017 Australasian Universities Power Engineering Conference (AUPEC)*, 2017, pp. 1–6. DOI: 10.1109/AUPEC.2017.8282399.

[208] M. Bagheri-Sanjareh, M. H. Nazari, M. Ebadat-Parast, and S. H. Hosseinian, "Cooperative utilization of electrical and thermal storage systems for uninterruptible supply of a greenhouse microgrid", in *2021 11th Smart Grid Conference (SGC)*, 2021, pp. 1–6. DOI: 10.1109/SGC54087.2021.9664060.

[209] P. Trairat and D. Banjerdpongchai, "Optimal dispatch of cogeneration with thermal and battery energy storage for bems subject to load demand uncertainty", in *2022 19th International Conference on Electrical Engineering/Electronics, Computer, Telecommunications and Information Technology (ECTI-CON)*, 2022, pp. 1–4. DOI: 10.1109/ECTI-CON54298.2022.9795588.

[210] T. Ha, Y. J. ZHANG, and V. V. T. J. HUANG, "Energy hub modeling to minimize residential energy costs considering solar energy and bess", *Journal of Modern Power Systems and Clean Energy*, vol. 5, no. 3, pp. 389–399, 2017. DOI: 10.1007/s40565-017-0281-4.

[211] M. Geraedts, J. Alpízar-Castillo, L. Ramírez-Elizondo, and P. Bauer, "Optimal sizing of a community level thermal energy storage system", in *2022 IEEE 21st Mediterranean Electrotechnical Conference (MELECON)*, 2022, pp. 52–57. DOI: 10.1109/MELECON53508.2022.9842945.

[212] C. Thai and J. Brouwer, "Challenges estimating distributed solar potential with utilization factors: California universities case study", *Applied Energy*, vol. 282, Jan. 2021, ISSN: 03062619. DOI: 10.1016/j.apenergy.2020.116209.

[213] A. Ameur, A. Berrada, K. Loudiyi, and R. Adomatis, *Performance and energetic modeling of hybrid PV systems coupled with battery energy storage*. Elsevier, 2021, pp. 195–238, ISBN: 9780128214039. DOI: 10.1016/b978-0-12-821403-9.00008-1.

[214] M. C. Argyrou, C. C. Marouchos, S. A. Kalogirou, and P. Christodoulides, "Modeling a residential grid-connected pv system with battery–supercapacitor storage: Control design and stability analysis", *Energy Reports*, vol. 7, pp. 4988–5002, Nov. 2021, ISSN: 23524847. DOI: 10.1016/j.egyr.2021.08.001.

[215] J. Alpízar-Castillo, "Simplified model to approach the theoretical clear sky solar pv generation curve through a gaussian approximation", *Nigerian Journal of Technology*, vol. 40, pp. 44–48, 1 Mar. 2021, ISSN: 0331-8443. DOI: 10.4314/njt.v40i1.7.

[216] S. Newman, K. Shiozawa, J. Follum, *et al.*, "A comparison of pv resource modeling for sizing microgrid components", *Renewable Energy*, vol. 162, pp. 831–843, Dec. 2020, ISSN: 18790682. DOI: 10.1016/j.renene.2020.08.074.

[217] L. W. Chong, Y. W. Wong, R. K. Rajkumar, and D. Isa, "Modelling and simulation of standalone pv systems with battery-supercapacitor hybrid energy storage system for a rural household", vol. 107, Elsevier Ltd, Feb. 2017, pp. 232–236. DOI: 10.1016/j.egypro.2016.12.135.

[218] V. Vega-Garita, L. Ramirez-Elizondo, G. R. C. Mouli, and P. Bauer, "Review of residential pv-storage architectures", Institute of Electrical and Electronics Engineers Inc., Jul. 2016, ISBN: 9781467384636. DOI: 10.1109/ENERGYCON.2016.7514039.

3

Residential Multi-carrier Energy Management Systems: Description and Modelling

"People with talent often have the wrong impression that things will go as they think"

Karma Akabane, Assassination Classroom, Chapter 143, by Yusei Matsui.

This Chapter is based on:

- **J. Alpízar-Castillo**, L. Ramirez-Elizondo, and P. Bauer, "Modelling and Evaluating Different Multi-Carrier Energy System Configurations for a Dutch House," Applied Energy, 364, 123197, April. 2024, doi: 10.1016/j.apenergy.2024.123197.

3.1. Introduction

Heat generation in residential buildings consumed 13 % of the total energy consumption in the Netherlands in 2018 [1]. In response, the government has promoted the transition to fossil fuel-free alternatives, as 96 % of Dutch households still use gas for heating [2]. Two main approaches are considered to diminish the usage of boilers: the deployment of fifth-generation district heating networks and directly replacing the gas boilers with other equipment that does not consume gas. The former was studied in [3], proposing an optimal sizing for the components in a case study in the north of the Netherlands. The latter approach includes multiple alternatives, such as heat pumps (HP), photovoltaic-thermal (PVT), infrared panels, and, more recently, thermal energy storage systems (TESS). This Chapter focused on studying the second approach, considering only alternatives that use a hydraulic network for space heating, specifically photovoltaic-thermal systems, heat pumps, and thermal energy storage systems.

Photovoltaic-thermal modules combine the advantages of solar collectors and photovoltaic systems; they can generate electric and thermal power simultaneously. Although the initial intention of coupling a heating exchange mechanism was to improve the PV cell efficiency, during the last decade, the frequency of studies related to PVT systems has grown considerably, given their opportunities to provide heat to other systems [4]. There are many classifications for PVT modules, but the working principle is essentially the same for them. A fluid (gas or liquid) circulates through a heat exchanger in the PVT module, extracting the heat from direct radiation, ambient temperature, or both [5]. Then, the fluid circulates through another heat exchanger to release the heat absorbed from the module. The review presented by [5] shows the evolution of electrical and thermal efficiencies from 2009 to 2019, showing ranges of electrical efficiencies from 6.4 % to 28 % and thermal efficiencies ranging from 27 % to 79 %, resulting in total efficiencies between 45 % and 91 %. Nevertheless, most of the literature uses simplified models to estimate the energy balance without considering the transport phenomena within the module in detail [6], [7].

Thermal energy storage has been explored to increase the efficiency and reliability of thermal networks [8]. More specifically, [9] studied the actors related to deploying such systems in the Dutch context, including different configurations. Some authors like [10] and [11] have coupled thermal energy storage systems to heat pumps to minimize their electrical consumption. This kind of thermal energy storage application is called pumped thermal energy storage or Carnot batteries [12]. On the other hand, authors such as [13] and [14] studied how coupling a PVT system with a HP through a water tank can increase the system's overall performance. In their work, the water tank is referred to as thermal energy storage; however, due to its capacity, it mainly works as a buffer for short-term demand peaks, but it cannot sustain the supply for periods longer than a few hours. For the purposes of this dissertation, this tank is considered as an intrinsic component of the PVT system, as detailed in Section 3.2.3. Phase-changing materials have also been used to improve the efficiency of PVT modules [15]. Units of such materials added to the PVT modules are also referred to as thermal energy storage [16] or thermal energy storage units [17]. When adding any type of thermal energy storage, most of the literature (excluding the phase-change materials attached directly to the PVT) locates the storage device indoors [18]. To avoid confusion with the terminology, this work con-

siders *thermal energy storage* only the systems that can provide thermal power directly to the thermal network to supply the demand.

Heat pumps are the leading technology in residential heating electrification. They rely on a fluid with boiling points lower than typical outdoor temperatures. After boiling, the gas is compressed to increase its temperature. The hot gas then provides heat through a heat exchanger, to finally be depressurized, causing it to condense and restart the cycle. Thanks to this operation principle, they tend to be three to four times more efficient than fossil fuel boilers [19]. Still, many heat pump technologies have been reported in the literature. Some use ground heat exchangers, like coils, U pipes, and boreholes, which were compared in [20]. Air source technologies use evaporators in contact with the environment, which require less infrastructure costs than the ground heat exchangers but at the cost of more variable temperatures, reducing the COP of the device in cold climates [21]. For this reason, research is also required on working fluids [22] and alternatives to increase the temperature at the evaporator, for example, coupling a PVT system, as mentioned before.

However, literature [23] suggests that deploying heat pumps in low-voltage distribution networks can cause challenges in maintaining a stable and reliable network due to their high power consumption. Simultaneously, it might worsen the instability conditions caused by distributed renewable energy sources (DRES), like photovoltaic (PV), as, on the one hand, high penetration of DRES in the low-voltage networks leads to overvoltages, as the surplus of power not consumed by the users is sent back to the grid. On the other hand, the power peaks of the HP alone are higher than the typical residential load, which might cause undervoltages. This combination, if not addressed promptly, can lead to severe congestion in the network.

One possible solution is to minimize the power exchange directly at the household level, including electrical or thermal energy storage systems. A combination of two or more different forms of energy is called a multi-carrier or multi-energy system. For instance, a PV and a battery energy storage system (BESS) would be a single carrier, whereas changing the PV to a PVT adds a thermal subsystem, resulting in a multi-carrier system. Recent works have demonstrated multi-carrier systems' opportunities to provide flexibility [24], [25]. However, due to the novelty of these systems, there is no standard terminology. Some literature refers to multi-carrier systems as hybrid [7]. However, the word "hybrid" has been used for multiple connotations, even within the context of energy engineering. For example, [26] refers to one or more generators (e.g., PV, hydro or diesel) coupled with a storage system as a hybrid system, [27] refers to a PVT system as a hybrid photovoltaic system combined with heat exchangers, and [28] calls hybrid energy storage to the couple of two different energy storage systems (in this case, BESS and hydrogen). In this dissertation, the term multi-carrier energy systems (MCES) is used to avoid confusion with the terminology.

This Chapter determines the contributions of a heat pump, a PVT system and an underground thermal storage, as part of a multi-carrier energy system, to meet the space heating and electric demands of a household in the Netherlands. The thermal losses of the TESS to the ground were modelled, and four device combinations, comprised of devices with different sizes were compared in terms of energy consumption from the grid, thermal comfort and equivalent $CO_{2,eq}$ emissions. To elaborate on the current state-

of-the-art of different asset configurations, a comprehensive search using Scopus was performed. Previous works in multi-carrier energy systems were searched using combinations of the terms: "photovoltaic thermal," "heat pump," "thermal energy storage," and "battery energy storage," as well as their respective acronyms, i.e., PVT, HP, TES, and BESS. Different ways of writing the terms using wildcards were also included, and the search was narrowed to only results available in English. After the first search, it became apparent that numerous publications use PVT for desalination, phase change materials to enhance the output of PVT systems, and combined BESS with HP in electric vehicles (including buses and ships); thus, those terms were excluded in the second query. Works dedicated exclusively to sizing the components instead of analyzing their interactions were also excluded. Then, the results were classified depending on the application. Table 3.1 summarises the number of publications found per application and some examples per application.

The literature review suggested that research has focused on residential applications. Of the 95 papers found, 64 correspond to residential, whereas for industrial and utility applications, we found 13 and 18, respectively. Most of the work regarding residential applications includes heat pumps as part of the overall system architecture, demonstrating their role in the energy transition and the challenges related to their limitations in conditions with lower temperatures. It was found that PVT systems and TESS are frequently used as support devices for the heat pump. In the case of TESS, they are usually water tanks with volumes below 1 m^3, thus can be located inside the house. However, TESS require higher volumes to provide sustained thermal power for space heating. To avoid occupying valuable space indoors, the TESS can be located underground outside the house, but this alternative still has to be studied regarding thermal losses to the soil. In addition, it is often assumed that the heat pumps would drastically reduce the equivalent emissions of the heating system compared to systems with gas boilers. However, emission contributions from increased use of the energy network still have to be investigated. This way, three main research gaps arise: the inclusion of PVT and TESS as part of the main thermal network and not as support devices, the effects of locating TESS underground outside the house, and the real equivalent emissions associated with heating electrification in residential buildings through heat pumps. Based on the research gaps found, this Chapter:

1. determines the thermal contributions of including photo-voltaic thermal and underground thermal energy storage systems into a residential space heating network,

2. proposes an analytical model for an underground water tank thermal energy storage system considering the soil's temperature gradient, and

3. evaluates the suitability of a MCES comprised of different combinations of a PVT, a HP, a TESS, and a BESS for household applications, based on electrical consumption from the grid, thermal power generation for space heating, and equivalent CO_2 emissions.

Table 3.1: Previous research in residential multi-carrier energy systems containing PVT, HP, TESS, BESS, or their combination.

Combination	Publications	Examples	Year	Contribution
PVT, HP	17	[29]	2020	Four PVT modules, a 150 L tank, and a HP were coupled, resulting in an average heating power of 4.7 kW and a COP of 6.16, under the environmental conditions of Northern China.
		[30]	2020	A simulation of a PVT coupled to the regenerator of the HP with TRNSYS suggested higher performance than a HP alone and electric output 4.2 % higher than a PV. However, the additional costs of the PVT do not compensate for the benefits.
PVT, TESS	1	[31]	2022	Using a sorption TESS, it was possible to achieve energy efficiencies up to 38 % in Hangzhou, China, 33 % in Helsinki, Finland, and 35 % in Copenhagen, Denmark.
HP, TESS	19	[32]	2017	A design and operational optimization for a HP paired with a TESS in the UK demonstrated that the equipment and operational costs of the HP system alone are higher than traditional heating systems, but integrating a TESS and using time-of-use tariffs reduce the operational costs to a competitive range.
		[33]	2022	Using the National Grid's Future Energy Scenarios of the United Kingdom, the benefit of installing TESS alongside HP at the residential level has system values between £1.1-2.3 bn/year in 2050, with annual long-term benefits per customer between £200-300. Also, TESS can considerably reduce the peak loading of heating electrification by as much as 2.3 GW at 50 % TESS uptake.
PVT, HP, TESS	4	[34]	2023	A residential building was modelled using Simulink demonstrated that reducing the temperature required at the could source of the HP increases the fraction of thermal energy produced by the PVT stored in the TESS 6 %/°C, and increasing the capacity of the TESS increases the fraction of load covered by the PVT by up to 30 %.

		[35]	2022	Several technologies were simulated using TRNSYS to determine their integration with a building with seven floors and 51 apartments in Helsinki, Finland. The results suggest that the physical boundaries of the buildings might limit the amount of renewables needed to generate the power to supply the demand in Nordic countries, requiring the usage of extended or virtual boundaries of the building.
		[36]	2021	A TESS coupled with a HP was evaluated when combined either with PVT or solar collectors, simulating in TRNSYS a case study in Busan, Korea. The solar collectors were able to provide 27 % of the annual cooling, heating, and domestic hot water demand, whereas the PVT covered 9 %. The PVT produced 19.1 % less electrical power than a PV due to continuous low temperatures.
PVT, BESS	11	[37]	2018	A system was optimally sized and simulated for conditions in Athens, Greece, London, United Kingdom, and Zaragoza, Spain. The results covered up to 65 % of the electric demand and 60, 30, and 45 % of the thermal demand, respectively, displacing 3.87, 1.65, and 1.54 tons of $CO_{2,eq}$. The payback times were 15.6 years in Athens and 11.6 in Zaragoza.
		[38]	2021	PV and PVT systems were modelled and tested in Ghana. A techno-economic analysis over 25 suggests that the PVT performs better than the PV despite having higher initial costs, as the levelized cost of exergy is 0.33 US$/kWh for the PVT and 0.45 US$/kWh for the PV when installed with BESS.
		[39]	2015	A system was simulated for Khuznin, Iran, suggesting that covering the thermal and electrical demands would require an over-dimensioned BESS.
HP, BESS	-	-	-	-
TESS, BESS	2	[40]	2023	A power management system with reinforcement learning, a BESS and TESS were controlled for peak shaving, achieving a 42.2 % reduction in the BESS capacity.

		[41]	2015	A demand response program was simulated for a residential energy hub, including load shifting and curtailing, and flexible storage usage, leading to cost savings of up to 40 %.
PVT, HP, BESS	2	[42]	2019	A residential building was simulated using Matlab/Simulink in Central Europe. HP performance increases when coupled with the PVT system.
		[43]	2015	An experimental setup was deployed in Spain and tested from December 2012 to April 2013. The HP had a maximum COP of 6, with an average of 3.2. The overall system saved between 574 to 836 kg of $CO_{2,eq}$, depending on the type of boiler used as reference.
PVT, TESS, BESS	-	-	-	-
HP, TESS, BESS	8	[44]	2022	Detached houses in southern Finland were simulated to evaluate the advantages of multi-carrier energy storage. The possibility of selling surplus energy stored in BESS improves the profitability to a renewable fraction of 20 % for 2019 and 50 % for 2021. However, hydrogen and TESS resulted in less profitable scenarios than using the grid unless sustained high market prices or subsidies are present.
		[45]	2022	Different control algorithms for multi-carrier systems were evaluated, highlighting the performance of the self-consumption maximization prioritizing the TESS over the BESS.
		[46]	2021	A multi-objective approach for peak-shaving and flexibility capacity was proposed, minimizing user costs and equipment degradation, tested with 2000 cases of buildings, resulting in an energy bill increase of less than 0.5 %, a peak demand reduction of 11 %, and increased flexibility capacity of 16.5 %.
PVT, HP, TESS, BESS	-	-	-	-

3.2. System Description

The thermal network of the proposed multi-carrier energy system considers a water tank thermal energy storage system, a PVT, and a heat pump to meet the thermal demand for space heating. Sections 3.2.1 to 3.2.5 present a discrete analytical model for each component, allowing us to couple them into a thermal network model. A similar approach is done for the thermal carrier of the system. It was considered a PVT and a battery energy storage system that, supported by the grid, can meet the base electric demand plus the heat pump consumption, which are described from section 3.2.6 to 3.2.9. Most of these models are validated in the literature; thus, Section 3.3.1 is dedicated to validating the thermal demand, the PVT and the underground TESS, using data available of measurements for those systems. Note that the models in this Chapter can be extrapolated to other case scenarios provided adequate constant values. Finally, four different combinations of the components are studied to determine their suitability for combined residential electric and thermal loads. The electric, thermal and equivalent emission performances were used as KPIs to determine the best combination.

3.2.1. Thermal Demand

For this dissertation, the thermal demand is considered only for space heating. Domestic hot water is another category of residential thermal loads. The work in [47] demonstrated that domestic hot water accounts for up to 2135 kWh/year in medium-sized European residences. However, the interaction with the overall system is different. Normally, domestic hot water requires high thermal power during short periods [18] and has a separate thermal network [48]. As this thesis focuses on the space heating thermal network, the thermal demand of domestic hot water will not be studied. An approach similar to [49] was used to model a house. The house comprises four rooms with specific thermal masses and losses to the environment through walls, double-glass windows and the roof, as shown in Figure 3.1. Each room's internal energy change can be calculated with

$$\frac{dU}{dt} = \sum_{j=1}^{m} \dot{Q}_j = \sum_{i=1}^{n} \frac{d(m\,c\,T)_i}{dt}. \tag{3.1}$$

Since no mass exchange is considered between the exterior and interior of the house, one can rewrite (3.1) as

$$\frac{\Delta T}{\Delta t} \sum_{i=1}^{n} m_i\, c_i = \sum_{j=1}^{m} \dot{Q}_j\,, \tag{3.2}$$

thus, if an uniform indoor temperature is considered, then

$$\frac{\Delta T_{\text{in}}}{\Delta t} \sum_{i=1}^{n} m_i c_i = \dot{Q}_{\text{PVT}} + \dot{Q}_{\text{TESS}} + \dot{Q}_{\text{HP}} - \dot{Q}_{\text{D}}\,, \tag{3.3}$$

where $\dot{Q}_{\text{D}}$ includes the heat losses to the environment (thermal demand), $\dot{Q}_{\text{PVT}}$ the heat supplied by the PVT, $\dot{Q}_{\text{TESS}}$ the heat supplied by the thermal energy storage and $\dot{Q}_{\text{HP}}$ the heat supplied by the heat pump. m_i and c_i are the thermal mass of the air in the room, the walls, the roof and windows, and their specific heats, respectively. ΔT_{in} is the change in the room temperature during the timestep Δt. Thus, the temperature in the room can

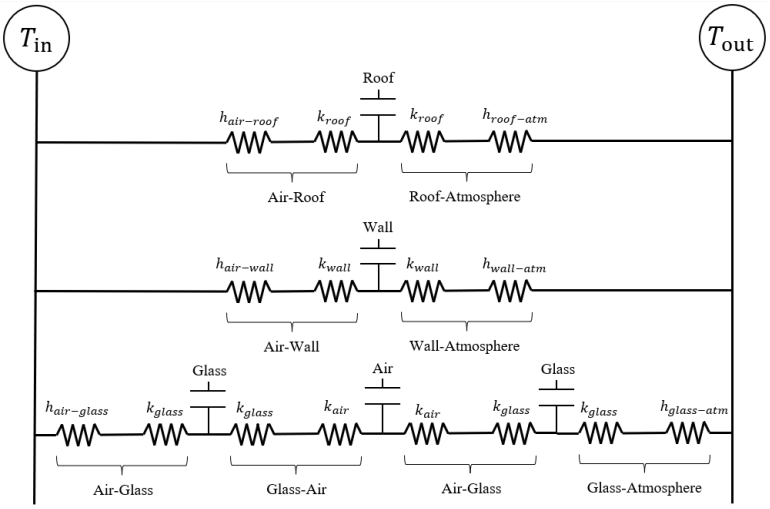

Figure 3.1: Convective and conductive thermal losses through the roof, walls, and windows considered per house room.

be approximated using a discrete timestep k as:

$$T_{\text{in}}(k+1) = T_{\text{in}}(k) + \frac{\Delta t \left[\dot{Q}_{\text{PVT}}(k) + \dot{Q}_{\text{TESS}}(k) + \dot{Q}_{\text{HP}}(k) - \dot{Q}_{\text{D}}(k)\right]}{\sum_{i=1}^{n} m_i c_i}. \tag{3.4}$$

The heat transfer between rooms, to the ground, and radiative heat transfer are neglected. Although radiative heat through the windows can provide some heat to the inside of the house, this heat would be more significant during the Summer, when heating is less likely to be needed. In this work, we do not consider cooling mechanisms.

Each room's overall heat transfer coefficient depends on the conductive and convective losses coefficients, as shown in Figure 3.1. Note that the conductive losses are divided into two identical sections with half of the distance, as we modelled the thermal mass in between. This coefficient can be calculated as

$$U = \left(\sum_{i=1}^{n} \frac{1}{h_i} + \sum_{j=1}^{m} \frac{L_j}{k_j}\right)^{-1}, \tag{3.5}$$

where h_i are the convection heat transfer coefficients, k_j the materials' conductivity and L_j the thickness of the convective materials. This way, the heat losses of the house to the environment through the walls, roof and windows can be calculated as:

$$\dot{Q}_L(k) = \sum_{i=1}^{n} U_i A_i \Delta T(k), \tag{3.6}$$

where U_i and A_i are the total convection heat transfer coefficient and the surface area, respectively, and ΔT is the temperature difference between the outside and the inside of the house.

On the other hand, the losses through ventilation and infiltration can be calculated following the method presented in [50]. In both cases, the equation is governed by the air mass exchange inside and outside the house. The ventilation losses $\dot{Q}_v$ can be calculated as:

$$\dot{Q}_v(k) = c_a \rho_a q_v \Delta T(k), \tag{3.7}$$

where c_a and ρ_a are the specific heat capacity and density of the air, $\Delta T(k)$ is the temperature difference between the outside and inside of the house (in degree Fahrenheit). To estimate the required ventilation airflow q_v (in cubic feet per minute), [50] suggest using

$$q_v = 0.03 A_{\text{cf}} + 7.5 (N_{\text{br}} + 1), \tag{3.8}$$

where A_{cf} is the building conditioned area (in feet squared) and N_{br} is the number of bedrooms in the house. Similarly, the infiltration losses can be estimated with

$$\dot{Q}_i(k) = c_a \rho_a q_i \Delta T(k). \tag{3.9}$$

The infiltration airflow q_i can be estimated using

$$q_i(k) = A_{\text{es}} A_u \sqrt{C_s |\Delta T(k)| + C_w u^2(k)}, \tag{3.10}$$

where A_{es} is the building's exposed area (in feet squared), A_u is the unit leakage area (in inches squared per feet squared), C_s is the stacking coefficient, C_w is the wind coefficient and u is the wind speed (in miles per hour).

In addition, buildings can have internal sources of heat. In residential buildings, the occupants of the building and appliances like stoves, ovens and incandescent lighting could contribute to increasing the temperature. In this case, the building considered is a two-person house with highly efficient appliances, induction cooking and LED lighting; thus, internal heat gains can be neglected in this case [50]. This way, the total thermal demand of the house is

$$\dot{Q}_D = \dot{Q}_L + \dot{Q}_v + \dot{Q}_i \tag{3.11}$$

3.2.2. THERMAL ENERGY STORAGE SYSTEM

The thermal energy storage system was considered to be an underground, perfectly mixed water tank. To model the tank, an analysis similar as in Section 3.2.1 was performed, i.e., no mass exchange was considered between the TESS and the heating system of the house or with the ground; thus, (3.1) can be rewritten as:

$$\dot{Q}_{\text{PVT}}^{\text{TESS}}(k) + \dot{Q}_{\text{HP}}^{\text{TESS}}(k) - \dot{Q}_{\text{TESS}}(k) - \dot{Q}^{\text{SD}}(k) = \sum_{i=1}^{n} m_i c_i \frac{\Delta T_{\text{TESS}}}{\Delta t}, \tag{3.12}$$

where $\dot{Q}_{\text{PVT}}^{\text{TESS}}$ and $\dot{Q}_{\text{HP}}^{\text{TESS}}$ are the heat supplied by the solar collectors and heat pump to charge the TESS, respectively. $\dot{Q}_{\text{TESS}}$ the heat supplied by the thermal energy storage to the thermal demand, $\dot{Q}^{\text{SD}}$ is the thermal loss to the soil around the TESS, m_i and c_i are the thermal mass fluid in the TESS and the walls and their specific heats, respectively,

and ΔT_{TESS} is the change in the TESS temperature during the timestep Δt. Thus, one can use

$$T_{\text{TESS}}(k+1) = T_{\text{TESS}}(k) + \frac{\Delta t \left[\dot{Q}^{\text{TESS}}_{\text{PVT}}(k) + \dot{Q}^{\text{TESS}}_{\text{HP}}(k) - \dot{Q}_{\text{TESS}}(k) - \dot{Q}^{\text{SD}}(k)\right]}{\sum_{i=1}^{n} m_i c_i}, \tag{3.13}$$

to approximate the temperature of the TESS.

The charge $\dot{Q}^{\text{c}}_{\text{TESS}}$ or discharge power $\dot{Q}_{\text{TESS}}$ are

$$\dot{Q}^{\text{c}}_{\text{TESS}}(k) = \eta^{c}_{\text{TESS}}(k)\, \dot{m} c_{\text{f}} \Delta T, \tag{3.14}$$

and

$$\dot{Q}_{\text{TESS}}(k) = \eta^{d}_{\text{TESS}}(k)\, \dot{m} c_{\text{f}} \Delta T, \tag{3.15}$$

where η_{TESS} is the charge or discharge efficiency as corresponds, $\dot{m}$ is the mass flow through the heat exchangers of the TESS, c_{f} is the fluid specific heat capacity, and ΔT is the temperature difference between the inlet and outlet of the heat exchanger. In this case, it was considered a TESS with separate charge and discharge coils; therefore, the TESS can be charged and discharged simultaneously. During the charge, the outlet temperature was assumed to be the same as the fluid in the tank. During the discharge, an output temperature equal to the supply temperature of the thermal network was considered.

The thermal energy stored in the tank can be expressed as

$$Q_{\text{TESS}}(k) = C_{\text{TESS}} SoC_{\text{TESS}}(k), \tag{3.16}$$

and its capacity C_{TESS} as

$$C_{\text{TESS}} = \rho_{\text{f}} V c_{\text{f}} \left(T^{\max} - T^{\min}\right), \tag{3.17}$$

where ρ_{f} is the fluid density, V is the tank volume, and $T^{\max}$ and $T^{\min}$ are the maximum and minimum temperatures allowed in the tank. As there are no changes in the fluid's mass or composition, the state-of-charge of the TESS depends only on its temperature, i.e.,

$$SoC_{\text{TESS}} = \frac{C_{\text{TESS}}(k)}{C_{\text{TESS}}} = \frac{\Delta T(k)}{\Delta T^{\max}} = \frac{T(k) - T^{\min}}{T^{\max} - T^{\min}}. \tag{3.18}$$

where $T(k)$ is the current temperature of the fluid.

The self-discharge of the tank, $\dot{Q}^{\text{SD}}$, is produced by the heat transferred to the soil around the tank. Figure 3.2a shows a diagram of the losses considered for the tank. Soil's temperature was assumed constant at any specific depth y. This way, convective heat transfers from the water to the tank's walls and conductive heat from the walls to the soil. To determine the soil's temperature, the soil was modelled as a semi-infinite solid with one-dimensional depth coordinates y, considering rotational symmetry, as proposed by [51] and [52]. The heat diffusion in the soil follows the equation

$$\frac{\partial^2 T_{\text{s}}(y,t)}{\partial y^2} = \frac{1}{\alpha} \frac{\partial T_{\text{s}}(y,t)}{\partial t}. \tag{3.19}$$

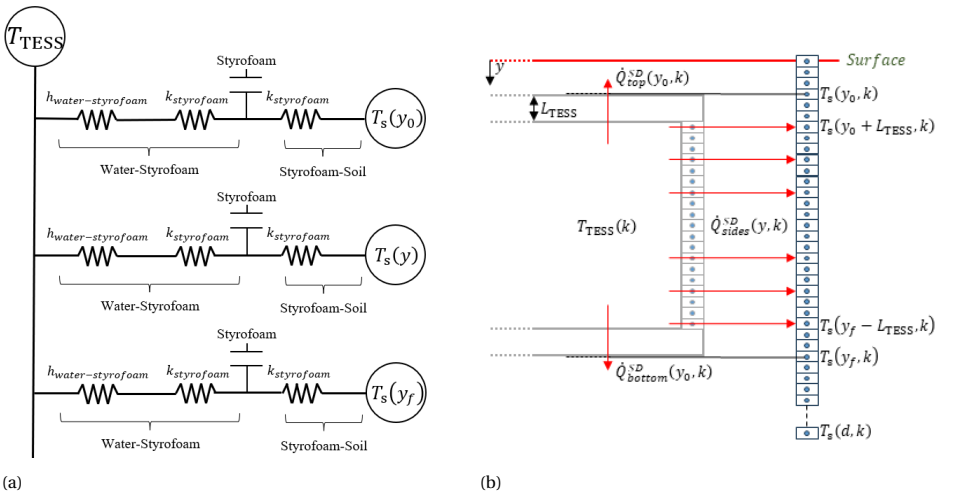

Figure 3.2: Thermal model used for the TESS. (a) Conductive thermal losses through the walls. (b) Discrete represesentation.

Using the finite difference method to discretize the equation, the space-dependant side of (3.19) can be rewritten using central differencing as

$$\frac{\partial^2 T_s(y,t)}{\partial y^2} = \frac{T_s(y-\Delta y,k) - 2T_s(y,k) + T_s(y+\Delta y,k)}{\Delta y^2}. \tag{3.20}$$

Similarly, using forward differencing, the time-dependant side of (3.19) can be rewritten as

$$\frac{\partial T_s(y,t)}{\partial t} = \frac{T_s(y,k+1) - T_s(y,k)}{\Delta t}. \tag{3.21}$$

This way, and gathering the time Δt between timesteps, the grid size sqared Δy^2, and the thermal diffusivity of the soil α as

$$r = \frac{\alpha \Delta t}{\Delta y^2}, \tag{3.22}$$

(3.19) can be reorganized as

$$T_s(y,k+1) = r\left[T_s(y-\Delta y,k) - 2T_s(y,k) + T_s(y+\Delta y,k)\right] + T_s(y,k) \tag{3.23}$$

The boundary conditions for (3.23) are the temperatures at the surface and at a point underground, at a depth d, with a known and constant temperature. The first boundary condition can be obtained by considering Fourier's Conductivity Law, Newton's Law of Cooling, and Stefan-Boltzmann's Law of Radiation, resulting in

$$-k_{soil}\frac{\partial T_s(y,t)}{\partial y} = h\left[T_{sky}(t) - T_s(y=0,t)\right] - \varepsilon \Delta R(t) + \alpha_0 G(t), \tag{3.24}$$

where T_{amb} is the ambient temperature, $T_s\left(y=0,t\right)$ is the temperature at the surface, ε is the soil's thermal emissivity, α_0 is the soil's diffusivity, G is the solar radiation and

$$\Delta R\left(t\right)=\sigma\left[T_{\mathrm{s}}^{4}\left(t-\Delta t\right)-T_{\mathrm{sky}}^{4}\left(t\right)\right] \tag{3.25}$$

is the thermal radiation. There are many empirical expressions that can be used to estimate the sky temperature. The recalibrated Brunt model

$$T_{\mathrm{sky}}\left(t\right)=0.62+0.056\left[6.11\left(\frac{RH}{100}\right)e^{\left(\frac{17.63\,T_{\mathrm{amb}}\left(t\right)}{243.04+T_{\mathrm{amb}}\left(t\right)}\right)}\right]^{0.5} \tag{3.26}$$

was selected as a widely used expression to estimate the sky temperature [53], where RH is the relative humidity.

The total heat transfer coefficient h can be written as

$$h\left(t\right)=h^{\mathrm{conv}}\left(t\right)+h^{r}\left(t\right), \tag{3.27}$$

where

$$h^{\mathrm{conv}}\left(t\right)=\begin{cases}5.7+3.8\,v_{\mathrm{w}}\left(t\right) & \forall\, v_{\mathrm{w}}\in[0,5[\,\mathrm{m/s}\\ 6.47+\,v_{\mathrm{w}}^{0.78}\left(t\right) & \forall\, v_{\mathrm{w}}\in[5,10[\,\mathrm{m/s}\end{cases} \tag{3.28}$$

corresponds to the coefficient of convective heat transfer, depending on the wind speed v_{w}, and

$$h^{r}\left(t\right)=\varepsilon\sigma\left[T_{\mathrm{s}}^{2}\left(t-\Delta t\right)+T_{sky}^{2}\left(t\right)\right]\left[T_{\mathrm{s}}\left(t-\Delta t\right)+T_{sky}\left(t\right)\right] \tag{3.29}$$

corresponds to the coefficient of radiant heat transfer [54].

Discretizing the Fourier term in (3.30) as

$$-k_{\mathrm{soil}}\frac{\partial T_{\mathrm{s}}\left(y,t\right)}{\partial y}=-k_{\mathrm{soil}}\frac{T_{\mathrm{s}}\left(y=d,t\right)-T_{\mathrm{s}}\left(y=0,t\right)}{d}, \tag{3.30}$$

allows to obtain the discrete expression for the temperature at the surface at any timestep

$$T_{\mathrm{s}}\left(y=0,k\right)=\frac{k_{\mathrm{soil}}T_{\mathrm{s}}\left(y=d,k\right)+dhT_{\mathrm{amb}}\left(k\right)-d\varepsilon\Delta R\left(k\right)+d\alpha_{o}G\left(k\right)}{dh+k_{\mathrm{soil}}}, \tag{3.31}$$

or in terms of the effective temperature T_e

$$T_{\mathrm{s}}\left(y=0,k\right)=\frac{k_{\mathrm{soil}}T_{\mathrm{s}}\left(y=d,k\right)+dhT_{e}\left(k\right)}{dh+k_{\mathrm{soil}}}, \tag{3.32}$$

where

$$T_{e}\left(k\right)=T_{\mathrm{amb}}\left(k\right)-\frac{\varepsilon\Delta R\left(k\right)}{h}+\frac{\alpha_{o}G\left(k\right)}{h} \tag{3.33}$$

The second boundary condition for (3.23) is the annual mean effective temperature, $\bar{T}_e$. This temperature is found at a point underground, where the effects at the surface and the geothermal heating are neglectable. This point was considered at a depth of 6 m [51].

Given the above, one can use

$$\dot{Q}^{\mathrm{SD}} = \dot{Q}^{\mathrm{SD}}_{\mathrm{top}} + \dot{Q}^{\mathrm{SD}}_{\mathrm{sides}} + \dot{Q}^{\mathrm{SD}}_{\mathrm{bottom}} \tag{3.34}$$

to estimate the heat lost by the TESS to the ground. Considering a constant temperature for the top and bottom walls of the tank, $T_{\mathrm{s}}\left(y = y_0, k\right)$ and $T_{\mathrm{s}}\left(y = y_f, k\right)$, respectively, and a discrete gradient of temperature in the soil, $T_{\mathrm{s}}\left(y_i, k\right)$ where $y_i \in \{y_0 + L_{\mathrm{TESS}}, y_0 + L_{\mathrm{TESS}} + \Delta y, ..., y_f - L_{\mathrm{TESS}}\}$, as shown in Figure 3.2b, (3.6) allows to estimate the components of (3.34) as

$$\dot{Q}^{\mathrm{SD}}_{\mathrm{top}} = U_{\mathrm{TESS}} A_{\mathrm{top}} \left[T_{\mathrm{TESS}}(k) - T_{\mathrm{s}}\left(y = y_0, k\right)\right], \tag{3.35}$$

$$\dot{Q}^{\mathrm{SD}}_{\mathrm{sides}} = \sum_{i=1}^{n} U_{\mathrm{TESS}} A_{\Delta y} \left[T_{\mathrm{TESS}}(k) - T_{\mathrm{s}}\left(y_i, k\right)\right], \tag{3.36}$$

and

$$\dot{Q}^{\mathrm{SD}}_{\mathrm{bottom}} = U_{\mathrm{TESS}} A_{\mathrm{bottom}} \left[T_{\mathrm{TESS}}(k) - T_{\mathrm{s}}\left(y = y_f, k\right)\right]. \tag{3.37}$$

3.2.3. PHOTOVOLTAIC-THERMAL SYSTEM

A similar approach to [54] was used to approach to model the PVT module. However, a different grouping strategy was used for the constants in the equations, and considered the tank and the modules connected in series as part of a hydraulic system. The model considers a layered PVT module, as shown in Figure 3.3a, and includes reflective, radiative, convective, and conductive losses, as shown in Figure 3.3b. Note that the PV layer comprises glass, two layers of ethylene vinyl acetate (EVA), the Si cell, and a tedlar layer. The governing equations of the model, as a function of the surface temperatures of the glass cover, the Si cell, the thermal absorber, and the fluid, T_{glass}, T_{PV}, T_{a} and T_{f}, respectively, are

$$\begin{cases} T_{\mathrm{glass}}(k+1) = C_1(k)\, T_{\mathrm{glass}}(k) + C_2(k)\, T_{\mathrm{PV}}(k) - D_1(k) \\ T_{\mathrm{PV}}(k+1) = C_3(k)\, T_{\mathrm{glass}}(k) + C_4(k)\, T_{\mathrm{PV}}(k) + C_5(k)\, T_{\mathrm{a}}(k) - D_2(k) \\ T_{\mathrm{a}}(k+1) = C_6(k)\, T_{\mathrm{PV}}(k) + C_7(k)\, T_{\mathrm{a}}(k) + C_8(k)\, T_{\mathrm{f}}(k) - D_3(k) \\ T_{\mathrm{f}}(k+1) = C_9(k)\, T_{\mathrm{a}}(k) + C_{10}(k)\, T_{\mathrm{f}}(k) - D_4(k) \end{cases}, \tag{3.38}$$

where

$$C_1(k) = \frac{A_{\mathrm{glass}}\Delta t}{m_{\mathrm{glass}} c_{\mathrm{glass}}} \left[\frac{m_{\mathrm{glass}} c_{\mathrm{glass}}}{A_{\mathrm{glass}}\Delta t} - h^{\mathrm{conv}}_{\mathrm{glass}}(k) - h^{r}_{\mathrm{glass}}(k) - h_{\mathrm{gap}}(k) - h^{r}_{\mathrm{glass\text{-}PV}}(k)\right], \tag{3.39}$$

$$C_2(k) = \frac{A_{\mathrm{glass}}\Delta t}{m_{\mathrm{glass}} c_{\mathrm{glass}}} \left[h_{\mathrm{gap}}(k) + h^{r}_{\mathrm{glass\text{-}PV}}(k)\right], \tag{3.40}$$

$$C_3(k) = \frac{A_{\mathrm{PV}}\Delta t}{m_{\mathrm{PV}} c_{\mathrm{PV}}} \left[h_{\mathrm{gap}}(k) + h^{r}_{\mathrm{glass\text{-}PV}}(k)\right], \tag{3.41}$$

$$C_4(k) = \frac{A_{\mathrm{PV}}\Delta t}{m_{\mathrm{PV}} c_{\mathrm{PV}}} \left[\frac{m_{\mathrm{PV}} c_{\mathrm{PV}}}{A_{\mathrm{PV}}\Delta t} - h_{\mathrm{gap}}(k) - h^{r}_{\mathrm{glass\text{-}PV}}(k) - h^{\mathrm{cond}}_{\mathrm{PV\text{-}a}}(k)\right], \tag{3.42}$$

$$C_5(k) = \frac{A_{\mathrm{PV}}\Delta t}{m_{\mathrm{PV}} c_{\mathrm{PV}}} h^{\mathrm{cond}}_{\mathrm{PV\text{-}a}}(k), \tag{3.43}$$

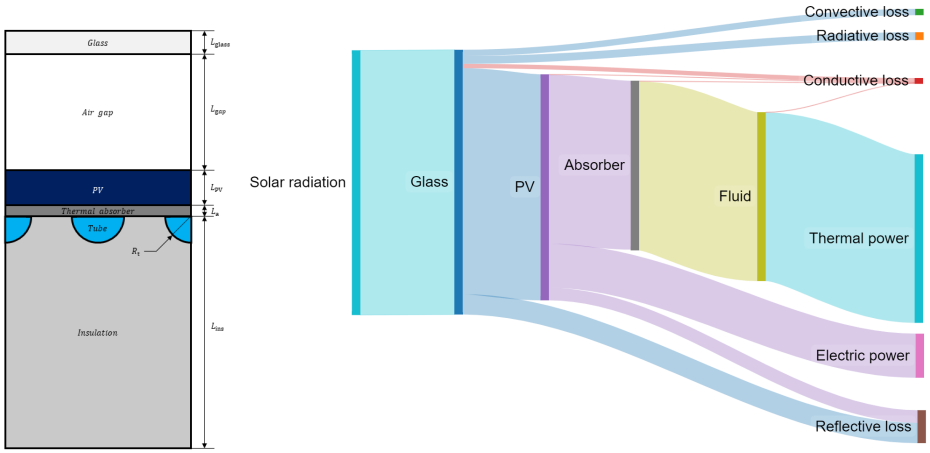

(a) (b)

Figure 3.3: Representation of the thermal model for the PVT. (a) Schematic of the PVT layers. (b) Heat transfer and loss distribution.

$$C_6(k) = \frac{A_a \Delta t}{m_a c_a} h_{\text{PV-a}}^{\text{cond}}(k), \tag{3.44}$$

$$C_7(k) = \frac{\Delta t}{m_a c_a}\left[\frac{m_a c_a}{\Delta t} - h_{\text{PV-a}}^{\text{cond}}(k) A_a - h_{\text{a-f}}(k) A_t^{\text{cross}} - h_a^{\text{cond}}(k) A_a\right], \tag{3.45}$$

$$C_8(k) = \frac{\Delta t}{m_a c_a} h_{\text{a-f}}(k) A_t^{\text{cross}}, \tag{3.46}$$

$$C_9(k) = \frac{A_t^{\text{cross}} \Delta t}{m_f c_f} h_{\text{a-f}}(k), \tag{3.47}$$

$$C_{10}(k) = \frac{\Delta t}{m_f c_f}\left[\frac{m_f c_f}{\Delta t} - h_{\text{a-f}}(k) A_t^{\text{surf}} - 2\dot{m}_f c_f\right], \tag{3.48}$$

$$D_1(k) = \frac{A_{\text{glass}} \Delta t}{m_{\text{glass}} c_{\text{glass}}}\left[h_{\text{glass}}^{\text{conv}} T_{\text{amb}}(k) + h_{\text{glass}}^{r}(k) T_{\text{sky}}(k) + \alpha_{\text{glass}} G(k)\right], \tag{3.49}$$

$$D_2(k) = \frac{A_{\text{PV}} \Delta t}{m_{\text{PV}} c_{\text{PV}}} \alpha_{\text{PV}} \tau_{\text{glass}} G(k)\left[1 - \eta_{\text{PV}}(k)\right], \tag{3.50}$$

$$D_3(k) = \frac{A_a \Delta t}{m_a c_a} h_a^{\text{cond}}(k) T_{\text{amb}}(k), \tag{3.51}$$

and

$$D_4(k) = 2\frac{\Delta t}{m_f} \dot{m}_f T_f^{\text{in}}(k). \tag{3.52}$$

The nomenclature for parameters of the equations (3.39)-(3.52) is as follows: h_{i-j}^{cond} and h_{i-j}^{r} represent the conductive and radiative thermal coefficients from the $i-$th to the $j-$th layer, respectively, h_i and h_i^{conv} represent the total thermal coefficient and the convective thermal coefficient (released to the environment) for the $i-$th layer. A_i, m_i, c_i,

L_i, α_i and τ_i are the area, mass, specific heat, thickness, absorbance and transmittance of the $i-$th layer. $A_{\mathrm{t}}^{\mathrm{cross}}$ is the tube's cross area (in contact with the thermal absorber), and $A_{\mathrm{t}}^{\mathrm{surf}}$ is the tube's lower surface area (in contact with the isolation layer). G is the solar radiation and η_{PV} is the PV cell efficiency.

In this case $h_{\mathrm{glass}}^{\mathrm{conv}}$ can be calculated using (3.28), $h_{\mathrm{glass}}^{\mathrm{r}}$ using (3.29), and h_{gap} using (3.5) for the convective heat transfer through the glass and the first layer of EVA, and

$$h_{\text{glass-PV}}^{\mathrm{conv}}(k) = \frac{\mathrm{Nu}_{\mathrm{gap}} k_{\mathrm{gap}}}{L_{\mathrm{gap}}}, \tag{3.53}$$

for the convective term, where $\mathrm{Nu}_{\mathrm{gap}}$ and k_{gap} are the Nusselt number and thermal conductivity of the air. The radiative heat transfer coefficient between the glass and the PV layer can be calculated with

$$h_{\text{glass-PV}}^{\mathrm{r}}(k) = \frac{1}{\frac{1}{\varepsilon_{\mathrm{glass}}} + \frac{1}{\varepsilon_{\mathrm{PV}}} - 1} \sigma \left[T_{\mathrm{glass}}^2(k-1) + T_{PV}^2(k-1) \right] \left[T_{\mathrm{glass}}(k-1) + T_{PV}(t-\Delta) \right]. \tag{3.54}$$

The conductive heat transfer coefficient through the layers of the PV (glass, EVA, Si cell and tedlar) to the thermal absorber, $h_{\text{PV-a}}^{\mathrm{con}}$, can be calculated using the conductive component of (3.5) [55]. The heat transfer coefficient between the fluid and the thermal absorber depends on the flow and can be calculated as

$$h_{\text{a-f}}(k) = \begin{cases} 2\dfrac{k_{\mathrm{f}}}{D_{\mathrm{H}}} & \forall\, \mathrm{Re} = 0 \\ 4.36\dfrac{k_{\mathrm{f}}}{D_{\mathrm{H}}} & \forall\, 0 < \mathrm{Re} < 2300 \\ 0.023\dfrac{k_{\mathrm{f}}}{D_{\mathrm{H}}} \mathrm{Re}^{0.8} \mathrm{Pr}^{0.4} & \forall\, \mathrm{Re} \geq 2300 \end{cases}, \tag{3.55}$$

where $\mathrm{D_H}$ is the hydraulic diameter of the tube, and Re and Pr are the Reynolds and Prandtl numbers, respectively. For the fluid temperature in the tubes, it was considered that

$$T_{\mathrm{f}}(k) = \frac{T_{\mathrm{f}}^{\mathrm{in}}(k) + T_{\mathrm{f}}^{\mathrm{out}}(k)}{2} \tag{3.56}$$

is the relation between the inlet and outlet temperatures, $T_{\mathrm{f}}^{\mathrm{in}}$ and $T_{\mathrm{f}}^{\mathrm{out}}$. Last, as the PV efficiency depends on the PV temperature, it can be calculated using

$$\eta_{\mathrm{PV}}(k) = \eta_{\mathrm{PV}}^{\mathrm{STC}} \left[1 - \beta_{\mathrm{PV}} \left(T_{\mathrm{PV}}(k) - T_{\mathrm{ref}} \right) \right], \tag{3.57}$$

where $\eta_{\mathrm{PV}}^{\mathrm{STC}}$ is the PV efficiency under standard test conditions, and T_{ref} is the reference temperature for the standard test conditions.

Finally, the thermal power generated by the module can be expressed as

$$\dot{Q}_{\mathrm{PVT,\,mod}}(k) = \eta_{\mathrm{T}} N \dot{m}_{\mathrm{f}} c_{\mathrm{f}} \left[T_{\mathrm{f}}^{\mathrm{out}}(k) - T_{\mathrm{f}}^{\mathrm{in}}(k) \right] = 2\eta_{\mathrm{T}} N \dot{m}_{\mathrm{f}} c_{\mathrm{f}} \left[T_{\mathrm{f}}(k) - T_{\mathrm{f}}^{\mathrm{in}}(k) \right], \tag{3.58}$$

where η_{T} is the efficiency of the heat exchanger and N is the number of tubes in the PVT.

The PVT module generally uses fluids and mass flows different than the tank and the thermal network; thus, the heat transferred from the PVT system to the thermal network uses a water tank as the coupling device. In this case, the inlet temperature of the PVT module is the tank temperature. To estimate the temperature in the tank T_{PVT}, one can adapt (3.13) for the PVT system, resulting in

$$T_{\text{PVT}}(k+1) = T_{\text{PVT}}(k) + \frac{\Delta t\left[\dot{Q}_{\text{PVT, mod}}(k) - \dot{Q}_{\text{PVT}}(k) - \dot{Q}_{\text{PVT}}^{\text{TESS}}(k)\right]}{m_{\text{tank}} c_{\text{tank}}}, \tag{3.59}$$

where $\dot{Q}_{\text{PVT}}$ is the thermal power from the PVT system to the thermal network, and $\dot{Q}_{\text{PVT}}^{\text{TESS}}$ is the thermal power from the PVT system to the TESS.

3.2.4. HEAT PUMP

As the PVT depends on the weather conditions, a heat pump was included to ensure at least one heat source when weather conditions are unfavourable and the TESS is unavailable. To model the behaviour of the heat pump, we used

$$\text{COP}(k) = 7.90471 e^{-0.024\left[T_{\text{ret}}(k) - T_{\text{amb}}(k)\right]} \tag{3.60}$$

as proposed by [56], where T_{ret} is the temperature of the working fluid at the inlet of the heat pump, and the constants were obtained after a linear regression from 10 different models of residential heat pumps.

The relation between the electric power consumption and the thermal power delivered by the HP is

$$P_{\text{HP}}(k) = \frac{\dot{Q}_{\text{HP}}(k)}{\text{COP}(k)}, \tag{3.61}$$

where the thermal power delivered by the HP is a function of the mass flow rate $\dot{m}_f$, the fluid specific heat c_f, the required supply temperature T_{sup} the return temperature T_{ret}, and the heat exchanger efficiency η_{HP} given by

$$\dot{Q}_{\text{HP}}(k) = \eta_{\text{HP}} \dot{m}_f c_f \left[T_{\text{sup}} - T_{\text{ret}}(k)\right]. \tag{3.62}$$

3.2.5. THERMAL NETWORK

The thermal network shown in Figure 3.4 was used to coupled the thermal demand with the PVT, the TESS, and the HP. From the thermal balance for the coupled system given in (3.3), one can approximate the return temperature at the different points of the network as

$$T_1(k) = T_4(k-1) - \frac{\dot{Q}_{\text{D}}(k-1)}{\dot{m}_f c_f}, \tag{3.63}$$

$$T_2(k) = T_4(k-1) + \frac{\dot{Q}_{\text{PVT}}(k) - \dot{Q}_{\text{D}}(k-1)}{\dot{m}_f c_f}, \tag{3.64}$$

$$T_3(k) = T_4(k-1) + \frac{\dot{Q}_{\text{PVT}}(k) + \dot{Q}_{\text{TESS}}(k) - \dot{Q}_{\text{D}}(k-1)}{\dot{m}_f c_f}, \tag{3.65}$$

$$T_4(k) = T_4(k-1) + \frac{\dot{Q}_{\text{PVT}}(k) + \dot{Q}_{\text{TESS}}(k) + \dot{Q}_{\text{HP}}(k) - \dot{Q}_{\text{D}}(k-1)}{\dot{m}_f c_f}, \tag{3.66}$$

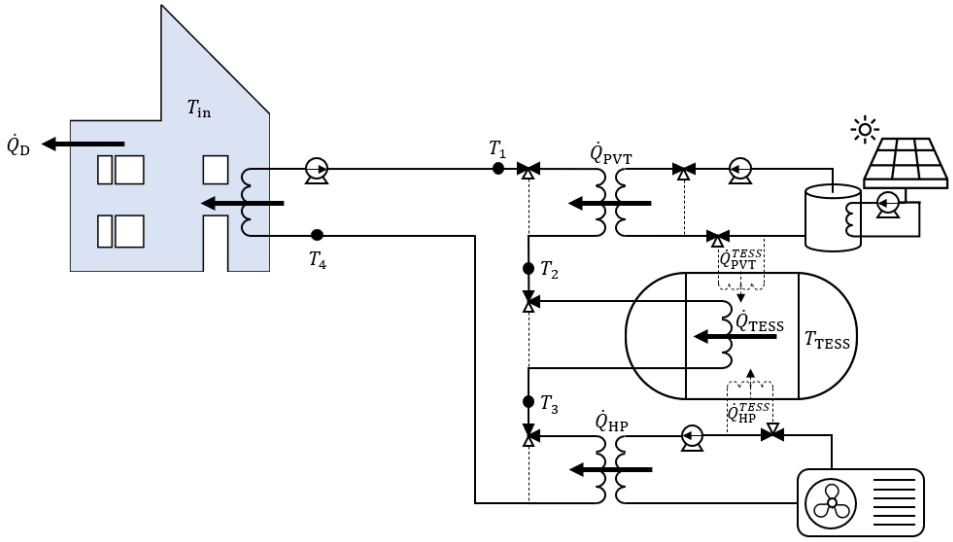

Figure 3.4: Thermal network diagram.

Given that (3.15), (3.58) and (3.62) depends on the inlet and outlet temperatures of the heat exchangers of the TESS and the HP, respectively. This way, using (3.63)-(3.65), they can be rewritten as

$$\dot{Q}_{\mathrm{TESS}}(k) = \eta_{\mathrm{TESS}}^{d} \dot{m} c_{\mathrm{f}} \left[T_{\mathrm{sup}} - T_2(k) \right], \tag{3.67}$$

$$\dot{Q}_{\mathrm{HP}}(k) = \eta_{\mathrm{HP}} \dot{m}_f c_f \left[T_{\mathrm{sup}} - T_3(k) \right]. \tag{3.68}$$

$$\dot{Q}_{\mathrm{PVT}} = 2\eta_{\mathrm{PVT}} N \dot{m}_{\mathrm{f}} c_{\mathrm{f}} \left[T_{\mathrm{f}}(k) - T_1(k) \right], \tag{3.69}$$

The energy management system uses the cascade control shown in Figure 3.5. First, it evaluates the indoor temperature; if it is above the setpoint, no heating is needed. Suppose the indoor temperature is below the setpoint. In that case, the control evaluates the temperatures T_1, T_2 and T_3, as the supply temperature to the domestic heating system, T_4, should be at least 50 °C. This way, the PVT, TESS, or HP would add heat to the working fluid as needed.

3.2.6. Electric Demand

A synthetic load profile was created based on the power of different appliances and their probabilities of being used at the current timestep. Thus, the total electrical power demanded was calculated as

$$P_L(k) = \sum_{i=1}^{n} P_i(k)\, \mathbb{P}_i\left(\{\omega_i(k) \in \Omega_i(k)\}\right) \tag{3.70}$$

where P_i is the power for each appliance considered, and $\mathbb{P}_i$ and $\Omega_i(t)$ are the probability of that appliance to be used and the event space at the instant k, respectively, based on

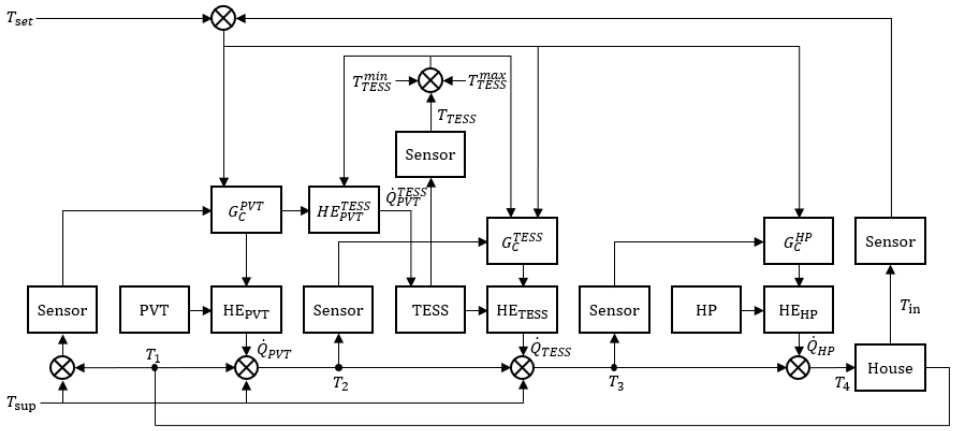

Figure 3.5: Control strategy used by the EMS in the thermal carrier.

typical power consumptions [57]. Note that the heat pump's power is excluded from the electrical demand of the house in (3.70), as it does not have a probabilistic behaviour. Instead, it reacts to the thermal demand, following the EMS instructions.

3.2.7. PHOTOVOLTAIC-THERMAL SYSTEM

Section 3.2.3 detailed the thermal model for the PVT modules used in this thesis. This model provides the temperature of the PV cell as a function of the ambient temperature, wind speed, and irradiance at any particular moment. Given the cell temperature, one can use

$$\eta_{\mathrm{PV}}(k) = \eta_{\mathrm{STC}}\left(1 - \beta\left[T_{\mathrm{PV}}(k) - T_{\mathrm{ref}}\right]\right) \tag{3.71}$$

to estimate the PV efficiency of the PVT, based on the environmental conditions, where η_{STC} and T_{ref} are the reference efficiency and temperature at standard test conditions. Therefore, the electrical power produced by a PVT module, with a total cell area A_{PV}, is

$$P_{\mathrm{PV}}(k) = \eta_{\mathrm{PV}}(k)\, A_{\mathrm{PV}} G(k)\,. \tag{3.72}$$

3.2.8. BATTERY ENERGY STORAGE SYSTEM

The BESS comprised Li-Ion batteries. Consistently with most of the literature, they modelled using an energy-balance approach. This way, the energy stored in the BESS at a particular moment depends on its previous state and the amount of power extracted or provided between sampling times [58], i.e.,

$$E_{\mathrm{BESS}}(k) = C_{\mathrm{BESS}}(k-1)\, SoC(k-1) + \frac{P_{\mathrm{BESS}}(k)}{\eta^{\mathrm{c,d}}(k)}\Delta t - E_{\mathrm{BESS}}^{\mathrm{SD}}(k)\,, \tag{3.73}$$

where E_{BESS} is the future amount of energy stored in the battery, C_{BESS} is the capacity of the battery, SoC is the state-of-charge of the battery, $\eta^{\mathrm{c,d}}$ is the charge or discharge efficiency as correspond, P_{BESS} is the charge or discharge power as corresponds, Δt is the sampling time and $E_{\mathrm{BESS}}^{\mathrm{SD}}$ is the self-discharge of the battery between time samples.

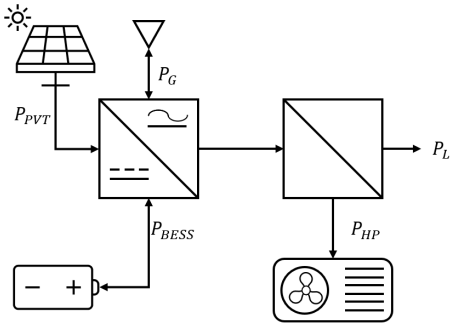

Figure 3.6: Electric network diagram.

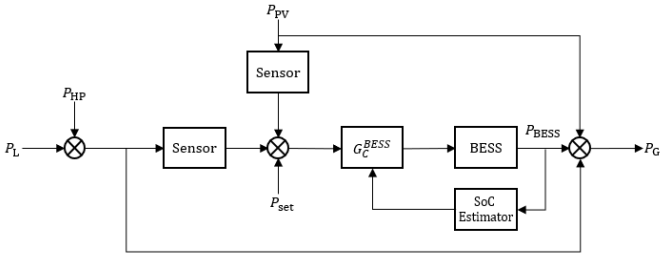

Figure 3.7: Control strategy used by the EMS in the electric carrier.

3.2.9. ELECTRIC NETWORK

A power electronics converter is the coupling point for the electric components, as shown in Figure 3.6. For the EMS, the hierarchical self-consumption strategy proposed in [58] was used, governed by the power balance equation

$$P_{\mathrm{G}} - P_{\mathrm{L}} - P_{\mathrm{HP}} + P_{\mathrm{PVT}} + P_{\mathrm{BESS}} = 0\,, \tag{3.74}$$

where P_{G} and P_{L} are the power purchased from the grid and the power consumed by the loads in the house. The control diagram is shown in Figure 3.7. As can be seen, the algorithm will prioritize the PV generation, then the BESS, and, at last, the purchase from the grid. The charging and discharging powers of the BESS are constrained to the battery's inverter capacity

3.3. RESULTS AND DISCUSSION

This Section presents the results of four different system architectures. First, the individual behaviour of the thermal components is demonstrated and compared the results with reference values for systems with similar characteristics. Then, the thermal components are classified as controllable and non-controllable to create the different case scenarios. This way, the heat pump and the thermal energy storage system are controllable, and the PVT is non-controllable, as it depends on the instantaneous meteorological conditions. However, it should be noted that the TESS cannot meet the thermal energy de-

Table 3.2: Parameters used to simulate the BESS.

Parameter	Symbol	Value	Units
Capacity	E_{BESS}	3.36	kWh
Power	P_{BESS}	1.28	kW
Charge/Discharge efficiency	$\eta_{c,\,d}$	0.943	-
Minimum SoC	SoC_{min}	0.2	-
Maximum SoC	SoC_{max}	0.9	-

mand as a whole and should be coupled with an external energy source. This is because water is its working fluid, which can store around 50 kWh/m^3 for the given temperature range, and the yearly space heating thermal demand is approximately 8207 kWh. For this reason, the only component robust enough to meet the thermal demand independently is the heat pump. Given the above, this Section evaluates the following four scenarios:

- *Scenario I:* only heat pump.
- *Scenario II:* heat pump coupled with a thermal energy storage system (with two different charging protocols).
- *Scenario III:* a PVT system coupled with a thermal energy storage system (with two different charging protocols).
- *Scenario IV:* a PVT system coupled with a thermal energy storage system (with two different charging protocols) and a heat pump.

All the cases were evaluated using up to 10 PVT modules, TESS volumes up to 10 m^3 and a BESS. Tables 3.3, 3.5, 3.6 and 3.2 show the parameters used to model the system.

3.3.1. INDIVIDUAL BEHAVIOUR OF THE THERMAL COMPONENTS

This work proposed analytical models for every component of the multi-carrier energy system. Previously validated models were used for the heat pump, the battery storage system, and the electric demand. In addition, modified models from previous research were used for the soil thermodynamics and the PVT. Finally, models for the space heating thermal demand and the underground thermal energy storage system were proposed. This Section is dedicated to validating the simulation results with data available on similar systems installed in the Netherlands.

THERMAL DEMAND

For this case, a 120 m^2 house built between 1990 and 2000, with an energy label C (using the Dutch energy efficiency standard) was simulated during 2021. The house is occupied by two adults and has highly efficient appliances and LED lighting. The parameters used are shown in Tables 3.3 and 3.4, and the weather data was retrieved from the Royal Netherlands Meteorological Institute database [59]. The free response of the indoor temperature (without any heating) is shown in Figure 3.8a. Then, a setpoint for

the comfortable temperature inside the house was defined. The heat balance in the system should ensure the indoor temperature is equal to or higher than the temperature profile throughout the year. This temperature ranges from 20 °C between 6:00 and 22:00, and 17 °C for the remaining time. The thermal losses to the environment are shown in Figure 3.8b when the indoor temperature matches the setpoint temperature, which adds 8 207 kWh per year. The values of energy consumption reported by [60] and [49] were used as a reference, as they provide data for different types of houses in the Netherlands (including age and area). The simulation results suggest an average specific heat demand of 68.4 kWh/(m^2-year), which is between the reported range of 45 to 86 kWh/(m^2-year).

Table 3.3: Parameters used to simulate the house [61].

Parameter	Symbol	Value				Units
		Roof (glass fiber)	Walls (concrete)	Windows (glass)	Windows (cavity)	
Density	ρ	2440	2400	2500	1.025	kg/m^3
Area	A	120.3	111.6	8	8	m^2
Thickness	L	0.2	0.25	0.004	0.014	m
Specific heat	c	835	750	840	1005.4	J/(kg-K)
Conductivity	k	0.04	0.14	0.8	0.0257	W/(kg-K)
Air specific heat	c_a	1012				J/(kg-K)
Air density	ρ_a	1.293				kg/m^3
No. of bedrooms	N_{br}	1				-
Exposed area	A_{es}	119.6				m^2
Unit leak area	A_u	0.01				in^2/ft^4
Stack coefficient	C_s	0.015				cfm^2/(in^4°F)
Wind coefficient	C_w	0.0012				cfm^2/(in^{4}mph^2)
Time step	Δt	900				s

THERMAL ENERGY STORAGE SYSTEM

A 4 m^3 underground water tank TESS, located 0.2 m below the surface, was modelled using the parameters shown in Table 3.5, and the weather data from the Royal Netherlands

Table 3.4: Convective heat transfer coefficients used to simulate the house [61].

Interface	Value [W/(m^2-K)]
Indoor air - wall	0.9
Wall - atmosphere	0.9
Indoor air - window (glass)	25
Window (glass) atmosphere	32
Indoor air - roof	12
Roof - atmosphere	38

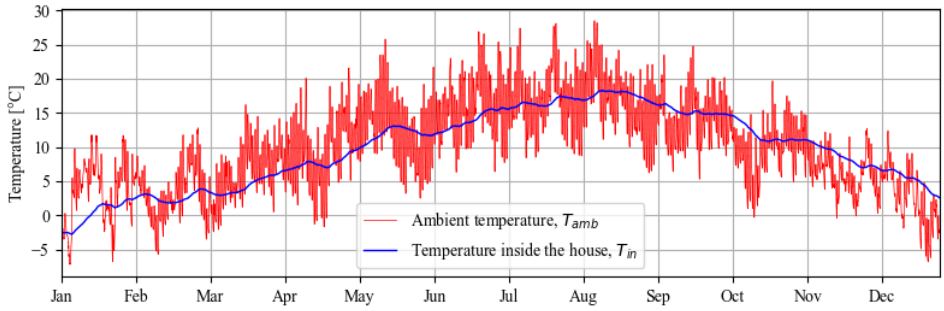

(a)

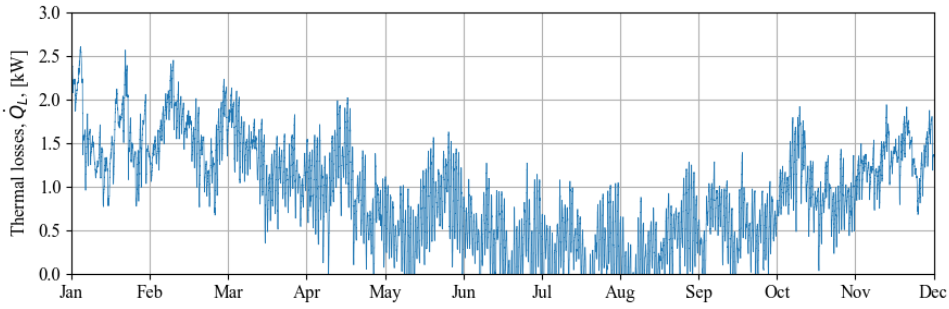

(b)

Figure 3.8: Results of the thermal model of the house. (a) Indoor temperature behaviour without thermal sources (b) Thermal losses when the indoor temperature follows the setpoint temperature.

Table 3.5: Parameters used to simulate the TESS and its losses to the soil.

Parameter	Symbol	Value	Units
	TESS		
Density (water)	ρ_f	1000	kg/m^3
Volume (water)	V_f	4	m^3
Specific heat (water)	c_f	4200	J/(kg-K)
Maximum temperature	T^{max}	95	°C
Minimum temperature	T^{min}	50	°C
Charge/Discharge efficiency	$\eta_{c,d}^{TESS}$	0.8	-
Area (top, bottom)	$A_{top,\ bottom}$	11.02	m^2
Discrete differential side area	$A_{\Delta y}$	0.134	m^2
Area (sides)	A_{sides}	21.44	m^2
Thickness (styrofoam)	L_{TESS}	0.314	m
Specific heat (styrofoam)	c_{styro}	1.34	J/(kg-K)
Conductivity (styrofoam)	k_{styro}	0.033	W/(kg-K)
Depth of the TESS top wall	y_0	0.2	m
Depth of the TESS bottom wall	y_f	1.8	m
	Soil		
Thermal diffusivity	α_s	3.877×10^{-7}	-
Absorbtivity	α_0	0.25	-
Emissivity	ε_s	0.25	-
Conductivity	k_s	1.19	W/(kg-K)
Density	ρ_s	2029.80	kg/m^3
Specific heat	c_s	1512.22	J/(kg-K)
Depth of the reference temperature	d	6	m
Grid size	Δy	0.01	m
Time step	Δt	60	s

Meteorological Institute database [59]. The thermal behaviour of the soil is presented in Figure 3.9, showing more variability in shallow depths, which is consistent with [62], [63] and [52]. To demonstrate the TESS's response, a three-step test cycle was used. The TESS starts charged at 90 °C (SoC of 100 %) and is left to discharge to 50 °C (SoC of 0 %) due to self-discharge. Then, it is charged back to 90 °C using a constant charging temperature of 95 °C. Finally, it is discharged to 50 °C using a network temperature of 40 °C. The behaviour of the temperature is shown in Figure 3.10a. As expected, the isolation of the TESS walls kept the thermal power loss between 250 W and 140 W, proportional to the TESS temperature, causing a slow self-discharge during the first step of the test cycle (see Figure 3.10b). During the second step, 250 kWh are used to charge the TESS, whereas 150 kWh can be retrieved from the TESS in the third due to the roundtrip efficiency of the heat exchanger (see Figure 3.10c). Simultaneously, the charging and discharging steps had thermal losses of 13.14 and 6.72 kWh, respectively.

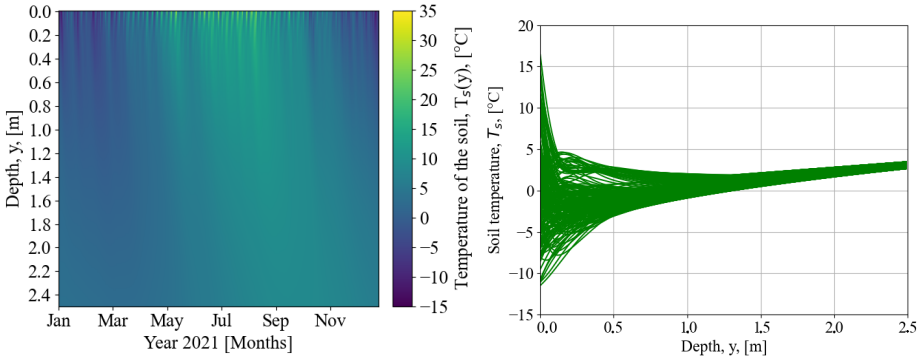

(a) (b)

Figure 3.9: Results of the thermal model of the soil for 2022. (a) Soil temperature throughout the year. (b) Soil temperature, measured every two days.

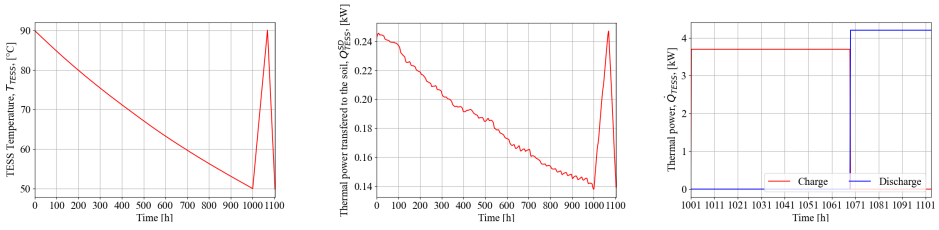

(a) (b) (c)

Figure 3.10: Results of the test cycle for the TESS: (a) temperature, (b) Self-discharge, and (c) Charge and discharge powers during steps 2 and 3 of the test.

PHOTOVOLTAIC-THERMAL SYSTEM

To evaluate the PVT model, a system comprised of 10 modules in series was simulated for 2022; the parameters used are shown in Table 3.6. The HP is activated when the PVT cannot provide heat to meet the thermal demand. From the year, a representative period from summer and winter were selected to demonstrate the system's behaviour under different weather conditions. Figure 3.11 presents the temperature in the different layers of the PVT (glass, T_{glass}, PV cell, T_{PV}, absorber, T_a), of the fluid in the return of thermal network, T_{net}, of the fluid in the PVT tubes T_f and in the PVT tank, T_{PVT}, as a function of the global irradiance, G, and the ambient temperature, T_{amb}.

During summer, less thermal power is demanded due to higher temperatures. This is reflected in Figure 3.11a, as the PVT is not used during June 30 and July 1, despite the tank temperature being above the supply temperature, whereas from June 27 to 29, there are moments where thermal power is demanded, increasing the temperature in the network and reducing the temperature in the tank. In contrast, winter weather conditions do not allow the PVT to warm the tank above the supply temperature (see Figure 3.11b); thus, the PVT cannot provide thermal power to the network, and the HP is activated. Still, both cases have similar temperature behaviours, increasing sharply when irradiance is available and decreasing slowly in its absence. Likewise, the temperature in the glass remains the coldest among the PVT layers, as it is exposed to the ambient, and the temperature in the PV cell and the absorber is near the same as they are in direct contact. Such results are consistent with [54].

3.3.2. SCENARIO I: BOILER VS. HP

A traditional natural gas boiler was used as the reference to evaluate the behaviour of the traditional, gas-based heating system. The power required to keep the house above the setpoint temperature is depicted in Figure 3.8b, and consists of 8207 kWh per year. To estimate the amount of $CO_{2,eq}$ the boiler produces to supply the space heating thermal demand, a 20 kW gas boiler with an efficiency of 92 % was considered, resulting in consuming in total 601 kg (718 m^3) of natural gas, corresponding to 1497 kg of $CO_{2,eq}$, given the Dutch emission factor of 2.085 kg $CO_{2,eq}$/ m^3. On the other hand, the alternative for this scenario is a fully electric heat pump as the thermal energy source. Using the model described in Section 3.2.4, the results showed a total electrical consumption of 5255 kWh, of which the heat pump consumed 2886 kWh. The COP of the heat pump ranged from 2.18 in colder days to 3.92 in warmer days throughout the year. Considering the Dutch emission factor of 0.523 kg $CO_{2,eq}$ per kWh of energy, the heat pump operation produces 1509 kg of $CO_{2,eq}$.

3.3.3. SCENARIO II: HP AND TESS

Two charging protocols for coupling the heat pump with a thermal energy storage system were considered. The first protocol, called from now on *fully-charged*, keeps the SoC of the TESS as close to 100 % as possible (90 °C), as shown in Figure 3.12a. This protocol minimizes the heat required from the heat pump, given that it depends on the difference between the temperature in the TESS and its maximum temperature (set as the charging temperature), as shown in (3.62). The second protocol, called *cycling*, leaves the TESS to discharge to 50 °C, then charges to the maximum SoC, as shown in Figure 3.12b,

Table 3.6: Parameters used to simulate the PVT module.

Parameter	Symbol	Value	Units
Glass area	A_{glass}	1.48	m^2
PV area	A_{PV}	1.46	m^2
Absorber area	A_a	1.48	m^2
Tube area	A_t	1.48	m^2
Glass density	ρ_{glass}	2200	kg/m^3
PV density	ρ_{PV}	2330	kg/m^3
Absorber density	ρ_a	2699	kg/m^3
Tube density	ρ_f	1050	kg/m^3
Glass thickness	L_{glass}	0.004	m
Air gap thickness	L_{air}	0.02	m
PV glass thickness	$L_{PV,\,glass}$	0.003	m
PV EVA thickness	L_{EVA}	0.0005	m
PV tedlar thickness	L_{ted}	0.0001	m
Absorber thickness	L_a	0.001	m
Insulation thickness	L_{ins}	0.04	m
Mass flow	$\dot{m}_f$	0.029	kg/s
Tank mass	m_{tank}	200	kg
Time step	Δt	1	s

Parameter	Symbol	Value	Units
Glass thermal conductivity	k_{glass}	1.8	W/(m-K)
Air thermal conductivity	k_a	0.024	W/(m-K)
PV glass thermal conductivity	k_{PV}	1.8	W/(m-K)
PV EVA thermal conductivity	k_{EVA}	0.35	W/(m-K)
PV tedlar thermal conductivity	k_{PV}	0.2	W/(m-K)
Fluid thermal conductivity	k_f	0.6071	W/(m-K)
Insulation thermal conductivity	k_{ins}	0.035	W/(m-K)
Glass specific heat	c_{glass}	670	J/(kg-K)
PV specific heat	c_{PV}	900	J/(kg-K)
Absorber specific heat	c_a	800	J/(kg-K)
Fluid specific heat	c_f	3800	J/(kg-K)
Glass diffusivity	α_{glass}	0.1	-
PV diffusivity	α_{PV}	0.9	-
Glass emmisivity	ε_{glass}	0.9	-
PV emmisivity	ε_{PV}	0.96	-
Glass transmitance	τ_{glass}	0.1	-
Heat exchanger efficiency	η_T	0.8	-
PV cell reference efficiency	η_{PV}	0.184	-
PV temperature coefficient	β_{PV}	0.3	%/°C

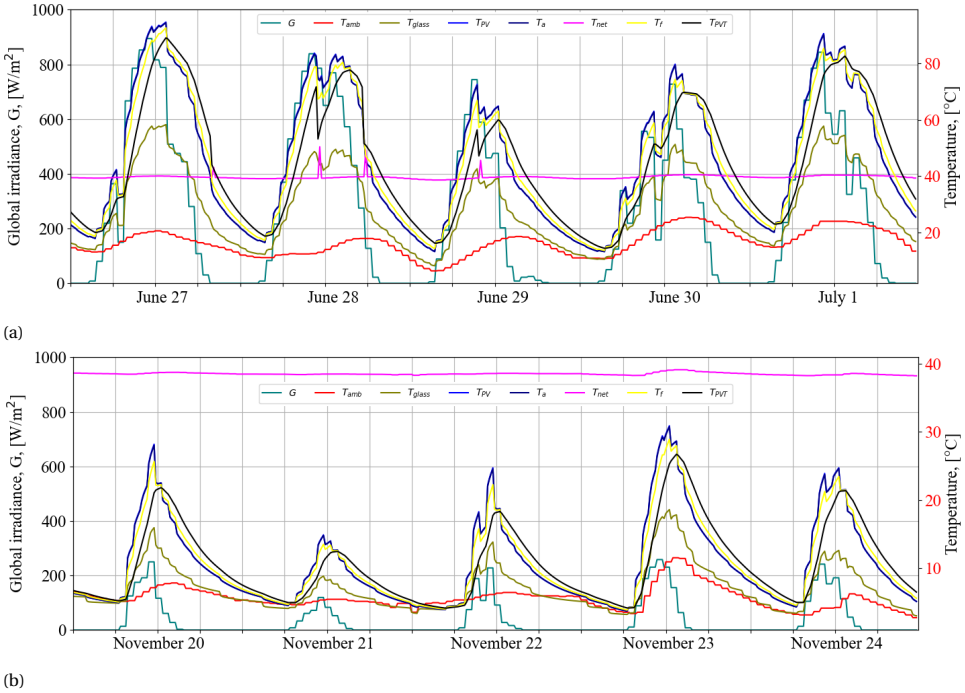

Figure 3.11: Results of the thermal model of the PVT during (a) summer and (b) winter.

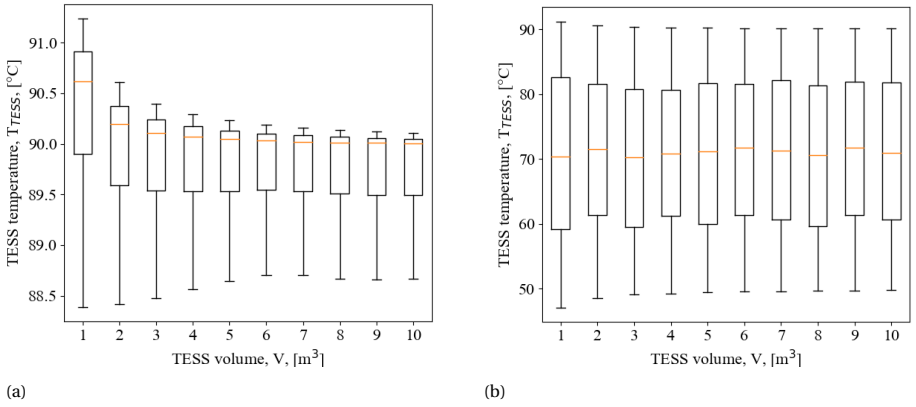

Figure 3.12: Distribution of the temperature in the TESS when using the (a) fully-charged and (b) cycling protocols.

improving the COP since it depends on the difference between the TESS and ambient temperatures, as shown in (3.60).

To evaluate the performance of each charging protocol, TESS sizes from 0 to 10 m^3 were considered and compared using three indicators: the amount of energy lost to the soil due to self-discharge of the TESS, the ratio of thermal energy extracted from the TESS to the thermal energy stored, and the ratio of thermal energy extracted from the TESS to the required electrical energy used to generate the thermal energy stored in the TESS. The first ratio is defined as thermal performance and the second as electric performance; for both cases, the energy associated with the initial state of charge is excluded. The self-discharge results presented in Figure 3.13a show an increasing trend in the accumulated energy lost to the soil with the volume of the TESS. This is related to the contact area of the tank with the soil since (3.35)-(3.37) establish a direct relationship between the thermal losses and the area of the TESS. Moreover, the fully-charged protocol keeps the TESS at a higher temperature, increasing the heat flux to the surrounding soil.

The thermal and electric performances for all considered TESS volumes are shown in Figure 3.13b. The results suggest a higher thermal performance for the fully-charged TESS protocol. The thermodynamics of the heat transfer can explain this, as the higher the temperature in the TESS, the easier the energy flows towards the thermal network. Nevertheless, keeping the TESS in a higher SoC requires a more frequent use of the HP, summed to a lower COP due to the higher difference between the temperature required to heat the TESS and the ambient temperature. On the other hand, the cycling protocol leaves the TESS temperature to reach temperatures closer to the supply temperature required by the thermal network, leading to a slower response. However, the reduced frequency at which the HP is used and better COPs for most of the charging time result in better electric performance. Still, the COP for both protocols was very low, averaging 0.88 to 0.95 in the fully-charged protocol and 1.29 to 1.38 for the cycling protocol. In both cases, the smaller the capacity of the TESS, the higher the COP. Such low COPs lead to energy consumption several times the consumption of the HP in Section 3.3.2, as shown in Figure 3.13c. Similarly, the overall equivalent emissions also increase considerably, as shown in Figure 3.13d.

3.3.4. SCENARIO III: PVT AND TESS

Solar-dependent technologies, such as PV or PVT, are usually unsuitable as stand-alone energy sources. Adding BESS or TESS, respectively, would allow the energy to be stored when there is no demand for the supply. Therefore, the suitability of a PVT system combined with a TESS was evaluated as an alternative to gas boilers, considering TESS sizes from 0 to 10 m^3, combined with PVT systems varying from 0 to 10 modules. The indicators used for this scenario are: the number of days when the indoor temperature was below 16 °C at any moment, called "cold days", the energy lost to the soil due to self-discharge of the TESS, the thermal performance, and the ratio of thermal energy used from the PVT to the electrical energy produced.

In this case, the results suggest that the combination is unsuitable due to the number of cold days shown in Figure 3.14a. One can notice that the number of cold days increases with the size of the TESS. This is because the thermal power from the PVT system used to charge the TESS reduces the temperature in the PVT tank. Therefore, when

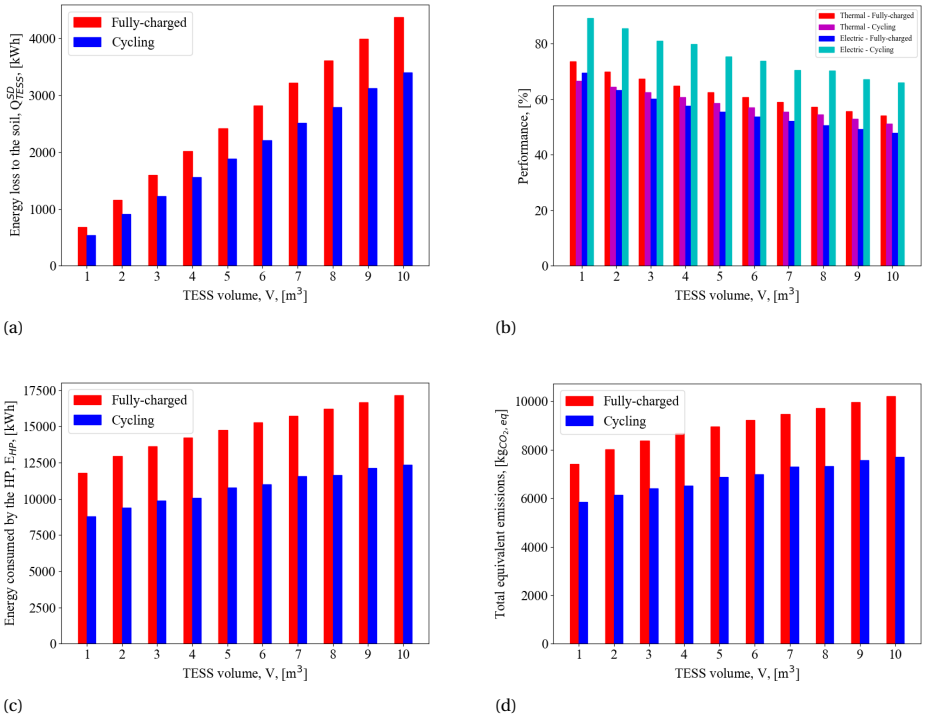

Figure 3.13: Assesment of the energy performance of Scenario 2 for each charging protocol. (a) Energy loss to the soil due to self-discharge of the TESS. (b) Thermal and electric performance of the coupled system. (c) Electrical energy consumption of the HP. (d) Equivalent CO_2 emissions.

thermal power is required to heat the house, the temperature the PVT system can provide is lower than in the case without TESS. Likewise, the bigger the capacity of the TESS, the higher the heat absorption rate from the PVT, as it requires more thermal energy to increase the temperature. Additionally, as shown in Section 3.3.3, increasing the volume of the TESS increases the self-discharge rate. Thus, the overall system becomes less efficient.

The phenomenon is demonstrated by correlating the results in Figures 3.14b and 3.14c, where it is shown that the thermal energy sent from the PVT to the thermal network decreases. In contrast, the energy sent to the TESS increases when the capacity of the TESS is increased. Simultaneously, increasing the SoC of the TESS increases the energy lost due to self-discharge, as shown in Figure 3.14d. Figure 3.14e shows the thermal energy supplied by the TESS, which is consistently lower than the thermal energy it received from the PVT. Note that increasing the temperature of the TESS sometimes requires less temperature than heating the house. As shown in Figure 3.15, the temperature in the TESS reaches values below the supply temperature required to heat the house, allowing it to charge with lower temperatures from the PVT, increasing the amount of usable thermal energy from the PVT. Nonetheless, the performance of the system is poor.

As shown in Figure 3.16a, the TESS can only provide energy to the thermal network with small capacities and many PVT modules. The negative results account for the energy delivered from the initial state-of-charge (55 %). Also, the PVT's thermal production is consistently below its electrical production. As shown in Figure 3.16b, although it is generally mentioned that the thermal output of the PVT outperforms the electric counterpart, it depends on the required output temperature. The high temperatures demanded by the TESS diminish the thermal output of the PVT. The PVT can deliver thermal energy to the TESS only when it reaches very low temperatures, which happens with higher capacities and few PVT modules and with small capacities and many PVT modules as shown in Figure 3.15. However, the electrical output grows linearly with the number of modules, but this relationship is not valid for the thermal output. For this reason, the thermal performance is better with small capacities and many modules, and the thermal-to-electric output ratio is not optimal in that region.

From the electrical perspective, it is possible to achieve a net-zero building when the number of PVT modules is increased. For this case scenario, the base energy consumption is 2375 kWh/year, which can be achieved with 7 PVT modules, as shown in Figures 3.17a and Figure 3.17b. However, the temporal mismatch between production and consumption prevents the energy from being consumed immediately, urging energy storage to avoid sending energy back to the grid. In contrast with the previous scenarios, this one can benefit from a battery energy storage system. As shown in Figure 3.17c, the BESS can store up to one-third of the yearly energy consumption but saturates after the seventh PVT module. This is because, at that point, the energy generation is greater than the consumption, and the energy sent back to the grid increases proportionally to the generation, as shown in Figure 3.17d. At this point, congestion issues might emerge.

3.3.5. SCENARIO IV: PVT, TESS, AND HP

This section evaluates the combination of all the components; however, only two of the five possible modes of operation are considered: the two charging protocols with

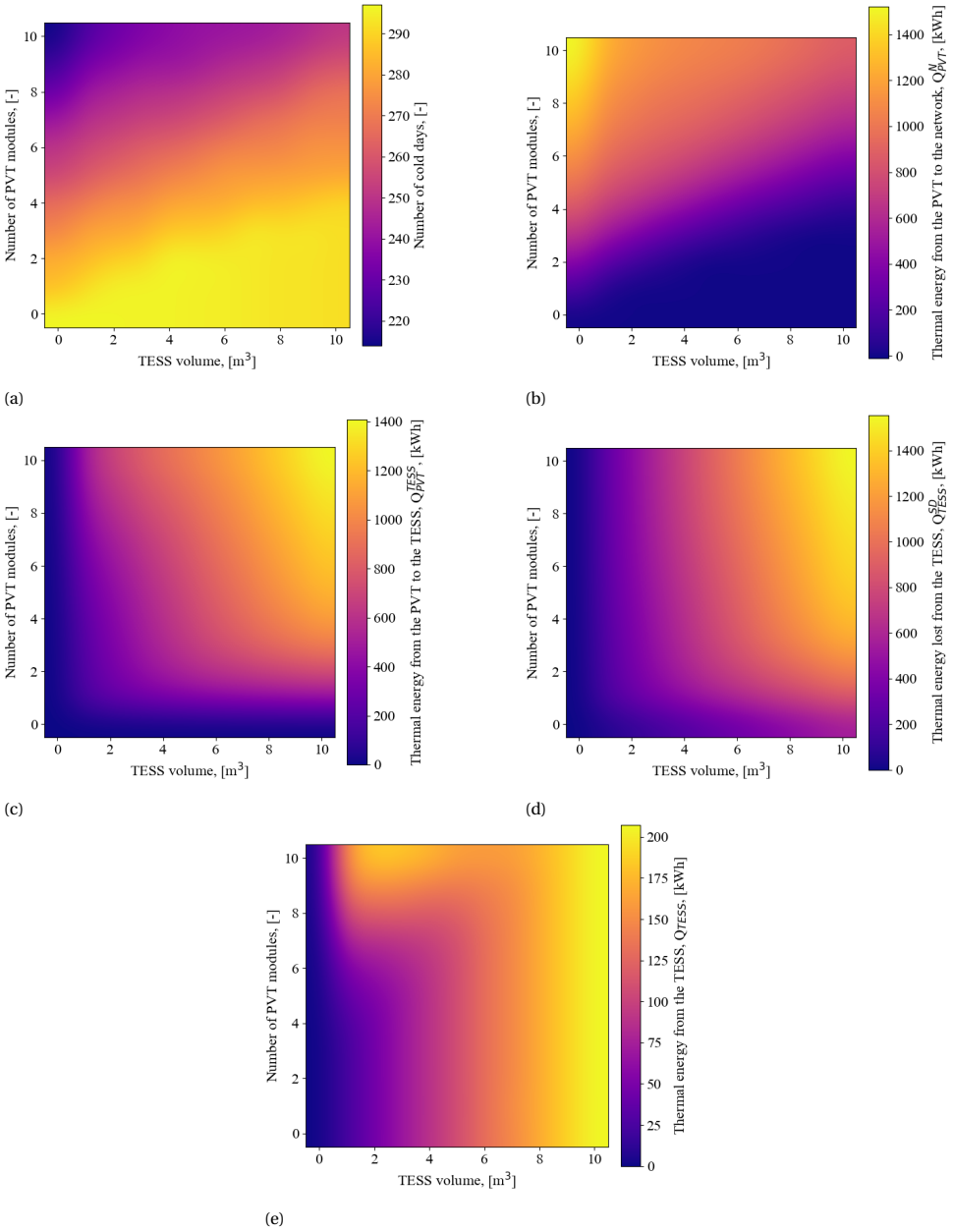

Figure 3.14: Thermal power flow in Scenario 3. (a) Cold days. (b) Thermal energy from the PVT to the thermal network. (c) Thermal energy from the PVT is used to charge the TESS. (d) Energy loss to the soil due to self-discharge. (e) Thermal energy from the TESS to the thermal network.

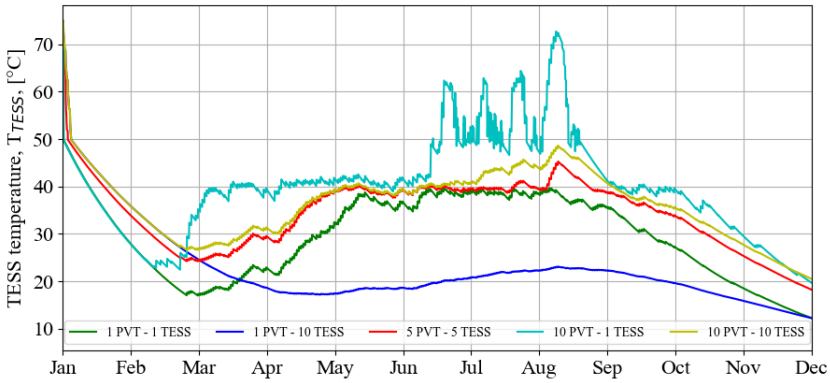

Figure 3.15: Temperature in the TESS during the year for different numbers of PVT modules and TESS volumes in Scenario 3.

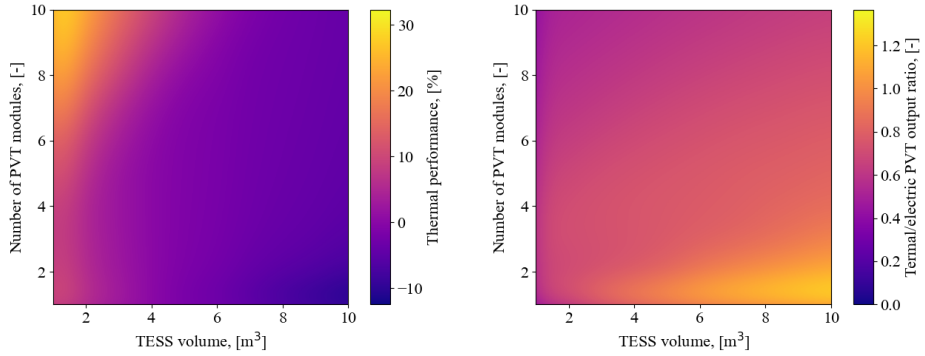

(a) (b)

Figure 3.16: Thermal performance in Scenario 3. (a) Thermal performance. (b) Ratio of the thermal and electrical output of the PVT.

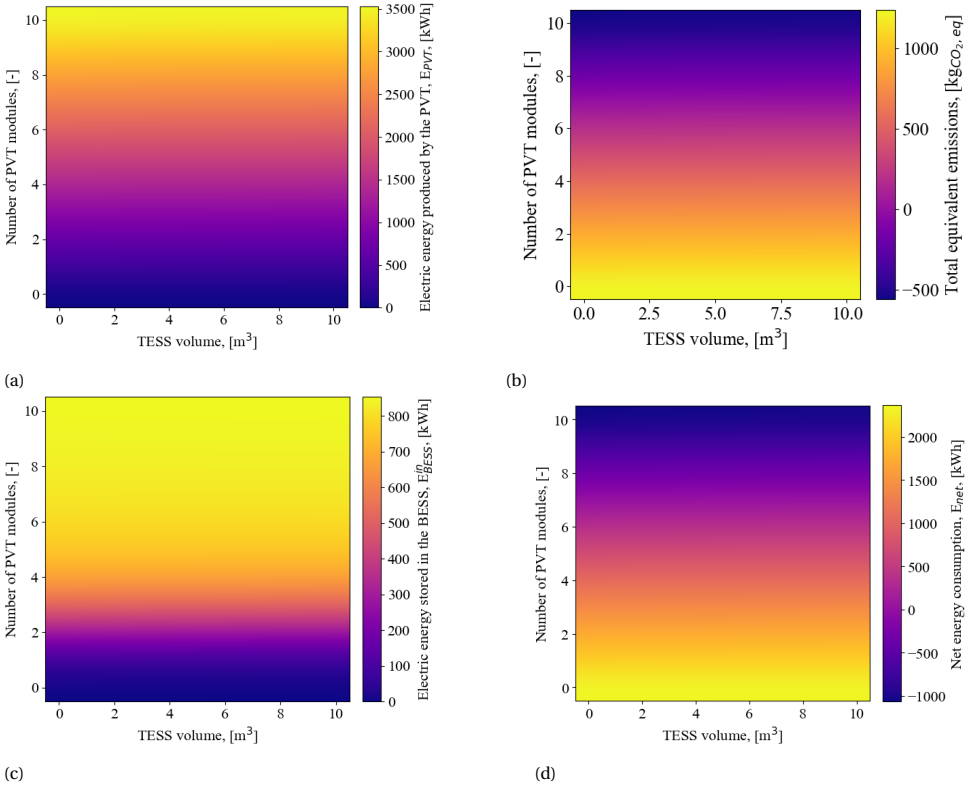

Figure 3.17: Electric performance in Scenario 3. (a) PVT electric output. (b) Equivalent CO_2 emissions. (c) Energy stored in the BESS. (d) Net energy consumption from the grid.

the heat pump alone, without considering the PVT to charge the TESS. This decision is based on the results of the previous sections. In Section 3.3.3, it was demonstrated that charging the TESS only with the HP has a trade-off between thermal and electrical performance based on the charging protocol. However, it was possible to meet the thermal demand. Section 3.3.4, on the other hand, demonstrated that using the PVT to charge the TESS is not possible due to the low temperatures the PVT can achieve. For this reason, the three combinations that would use the PVT to charge the TESS, i.e., using only the PVT, and using both the PVT and the HP with its two charging protocols were excluded. Thus, the indicators are the same as Section 3.3.4.

First, the role of the PVT as a thermal energy source was evaluated. For both charging protocols, the contribution of the PVT is approximately the same, as shown in Figures 3.18a and 3.18b. In this scenario, the energy sent from the PVT to the thermal network is one order of magnitude less than in Scenario 3. The thermal network temperature difference for both cases can explain this. As the indoor temperature in Scenario 3 is consistently lower than in Scenario 4, the temperature in the network would also be lower, allowing the PVT to provide thermal power in lower temperatures. However, this does not prevent the indoor temperature from reaching values below the setpoint, unlike in Scenario 4, where the TESS and the HP can ensure an indoor temperature above the setpoint, requiring higher temperatures from the PVT to be able to contribute. Nevertheless, the PVT cannot reach such temperatures consistently, thus reducing the amount of thermal energy it provides to the network.

Given the small contribution of the PVT to the thermal network, this scenario becomes similar to Scenario 2 in terms of thermal power flow. Figures 3.18c and 3.18d demonstrate that increasing the number of PVT modules does not affect the amount of thermal energy the HP provides to the TESS for any given capacity. In addition, those results and the self-discharge losses presented in Figures 3.18e and 3.18f are approximately the same as in Scenario 2, regardless of the charging protocol. Albeit the COPs for the fully-charged protocol improve slightly, ranging between 0.88 and 0.95, the yearly average only increased to 0.89. Similarly, the COP in the cycling protocol ranged between 1.28 and 1.38. Therefore, both scenarios present comparable thermal performances to Scenario 2, as shown in Figure 3.19.

The electric behaviour, on the other hand, differs from the previous scenarios. In this scenario, the PVT generation is not enough to achieve a net-zero condition (see Figures 3.20a, 3.20b, 3.20c and 3.20d). This also translates into less energy stored in the BESS than Scenario 3. Figures 3.20e and 3.20f demonstrate that the increased frequency of use of the HP allows more energy to be consumed directly from the PVT instead of being stored in the BESS. Also, the convergence in the energy stored in the BESS shown in Scenario 3 no longer occurs due to the increased load. However, given the stochasticity of both the PVT generation and the HP activation, added to the limited capacity of the BESS inverter, energy is still sent back to the grid, as shown in Figures 3.20g and 3.20h.

When comparing the two protocols in this scenario, one can notice that keeping the TESS with a high SoC reduces the energy stored in the BESS and sent back to the grid. In contrast, the net energy consumption is around 30 % more than with the cycling protocol. This behaviour was also present in Scenario 2. However, in Scenario 2, no energy was sent back to the grid due to the absence of PVT. This creates a dual challenge for grid

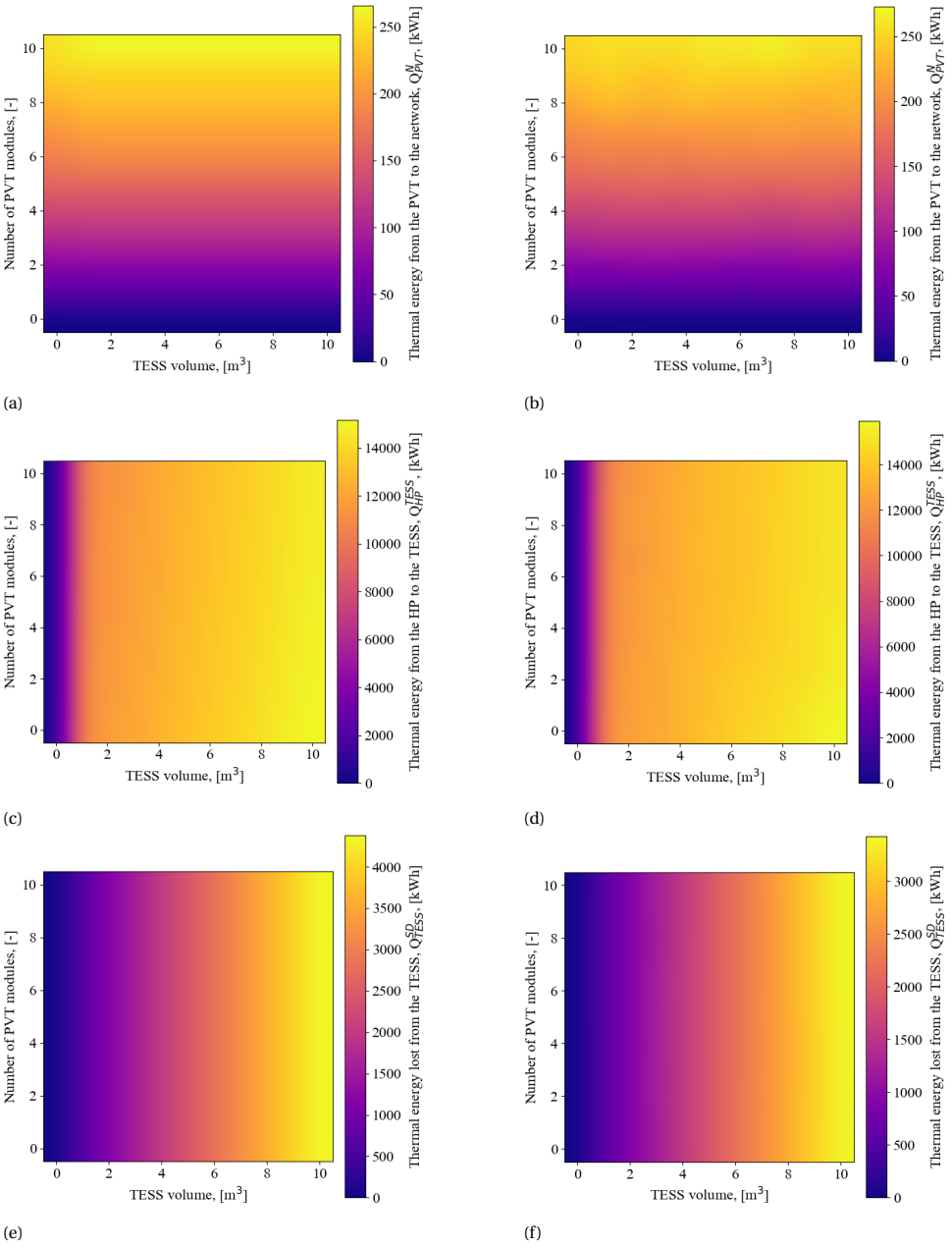

Figure 3.18: Thermal power flow in Scenario 4. Thermal energy from the PVT to the thermal network using (a) the fully-charged and (b) the cycling protocol. Thermal energy from the HP to the TESS using (c) the fully-charged and (d) the cycling protocol. Energy loss to the soil due to self-discharge using (e) the fully-charged and (f) the cycling protocol.

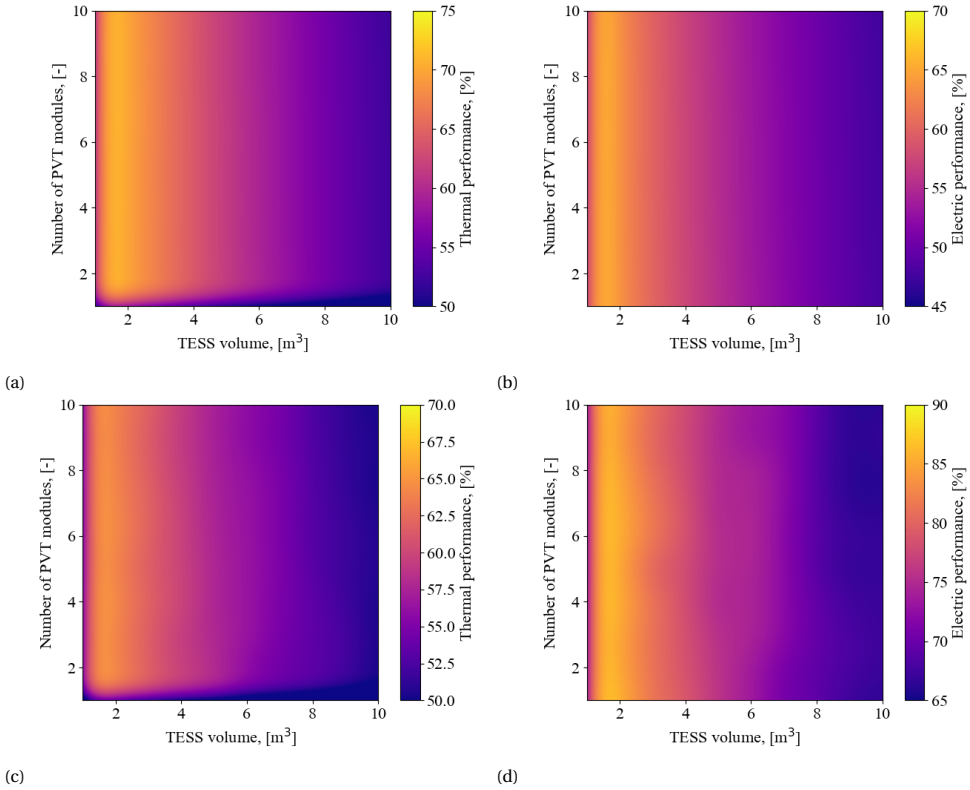

Figure 3.19: Performance in Scenario 4. Thermal performance using (a) the fully-charged and (c) the cycling protocol. Electric performance using (b) the fully-charged and (d) the cycling protocol.

operators. On the one hand, the stress in the network increases as the energy consumption increases between four to six times with the fully-charged protocol and three to five times with the cycling protocol. On the other hand, overvoltages can occur as energy is being sent back to the grid.

3.3.6. SCENARIOS COMPARISON

After analyzing each scenario, this section compares the advantages and disadvantages between scenarios. Three comparison points were considered: thermal performance, electrical performance, and equivalent emissions. The reference point is the base case with only the gas boiler defined in Section 3.3.2, which always meets the thermal demand, produces 1497 kg of $CO_{2,eq}$, and has a net consumption of 2375 kWh from the grid. Table 3.7 summarises the previous sections' results.

From the perspective of the space heating thermal demand, all scenarios except Scenario 3 ensure an indoor temperature above the setpoint temperature. The results suggest that, given the priority of the TESS over the heat pump in Scenarios 2 and 4, the contributions of the HP to the thermal demand are almost negligible. The HP is only used to keep the TESS charged when using the fully-charged protocol. In the cycling protocol, the HP provides thermal power to the network if the TESS gets discharged and thermal power is still needed. Then, the HP remains active to charge back the TESS. Nevertheless, using the HP to provide thermal power through the TESS reduces the system's thermal performance. When comparing Scenario 1 with Scenarios 2 and 4, the difference between the amount of energy generated vs. the thermal demand is noticeable. Figures 3.16a, 3.19a and 3.19c show that the thermal performance is between 40 and 70 % in the presence of TESS, whereas is 100 % in Scenario 1.

Low thermal performance also leads to poor electric performance. In Scenario 1, the COP of the HP oscillates between 2.18 to 3.92. In contrast, Scenarios 2 and 4 have maximum COPs below 1 (fully-charged protocol) and 1.4 (cycling protocol). This considerably increases the yearly electric energy consumption, even in Scenario 4 with the PVT, increasing the chances of undervoltages in the distribution network. Moreover, energy is returned to the grid despite using a BESS. This is undesired in most cases, as it can lead to overvoltages and congestion in the distribution network. Therefore, Scenarios 2 and 4 represent a significant challenge for grid operators. Similarly, Scenario 3 achieves net-zero consumption, even reaching net-positive conditions. Nevertheless, the stochasticity of the PVT generation causes a bidirectional energy exchange with the grid, potentially causing congestion and more severe overvoltages than previous scenarios due to the lower energy consumption and the same energy generation.

In Section 3.3.2 it was mentioned that, given the Dutch emission factors, an improvement in $CO_{2,eq}$ from the base case with the boiler can be achieved with a net electric consumption increase below 2900 kWh/year, i.e., the total net energy consumption should be 5250 kWh/year or less. Using only the heat pump, as in Scenario 1, it is possible to meet this criteria. Scenario 3 consistently reduced the net consumption from the grid at the expense of thermal comfort. In this scenario, the net energy consumption can reach even negative values, turning the house into a net-positive building when there are more than seven PVT modules, but the heat production cannot meet the thermal demand, making this scenario unfeasible. On the other hand, Scenario 4 can meet this

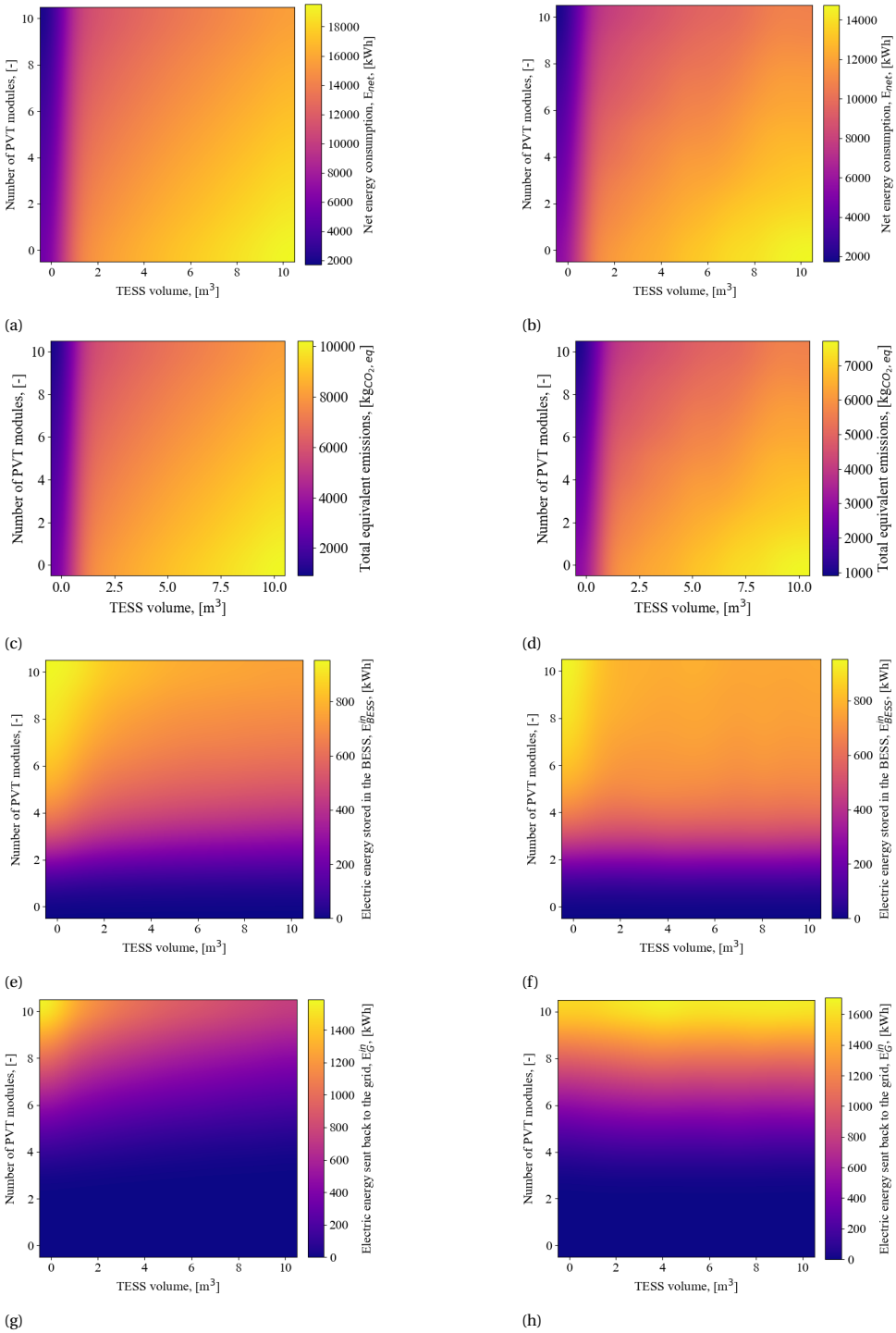

Figure 3.20: Electric energy flow in Scenario 4. Net energy consumption from the grid when using (a) the fully-charged and (b) the cycling protocol. Equivalent CO_2 emissions when using (c) the fully-charged and (d) the cycling protocol. Energy stored in the BESS when using (e) the fully-charged and (f) the cycling protocol. Energy returned to the grid when using (g) the fully-charged and (h) the cycling protocol.

requirement only in the case without TESS. In fact, the only difference between this case and Scenario 2 is the PVT. In Scenario 2, the absence of PVT considerably increases the equivalent emissions compared with only the HP or the gas boiler in Scenario 1, ranging from 3087 $kg_{CO_{2,eq}}$ more in the case with the smaller TESS, up to 4960 $kg_{CO_{2,eq}}$ for the cycling protocol. The equivalent emissions increase for the fully-charged protocol is worse, ranging from 4654 to 7467 $kg_{CO_{2,eq}}$. Scenario 4 has a lower equivalent emissions impact than Scenario 2, as the PVT can compensate for up to 1870 $kg_{CO_{2,eq}}$ when using 10 modules, but it is insufficient to justify the usage of the usage of the TESS from an emissions perspective. It was also demonstrated that the PVT does not provide any significant advantage on the thermal side. For this reason, a PV system would add the same value towards reducing the equivalent emissions, with a lower cost, as it would not require the hydraulic components. Then, adding thermal storage increased several times the electrical consumption, thus, the $CO_{2,eq}$.

Assuming the same weight for the three criteria, Scenario 1 shows the best performance overall. This scenario can meet the thermal demand with the lower electric and net grid consumption; therefore, its $CO_{2,eq}$ is just below Scenario 3. Scenarios 2 and 4 have almost the same thermal performance; however, Scenario 4 has better electric behaviour from the user perspective due to the solar energy from the PVT, reducing its $CO_{2,eq}$. Still, from the grid perspective, Scenario 4 represents the most significant challenge among the four scenarios due to the notable increase in consumption and stochastic bidirectional energy flow. Scenario 3 outperforms the other scenarios in terms of net grid consumption, but it cannot meet the thermal demand, which makes it an unsuitable architecture. Notably, all scenarios can provide ancillary services if the multi-carrier system is sized according to a specific ancillary service, such as voltage control or congestion management, and an adequate EMS strategy is implemented, as will be detailed in Chapters 4, 5 and 6. If so, Scenarios 2 or 4 might become more attractive than Scenario 1, thanks to the combination of the HP and the TESS. For instance, variable energy prices would make it more profitable to use the heat pump when heating demand is not necessarily needed, thus requiring thermal energy storage, resulting in a cost-driven demand response. Similarly, using the heat pump to charge the TESS in high-power injection periods despite no heating being needed could potentially support the grid in reducing overvoltages without affecting the thermal comfort of the occupants of the house.

3.4. CONCLUSIONS

This Chapter described analytical models for a multi-carrier energy system to replace gas boilers for space heating in residential houses in the Netherlands. An underground water tank thermal energy storage system was used for the analysis, providing an analytical model to estimate its self-discharge to the surrounding soil. Then, four architecture scenarios were evaluated to determine their electrical consumption from the grid, thermal power generation for space heating and $CO_{2.eq}$ emissions. It was demonstrated that using a heat pump generates approximately the same equivalent emissions as the gas boiler in households (around 1500 kg of $CO_{2,eq}$); however, a more renewable network would improve the heat pump result. Coupling a PVT to the heat pump did not provide any value from the thermal perspective; thus, a PV system could be used instead if the target is a net-zero building at the cost of more stochasticity added to the grid.

Table 3.7: Summary of the results for the different scenarios.

Scenario	Architecture	TESS charge	Conclusions
Scenario I	HP	-	The $CO_{2,eq}$ produced by the HP is 1509 kg, vs 1497 kg when using the boiler, given the Dutch emission factor. The HP consumes 2886 kWh/year, with COPs ranging from 2.18 to 3.92.
Scenario II	HP and TESS	Fully-charged	The TESS loses between 684 and 4378 kWh/year to the soil and receives 11 139 to 15 159 kWh from the HP, depending on the volume (ascending), with COPs varying from 0.88 to 0.95. $CO_{2,eq}$ increases between 4654 to 7467 $kg_{CO_{2,eq}}$.
		Cycling	Loses between 533 and 3405 kWh/year to the soil and receives 11 766 to 15 905 kWh from the HP, depending on the volume (ascending), with COPs varying from 1.29 to 1.38. $CO_{2,eq}$ increases between 3087 to 4960 $kg_{CO_{2,eq}}$.
Scenario III	PVT and TESS	-	The PVT cannot charge the TESS for any combination of volumes and number of modules considered. More modules with smaller TESS capacities can keep the tank near 40 °C. However, more than seven modules would create a net-positive building, which could potentially cause instabilities in the low-voltage network.
Scenario IV	PVT, TESS and HP	Fully-charged	The PVT contribution to meet the thermal demand is below 3.25 % of the total thermal energy needed; thus, the behaviour of the HP is almost identical to Scenario II. The consumption of the HP prevents a net-zero building; nevertheless, up to 1587 kWh/year, depending on the number of modules, are sent back to the grid due to the storage and inverter capacities of the BESS. $CO_{2,eq}$ increases between 2784 to 7467 $kg_{CO_{2,eq}}$.
		Cycling	The PVT contribution to meet the thermal demand is below 3.25 % of the total thermal energy needed; thus, the behavior of the HP is almost identical to Scenario II. The consumption of the HP prevents a net-zero building; nevertheless, up to 1708 kWh/year, depending on the number of modules, are sent back to the grid due to the storage and inverter capacities of the BESS. $CO_{2,eq}$ increases between 1217 to 4960 $kg_{CO_{2,eq}}$.

It also proved that water tank TESS and PVT systems are incompatible due to the low temperature the latter can generate. When coupled with a heat pump, the electrical consumption, thus, the $CO_{2,eq}$, increased from three to six times than when using the heat pump alone. This is because the temperature difference between the fluid stored in the TESS (50 – 95 °C) and the ambient (-5 – 30 °C) reduces the COP to values near 1, regardless of the charging cycle. It was noted, however, that using the cycling protocol reduces the frequency of activation of the heat pump to charge the tank. This way, the TESS can provide enough thermal power for space heating independently, but the overall performance of the HP coupled with the TESS depends on the charging and discharging strategy. Such strategies could provide flexibility in a scenario where the TESS does not depend solely on the HP to charge, as adding the HP consistently increases the energy consumption and adds power peaks to the base demand. Combining with PVT systems can reduce the net energy consumption from the grid, but it could contribute to voltage stability issues for grid operators, given the amount of electrical power injected into the grid.

The previous conclusions set the base for the multi-carrier energy system to be used in further chapters. Given that the PVT and the TESS are incompatible systems, the PVT will be replaced, as recommended, by a PV system. Similarly, a deeper study on how the EMS affects the system's behaviour is done in Chapter 4, considering, aside from the thermal comfort, the energy price and the setpoints given by the DSOs. Similarly, it sets the base for the customer segments used in Chapter 5 to investigate prosumers' requirements to participate in the most feasible ancillary services, as recommended in Chapter 2.

BIBLIOGRAPHY

[1] "The netherlands 2020 - energy policy review", International Energy Agency, Tech. Rep., 2020. [Online]. Available: https://iea.blob.core.windows.net/assets/93f03b36-64a9-4366-9d5f-0261d73d68b3/The_Netherlands_2020_Energy_Policy_Review.pdf.

[2] A. Oei, R. Haffner, H. van Til, L. Heidecke, and A. Slaakweg, "Van cv-ketel naar duurzame warmte - twee toekomstbeelden voor een warme nederlandse gebouwde omgeving in 2030", Ecorys, 2018. [Online]. Available: https://iea.blob.core.windows.net/assets/93f03b36-64a9-4366-9d5f-0261d73d68b3/The_Netherlands_2020_Energy_Policy_Review.pdf.

[3] M. Geraedts, J. Alpízar-Castillo, L. Ramírez-Elizondo, and P. Bauer, "Optimal sizing of a community level thermal energy storage system", in *2022 IEEE 21st Mediterranean Electrotechnical Conference (MELECON)*, 2022, pp. 52–57. DOI: 10.1109/MELECON53508.2022.9842945.

[4] J. Oh, S. Bae, H. Chae, J. Jeong, and Y. Nam, "Photovoltaic–thermal advanced technology for real applications: Review and case study", *Energy Reports*, vol. 10, pp. 1409–1433, 2023, ISSN: 2352-4847. DOI: https://doi.org/10.1016/j.egyr.2023.08.002. [Online]. Available: https://www.sciencedirect.com/science/article/pii/S2352484723011435.

[5] A. K. Tiwari, K. Chatterjee, S. Agrawal, and G. K. Singh, "A comprehensive review of photovoltaic-thermal (pvt) technology: Performance evaluation and contemporary development", *Energy Reports*, vol. 10, pp. 2655–2679, 2023, ISSN: 2352-4847. DOI: https://doi.org/10.1016/j.egyr.2023.09.043. [Online]. Available: https://www.sciencedirect.com/science/article/pii/S2352484723012878.

[6] S. Ranjbar Golafshani, M. Fatehpour, and E. Houshfar, "Optimization and dynamic techno-economic assessment of integrated combined ejector cooling, heating, and power system", *Energy*, vol. 282, p. 128 829, 2023, ISSN: 0360-5442. DOI: https://doi.org/10.1016/j.energy.2023.128829.

[7] S. Kallio and M. Siroux, "Hybrid renewable energy systems based on micro- cogeneration", *Energy Reports*, vol. 8, pp. 762–769, 2022, 2021 The 8th International Conference on Power and Energy Systems Engineering, ISSN: 2352-4847. DOI: https://doi.org/10.1016/j.egyr.2021.11.158. [Online]. Available: https://www.sciencedirect.com/science/article/pii/S2352484721013056.

[8] L. Herre, B. Nourozi, M. R. Hesamzadeh, Q. Wang, and L. Söder, "Provision of multiple services with controllable loads as multi-area thermal energy storage", *Journal of Energy Storage*, vol. 63, p. 107 062, 2023, ISSN: 2352-152X. DOI: https://doi.org/10.1016/j.est.2023.107062. [Online]. Available: https://www.sciencedirect.com/science/article/pii/S2352152X23004590.

[9] S. Wang, P.-J. Hoes, J. L. M. Hensen, O. C. G. Adan, and P. A. J. Donkers, "Investigating the use cases of a novel heat battery in dutch residential buildings", *Building Simulation*, vol. 16, no. 9, pp. 1675–1689, 2023. DOI: 10.1007/s12273-023-1069-2. [Online]. Available: https://www.scopus.com/inward/record.uri?eid=2-s2.0-85168571099&doi=10.1007%2fs12273-023-1069-2&partnerID=40&md5=ef6d91aebc5a9fbf21a8f6bb9bc74653.

[10] D. H. Clift, J. Leerson, K. N. Hasan, and G. Rosengarten, "Maximising the benefit of variable speed heat-pump water heater with rooftop pv and intelligent battery charging", *Solar Energy*, vol. 265, 2023. DOI: 10.1016/j.solener.2023.112049. [Online]. Available: https://www.scopus.com/inward/record.uri?eid=2-s2.0-85175805870&doi=10.1016%2fj.solener.2023.112049&partnerID=40&md5=79f575686dac560ddc40886c0670d95e.

[11] J. Hirschey, Z. Li, K. R. Gluesenkamp, T. J. LaClair, and S. Graham, "Demand reduction and energy saving potential of thermal energy storage integrated heat pumps", *International Journal of Refrigeration*, vol. 148, pp. 179–192, 2023, ISSN: 0140-7007. DOI: https://doi.org/10.1016/j.ijrefrig.2023.01.026. [Online]. Available: https://www.sciencedirect.com/science/article/pii/S0140700723000348.

[12] N. Torricelli, L. Branchini, A. De Pascale, O. Dumont, and V. Lemort, "Optimal management of reversible heat pump/organic rankine cycle carnot batteries", *Journal of Engineering for Gas Turbines and Power*, vol. 145, no. 4, 2023. DOI: 10.1115/1.4055708. [Online]. Available: https://www.scopus.com/inward/record.uri?eid=2-s2.0-85159203479&doi=10.1115%2f1.4055708&partnerID=40&md5=6f62e158e318bf645891797ddd6a4bac.

[13] A. Ramos, M. A. Chatzopoulou, I. Guarracino, J. Freeman, and C. N. Markides, "Hybrid photovoltaic-thermal solar systems for combined heating, cooling and power provision in the urban environment", *Energy Conversion and Management*, vol. 150, pp. 838–850, 2017, ISSN: 0196-8904. DOI: https://doi.org/10.1016/j.enconman.2017.03.024. [Online]. Available: https://www.sciencedirect.com/science/article/pii/S0196890417302273.

[14] M. Emamjome Kashan, A. S. Fung, and J. Swift, "Integrating novel microchannel-based solar collectors with a water-to-water heat pump for cold-climate domestic hot water supply, including related solar systems comparisons", *Energies*, vol. 14, no. 13, 2021, ISSN: 1996-1073. DOI: 10.3390/en14134057. [Online]. Available: https://www.mdpi.com/1996-1073/14/13/4057.

[15] S. Navakrishnan, E. Vengadesan, R. Senthil, and S. Dhanalakshmi, "An experimental study on simultaneous electricity and heat production from solar pv with thermal energy storage", *Energy Conversion and Management*, vol. 245, p. 114 614, 2021, ISSN: 0196-8904. DOI: https://doi.org/10.1016/j.enconman.2021.114614. [Online]. Available: https://www.sciencedirect.com/science/article/pii/S0196890421007901.

[16] M. Carmona, A. Palacio Bastos, and J. D. García, "Experimental evaluation of a hybrid photovoltaic and thermal solar energy collector with integrated phase change material (pvt-pcm) in comparison with a traditional photovoltaic (pv) module", *Renewable Energy*, vol. 172, pp. 680–696, 2021, ISSN: 0960-1481. DOI: https://doi.org/10.1016/j.renene.2021.03.022.

[17] F. Selimefendigil and C. Şirin, "Energy and exergy analysis of a hybrid photovoltaic thermal-air collector modified with nano-enhanced latent heat thermal energy storage unit", *Journal of Energy Storage*, vol. 45, p. 103 467, 2022, ISSN: 2352-152X. DOI: https://doi.org/10.1016/j.est.2021.103467. [Online]. Available: https://www.sciencedirect.com/science/article/pii/S2352152X21011518.

[18] D. Fischer, K. Byskov-Linbder, A. Flunk, B. Wille-Haussmann, N. Kreifels, and J. Scherer, "Impact of hp, chp, pv and evs on households' electric load profiles", Jul. 2015. DOI: 10.1109/PTC.2015.7232784.

[19] B. Mitterrutzner, C. Z. Callegher, R. Fraboni, E. Wilczynski, and S. Pezzutto, "Review of heating and cooling technologies for buildings: A techno-economic case study of eleven european countries", *Energy*, vol. 284, p. 129 252, 2023, ISSN: 0360-5442. DOI: https://doi.org/10.1016/j.energy.2023.129252. [Online]. Available: https://www.sciencedirect.com/science/article/pii/S0360544223026464.

[20] P. Cui, W. Yang, W. Zhang, K. Zhu, J. D. Spitler, and M. Yu, "Advances in ground heat exchangers for space heating and cooling: Review and perspectives", *Energy and Built Environment*, vol. 5, no. 2, pp. 255–269, 2024, ISSN: 2666-1233. DOI: https://doi.org/10.1016/j.enbenv.2022.10.002. [Online]. Available: https://www.sciencedirect.com/science/article/pii/S2666123322000733.

[21] M. E. Konrad and B. D. MacDonald, "Cold climate air source heat pumps: Industry progress and thermodynamic analysis of market-available residential units", *Renewable and Sustainable Energy Reviews*, vol. 188, p. 113 739, 2023, ISSN: 1364-0321. DOI: https://doi.org/10.1016/j.rser.2023.113739. [Online]. Available: https://www.sciencedirect.com/science/article/pii/S1364032123005968.

[22] L. Ji, S. K. Shukla, Z. Zuo, X. Lu, X. Ji, and C. Wang, "An overview of the progress of new working pairs in absorption heat pumps", *Energy Reports*, vol. 9, pp. 703–729, 2023, ISSN: 2352-4847. DOI: https://doi.org/10.1016/j.egyr.2022.11.143. [Online]. Available: https://www.sciencedirect.com/science/article/pii/S235248472202532X.

[23] J. Alpízar-Castillo, L. Ramírez-Elizondo, and P. Bauer, "The effect of non-coordinated heating electrification alternatives on a low-voltage distribution network with high pv penetration", in *2023 IEEE 17th International Conference on Compatibility, Power Electronics and Power Engineering (CPE-POWERENG)*, 2023, pp. 1–6. DOI: 10.1109/CPE-POWERENG58103.2023.10227394.

[24] S. S. Foslie, B. R. Knudsen, and M. Korpås, "Integrated design and operational optimization of energy systems in dairies", *Energy*, vol. 281, p. 128 242, 2023, ISSN: 0360-5442. DOI: https://doi.org/10.1016/j.energy.2023.128242. [Online]. Available: https://www.sciencedirect.com/science/article/pii/S0360544223016365.

[25] J. Alpízar-Castillo, L. Ramirez-Elizondo, and P. Bauer, "Assessing the role of energy storage in multiple energy carriers toward providing ancillary services: A review", *Energies*, vol. 16, no. 1, 2023, ISSN: 1996-1073. DOI: 10.3390/en16010379. [Online]. Available: https://www.mdpi.com/1996-1073/16/1/379.

[26] S. Kumar, T. Kaur, M. Arora, and S. Upadhyay, "Resource estimation and sizing optimization of pv/micro hydro-based hybrid energy system in rural area of western himalayan himachal pradesh in india", *Energy Sources, Part A: Recovery, Utilization and Environmental Effects*, vol. 41, no. 22, pp. 2795–2807, 2019. DOI: 10.1080/15567036.2019.1576075.

[27] M. Barbu, E. Minciuc, D. C. Frusescu, and D. Tutica, "Integration of hybrid photovoltaic thermal panels (pvt) in the district heating system of bucharest, romania", in *2021 10th International Conference on ENERGY and ENVIRONMENT (CIEM)*, 2021, pp. 1–5. DOI: 10.1109/CIEM52821.2021.9614721.

[28] M. Jafari, D. Armaghan, S. Seyed Mahmoudi, and A. Chitsaz, "Thermoeconomic analysis of a standalone solar hydrogen system with hybrid energy storage", *International Journal of Hydrogen Energy*, vol. 44, no. 36, pp. 19 614–19 627, 2019, ISSN: 0360-3199. DOI: https://doi.org/10.1016/j.ijhydene.2019.05.195. [Online]. Available: https://www.sciencedirect.com/science/article/pii/S036031991932110X.

[29] C. Zhou, R. Liang, J. Zhang, and A. Riaz, "Experimental study on the cogeneration performance of roll-bond-pvt heat pump system with single stage compression during summer", *Applied Thermal Engineering*, vol. 149, pp. 249–261, 2019. DOI: 10.1016/j.applthermaleng.2018.11.120. [Online]. Available: https://www.scopus.com/inward/record.uri?eid=2-s2.0-85058216317&doi=10.1016%2fj.applthermaleng.2018.11.120&partnerID=40&md5=cb00d57a24d8cce4e5e2d028f65229fa.

[30] F. Hengel, C. Heschl, F. Inschlag, and P. Klanatsky, "System efficiency of pvt collector-driven heat pumps", *International Journal of Thermofluids*, vol. 5-6, 2020. DOI: 10.1016/j.ijft.2020.100034.

[31] L. Jiang, W. Liu, Y. Lin, R. Wang, X. Zhang, and M. Hu, "Hybrid thermochemical sorption seasonal storage for ultra-low temperature solar energy utilization", *Energy*, vol. 239, 2022. DOI: 10.1016/j.energy.2021.122068. [Online]. Available: https://www.scopus.com/inward/record.uri?eid=2-s2.0-

85115611628&doi=10.1016%2fj.energy.2021.122068&partnerID=40&md5=484c3650ea585574f9fa7ac178bb20c3.

[32] R. Renaldi, A. Kiprakis, and D. Friedrich, "An optimisation framework for thermal energy storage integration in a residential heat pump heating system", *Applied Energy*, vol. 186, pp. 520–529, 2017. DOI: 10.1016/j.apenergy.2016.02.067. [Online]. Available: https://www.scopus.com/inward/record.uri?eid=2-s2.0-84959144692&doi=10.1016%2fj.apenergy.2016.02.067&partnerID=40&md5=164f2c5cc2b54592e159df2d5315749d.

[33] M. Aunedi and G. Strbac, "System benefits of residential heat storage for electrified heating sector in the united kingdom", in *2022 IEEE PES Innovative Smart Grid Technologies Conference Europe (ISGT-Europe)*, 2022, pp. 1–5. DOI: 10.1109/ISGT-Europe54678.2022.9960709.

[34] A. Vallati, C. V. Fiorini, G. L. Basso, F. Muzi, P. Oclon, and M. di Matteo, "Optimization of a thermal storage tank for a water water heat pump solar assited", in *2023 8th International Conference on Smart and Sustainable Technologies (SpliTech)*, 2023, pp. 1–7. DOI: 10.23919/SpliTech58164.2023.10192989.

[35] H. ur Rehman, A. Hasan, and F. Reda, "Challenges in reaching positive energy building level in apartment buildings in the nordic climate: A techno-economic analysis", *Energy and Buildings*, vol. 262, p. 111 991, 2022, ISSN: 0378-7788. DOI: https://doi.org/10.1016/j.enbuild.2022.111991.

[36] M.-H. Kim, Y. An, H.-J. Joo, D.-W. Lee, and J.-H. Yun, "Self-sufficiency and energy savings of renewable thermal energy systems for an energy-sharing community", *Energies*, vol. 14, no. 14, 2021. DOI: 10.3390/en14144284.

[37] M. Herrando, A. Ramos, J. Freeman, I. Zabalza, and C. N. Markides, "Technoeconomic modelling and optimisation of solar combined heat and power systems based on flat-box pvt collectors for domestic applications", *Energy Conversion and Management*, vol. 175, pp. 67–85, 2018. DOI: 10.1016/j.enconman.2018.07.045. [Online]. Available: https://www.scopus.com/inward/record.uri?eid=2-s2.0-85052890685&doi=10.1016%2fj.enconman.2018.07.045&partnerID=40&md5=bef699b640829fcb05004208045171d1.

[38] S. Abdul-Ganiyu, D. A. Quansah, E. W. Ramde, R. Seidu, and M. S. Adaramola, "Techno-economic analysis of solar photovoltaic (pv) and solar photovoltaic thermal (pvt) systems using exergy analysis", *Sustainable Energy Technologies and Assessments*, vol. 47, 2021. DOI: 10.1016/j.seta.2021.101520. [Online]. Available: https://www.scopus.com/inward/record.uri?eid=2-s2.0-85112290300&doi=10.1016%2fj.seta.2021.101520&partnerID=40&md5=b8fea69671b51d40b62e83e061b272f7.

[39] H. Gholami, A. Khalilnejad, and G. Gharehpetian, "Electrothermal performance and environmental effects of optimal photovoltaic-thermal system", *Energy Conversion and Management*, vol. 95, pp. 326–333, 2015. DOI: 10.1016/j.enconman.2015.02.014. [Online]. Available: https://www.scopus.com/inward/record.uri?eid=2-s2.0-84923829852&doi=10.1016%2fj.enconman.2015.02.014&partnerID=40&md5=321094fe41a1066dc1e00be6483c66ef.

[40] Z. Rostmnezhad and L. Dessaint, "Power management in smart buildings using reinforcement learning", 2023. DOI: 10.1109/ISGT51731.2023.10066398. [Online]. Available: https://www.scopus.com/inward/record.uri?eid=2-s2.0-85151492082&doi=10.1109%2fISGT51731.2023.10066398&partnerID=40&md5=912d89ca3b23d400b11eea364f2285e0.

[41] F. Brahman, M. Honarmand, and S. Jadid, "Optimal electrical and thermal energy management of a residential energy hub, integrating demand response and energy storage system", *Energy and Buildings*, vol. 90, pp. 65–75, 2015. DOI: 10.1016/j.enbuild.2014.12.039.

[42] M. Koch and R. Dott, "Contributions to system integration of pv and pvt collectors with heat pumps in buildings", *E3S Web of Conferences*, vol. 111, p. 01 061, Jan. 2019. DOI: 10.1051/e3sconf/201911101061.

[43] M. Izquierdo and P. de Agustín-Camacho, "Solar heating by radiant floor: Experimental results and emission reduction obtained with a micro photovoltaic–heat pump system", *Applied Energy*, vol. 147, pp. 297–307, 2015, ISSN: 0306-2619. DOI: https://doi.org/10.1016/j.apenergy.2015.03.007.

[44] J. Hyvönen, A. Santasalo-Aarnio, S. Syri, and M. Lehtonen, "Feasibility study of energy storage options for photovoltaic electricity generation in detached houses in nordic climates", *Journal of Energy Storage*, vol. 54, 2022. DOI: 10.1016/j.est.2022.105330. [Online]. Available: https://www.scopus.com/inward/record.uri?eid=2-s2.0-85134710899&doi=10.1016%2fj.est.2022.105330&partnerID=40&md5=d5665bbeee430c39dc8051c285996c23.

[45] N. A. Efkarpidis, G. C. Christoforidis, and G. K. Papagiannis, "Assessment of energy management strategies in buildings equipped with modulating heat pumps", 2022. DOI: 10.1109/SyNERGYMED55767.2022.9941406. [Online]. Available: https://www.scopus.com/inward/record.uri?eid=2-s2.0-85142886916&doi=10.1109%2fSyNERGYMED55767.2022.9941406&partnerID=40&md5=7c16a1608c0d12b14362a7cd758d1b42.

[46] M. Banaei, F. D'Ettorre, R. Ebrahimy, E. M. V. Blomgren, and H. Madsen, "Mutual impacts of procuring energy flexibility and equipment degradation at the residential consumers level", in *2021 IEEE PES Innovative Smart Grid Technologies Europe (ISGT Europe)*, 2021, pp. 1–6. DOI: 10.1109/ISGTEurope52324.2021.9640142.

[47] E. Fuentes, L. Arce, and J. Salom, "A review of domestic hot water consumption profiles for application in systems and buildings energy performance analysis", *Renewable and Sustainable Energy Reviews*, vol. 81, pp. 1530–1547, 2018, ISSN: 1364-0321. DOI: https://doi.org/10.1016/j.rser.2017.05.229. [Online]. Available: https://www.sciencedirect.com/science/article/pii/S1364032117308614.

[48] "EN standard 806-3 - specification for installations inside buildings conveying water for human consumption.", Tech. Rep., 2012.

[49] I. Pothof, T. Vreeken, and M. van Meerkerk, "Field measurements on lower radiator temperatures in existing buildings", Warming Up, Tech. Rep., 2022. [Online]. Available: https://www.warmingup.info/documenten/11205149-hye-001_field-measurements-on-lower-radiator-temperatures-in-existing-buildings_def.pdf (visited on 11/10/2023).

[50] R. American Society of Heating and I. (Air-Conditioning Engineers, *2021 ASHRAE® Handbook - Fundamentals (SI Edition)*. American Society of Heating, Refrigerating and Air-Conditioning Engineers, Inc. (ASHRAE), 2021, ISBN: 978-1-947192-90-4.

[51] R. K. Singh and R. V. Sharma, "Numerical analysis for ground temperature variation", *Geotherm. Energy*, vol. 5, no. 1, 2017. [Online]. Available: https://geothermal-energy-journal.springeropen.com/articles/10.1186/s40517-017-0082-z.

[52] D. Hillel, Ed., *Composite Phenomena*. Burlington: Academic Press, 2003, p. xi, ISBN: 978-0-12-348655-4. DOI: https://doi.org/10.1016/B978-012348655-4/50000-9. [Online]. Available: https://www.sciencedirect.com/science/article/pii/B9780123486554500009.

[53] R. Y. Wong, C. Tso, S. Jeong, S. Fu, and C. Y. Chao, "Critical sky temperatures for passive radiative cooling", *Renewable Energy*, vol. 211, pp. 214–226, 2023, ISSN: 0960-1481. DOI: https://doi.org/10.1016/j.renene.2023.04.142. [Online]. Available: https://www.sciencedirect.com/science/article/pii/S0960148123006080.

[54] M. Barbu, M. Siroux, and G. Darie, "Numerical model and parametric analysis of a liquid based hybrid photovoltaic thermal (pvt) collector", *Energy Reports*, vol. 7, pp. 7977–7988, 2021, ISSN: 2352-4847. DOI: https://doi.org/10.1016/j.egyr.2021.07.058. [Online]. Available: https://www.sciencedirect.com/science/article/pii/S2352484721005242.

[55] L. Wai Zhe, M. Yusoff, S. Ibrahim, *et al.*, "Simulation study on photovoltaic panel temperature under different solar radiation using computational fluid dynamic method", *Journal of Physics: Conference Series*, vol. 1432, Jan. 2020. DOI: 10.1088/1742-6596/1432/1/012052.

[56] N. Damianakis, G. C. R. Mouli, and P. Bauer, "Risk-averse estimation of electric heat pump power consumption", in *2023 IEEE 17th International Conference on Compatibility, Power Electronics and Power Engineering (CPE-POWERENG)*, 2023, pp. 1–6. DOI: 10.1109/CPE-POWERENG58103.2023.10227424.

[57] M. Pipattanasomporn, M. Kuzlu, S. Rahman, and Y. Teklu, "Load profiles of selected major household appliances and their demand response opportunities", *IEEE Transactions on Smart Grid*, vol. 5, no. 2, pp. 742–750, 2014. DOI: 10.1109/TSG.2013.2268664.

[58] J. Alpízar-Castillo, V. Vega-Garita, N. Narayan, and L. Ramirez-Elizondo, "Open-access model of a pv-bess system: Quantifying power and energy exchange for peak-shaving and self consumption applications", *Energies*, vol. 16, no. 14, 2023, ISSN: 1996-1073. DOI: 10.3390/en16145480. [Online]. Available: https://www.mdpi.com/1996-1073/16/14/5480.

[59] KNMI, *Uurgegevens van het weer in nederland*, 2022. [Online]. Available: https://www.knmi.nl/nederland-nu/klimatologie/uurgegevens (visited on 08/16/2023).

[60] S. D. Energie, *Duurzame warmte, de technieken van de warmtetransitie*. Oct. 2019. [Online]. Available: https://servicepuntduurzameenergie.nl/wp-content/uploads/2019/10/Duurzame-warmte.pdf (visited on 11/10/2023).

[61] C. van der Veen, *Analysing thermal energy storage in residential buildings: Towards decarbonization of the heating sector*, The Netherlands, 2022. [Online]. Available: https://repository.tudelft.nl/islandora/object/uuid:c1fca7b7-a7cb-4ddc-936e-239a8f0a6cb7?collection=education.

[62] J. M. van Esch, *BTM+ model and Expert tool*. Sep. 2022. [Online]. Available: https://backend.tkiwatertechnologie.nl/wp-content/uploads/2020/10/Engine-BTM-and-EXPERT.pdf.

[63] J. G. Veldkamp and D. Hegen, *Temperature modelling of the Dutch subsurface at the depth of the Dinantian*. Apr. 2020. [Online]. Available: https://www.nlog.nl/sites/default/files/2020-04/SCAN%20Dinantian%20Temperature%20modelling%20Dutch%20subsurface%20at%20depth%20Dinantian%20report.pdf.

4

Energy Management Systems: Power Allocation Methods in Residential Multi-Carrier Energy Systems

"I wish I were that strong... but reality is disappointing."

Snek, One-Punch Man, volume 63, by One and Yosuke Murata.

This Chapter is based on

- **J. Alpízar-Castillo**, V. Vega-Garita, N. Narayan, L. Ramirez-Elizondo, "Open-Access Model of a PV–BESS System: Quantifying Power and Energy Exchange for Peak-Shaving and Self Consumption Applications," Energies, vol. 16, no. 14, Jul. 2023, pp.5480, doi: 10.3390/en16145480.
- **J. Alpízar-Castillo**, A. Fu, L. Ramírez-Elizondo, M. Cvetkovic and P. Bauer, "Multi-Carrier Home Energy Management System Using Genetic Algorithms and Random Forest Regression Estimations," IEEE Energy Conversion Conference and Expo (ECCE USA), Phoenix, United States of America, 2024, pp. 1037-1044, doi: 10.1109/ECCE55643.2024.10861342.
- D. Slaifstein, **J. Alpízar-Castillo**, A. M. Agudin, L. Ramírez-Elizondo, G. R. C. Mouli and P. Bauer, "Aging-Aware Battery Operation for Multicarrier Energy Systems," IECON 2023- 49th Annual Conference of the IEEE Industrial Electronics Society, Singapore, Singapore, 2023, pp. 1-8, doi: 10.1109/IECON51785.2023.10312455.

4.1. INTRODUCTION

The inclusion of distributed renewable energy sources and electric vehicles in the energy mix has accelerated the energy transition in the last decade. More recently, heating electrification has gained momentum, albeit still heavily dependent on fossil fuels. Therefore, current research proposes the creation of multi-carrier energy systems (MCES) to combine heat and electrical generation, consumption and storage [1]. Recent studies have demonstrated that such combinations help minimize the impact of distributed renewable energy systems (DRES) in the distribution networks if an adequate control strategy is implemented [2]. However, controlling such complex systems has proven challenging for energy management system (EMS) designers, as their combined models are generally non-linear, non-convex, and heavily constrained, resulting in high computation costs and convergence difficulties [3].

Different energy management system strategies have been proposed in the literature in an attempt to overcome those challenges. Rule-based controls (RB), also known as heuristics, have been commonly used in implementations despite requiring numerous correlations and operation cases since they usually do not show convergence challenges [4]. Nevertheless, they cannot guarantee optimality and rarely use predictions. Thus, more complex optimization strategies have been proposed to handle uncertainty, consider multiple objectives simultaneously, or ensure optimality. For instance, [5] proposed a real-time home energy management system controller using mixed-integer linear programming for a multi-objective problem, achieving cost minimization. An optimization for controlling a multi-carrier system for demand response applications was solved using mixed-integer linear programming by [6] to minimize the operative costs, highlighting the importance of energy storage to provide flexibility to the grid. Day-ahead and real-time participation of an aggregated MCES were studied in [7], using an event-triggered-based distributed algorithm, but the internal energy flow control between the assets was not considered. In [8], the EMS minimized the ageing of the battery energy storage system (BESS) and total energy cost in a residential MCES, reducing the grid costs up to 45 % when compared with controllers that do not consider the degradation of the batteries. A distributed energy management system using sub-gradient averaging consensus was proposed in [9] for real-time control of coupled energy hubs, achieving optimality despite challenges in the convergence rate.

A review in [10] evaluated different artificial intelligence techniques used for power allocation optimization and parameter prediction, concluding that more research is still required to couple such applications given their complexity and computational cost. The work in [11] used the non-dominated sorting genetic algorithm II to control in real-time the power flow of a multi-carrier energy system in Italy comprised of a renewable energy source system, an EV charger, a water electrolyzer and a fuel cell. The objective functions included the total energy cost and the deviation of a setpoint the distribution system operator (DSO) requested to assist in grid balancing. Dynamic fuzzy logic was used by [12] to optimize renewable energy utilization and minimize electric and gas purchases from the grid, achieving a reduction of up to 80 % in the electric grid. A comparison of gate recurrent unit temporal convolutional network and deep Q-network was done by [13] as energy management strategies for a multi-carrier system, resulting in an economical cost reduction of 14.5 % when using the former.

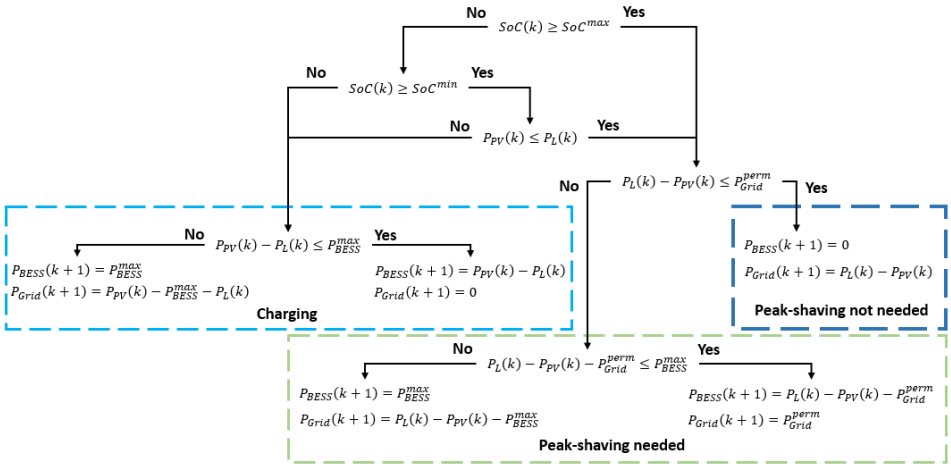

Figure 4.1: Decision sequence for the electric power dispatch of the rule-based control.

The literature agrees that computational cost is one of the main challenges to implementing successful energy management systems, especially for multi-carrier energy systems. In addition, [14] reviewed the available simulation and optimization tools, highlighting that coupling the different carriers remains challenging and that many available tools require a license, urging for modular, open-source alternatives. For this reason, an accessible EMS strategy that balances the computational cost and the accuracy is required. Thus, the contributions of this Chapter are:

- proposing a modular genetic algorithm (GA) EMS strategy for short-term control of the power flow between the assets of a household multi-carrier energy system, intrinsically adaptable to different system architectures, forecasting methods and time horizons, and
- analyzing an ageing-aware strategy operation that exploits the trade-off between battery operation and its degradation in the context of energy systems with multiple carriers

4.2. RULE-BASED CONTROL

Many controllers available use sets or conditional rules for their operation. This strategy has individual controls for the electric and thermal carriers, following the control schemes shown in Figures 3.7 for the electric carrier, and 3.5 for the thermal. For the former, the control is defined to limit the power purchased from the grid to a maximum value $P_{\text{Grid}}^{\text{perm}}$; loads above such value would be shaved using the energy from the PV system first and then from the BESS. The decision sequence is shown in Figure 4.1.

For the thermal carrier, following the recommendations from Chapter 3, the PVT system was replaced by a solar thermal collector, which can reach temperatures high enough to charge the TESS. This way, the control will prioritize the solar collectors, then the thermal storage system, and at last, the heat pump, as shown in Figure 4.2.

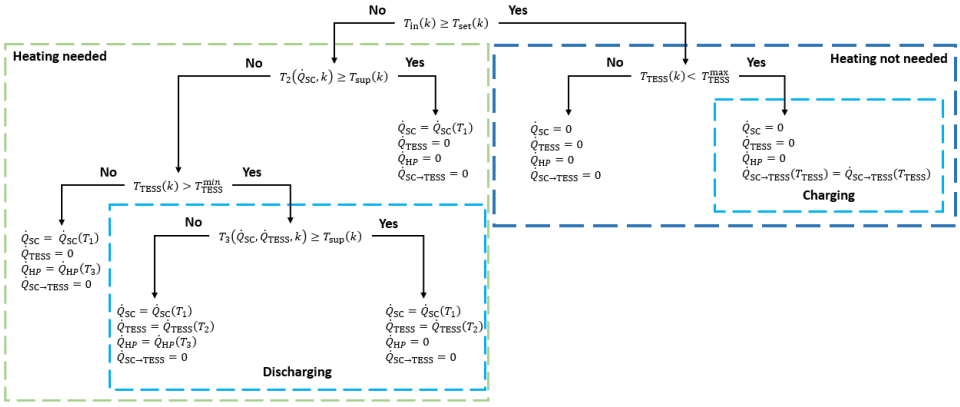

Figure 4.2: Decision sequence for the thermal power dispatch of the rule-based control.

4.3. GENETIC ALGORITHM REAL-TIME CONTROL

Literature offers many methods to solve the local power allocation, considering different optimization objectives. Generally, the optimization problem requires minimising a cost function while electric power balances. However, few works have included satisfying the thermal power balance to ensure thermal comfort. Therefore, this Section proposes a novel approach using genetic algorithms to solve the multi-objective problem for real-time control. Based on the thermo-electrical models provided in Chapter 3, the thermal energy balance is given by

$$\dot{Q}_D = \dot{Q}_L + \dot{Q}_v + \dot{Q}_i \tag{4.1}$$

as a function of the thermal power loss through walls, windows and roof due to the thermal difference between indoor and outdoor temperatures, T_{in} and T_{out} respectively,

$$\dot{Q}_L(k) = \sum_{i=1}^{n} U_i A_i \left[T_{\text{in}}(k) - T_{\text{out}}(k)\right], \tag{4.2}$$

the ventilation losses

$$\dot{Q}_v(k) = c_a \rho_a q_v \left[T_{\text{in}}(k) - T_{\text{out}}(k)\right], \tag{4.3}$$

and infiltration losses

$$\dot{Q}_i(k) = c_a \rho_a q_i \left[T_{\text{in}}(k) - T_{\text{out}}(k)\right], \tag{4.4}$$

allowing one to estimate the indoor temperature, as

$$T_{\text{in}}(k+1) = T_{\text{in}}(k) + \frac{\Delta t \left[\dot{Q}_{\text{SC}}(k) + \dot{Q}_{\text{TESS}}(k) + \dot{Q}_{\text{HP}}(k) - \dot{Q}_{\text{D}}(k)\right]}{\sum_{i=1}^{n} m_i c_i}. \tag{4.5}$$

The power purchased from the grid ensures the electric power balance as

$$P_{\text{G}} = P_{\text{L}} + P_{\text{HP}} - P_{\text{PV}} - P_{\text{BESS}}, \tag{4.6}$$

where, P_{PV}, P_{BESS}, P_L and P_{HP} are the powers from the PV, the BESS, the load and the heat pump, respectively. A negative P_{BESS} means the BESS is charging.

For the chromosome structure shown in Figure 4.3, each gene controls a different device within the MCES (called *setpoint genes*), and the last one represents the cost associated with those control values (called *suitability gene*). Unlike traditional implementations of GA, this work proposes a discrete-continuous approach, where some genes are binary and others continuous within the same chromosome, reducing the maximum possible combinations and computational cost. For the thermal carrier, the genes are binary, as the technologies for solar collectors, thermal storage and heat pumps work at an on/off pace. Curtailment in the PV system was considered, so the corresponding setpoint gene goes from 0 to 1 of the available power at the timestep. Finally, the power delivered or consumed by the BESS is constrained by its SoC. To avoid adding constraints to the cost function, a function of the capacity (C_{BESS}), the inverter maximum power (P^{max}_{BESS}), and the current SoC of the battery is proposed to determine the maximum and minimum power the battery can exchange P^{perm}_{BESS}. Such values are

$$\overline{P}^{perm}_{BESS}(k) = \begin{cases} P^{max}_{BESS} & \forall \quad P_{BESS}(k) \geq P^{max}_{BESS} \\ C_{BESS}\dfrac{SoC_{BESS}(k) - SoC^{min}_{BESS}}{\Delta t} & \forall \quad P_{BESS}(k) < P^{max}_{BESS} \end{cases}, \tag{4.7}$$

and

$$\underline{P}^{perm}_{BESS}(k) = \begin{cases} C_{BESS}\dfrac{SoC_{BESS}(k) - SoC^{max}_{BESS}}{\Delta t} & \forall \quad P_{BESS}(k) > -P^{max}_{BESS} \\ -P^{max}_{BESS} & \forall \quad P_{BESS}(k) \leq -P^{max}_{BESS} \end{cases}. \tag{4.8}$$

This way, the gene that controls the BESS can only have values within a range that will not violate the SoC constraint, reducing the complexity of the optimization problem. On the other hand, the SoC constraint for the TESS has to remain as a formal constraint, where the thermal power from the TESS has to be 0 W if the temperature in the TESS is below the minimum allowed temperature (50 °C), and it cannot charge if its temperature is above the maximum allowed temperature (95 °C).

The optimization proposed aims to minimize a weighted multi-objective function that considers the economic cost of using each device per timestep and the thermal comfort the residents in the house will have due to such control actions. This function can be written as

$$\min(C(k)) = \min\left(\theta_T C_T(k), \theta_E C_E(k), \theta_{CO_2} C_{CO_2}(k)\right), \tag{4.9}$$

where C_T, C_E and C_{CO_2} are the cost functions for the thermal comfort, the economic energy costs and the CO_2 equivalent emissions, and θ_T, θ_E and θ_{CO_2} are their balance weights. The only constraint for the problem is

$$T^{min}_{TESS} < T_{TESS}(k) < T^{max}_{TESS} \tag{4.10}$$

The cost for thermal comfort depends on the relation of the indoor temperature and the setpoint temperature at a certain instant k. If the indoor temperature T_{in} is above

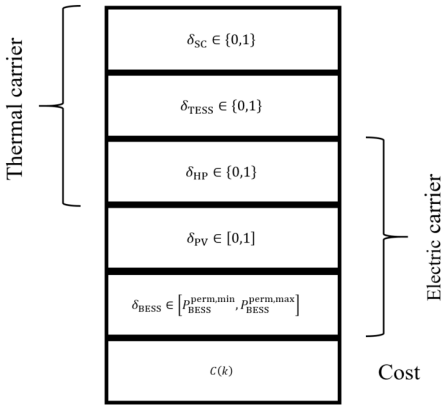

Figure 4.3: Individual chromosome proposed for the genetic algorithm.

the setpoint temperature T_{set}, heating will be penalized. In contrast, heating will be rewarded if the indoor temperature is below the setpoint, using a comfort factor β [15]. This way, the function is defined as

$$C_T(k) = \beta |T_{\text{set}} - T_{\text{in}}| \tag{4.11}$$

For the energy cost, the function depends on the operational cost of energy for each device of the MCES i considered (λ_i), as well as the cost of the energy purchased from the grid λ_G under a feed-in scheme. Thus, the function is defined as:

$$C_E(k) = \left(\sum_{i=1}^{n} P_i \lambda_i + \sum_{i=1}^{n} \dot{Q}_i \lambda_i \right) \Delta t. \tag{4.12}$$

Similarly, the total CO_2 emissions are calculated as

$$C_{CO_2}(k) = \left(\sum_{i=1}^{n} P_i \, \text{CI}_i \right) \Delta t. \tag{4.13}$$

where CI is the CO_2 intensity per kWh.

The genetic algorithm used to solve the optimization problem is shown in Figure 4.4. Considering the number of genes in the chromosome and their possible values, the maximum number of combinations is 2080. Note that the pool of possible gene combinations is relatively small; this is possible because three of the five genes are binary, and we considered steps of 0.1 for the PV curtailment and the BESS power setpoint genes. A population of 200 individuals was considered for each generation, with an elitist approach to generating new individuals. The crossing included the 5 % of individuals with the lowest cost and a random sample of 15 % of the remaining individuals. The new population was selected randomly from the previous one, plus the new individuals. No mutation was considered. To determine the individual that best solves the optimization problem, we established a permanence of 5 consecutive generations.

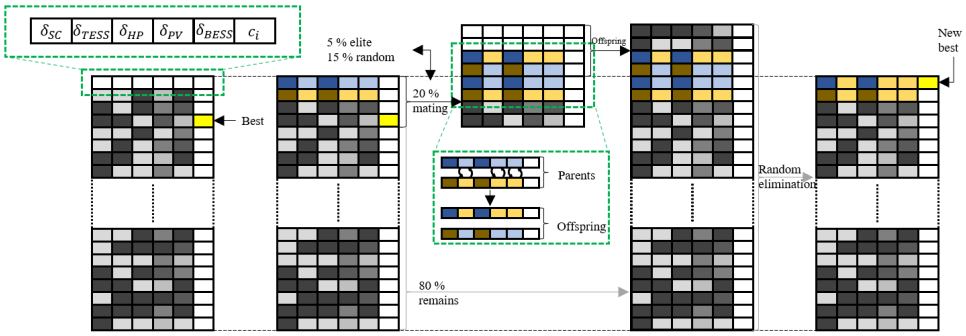

Figure 4.4: Genetic algorithm proposed to minimize the cost function for the real-time controller.

4.3.1. SENSITIVITY ANALYSIS

An appropriate population size is required to balance the time the algorithm requires to solve the cost function and how close to the theoretical optimal such solution would be. Larger populations would provide a more diverse set of possible solutions, albeit having a higher computational cost. Nevertheless, it is expected that, at some point, increasing the population's size does not significantly improve the result.

Figure 4.5 shows the normalized cost during one year as a function of the size of the population and the shoulder identification curve given by

$$K\left(c\left(X\right),X\right)=\left[\frac{c\left(X\right)_{\max}-c\left(X\right)}{c\left(X\right)_{\max}}\right]\left[X_{\max}-X\right], \tag{4.14}$$

where $c\left(X\right)$ is the cost associated with an X-size population, and $\max\left(K\right)$ is the shoulder point. The results suggest that increasing the population beyond 75 will not substantially improve the algorithm's performance.

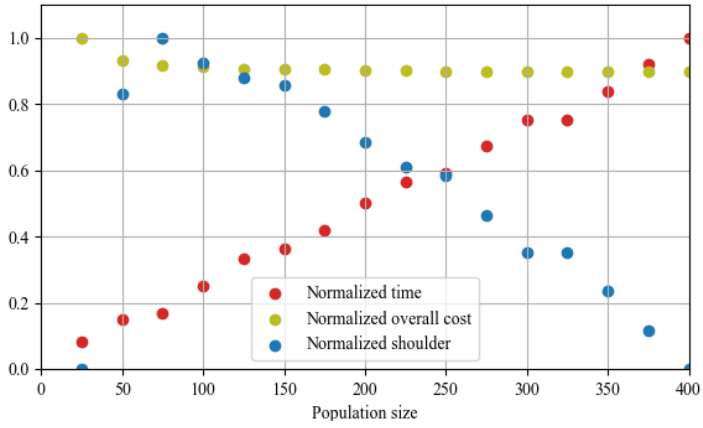

Figure 4.5: Overall cost vs. population size.

For the weights in (4.9), the energy and carbon intensity cost weights were deter-

mined considering a case where all the components were working at full capacity; this way, the weighting factor θ normalizes the results. A boundary for the setpoint temperature of ±1 °C was considered before thermal discomfort, following the standard ASHRAE 55 [16]. Then, a simulation was done for 2022 to evaluate the costs individually and determine the maximum value per cost during the year to normalize the results. The process was iterated until no weight adjustment was needed to obtain normalized results. The values obtained are: $\theta_E = 0.06$, $\theta_T = 1$, and $\theta_{CO_2} = 0.4$. Five consecutive generations were considered.

The diversity (proportion of unique individuals in a population) was also analyzed as a function of the population size. Given that the algorithm does not filter individuals with the same genes, the possibility of having identical individuals arises when increasing the population size. To this extent, Figure 4.6 shows the diversity associated with different population sizes. The results confirm that increasing the population size reduces the proportion of unique individuals. Note that the absolute number of unique individuals does increase.

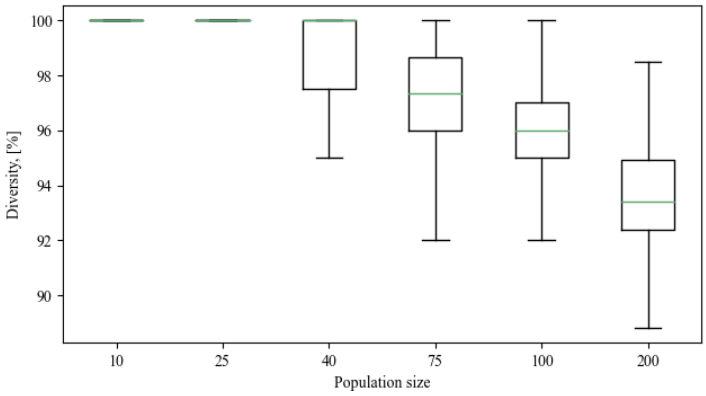

Figure 4.6: Diversity vs. population size.

4.3.2. RESULTS ANALYSIS

To evaluate the performance of the proposed approach, the rule-based control described in Section 4.2 was used as a reference. The rule-based algorithm prioritizes supplying the demand with the PV generation in the electric carrier. If it is not enough, it will use the BESS and, as the last resource, it will buy energy from the grid. If there is a surplus of PV, the EMS will prioritize charging the battery to sell the energy to the grid when possible. The BESS inverter limitations are considered during charge and discharge. Similarly, for the thermal carrier, if the indoor temperature is below the setpoint, the EMS will prioritize the power from the solar collectors, then the TESS and at last the HP. When not used to heat the house, the excess of power from the solar collectors will charge the TESS. Table 4.1 shows the parameters used for the simulation. The values considered for the thermal losses of the house are described in Chapter 3, and the load conditions used are based on typical power consumptions of household appliances [17]. The costs and

intensity factors were taken from [18], [19].

Table 4.1: Parameters considered for the simulation

Symbol	Value	Units	Parameter
		Electric sub-system	
$P_{\text{PV}}^{\text{peak}}$	4	kW	PV system peak power
$P_{\text{BESS}}^{\text{max}}$	1.28	kW	BESS inverter maximum power
C_{BESS}	3.36	kWh	BESS capacity
$\eta_{\text{BESS}}^{c,d}$	0.943	-	BESS charge and discharge efficiency
$SoC_{\text{BESS}}^{\text{min}}$	20	%	BESS minimum SoC
$SoC_{\text{BESS}}^{\text{max}}$	90	%	BESS maximum SoC
P_{HP}	2.7	kW	HP electrical power
		Thermal sub-system	
A_{SC}	6	m^2	SC area
η_{SC}	0.45	-	SC efficiency
V_{TESS}	4	m^3	TESS volume
$\dot{Q}^{\text{SD}}$	0.1	kW	TESS self discharge power
Q_{TESS}	210	kWh	TESS capacity
$T_{\text{TESS}}^{\text{min}}$	50	°C	TESS minimum temperature
$T_{\text{TESS}}^{\text{max}}$	95	°C	TESS maximum temperature
$\eta_{\text{TESS}}^{c,d}$	0.8	-	TESS heat exchanger efficiency
		Optimization	
λ_{G}	0.483	€/kWh	Grid energy cost
λ_{BESS}	0.13	€/kWh	BESS energy cost
θ_E	0.06	$€^{-1}$	Energy costs weight
β	6	-	Temperature comfort factor
θ_T	1	$°\text{C}^{-1}$	Temperature comfort weight
$T_{\text{set}}^{\text{day}}$	20	°C	Setpoint temperature (06:00-20:00)
$T_{\text{set}}^{\text{night}}$	17	°C	Setpoint temperature ($20{:}00\text{-}06{:}00^{+1}$)
CI_{G}	0.325	kg_{CO_2}/kWh	Grid energy carbon intensity
θ_{CO_2}	0.4	$\text{kg}_{\text{CO}_2}{}^{-1}$	Carbon intensity weight

An evaluation of how each control algorithm allocated the power among the devices of the MCES to supply the thermal and electrical demand was performed. Figure 4.7 shows the results for the GA EMS. The main difference between the algorithms is the usage of the solar collectors and the TESS, as shown in Figure 4.8. The GA EMS prioritized supplying the thermal demand directly from the SC to minimize the usage of the TESS. In contrast, the RB control preferred charging the TESS with the SC and splitting the thermal demand almost evenly between the TESS and the HP. As a result, the HP is used 18 % less with the GA, reducing the overall load supplied from the PV and the grid. Similarly, given the cost associated with the degradation of the BESS, the GA reduced its usage and curtailed the power of the PV, reducing the energy stored in the BESS, but also

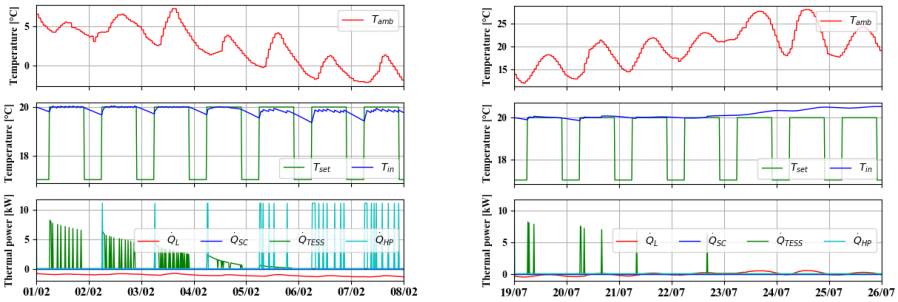

(a) (b)

Figure 4.7: Thermal power allocation during (a) winter and (b) summer using the real-time GA controller.

the energy sent back to the grid. Overall, the GA purchased 3 % less energy from the grid, reducing the $CO_{2,eq}$ associated with the system's operation.

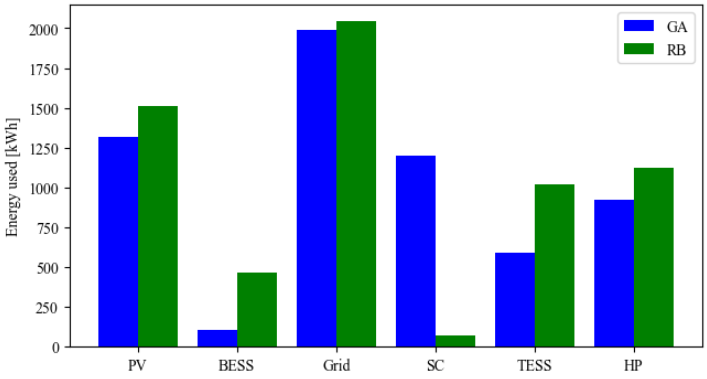

Figure 4.8: Energy consumption comparison per component of the MCESS while simulating the GA and RB control strategies for one year.

The thermal comfort is evaluated based on the difference between the indoor and setpoint temperatures ($T_{\text{in}}(k) - T_{\text{set}}(k)$). Figure 4.9 shows that the deviation distribution has two peaks, one centred near 0 °C, and the other near 3 °C. This can be explained because, during the day (06:00-20:00), the temperature inside the house is set at 20 °C, so both controllers keep it near that value. When the setpoint changes to 17 °C at night, there is a positive difference of 3 °C, which decays in time as the house loses heat to the environment. The GA keeps the indoor temperature slightly below the setpoint because it accounts for thermal comfort; therefore, it does not necessarily need to reach the setpoint exactly to be considered comfortable. On the other hand, the RB usually overshoots the temperature above the setpoint as it is set to always keep the temperature above

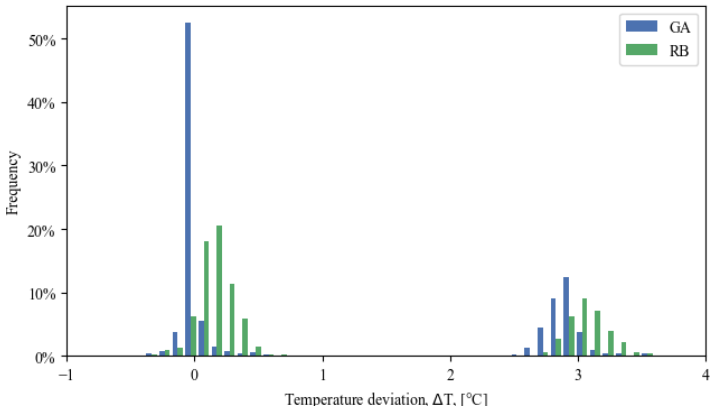

Figure 4.9: Distribution of the temperature deviation with respect to the setpoint ($T_{\text{in}}(k) - T_{\text{set}}(k)$) while simulating the GA and RB control strategies for one year.

A 16 GB RAM laptop with an Intel i7-1185G7 processor was used to run the full year ten times. On average, the GA takes 16.83 s to complete each day, whereas the RB model takes 0.0348 s. Albeit the RB control is considerably faster, the GA allows more complex decisions, which can be easily escalated in cases where operation costs should be considered or where the assets do have a direct $CO_{2,\text{eq}}$ emission, as will be demonstrated in Section 4.4. The results showed that the GA reduced the energy costs compared to a rule-based model while supplying the electric and thermal demands and ensuring thermal comfort. The proposed GA is also suitable for real-time controllers as each timestep requires 0.175 s on average, demonstrating that it does not have dimensionality issues. Section 4.4 includes a prediction horizon so the EMS can take the future state of the model to make better decisions.

4.4. GENETIC ALGORITHM SHORT-TIME PREDICTIVE CONTROL

Section 4.3 presented a real-time control EMS strategy to consider simultaneously energy cost, thermal comfort and equivalent CO_2 emissions. This Section generalizes the expression to determine the power setpoint for each controllable element within a prediction horizon h. This way, a gene determines the setpoint value δ for each device at a particular instant in the future i with respect to the current time step $(k+i|k)$. Those genes are grouped per timestep; this way, there is a chromosome section that includes the *setpoint genes* of all the devices for each instant $(k+i|k)$ between $(k|k)$ and $(k+h|k)$, as shown in Figure 4.10. Similarly to the real-time implementation, the last gene of the chromosome (*suitability gene*) contains the overall performance of that control profile, which is used to build the Pareto front. To overcome possible dimensionality issues, the same discrete-continuous approach used for the real-time control was used for the setpoints during the horizon, as, in reality, some devices work on an on/off basis. Such devices are the solar collectors, the TESS and the HP. In the case of the solar collectors, the power is sent by default to the house; if they are not activated and there is power available, it will be used to charge the TESS. On the other hand, the BESS is intrinsically continuous, and power curtailment was considered; therefore, the PV is also continu-

ous, ranging from 0 to 1, where 1 is the maximum available PV power at the particular timestep. For the BESS, equations (4.15) and (4.16) are also considered to avoid unfeasible solutions to set the gene boundaries. Those functions are adapted for the prediction horizon as

$$\overline{P}^{\text{perm}}_{\text{BESS}}(k+i|k) = \begin{cases} P^{\max}_{\text{BESS}} & \forall \quad P_{\text{BESS}} \geq P^{\max}_{\text{BESS}} \\ C_{\text{BESS}} \Delta SoC^{\max}_{\text{BESS}}(k+i|k) & \forall \quad P_{\text{BESS}} < P^{\max}_{\text{BESS}} \end{cases} \tag{4.15}$$

and

$$\underline{P}^{\text{perm}}_{\text{BESS}}(k+i|k) = \begin{cases} C_{\text{BESS}} \Delta SoC^{\min}_{\text{BESS}}(k+i|k) & \forall \quad P_{\text{BESS}} > -P^{\max}_{\text{BESS}} \\ -P^{\max}_{\text{BESS}} & \forall \quad P_{\text{BESS}} \leq -P^{\max}_{\text{BESS}} \end{cases} \tag{4.16}$$

with

$$\Delta SoC^{\max}_{\text{BESS}}(k+i|k) = \frac{SoC_{\text{BESS}}(k+i|k) - SoC^{\min}_{\text{BESS}}}{\Delta t} \tag{4.17}$$

and

$$\Delta SoC^{\min}_{\text{BESS}}(k+i|k) = \frac{SoC_{\text{BESS}}(k+i|k) - SoC^{\max}_{\text{BESS}}}{\Delta t}. \tag{4.18}$$

This way, the only remaining constraint for the optimization problem is the TESS SoC. The thermal power from the TESS has to be 0 W if the temperature in the TESS is below the minimum allowed temperature (50 °C), and it cannot charge if its temperature is above the maximum allowed temperature (95 °C).

The optimization problem to solve is also (4.9). However, the costs have to be adjusted to include the prediction horizon h, thus the operational cost (OPEX) is

$$C_E(k) = \sum_{k=0}^{h} \left(\sum_{i=1}^{n} P_i(k)\, \lambda_i(k) + \sum_{i=1}^{n} \dot{Q}_i(k)\, \lambda_i(k) \right) \Delta t, \tag{4.19}$$

the thermal comfort cost is

$$C_T(k) = \beta \sum_{k=0}^{h} |T_{\text{set}}(k) - T_{\text{in}}(k)|, \tag{4.20}$$

and the equivalent CO_2 emissions cost is

$$C_{CO_2}(k) = \sum_{k=0}^{h} \left(\sum_{i=1}^{n} P_i(k)\, \text{CI}_i \right) \Delta t. \tag{4.21}$$

during the prediction horizon h. The best solution per objective will not necessarily be the best overall solution, i.e., the solutions are non-dominated. The Euclidean distance of the individual Pareto efficient solutions to the origin was used to select the best possible solution. This allows one to obtain an overall cost per chromosome profile. The cost associated with the individual setpoint profile is then stored in the suitability gene, which is compared after the mating to determine the most suitable individual in the population, as shown in Figure 4.10. The optimization is done every timestep and only the solution for k is used for the power allocation.

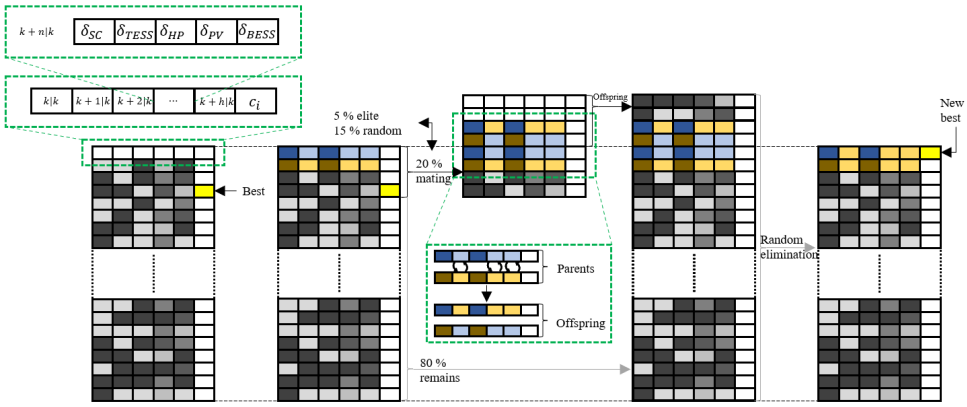

Figure 4.10: Genetic algorithm proposed to minimize the cost function for the short-term predictive controller

4.4.1. RESULTS ANALYSIS

The random forest regression approach was used as a proven short-term forecasting method [20]. This way, leveraging two years of historical data, the electric load demand, temperature (used to estimate the thermal demand), and irradiance (used to estimate the PV and solar collector production) were estimated. The model specifically includes time lag, hour of the day, and month as features to effectively capture both immediate temporal dynamics and broader seasonal patterns. The dataset was partitioned into training and testing subsets, allocating 99 % for training to develop the model robustly and reserving 1 % for testing. The model is configured with 100 decision trees and a fixed random state of 42 to ensure consistent and repeatable outcomes. A representative sample of the estimated values using a prediction of 60 min is presented in Figure 4.11a and their respective error in Figure 4.11b. These results highlight the model's precision.

Two parameters were changed to evaluate the performance of the EMS: the season and the prediction horizon. For the former, a representative week was chosen for winter and summer. For the latter, a population size that ensures thermal comfort was determined, as shown in Tables 4.2 and 4.3, using the results from Section 4.3.2 as reference. The optimization used the dynamic prices shown in Figure 4.12 and a carbon intensity of 0.325 $gCO_{2,eq}$/kWh. During winter (see Figure 4.13), the EMS prioritizes the TESS over the HP as the latter would increase the electric load and energy cost (on 01/02). However, when the TESS SoC is lower, i.e., its temperature decreases, the thermal power it can deliver is reduced, and the EMS activates the HP to avoid uncomfortable temperatures (between 02/02 and 03/02). Finally, the HP becomes the dominant energy source once the TESS is discharged (between 04/02 and 07/02). The solar collectors provide some thermal power, but this is too small. During summer (see Figure 4.14), the system again prefers the TESS to supply thermal power in the few cases where the indoor temperature falls below the setpoint temperature (between 19/07 and 22/07). Once the outdoor temperature is higher than the setpoint temperature, the TESS and the HP are not active, as the outdoor temperature would increase the indoor temperature, and no cooling technologies are considered (after 23/07).

From Figure 4.13 and Table 4.2, one can notice that the EMS performs more effi-

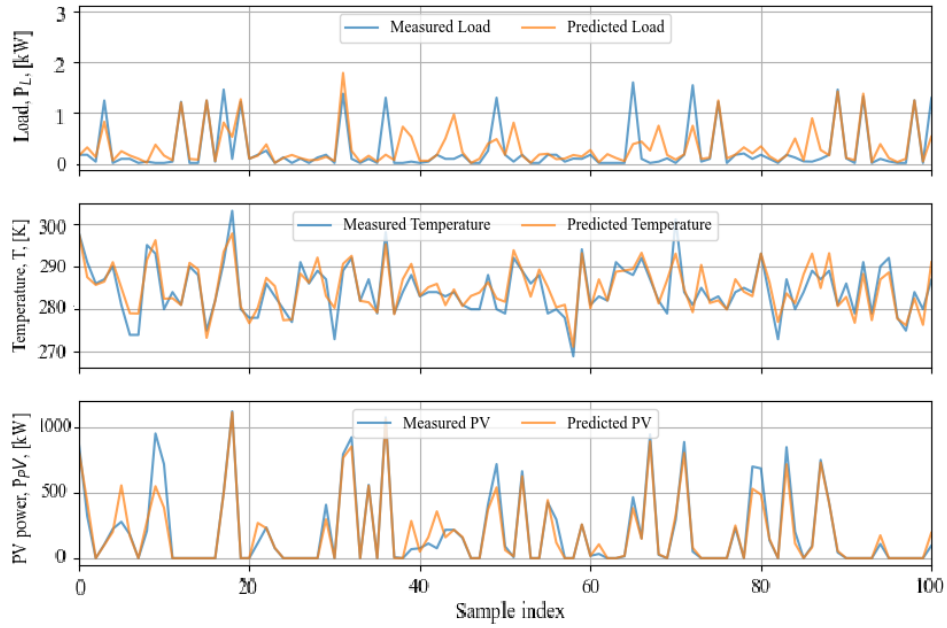

(a)

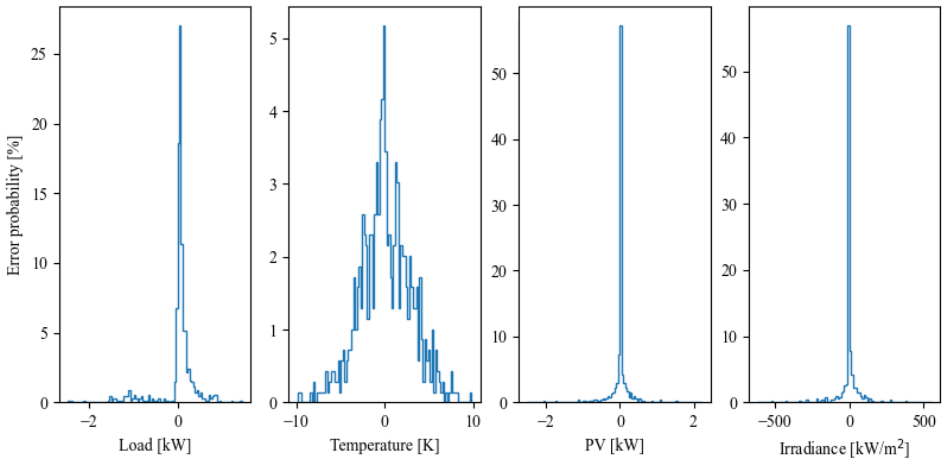

(b)

Figure 4.11: (a) Estimated and measured values and (b) error of the forecasted values using a prediction horizon of 60 min.

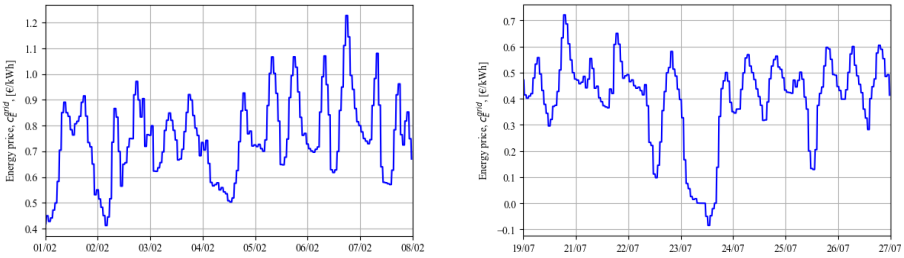

(a) (b)

Figure 4.12: Energy price from the grid during (a) winter and (b) summer.

Table 4.2: Parameters used for the short-term predictive GA optimization in winter.

Horizon [min]	Population	Generations	Timestep run time [s]
0	25	5	0.3 - 0.55
30	50	5	0.3 - 0.65
60	100	5	0.44 - 0.85
90	200	5	0.7 - 1.2
120	400	5	0.7 - 1.65

ciently in winter. Even for the longer prediction horizon, a small population can solve the power balance problem without increasing the indoor temperature. Similarly, having longer prediction horizons allows the EMS to keep the temperature closer to the setpoint when it reaches 20 °C. At night, when it lowers to 17 °C, the temperature drops naturally, and no thermal power is extracted from any source. Notice that the strategy can overcome the curse of dimensionality during winter, as achieving a control setpoint takes, on average, less than 1 s, as shown in Figure 4.15b, albeit the cardinality of possible solutions when using a prediction horizon of 60 min is in the order of 10^{13}.

On the other hand, temperature control during summer is more challenging for the EMS in longer prediction horizons, as shown in Figure 4.14 and Table 4.3. Despite increasing the population one order of magnitude compared to the respective case in winter, the EMS during summer still executes heating instructions when the indoor temperature is above the setpoint (see Figures. 4.14b and 4.14c). This can be explained due to the absence of cooling mechanisms. During winter, the EMS can successfully prioritize the available thermal power sources, as explained before. In summer, however, as the outdoor temperature is already above the setpoint, any thermal action would increase the indoor temperature, decreasing thermal comfort and requiring all the setpoint genes to be zero for the thermal generation devices. For this reason, a more diverse gene pool is required to achieve the suboptimal solutions, increasing the time of simulation needed, as shown in Figure 4.15 (the model was run on a laptop with a processor Intel i7-1185G7, and 16 GB of RAM). To overcome this challenge, one can take several action points aside

Table 4.3: Parameters used for the short-term predictive GA optimization in summer.

Horizon [min]	Population	Generations	Timestep run time [s]
0	25	5	0.3 - 0.7
30	200	5	0.4 - 1
60	750	5	1.3 - 2.2
90	1500	5	4 - 12
120	2000	5	5 - 9

from increasing the population or the number of generations. For example, the heating devices can be turned off at the gene level when the outdoor temperature reaches a specific value or a hard constraint can be included as a condition to reach a solution during the evolutionary process.

The optimization performance per objective is shown in Tables 4.4 and 4.5 for winter and summer, respectively. For both seasons, one can notice that the real-time control (h = 0 min) has the best performance. This can be associated with the forecast, as the real-time control case does not depend on the prediction value and, therefore, does not have to account for the uncertainty. In contrast, the cases with longer horizons tend to have the lowest performances. Nevertheless, it is interesting to notice that, although the performance decreases when increasing the horizon, the change is relatively small between consecutive cases (less than 1 % for winter and 5 % for summer).

The results suggest that the forecast method and the energy management system perform satisfactorily. Thanks to its design, the EMS is easily adaptable to any MCES architecture, as the devices are added as genes. Energy storage systems' physical constraints are set at the gene level using the approach demonstrated for BESS, based on their allowed power, capacity, and SoC, minimizing unfeasibilities. Also, considering the devices that work on an on/off pace, such as the heat pump or the solar collectors, as binary at the gene level demonstrates that the discrete-continuous approach for the power setpoints reduces the dimensionality issues. The random forest regression produced short-term estimations of the electric load, the temperature, and the irradiance with error distributions centred near 0 %, allowing us to estimate the thermal demand and PV output. With those estimations, the energy management system created a power setpoint profile for each device of the multi-carrier energy system, minimizing the economic cost, $CO_{2,eq}$ and ensuring thermal comfort. The low computational cost of the EMS proposed was also demonstrated for short-term prediction horizons. During winter, the EMS can solve the power allocation problem, including the prediction, in around 1 s on average for prediction horizons equal to or shorter than 120 min. In summer, the decisions might take up to 10 s per timestep, which is still acceptable, as the system works on a 15-minute timestep. Further research should be done to improve the performance of the algorithm during the summer and study longer prediction horizons.

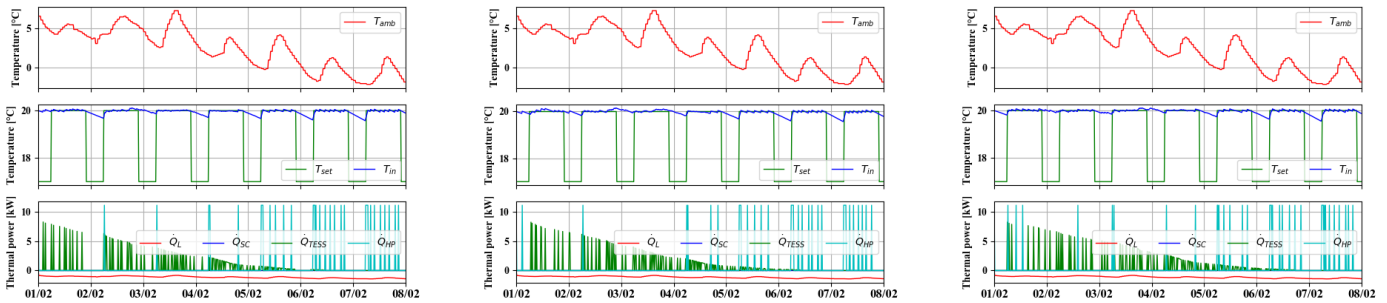

(a) (b) (c)

Figure 4.13: Thermal power allocation during winter for prediction horizons of (a) 60 min, (b) 90 min, and (c) 120 min.

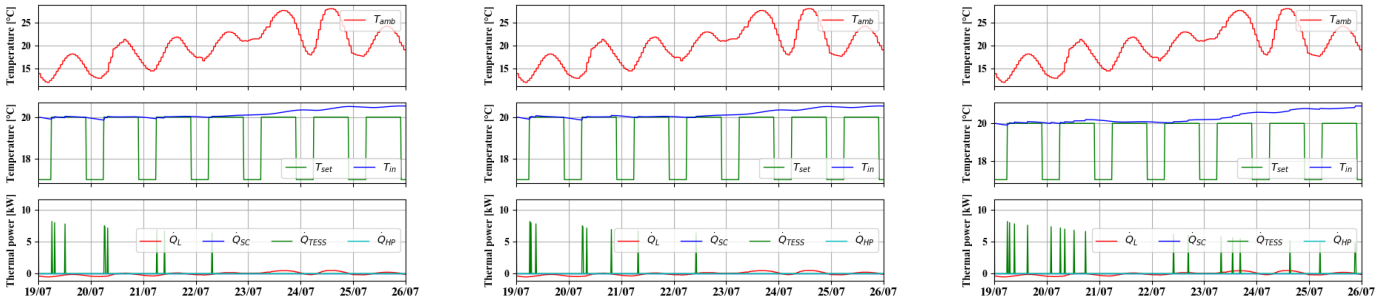

(a) (b) (c)

Figure 4.14: Thermal power allocation during summer for prediction horizons of (a) 60 min, (b) 90 min, and (c) 120 min.

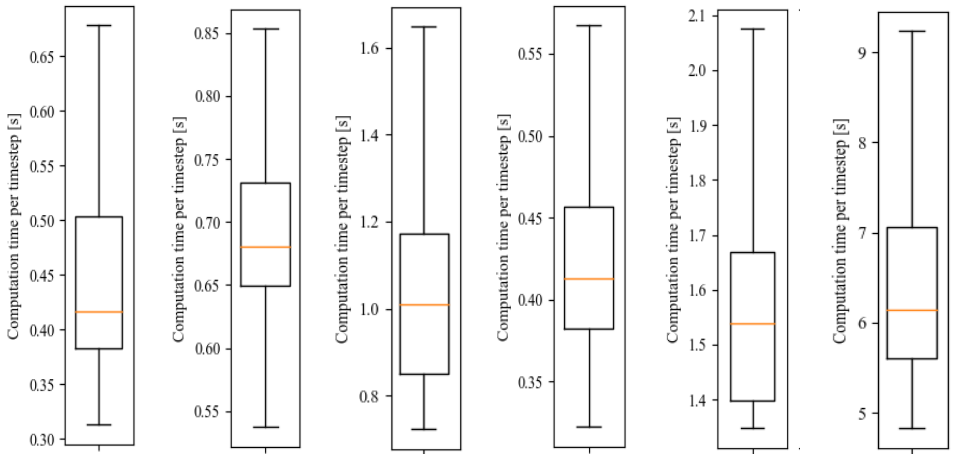

(a) 0 min (b) 60 min (c) 120 min (d) 0 min (e) 60 min (f) 120 min

Figure 4.15: Distribution of the computational time required to solve each control iteration for different prediction horizons during winter (a), (b) and (c), and summer (d), (e) and (f).

4.5. HEURISTIC CONTROL

Sections 4.3 and 4.4 proposed two EMS strategies using genetic algorithms to optimize the power dispatch. Individually, their performances were acceptable in terms of computational cost. However, to perform more complex analysis in distribution systems with hundreds of nodes and systems as required for Chapter 6, their accumulated computational cost might lead to simulation bottlenecks. Also, the CO_2 equivalent emissions were found to be proportional to the grid purchase, therefore the objectives were redundant [21]. In addition, to aggregate the assets, the EMS must be capable of including an external setpoint.

This Section describes a heuristic method that can integrate thermal comfort, represented as the deviation from a setpoint temperature, energy purchase costs under a day-ahead pricing scheme, and the deviation from a power exchange setpoint defined by an aggregator as objectives. These policies are recalculated for each time step k. The thermal comfort policy δ^T defines whether the HP and the TESS should be available to heat the house or not, thus $\delta^T = [\delta^T_{\text{HP}}, \delta^T_{\text{TESS}}]$, with

$$\delta^T_{\text{HP}} = \begin{cases} 0, & \forall \quad T_{\text{set}} \leq T_{\text{in}} \\ 1, & \forall \quad T_{\text{set}} > T_{\text{in}} \end{cases}, \tag{4.22}$$

and

$$\delta^T_{\text{TESS}} = \begin{cases} 0, & \forall \quad T_{\text{set}} \leq T_{\text{in}} \\ 1, & \forall \quad T_{\text{set}} > T_{\text{in}} \end{cases}. \tag{4.23}$$

The energy purchase cost policy $\delta^\lambda = [\delta^\lambda_{\text{HP}}, \delta^\lambda_{\text{TESS}}, \delta^\lambda_{\text{HP}\rightarrow\text{TESS}}, \delta^{HP}_{\text{HP}\rightarrow\text{TESS}}, \delta^{\text{SoC}}_{\text{HP}\rightarrow\text{TESS}}, \delta^{\text{SoC}}_{\text{TESS}}]$ suggests which heating device should be used at any given point k, based on the energy

Table 4.4: Optimization results in winter.

Horizon [min]	Grid purchase [kWh]	Grid cost [€]	Emissions [$gCO_{2,eq}$]	Thermal comfort [-]
0	67.28	13.80	21.87	3976
30	71.69	14.45	23.30	3891
60	72.81	14.62	23.66	3911
90	73.06	14.72	23.74	3926
120	73.35	14.84	23.84	3943

Table 4.5: Optimization results in summer.

Horizon [min]	Grid purchase [kWh]	Grid cost [€]	Emissions [$gCO_{2,eq}$]	Thermal comfort [-]
0	44.17	4.52	14.36	4584
30	46.38	4.71	15.08	4691
60	49.00	5.07	15.93	4650
90	49.23	5.18	16.00	4657
120	50.15	4.92	16.30	5679

price λ reported in the day-ahead list. To define the prices as high or low and thus increase or decrease the power exchanged with the grid, the distribution quartiles of the DA prices were calculated for every day. The *low prices* are those included in the first quartile, i.e., below λ_{Q25}. Therefore, the policy for the activation of the heat pump to heat the house is

$$\delta^{\lambda}_{\text{HP}} = \begin{cases} 1, & \forall \quad \lambda \leq \lambda_{Q25} \\ 0, & \forall \quad \lambda > \lambda_{Q25} \end{cases} , \tag{4.24}$$

the policy for the discharge of the TESS is

$$\delta^{\lambda}_{\text{TESS}} = \begin{cases} 0, & \forall \quad \lambda \leq \lambda_{Q25} \\ 1, & \forall \quad \lambda > \lambda_{Q25} \end{cases} , \tag{4.25}$$

and the policy for charging the TESS is

$$\delta^{\lambda}_{\text{HP}\rightarrow\text{TESS}} = \begin{cases} 1, & \forall \quad \lambda \leq \lambda_{Q25} \\ 0, & \forall \quad \lambda > \lambda_{Q25} \end{cases} . \tag{4.26}$$

Also, as the HP cannot heat the house and charge the TESS simultaneously, thus

$$\delta^{HP}_{\text{HP}\rightarrow\text{TESS}} = \begin{cases} 1, & \forall \quad \delta_{\text{HP}} = 0 \\ 0, & \forall \quad \delta_{\text{HP}} = 1 \end{cases} . \tag{4.27}$$

Then, to account for the SoC constraints of the TESS,

$$\delta^{\text{SoC}}_{\text{HP}\rightarrow\text{TESS}} = \begin{cases} 1, & \forall \quad T_{\text{TESS}} < T^{\max}_{\text{TESS}} \\ 0, & \forall \quad T_{\text{TESS}} \geq T^{\max}_{\text{TESS}} \end{cases} \tag{4.28}$$

was considered for the charge, and

$$\delta^{\text{SoC}}_{\text{TESS}} = \begin{cases} 1, & \forall \quad T^{\min}_{\text{TESS}} \leq T_{\text{TESS}} \\ 0, & \forall \quad T^{\min}_{\text{TESS}} > T_{\text{TESS}} \end{cases} \tag{4.29}$$

for the discharge.

Finally, the power from the PV and BESS depends on the grid exchange setpoint P^*. To minimise the degradation of the BESS and curtailment on the PV, the policy $\delta^{\text{P}} = [P^{\delta}_{\text{BESS}}, P^{\delta}_{\text{PV}}]$ prioritizes using as much power from the PV as possible. However, unlike the TESS, where its primary controller regulates the flow so that the output temperature reaches the supply temperature (which is a fixed value), the policy for the BESS defines its power -delivered or consumed- which is limited by its current state-of-charge and the available PV power. The power boundaries for the BESS follow (4.15) and (4.16). Then, the setpoint boundaries for the BESS, based on the available PV power, are

$$\overline{P}^{\text{set}}_{\text{BESS}} = P_L + P_{\text{HP}} + P_{\text{HP}\rightarrow\text{TESS}} - P^{\text{av}}_{\text{PV}} - P^* \tag{4.30}$$

and

$$\underline{P}^{\text{set}}_{\text{BESS}} = P_L + P_{\text{HP}} + P_{\text{HP}\rightarrow\text{TESS}} - P^*, \tag{4.31}$$

Thus, the policies for the PV and BESS are, respectively,

$$P^{\delta}_{\text{BESS}} = \begin{cases} \underline{P}^{\text{set}}_{\text{BESS}}, & \forall \quad \left(\underline{P}^{\text{set}}_{\text{BESS}} \geq \underline{P}^{\text{perm}}_{\text{BESS}}\right) \wedge \left(\underline{P}^{\text{set}}_{\text{BESS}} \leq \overline{P}^{\text{perm}}_{\text{BESS}}\right) \\ \underline{P}^{\text{perm}}_{\text{BESS}}, & \forall \quad \left(\underline{P}^{\text{set}}_{\text{BESS}} \leq \underline{P}^{\text{perm}}_{\text{BESS}}\right) \wedge \left(\overline{P}^{\text{set}}_{\text{BESS}} \geq \underline{P}^{\text{perm}}_{\text{BESS}}\right) \\ \overline{P}^{\text{perm}}_{\text{BESS}}, & \forall \quad \underline{P}^{\text{set}}_{\text{BESS}} \geq \overline{P}^{\text{perm}}_{\text{BESS}} \\ \underline{P}^{\text{perm}}_{\text{BESS}}, & \text{else} \end{cases} \tag{4.32}$$

and

$$P^{\delta}_{\text{PV}} = \begin{cases} P^{\text{av}}_{\text{PV}}, & \forall \quad \left(\underline{P}^{\text{set}}_{\text{BESS}} \geq \underline{P}^{\text{perm}}_{\text{BESS}}\right) \wedge \left(\underline{P}^{\text{set}}_{\text{BESS}} \leq \overline{P}^{\text{perm}}_{\text{BESS}}\right) \\ \underline{P}^{\text{perm}}_{\text{BESS}} - \underline{P}^{\text{set}}_{\text{BESS}}, & \forall \quad \left(\underline{P}^{\text{set}}_{\text{BESS}} \leq \underline{P}^{\text{perm}}_{\text{BESS}}\right) \wedge \left(\overline{P}^{\text{set}}_{\text{BESS}} \geq \underline{P}^{\text{perm}}_{\text{BESS}}\right) \\ 0, & \forall \quad \underline{P}^{\text{set}}_{\text{BESS}} \geq \overline{P}^{\text{perm}}_{\text{BESS}} \\ P^{\text{av}}_{\text{PV}}, & \text{else} \end{cases} \tag{4.33}$$

prioritizing meeting the thermal load for two reasons: first, thermal comfort is deemed more important than charging the TESS. Second, and perhaps less obvious, the HP's coefficient of performance is higher when heating the house than when charging the TESS due to the required supply temperatures, as demonstrated in Chapter 3. Therefore, prioritizing the thermal load will also reduce the purchase from the grid.

The general policy π_k for each timestep k is then comprised of the individual policies per device j and objective i, resulting in

$$\pi_k = [\delta^T, \delta^\lambda, \delta^P] \tag{4.34}$$

Table 4.6: Parameters used for the heuristic EMS

Symbol	Value	Units	Parameter
$P_{\text{PV}}^{\text{peak}}$	6.615	kW	PV system peak power
E_{L}	2491	kWh	Base yearly consumption
E_{BESS}	10	kWh	BESS capacity
$P_{\text{BESS}}^{\text{max}}$	10	kW	BESS power

thus, for each device, the control policy is given by

$$\delta_j = \prod_{\delta^i \in \pi_k} \delta_j^i, \tag{4.35}$$

4.5.1. RESULTS ANALYSIS

The results from Chapter 3, and Sections 4.3 and 4.4 provided insight into the role of the different components of the MCES. This way, it was determined that neither photovoltaic thermal systems nor solar collectors are suitable for charging the TESS. Thus, the heat pump was used, following the policy (4.34). In addition, the sizes of the PV and BESS were adjusted. The PV system was sized to reach a near-zero building, excluding the heat pump load. Also, the BESS capacity and power were increased. Table 4.6 shows the new parameters used for this house, with respect to Table 4.1.

The system was simulated for the same week in winter and summer. Figure 4.16 shows the results when the aggregator does not provide a setpoint, and Figure 4.17 when there is a setpoint (more details on how this sepoint was calculated can be found in Chapter 6). For the case without external grid power setpoints, it can be seen that the EMS ensures the indoor temperature, activating the HP during the daily low-price periods either for direct heating or to charge the TESS, which is later used to heat the house during high-price periods. During summer, the outside temperature surpasses the indoor temperature, creating a reverse thermal loss, heating the house. The heat pump then charges the TESS during low price periods up to near 100 % SoC, compensating for the TESS thermal losses to the soil. The BESS follows a similar pattern, charging in low-price periods and discharging during the high-priced. Adding an external setpoint drastically changes the power dispatch, as shown in Figure 4.17. First, the usage of the HP decreases considerably, both during winter and summer, relying on the TESS. During winter, the TESS reaches temperatures where it can no longer heat the house, and the HP is used only when the minimum allowed temperature of 16 °C is reached. During this period (7 of February), the EMS is incapable of following the setpoint, as the indoor temperature is too low and the TESS completely discharged. Similarly, the BESS has very short cycles, as it is required too often to charge over 50 % most of the time. During summer, the setpoint is consistently met; however, the power limit reduces the times when the HP can be used to charge the TESS. Therefore, it reaches an SoC of around 75 %. Considering the four simulations (both seasons with and without external setpoint), the algorithm took between 0.03 s and 0.06 s to run, which is one order of magnitude less than the real-time GA EMS presented in Section 4.3, and up to two orders of magnitude less than the short-term predictive GA EMS presented in Section 4.4.

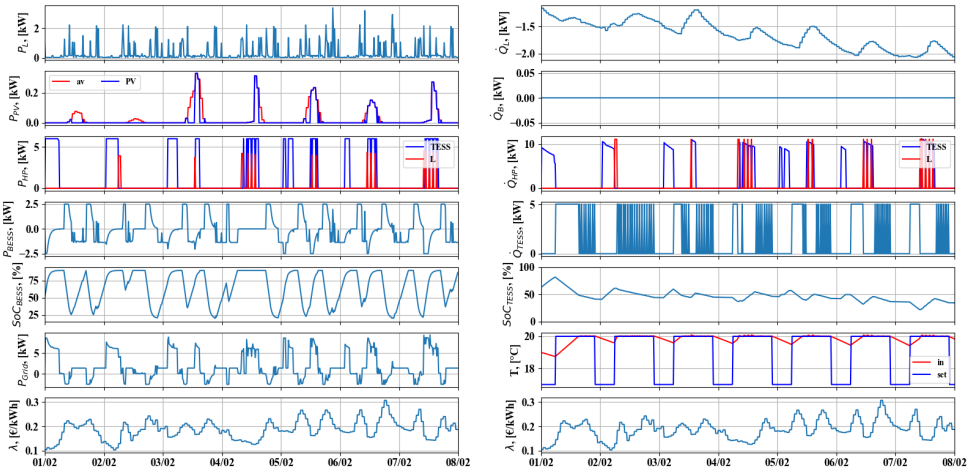

(a)

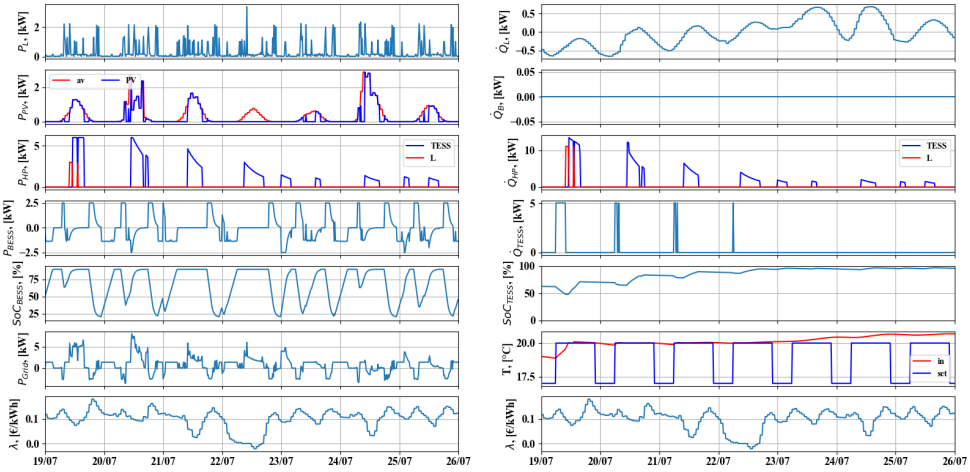

(b)

Figure 4.16: Results for the heuristic controller during (a) winter and (b) summer without a setpoint from the DSO.

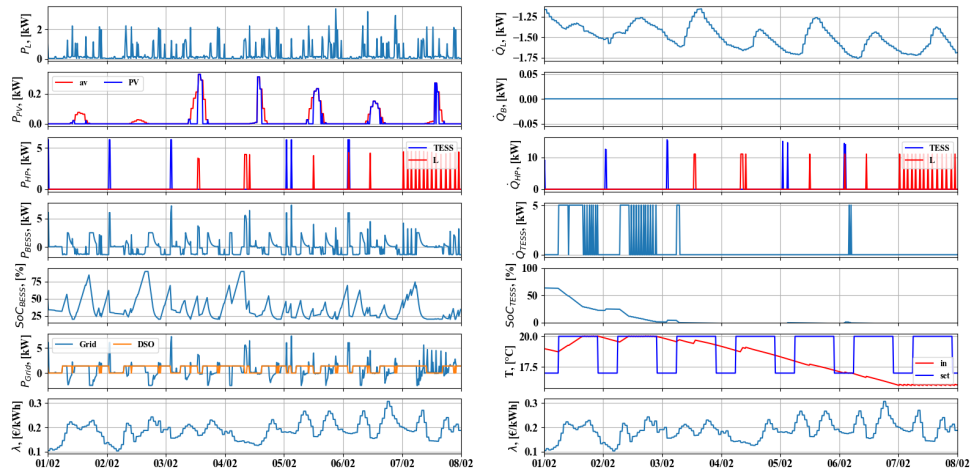

(a)

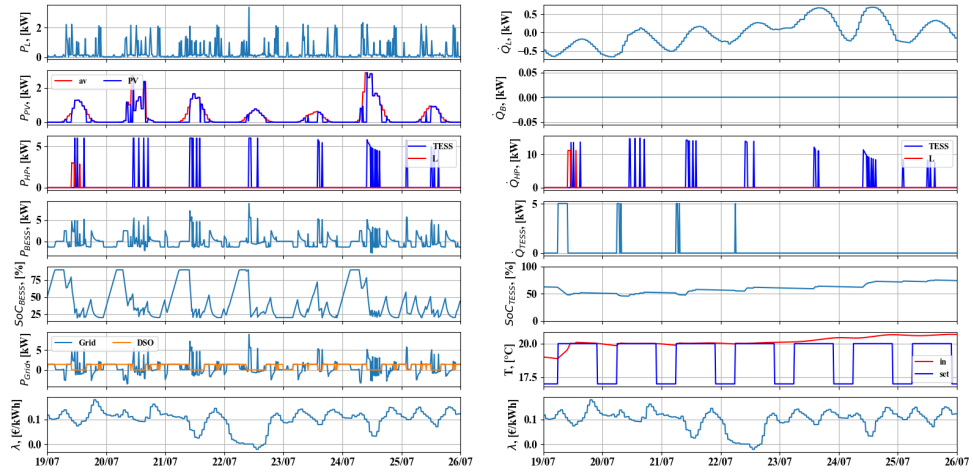

(b)

Figure 4.17: Results for the heuristic controller during (a) winter and (b) summer considering a setpoint from the DSO.

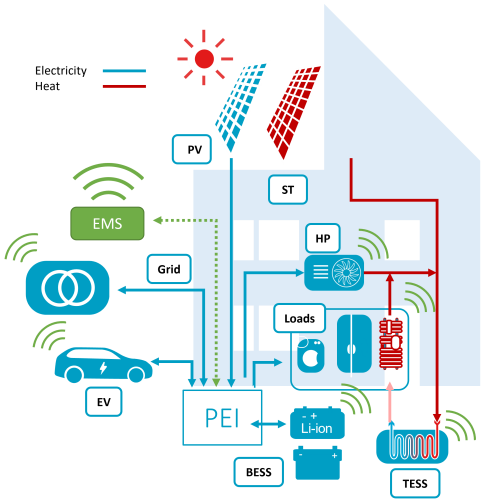

Figure 4.18: Schematic diagram of the proposed multi-carrier energy system.

4.6. Ageing-Aware Control

Despite this thesis does not intend to provide an in-depth analysis of the degradation of the batteries during their operation, recent literature advises its consideration to establish realistic business models [8], as will be detailed in Chapter 5. This Section provides an overview of how to implement an ageing-aware control EMS and its possible benefits and challenges without the intention of being an exhaustive analysis. A schematic of system the system to be analyzed is presented in Figure 4.18. The system is composed of a PV, a BESS, an electric vehicle (EV), a power electronics interface (PEI), a HP, a solar thermal system (ST), a TESS, a grid connection and loads. The modelling is done following the universal modeling framework by Powell [22]–[24].

The EMS plans a day-ahead operation, considering perfect information where the sizing of the components is known. Hence, the costs of the system are only its operation costs. These are the net grid cost C_{grid} and the battery degradation cost C_{loss}. Lastly, to account for the user's mobility requirement, a fictitious penalty p_{SoCDep} is incorporated to quantify possible deviations from the desired SoC of the EV at departure. The optimization problem is then reduced to

$$\begin{aligned} \min_{P^*_{a,t}} \quad & C_{\text{grid}} + p_{\text{SoCDep}} + C_{\text{loss}} \\ \text{s.t.} \quad & S_{a,t+1} = S^M_{a,t}(S_{a,t}, P^*_{a,t}, W_{t+1}|\theta_{a,t}) \\ & P^*_{a,t} = X^\pi(S_{a,t}) \in \mathscr{P} \qquad \forall a \in \mathbb{A} \\ & S_{a,t} \in \mathscr{S} \qquad \forall a \in \mathbb{A} \end{aligned} \tag{4.36}$$

with

$$a = \{\text{PV}, \text{grid}, n_{\text{EV}}, \text{BESS}, \text{HP}, \text{ST}, \text{TESS}\}. \tag{4.37}$$

The components of the objective are

$$C_{\text{grid}} = w_{\text{grid}} \sum_{0}^{T} \left(\lambda_{\text{buy}} P^{+}_{\text{grid}} + \lambda_{\text{sell}} P^{-}_{\text{grid}} \right) \Delta t, \tag{4.38}$$

$$p_{\text{SoCDep}} = w_{\text{SoC}} ||\varepsilon_{\text{SoC}}||_2^2, \tag{4.39}$$

and

$$C_{\text{loss}} = w_{\text{loss}} c_{\text{loss}} \sum_{0}^{T} \sum_{sa} i_{\text{loss}} \Delta t, \ \forall \ sa \subset a, \tag{4.40}$$

where $S_{a,t}$ is the state vector, $P^{*}_{a,t}$ is the optimal decision for timestep t, W_{t+1} is an exogenous process that introduces new information after making a decision. The mappings $S^{M}_{a,t}(.)$, and $X^{\pi}(.)$ are the transition function and optimal policy, respectively. The first is a set of equations describing the states and parameter evolution, and the second is the algorithm that finds the optimal setpoints. The vector $\theta_{a,t}$ contains all the parameters of each asset a and changes over time t. The subindex $a \in \mathbb{A}$ corresponds to the assets shown in Figure 4.18, which are PV modules, a grid connection, electric vehicles, a stationary battery, a heat pump, a solar thermal system and a thermal storage. Additionally, $sa = \{\text{BESS}, n_{\text{EV}}\} \subset a$ denotes the electric storage assets and $n_{\text{EV}} = 1...N_{\text{EV}}$ is the number of EV. The time window is $T = 24$ h, and the timestep $\Delta t = 15$ min. The three components of the objective function are the grid cost C_{grid}, the cost of lost energy capacity C_{loss}, and a penalty for not charging the EV to the desired setpoint p_{SoCDep}. C_{loss} is explained in Section 4.6.3.

The following definitions of the elements are considered. The state vector is

$$S_{a,t} = [P_{\text{PV}}, P_{\text{grid}}, \gamma_{n_{\text{EV}}}, P^{\text{th}}_{\text{HP}}, P_{\text{ST}}, P^{\text{e}}_{\text{load}}, P^{\text{th}}_{\text{load}}]^{T}_{t}.$$

where $P_{a,t}$ is the power of the assets and $\gamma_{n_{\text{EV}}}$ is the EV availability. The policy or decision variables are

$$P^{*}_{a,t} = [P_{n_{\text{EV}}}, P_{\text{BESS}}, P_{\text{TESS}}, P^{\text{e}}_{\text{HP}}]^{T}_{t}.$$

The superscripts e and th refer to electricity or thermal carriers. They are used when the subscript is the same. Both the policy and state vectors have upper and lower limits denoted as $\overline{P}^{*}_{a,t}$, $\underline{P}^{*}_{a,t}$, $\overline{S}_{a,t}$, and $\underline{S}_{a,t}$. All bidirectional variables, either policies or states, are modelled with the constraints

$$S^{+}_{t} + S^{-}_{t} = S_t \wedge \ S^{-}_{t} \leq 0, S^{+}_{t} \geq 0, \tag{4.41}$$

and

$$S^{+}_{t}.S^{-}_{t} = 0. \tag{4.42}$$

Uncertainty is tackled through a DLA $X^{\pi}(.)$ in a deterministic setup where at each timestep t we take the median of a forecast $W_{t+1} = 0$. In our case, our policy mapping is our optimization algorithm. The order of the subscript is *"name, device, time index"*, and the capital C denotes total cost in €, lowercase c denotes unit cost, and w indicates tunning/scaling weight. The inputs of the operation are the solar power P_{PV}, the prices $\lambda_{\text{buy/sell}}$, the electric demand $P^{\text{e}}_{\text{load}}$, and the thermal demand $P^{\text{th}}_{\text{load}}$.

To define transition function $S^M_{a,t}(.)$, all assets need to be modelled. The thermal assets are incorporated with the following linear models:

$$P^{\text{th}}_{\text{HP}} = \eta_{\text{HP}} P^{\text{e}}_{\text{HP}}, \tag{4.43}$$

$$P_{\text{ST}} = \eta_{\text{ST}} P_{\text{PV}}, \tag{4.44}$$

and

$$SoC_{\text{TESS},t+1} = SoC_{\text{TESS},t} - \frac{\Delta t}{Q_{\text{TESS}}.3600} \eta_{\text{TESS}} P_{\text{TESS},t}, \tag{4.45}$$

where η denotes a conversion factor or efficiency, Q_{TESS} is the capacity in kWh. Then, the thermal balance is

$$P_{\text{ST}} + P^{\text{th}}_{\text{HP}} + P_{\text{TESS}} = P^{\text{th}}_{\text{load}}. \tag{4.46}$$

The electric power balance, on the other hand, is

$$P_{\text{PV}} + P_{\text{BESS}} + \sum_{n_{\text{EV}}=1}^{N_{\text{EV}}} \gamma_{n_{\text{EV}}}.P_{n_{\text{EV}}} + P_{\text{grid}} = P^{\text{e}}_{\text{load}} + P^{\text{e}}_{\text{HP}}. \tag{4.47}$$

where $\gamma_{n_{\text{EV}}}$ is the EV availability, explained in Section 4.6.4.

The following sections elaborate on the models used to describe the performance and degradation of the electric storage denoted by sa. The performance model $S^M_{sa,t}(.)$ describes the evolution of the states $S_{sa,t}$, and the degradation model $g_{sa,t}(.)$ describes the dynamics of the parameters $\theta_{sa,t}$ that parameterize the performance model. These performance and ageing sub-models are part of the main transition function $S^M_{a,t}(.)$.

4.6.1. BUCKET MODEL

The bucket model (BM) is a basic model of the operation of a battery that assumes that its output voltage v_t is linear with the state of charge SoC, assuming no voltage drop [25]. Hence the only equations of this model are

$$SoC_{sa,t+1} = SoC_{sa,t} - \frac{\Delta t}{Q_{sa,t}3600} \eta_c i_{sa,t}, \tag{4.48}$$

$$i_{sa,t} = \frac{P_{sa,t}}{v_{sa,t} N_{s,sa} N_{p,sa}}, \tag{4.49}$$

and

$$OCV_{sa,t} = a_{OCV,sa} + b_{OCV,sa} SoC_{sa,t}, \tag{4.50}$$

$$v_{t,sa,t} = OCV_{sa,t}, \tag{4.51}$$

where $i_{sa,t}$ is the current passing through the cell, $OCV_{sa,t}$ is the open circuit voltage, $a_{OCV,sa}$ and $b_{OCV,sa}$ are the voltage model parameters, η_c is the Coulombic efficiency and $Q_{sa,t}$ is the cell capacity in Ah. Each battery pack is assumed to be organized as a series cell module where $N_{s/p,\ sa}$ are the series and parallel cells and branches, respectively.

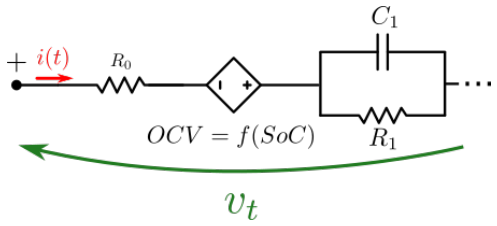

Figure 4.19: First order Equivalent Circuit Model.

4.6.2. EQUIVALENT CIRCUIT MODEL

To improve the accuracy of the model, a first-order equivalent circuit model (ECM) can be incorporated, as in Figure 4.19. The performance sub-model $S^M_{sa,t}(.)$ is then modified with:

$$i_{R_1,sa,t+1} = e^{-\frac{\Delta t}{R_{1,sa}C_{1,sa}}} i_{R_1,sa,t} + \left(1 - e^{-\frac{\Delta t}{R_{1,sa}C_{1,sa}}}\right) i_{sa,t} \tag{4.52}$$

$$v_{sa,t} = OCV_{sa,t} - i_{R_1,sa,t}R_{1,sa} - i_{sa,t}R_{0,sa}\,, \tag{4.53}$$

where $i_{R_1,sa,t}$ is the pole current, $R_{1,sa}$ and $C_{1,sa}$ are the pole elements and $R_{0,sa}$ is the series resistance as defined in Figure 4.19. Eqs. 4.48, 4.49 and 4.50 are maintained. The ECM incorporates the series voltage drop ($R_{0,sa}$) that limits power output and the first-order diffusion dynamics ($R_{1,sa}$ and $C_{1,sa}$) [25]. This sub-model further differentiates electric and thermal ESS technologies.

4.6.3. EMPIRICAL DEGRADATION MODEL

The degradation model follows the work from Wang et al. [26], which summarizes all aging mechanisms into calendar (i_{cal}) and cyclic (i_{cycle}) aging currents. The chosen empirical degradation model ($g_{sa,t}(.)$) only describes the capacity fade, neglecting the power fade, following

$$i_{\text{cycle},sa,t} = \frac{c_1.c_3}{c_4} e^{c_2|i_{sa,t}|}(1 - SoC_{sa,t})|i_{sa,t}|\,, \tag{4.54}$$

$$i_{\text{cal},sa,t} = c_5 e^{-\frac{24\,\text{kJ}}{RT}} \sqrt{t}\,, \tag{4.55}$$

$$i_{\text{loss},sa,t} = i_{\text{cycle},sa,t} + i_{\text{cal},sa,t}\,, \tag{4.56}$$

and

$$Q_{sa,t+1} = Q_{sa,t} - \frac{\Delta t}{3600} i_{\text{loss},sa,t}\,, \tag{4.57}$$

where $c_{1:5}$ are empirical parameters coming from curve fitting [26] shown in Table 4.7, R is the gas constant and T is the temperature.

Table 4.7: Parameters for the empirical degradation model [26]

Parameter	Value	Units
c_1	0.0008	-
c_2	0.39	A^{-1}
c_3	1.035	-
c_4	50	-
c_5	1.721×10^{-4}	$A/s^{0.5}$

4.6.4. ELECTRIC VEHICLES

From the point of view of a residential building, the EVs are a BESS with availability constraints and certain requirements regarding their SoC at departure time t_{dep}. For the availability γ, the probability distributions of departure (t_{dep}) and arrival (t_{arr}) times can be described as random variables with Gaussian distributions $t_{\text{dep/arr}} \sim \mathcal{N}(\mu_{\text{dep/arr}}, \sigma^2_{\text{dep/arr}})$. The availability γ_{EV} will then be

$$\gamma_{\text{EV}} = \begin{cases} 0 & t \in [t_{\text{dep}};\ t_{\text{arr}}] \\ 1 & \text{otherwise} \end{cases}. \tag{4.58}$$

The power balance of an EV is

$$P_{tot,n_{\text{EV}},t} = \gamma_{n_{\text{EV}},t} P_{n_{\text{EV}},t} + (1 - \gamma_{n_{\text{EV}},t}) P_{\text{drive},n_{\text{EV}}}, \tag{4.59}$$

where $P_{\text{tot},n_{\text{EV}},t}$ is the total power of the EV, $P_{n_{\text{EV}},t}$ is the charger power, and $P_{\text{drive},n_{\text{EV}}}$ is the power consumed while driving assuming no public charging. The total power $P_{\text{tot},n_{\text{EV}},t}$ is then used in (4.49) and later for calculating the ageing of the EV batteries. The average driving power is also sampled from a Gaussian distribution $P_{\text{drive},n_{\text{EV}}} \sim \mathcal{N}(\mu_{\text{drive}}, \sigma^2_{\text{drive}})$.

Additionally, the EV is required to be delivered with a minimum SoC as

$$SoC_{EV}(t_{\text{dep}}) = SoC_{\text{dep}}. \tag{4.60}$$

This is implemented as a penalty in the cost function (soft constraint) since an equality constraint might be too strict and cause non-convergence. This extra cost is defined by taking the squared L2 norm of the deviation ε_{SoC}, from (4.39), and defined as

$$\varepsilon_{\text{SoC}} = SoC_{\text{EV}}(t_{\text{dep}}) - SoC_{\text{dep}}, \tag{4.61}$$

4.6.5. RESULTS ANALYSIS

To assess the performance of incorporating ageing into the MCES operation, the proposed controller is benchmarked against a controller without a degradation sub-model. The first controller will be called *CEmpDeg* and contains a first-order ECM with an empirical ageing model. The second controller, called *BNoDeg*, has a bucket model without an ageing model, following (4.54) - (4.57). The two controllers are compared for typical Dutch summer and winter days in 2022 and were simulated in Julia, using the Knitro solver. Even though their objective functions and constraints/models are different, the final informed results are calculated with the full objective function presented in (4.36).

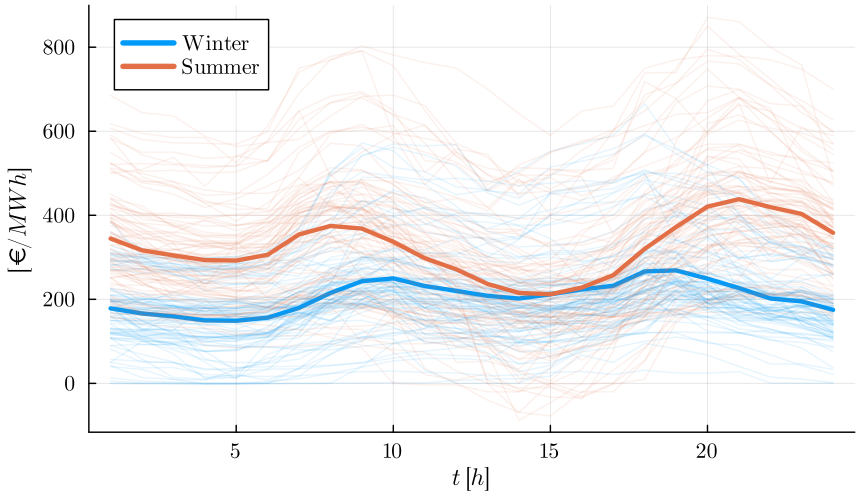

Figure 4.20: EPEX day-ahead auction prices for summer and winter. The bold lines show the mean hourly prices.

Table 4.8: Objective function weights.

Weight	Summer		Winter	
	CEmpDeg	*BNoDeg*	***CEmpDeg***	*BNoDeg*
w_{grid}	1000	1000	1000	500
w_{EVs}	1000	1000	1000	1000
w_{loss}	600	0	600	0

This means that for the *BNoDeg* controller, the created power setpoints are used to calculate C_{loss}.

The system is composed of a 5 kWp PV, a 20 kWh BESS with LFP cells, two 12.5 kW EV charging points, a 4 kW (electric) heat pump, a 2.7 kW (thermal) solar thermal collector, a 200 kWh TESS, a 6 kWp electrical load, a 1 kWp thermal demand, and a 10 kW LV grid connection. The output of the PV is taken from [27]–[29], the market prices λ are taken from the EPEX day-ahead auction, shown in Figure 4.20, considering $\lambda_{\text{buy}} = 0.95\lambda_{\text{sell}}$ [30]. The power demand was modelled taking the standard consumption patterns [31], and the heat demand was modelled as shown in Chapter 3. The $g_{sa,t}(.)$ model is parameterized for LIB cells with NMC cathodes and graphite anodes, and its parameters are presented in Table 4.7. The sampling time is $\Delta t = 15$ min, and the total number of EVs is $N_{\text{EV}} = 2$.

In this case study, the weights w used for the objective function $C(S_t, P_t)$ are presented in Table 4.8. The w is chosen for regularization purposes and tunning preferences. Hence the user has direct control over how the controller behaves by changing the ratio between w_{grid} and w_{loss}. Additionally, the reader has to remember that the submodels used for the performance $S^M_{sa}(.)$ and the ageing $g_{sa}(.)$ are different between the controllers.

The optimization algorithm results in the optimal scheduling of the power dispatch P_t^*. The optimal day-ahead strategy of the *CEmpDeg* controller is shown in Figure 4.21 for the typical summer day. The dashboard presents the electric power and thermal balances, the *SoC* of the storage devices, and the evolution of the capacities Q_{sa}. Figure 4.21 presents the P_t^* for the electric and thermal carriers. Given the signal prices and the high solar generation for this typical summer day, the highest electric load is the EV charging requirement at the beginning of the day. For the thermal carrier, the controller chooses to charge the TESS taking advantage of low prices of the first half of the day. The heat pump follows the thermal load and ramps down when solar heat generation occurs. The excess heat from the heat pipes charges the TESS. In this sense, for the chosen sizing the TESS is not used for daily variations. Further evidence is needed to quantify the impact of BESS modelling in its weekly and/or seasonal operation.

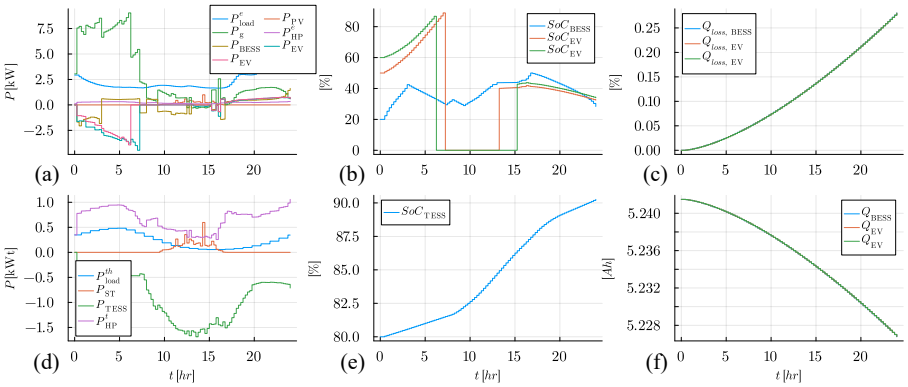

Figure 4.21: Results for the *CEmpDeg* EMS for a typical summer day of 2022, showing (a) electric balance, (b) electric storage, (c) relative lost capacity, (d) thermal balance, (e) thermal storage and (f) total cell capacity.

As for the battery ageing, Figure 4.21 shows that the total degradation $Q_{\text{loss},\,sa}$ is less than 0.3 % per cell. In this work, it is assumed that all cells are identical and hence their aging parameters are the same, thus their only difference would come from their utilization. Unfortunately, for the given 24 h period and set of initial parameters, calendar ageing is 2 orders of magnitude higher than cyclic ageing, in accordance to [26]. Since cyclic ageing represents the operation of the batteries, there's no significant difference between Q_{sa}.

The key difference between controllers is how they use electric storage, (see Figure 4.22). In the *CEmpDeg* controller, the *sa* are used more aggressively (understanding this as higher peak power values) during the summer to achieve higher earnings. On the other hand, for winter, the P_{sa}^* captures marginal prices. The results show how the EVs are not available during $t \in [t_{\text{dep}}, t_{\text{arr}}]$; nevertheless, they are used for bidirectional power when connected. The long-duration thermal storage stays mostly idle during the day, only changing 10-15 % in both seasons. The algorithm also successfully distinguishes between the fast dynamics of electrical storage and the slow dynamics of the TESS. Using the fast dynamics of the LIBs to balance out hourly and daily variations. This also impacts the operation of the TESS presented in Figures 4.22c and 4.22d. In the *CEm-*

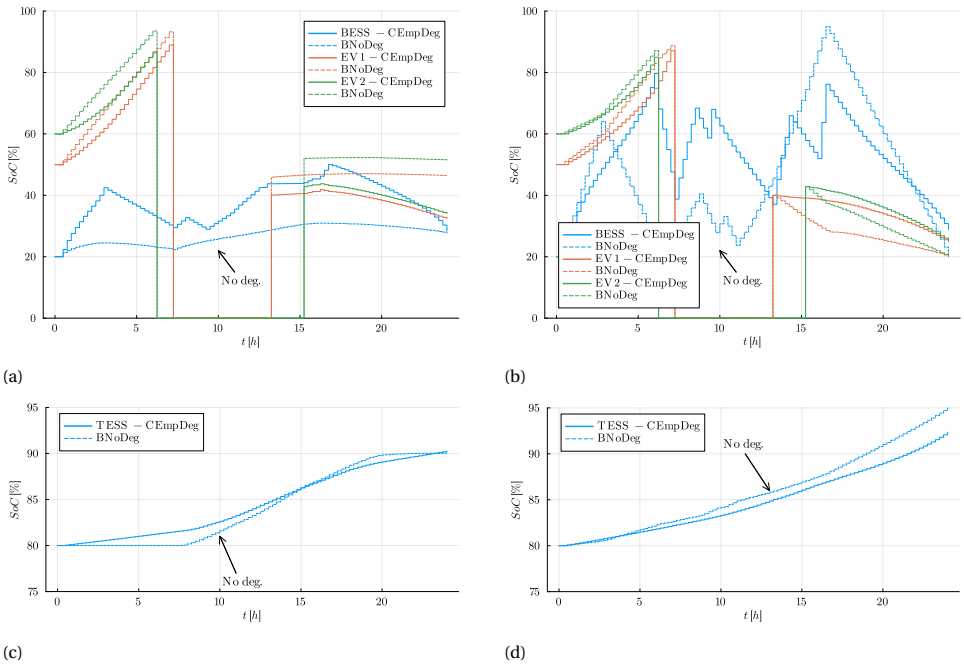

Figure 4.22: Electrical storage behaviour for a typical (a) summer and (b) winter day. Thermal storage behaviour for a typical (c) summer and (d) winter day.

pDeg, the *SoC* deviation of the thermal buffer is slightly less when compared to *BNoDeg*.

Finally, for the typical days analyzed, Figure 4.23 presents the cumulative grid cost C_{grid} curves. The results confirmed that enhancing the models used for the batteries allows a more aggressive strategy that pays off with 22 % and 48 % cost reductions for summer and winter, respectively. Additionally, calendar ageing dominates by almost 2 orders of magnitude over cyclic ageing, thus the difference in Q_{loss} between *CEmpDeg* and *BNoDeg* is negligible (less than 0.3 mAh/day per cell). This is why the change in objective function and constraints enables better grid costs C_{grid}. Since the total capacity fade is going to remain the same for both algorithms, the ageing submodel enhances the decisions taken by the *CEmpDeg*. Of course, this is a direct consequence of the period being simulated. For longer simulation times, this would not necessarily hold, and the trade-off between degradation and grid operation should be controlled by tunning w. Further research is needed to clarify this point.

4.7. CONCLUSIONS

This Chapter presented five different EMS strategies that can be used for residential multi-carrier energy storage systems. Depending on the objective, some strategies might be more suitable than others. It was demonstrated that the genetic algoritm EMS is suitable to integrate multiple objectives for real-time and short-time control. Also, adding or removing devices or objectives does not fundamentally changes the logic of the al-

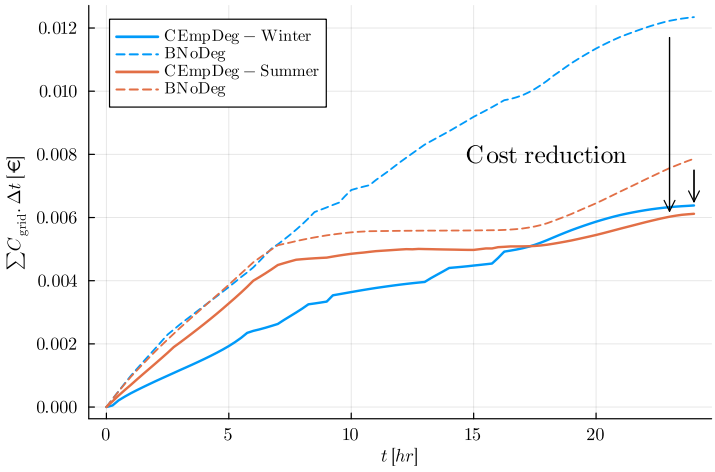

Figure 4.23: Cumulative grid cost C_{grid} for typical summer and winter days.

gorithm, making it the most flexible. However, prediction horizons over 2 h might cause suboptimality below what a rule-based control can achieve. This way, the heuristic method is preferred for cases where the computational cost is a barrier since the heuristic method takes between 1 and 2 order of magnitude less time, for instance, when many households are simulated together withing a distribution network, as will be described in Chapter 6. Additionally, a Section 4.6 was dedicated to study the importance of considering the ageing of the BESS into the EMS. It was demonstrated that there is a cost benefit of op to 48 %.

BIBLIOGRAPHY

[1] J. Alpízar-Castillo, L. Ramirez-Elizondo, and P. Bauer, "Assessing the role of energy storage in multiple energy carriers toward providing ancillary services: A review", *Energies*, vol. 16, no. 1, 2023, ISSN: 1996-1073. DOI: 10.3390/en16010379. [Online]. Available: https://www.mdpi.com/1996-1073/16/1/379.

[2] J. Alpízar-Castillo, L. Ramírez-Elizondo, and P. Bauer, "The effect of non-coordinated heating electrification alternatives on a low-voltage distribution network with high pv penetration", in *2023 IEEE 17th International Conference on Compatibility, Power Electronics and Power Engineering (CPE-POWERENG)*, 2023, pp. 1–6. DOI: 10.1109/CPE-POWERENG58103.2023.10227394. [Online]. Available: https://ieeexplore.ieee.org/document/10227394.

[3] A. R. Abbasi and D. Baleanu, "Recent developments of energy management strategies in microgrids: An updated and comprehensive review and classification", *Energy Conversion and Management*, vol. 297, p. 117 723, 2023, ISSN: 0196-8904. DOI: https://doi.org/10.1016/j.enconman.2023.117723. [Online]. Available: https://www.sciencedirect.com/science/article/pii/S0196890423010695.

[4] P. Horrillo-Quintero, P. García-Triviño, E. Hosseini, *et al.*, "Control of electrical/thermal multi-energy microgrid", in *2023 IEEE International Conference on Energy Technologies for Future Grids (ETFG)*, 2023, pp. 1–6. DOI: 10.1109/ETFG55873.2023.10408649.

[5] M. Kazemi, C. Papadimitriou, N. G. Paterakis, I. Dukovska, and K. Kok, "Optimal design of multi-carrier and multi-objective home energy management system", in *2023 International Conference on Smart Energy Systems and Technologies (SEST)*, 2023, pp. 1–6. DOI: 10.1109/SEST57387.2023.10257384.

[6] P. Di, Z. Su, Q. Lu, J. Liu, K. Xu, and G. Yan, "Optimal energy management for multi-energy microgrid considering demand response", in *2022 IEEE 6th Conference on Energy Internet and Energy System Integration (EI2)*, 2022, pp. 72–77. DOI: 10.1109/EI256261.2022.10117134.

[7] P. Li, Y. Huang, W. Qi, and J. Gan, "Capacity co-optimization of thermal and battery energy storage system in multi-energy complementary system", in *2019 IEEE Innovative Smart Grid Technologies - Asia (ISGT Asia)*, 2019, pp. 3815–3819. DOI: 10.1109/ISGT-Asia.2019.8881407.

[8] D. Slaifstein, J. Alpízar-Castillo, A. M. Agudin, L. Ramírez-Elizondo, G. R. C. Mouli, and P. Bauer, "Aging-aware battery operation for multicarrier energy systems", in *IECON 2023- 49th Annual Conference of the IEEE Industrial Electronics Society*, 2023, pp. 1–8. DOI: 10.1109/IECON51785.2023.10312455. [Online]. Available: https://ieeexplore.ieee.org/document/10312455.

[9] Y. Zhou and P. D. Lund, "Peer-to-peer energy sharing and trading of renewable energy in smart communities trading pricing models, decision-making and agent-based collaboration", *Renewable Energy*, vol. 207, pp. 177–193, 2023. DOI: 10.1016/j.renene.2023.02.125.

[10] T. M. Alabi, E. I. Aghimien, F. D. Agbajor, *et al.*, "A review on the integrated optimization techniques and machine learning approaches for modeling, prediction, and decision making on integrated energy systems", *Renewable Energy*, vol. 194, pp. 822–849, 2022, ISSN: 0960-1481. DOI: https://doi.org/10.1016/j.renene.2022.05.123. [Online]. Available: https://www.sciencedirect.com/science/article/pii/S0960148122007741.

[11] D. Arnone, M. Bertoncini, G. Paternò, A. Rossi, M. G. Ippolito, and E. R. Sanseverino, "Smart multi-carrier energy system: Optimised energy management and investment analysis", in *2016 IEEE International Energy Conference (ENERGYCON)*, 2016, pp. 1–6. DOI: 10.1109/ENERGYCON.2016.7513926.

[12] P. Horrillo-Quintero, P. García-Triviño, E. Hosseini, *et al.*, "Dynamic fuzzy logic energy management system for a multi-energy microgrid", *IEEE Access*, vol. 12, pp. 93 221–93 234, 2024. DOI: 10.1109/ACCESS.2024.3422009.

[13] H. Xiao, X. Pu, W. Pei, L. Ma, and T. Ma, "A novel energy management method for networked multi-energy microgrids based on improved dqn", *IEEE Transactions on Smart Grid*, vol. 14, no. 6, pp. 4912–4926, 2023. DOI: 10.1109/TSG.2023.3261979.

[14] D. Song, W. Meng, M. Dong, *et al.*, "A critical survey of integrated energy system: Summaries, methodologies and analysis", *Energy Conversion and Management*, vol. 266, p. 115 863, 2022, ISSN: 0196-8904. DOI: https://doi.org/10.1016/j.enconman.2022.115863. [Online]. Available: https://www.sciencedirect.com/science/article/pii/S0196890422006598.

[15] A. Baniasadi, D. Habibi, O. Bass, and M. A. S. Masoum, "Optimal real-time residential thermal energy management for peak-load shifting with experimental verification", *IEEE Transactions on Smart Grid*, vol. 10, no. 5, pp. 5587–5599, 2019. DOI: 10.1109/TSG.2018.2887232.

[16] *ANSI/ASHRAE Standard 55-2020: Thermal Environmental Conditions for Human Occupancy* (ASHRAE standard). ASHRAE, 2020. [Online]. Available: https://www.ashrae.org/technical-resources/bookstore/standard-55-thermal-environmental-conditions-for-human-occupancy.

[17] M. Pipattanasomporn, M. Kuzlu, S. Rahman, and Y. Teklu, "Load profiles of selected major household appliances and their demand response opportunities", *IEEE Transactions on Smart Grid*, vol. 5, no. 2, pp. 742–750, 2014. DOI: 10.1109/TSG.2013.2268664.

[18] C. van der Veen, *Analysing thermal energy storage in residential buildings: Towards decarbonization of the heating sector*, The Netherlands, 2022. [Online]. Available: https://repository.tudelft.nl/islandora/object/uuid:c1fca7b7-a7cb-4ddc-936e-239a8f0a6cb7?collection=education.

[19] G. Menzies and Y. Roderick, "Energy and carbon impact analysis of a solar thermal collector system", *International Journal of Sustainable Engineering*, vol. 3, pp. 9–16, Mar. 2010. DOI: 10.1080/19397030903362869.

[20] L. Gigoni, A. Betti, E. Crisostomi, *et al.*, "Day-ahead hourly forecasting of power generation from photovoltaic plants", *IEEE Transactions on Sustainable Energy*, vol. 9, no. 2, pp. 831–842, 2018. DOI: 10.1109/TSTE.2017.2762435.

[21] J. Alpízar-Castillo, L. M. Ramírez-Elizondo, and P. Bauer, "Modelling and evaluating different multi-carrier energy system configurations for a dutch house", *Applied Energy*, vol. 364, p. 123 197, 2024, ISSN: 0306-2619. DOI: https://doi.org/10.1016/j.apenergy.2024.123197.

[22] W. B. Powell, "A unified framework for stochastic optimization", *European Journal of Operational Research*, vol. 275, no. 3, pp. 795–821, Jun. 2019, ISSN: 0377-2217. DOI: 10.1016/J.EJOR.2018.07.014.

[23] W. B. Powell, *Sequential Decision Analytics and Modeling Modeling with Python*. Now Foundations and Trends, 2022, pp. 15–16.

[24] I. Halperin, "Reinforcement Learning and Stochastic Optimization: A Unified Framework for Sequential Decisions", *Quantitative Finance*, vol. 22, no. 12, pp. 2151–2154, Dec. 2022, ISSN: 1469-7688. DOI: 10.1080/14697688.2022.2135456. [Online]. Available: https://www.tandfonline.com/doi/full/10.1080/14697688.2022.2135456.

[25] G. L. Plett, *Battery Management Systems Volume II: Equivalent-Circuit Methods*. Artech House Power Engineering and Power Electronics, 2016.

[26] J. Wang, J. Purewal, P. Liu, *et al.*, "Degradation of lithium ion batteries employing graphite negatives and nickel–cobalt–manganese oxide + spinel manganese oxide positives: Part 1, aging mechanisms and life estimation", *Journal of Power Sources*, vol. 269, pp. 937–948, Dec. 2014, Empirical aging modelused by Wiljan, ISSN: 03787753. DOI: 10.1016/j.jpowsour.2014.07.030. [Online]. Available: https://linkinghub.elsevier.com/retrieve/pii/S037877531401074X.

[27] A. Smets, K. Jäger, O. Isabella, R. van Swaaij, and M. Zeman, *Solar Energy: The physics and engineering of photovoltaic conversion, technologies and systems*. UIT Cambridge Ltd, 2016, ISBN: 9781906860738. [Online]. Available: https://ebookcentral-proquest-com.tudelft.idm.oclc.org/lib/delft/detail.action?docID=4781743.

[28] I. Diab, B. Scheurwater, A. Saffirio, G. R. Chandra-Mouli, and P. Bauer, "Placement and sizing of solar PV and Wind systems in trolleybus grids", *Journal of Cleaner Production*, vol. 352, p. 131 533, Jun. 2022, ISSN: 0959-6526. DOI: 10.1016/J.JCLEPRO.2022.131533.

[29] I. Diab, A. Saffirio, G. R. Chandra-Mouli, and P. Bauer, "A simple method for sizing and estimating the performance of PV systems in trolleybus grids", *Journal of Cleaner Production*, vol. 384, p. 135 623, Jan. 2023, ISSN: 0959-6526. DOI: 10.1016/J.JCLEPRO.2022.135623.

[30] *EPEX Spot*, 2023. [Online]. Available: https://www.epexspot.com/en.

[31] Market Facilitation Forum (MFF) and the Beheerder Afspraken Stelsel (BAS), *mff-bas Sectordocuments*, 2023. [Online]. Available: https://www.mffbas.nl/en/documents/.

5

REQUIREMENTS FOR PROSUMERS TO PARTICIPATE IN THE ANCILLARY SERVICE MARKET: A CASE STUDY OF A DUTCH LOW-VOLTAGE RESIDENTIAL NETWORK

"I mustn't run away"

Shinji Ikari, Neon Genesis Evangelion, Episode 1, by Yoshiyuki Sadamoto.

This Chapter is based on:

- **J. Alpízar-Castillo**, L. Ramírez-Elizondo and P. Bauer, "Addressing Premature Reinforcement of Low-Voltage Distribution Infrastructure with Peak-Shaving and Power Curtailment: a Business Model," International Conference on European Energy Markets (EEM), Istanbul, Türkiye, 2024, pp. 1-6, doi: 10.1109/EEM60825.2024.10608931.
- **J. Alpízar-Castillo**, K. Linders, D. Slaifstein L. Ramírez-Elizondo and P. Bauer, "Economic Opportunities of Power Curtailment and Peak Shaving on Residential PV-BESS Systems," International Conference on European Energy Markets (EEM), Istanbul, Türkiye, 2024, pp. 1-6, doi: 10.1109/EEM60825.2024.10608921.
- **J. Alpízar-Castillo**, C. Engström, L. Ramírez-Elizondo and P. Bauer, "Investigating the Effect of Power Curtailment on the Switch of a Solar Boost Converter Under Residential Loads," IEEE Power Electronics and Motion Control Conference (PEMC), Pilsen, Czech Republic, 2024, pp. 1-6, doi: 10.1109/PEMC61721.2024.10726347.

5.1. Introduction

Energy transition has entailed changes in the energy mix and the transmission and distribution infrastructure. The intention is a generalized transition from fossil fuels to emission-free alternatives for generation, transportation and heating. From an infrastructure point of view, traditional energy systems are unidirectional; the power is generated in centralized power plants to be delivered to consumers through transmission and distribution networks. However, distributed renewable energy sources introduce bidirectional energy flows in distribution systems. In this new scheme, prosumers consume power from the grid when their generators do not meet the local demand and inject power into the grid when the generation surpasses the demand. Since the distribution networks were not initially designed for distributed power injections, those power injections increase the voltage at the connection point, which can cause overvoltages beyond the voltage quality standards, such as EN 50160 in the European Union [1].

To overcome this challenge, DSOs throughout the world have implemented different strategies. In some cases, the network infrastructure has been reinforced, requiring complex and expensive project planning and deployment. Nevertheless, this solution was insufficient due to the speed and cost at which the number of installations increased and the rate at which the grid is being reinforced [2]. Likewise, storage systems like BESS [3] and flywheels [4] have been used to compensate for power fluctuations, but the cost and complexity are still challenging. Alternatively, some local governments have entitled DSOs to request prosumers to curtail their power generation to cap the energy injected into the grid. The main argument is that those DRES systems should operate for self-consumption, not grid injection. In the Netherlands, curtailment is an essential assumption in the grid transformation plans for 2050 [5]. In the United Kingdom, the engineering recommendation EREC G100, by the Energy Networks Association (ENA), allows DSOs to limit their customer's energy import and export [2]. Similarly, Germany's Renewable Energy Sources Act EEG2012 sets the maximum feed-in power into the grid to 70 % of the installed DRES system capacity [6]. When prosumers do not have energy storage systems (EESs) available, they might need to curtail power to comply with those regulations.

This Chapter studies the market conditions that would make it attractive for residential prosumers to participate in the ancillary service market in the Netherlands. The scope for the analysis is: Dutch prosumers with a PV system and a HP, as will be detailed in Section 5.5. EV charging is excluded because, in the Netherlands, most EV owners use public infrastructure instead of charging at their own house [7]. Moreover, the existing energy tariff schemes for residential prosumers were considered, aiming to recreate a more realistic analysis, as many works in the literature consider the wholesale energy market price for similar estimations, but the participation of individual residential prosumers would not fit the wholesale bid market in terms of capacity or reliability.

First, relevant ancillary services at the residential low-voltage distribution networks were qualitatively compared, based on Chapter 2, to select the most suitable ones for short-term implementation by residential prosumers. Then, an analysis of current market-ready inverters and energy management systems for multi-carrier energy systems (based on Section 5.2.1) determined the technical feasibility of implementing those ancillary services in the short term, providing insight into the feasibility of including ancillary ser-

vices in the energy market. A description of the degradation and voltage behaviour of the components selected for the multi-carrier energy system is provided, as Chapter 3 is limited to energy-based modelling. The information is then summarized using the business model canvas, creating a framework for decision-makers to determine the value of ancillary services in residential low-voltage distribution networks. Finally, the impact of supporting the grid by power curtailment and peak-shaving on the levelized cost of energy and storage for individual prosumers in a residential case scenario in the Netherlands was investigated. Three representative case studies were selected for each ancillary service, considering the degradation of the batteries when working in peak-shaving mode, and on the power electronics of the solar converter when curtailing power.

This way, for the case studies of a Dutch low-voltage residential network presented in Section 5.5, this Chapter:

1. defines the requirements for a business model to provide value to Dutch DSOs and residential prosumers through peak-shaving and power curtailment,
2. quantifies the effect of peak-shaving and power curtailment for a case study of a Dutch low-voltage residential network,
3. provides insight into the power exchange conditions that would make it feasible for residential prosumers to provide voltage support to the low-voltage distribution network,
4. quantifies the PV energy lost due to power curtailment and its effect on the levelized cost of energy (LCoE), and the BESS degradation due to peak-shaving and its effect on the expected end-of-life (EoL) and levelized cost of storage (LCoS),
5. estimates the changes in the expected lifetime of the switch of a boost converter when operating in a voltage-controlled curtailment mode,
6. analyses the impacts on the levelized cost of energy caused by the accelerated degradation of a boost converter due to power curtailment, and
7. proposes limits for power curtailment and peak-shaving that minimize the impact on the levelized costs.

5.2. ROLE OF RESIDENTIAL PROSUMERS IN THE DUTCH LOW-VOLTAGE NETWORK

Heat and transport electrification incorporate sudden high-power demands in the distribution network. Heat electrification at the residential level is mainly done by heat pumps. A characterization of the power consumption of HP in the Netherlands is provided in [8]. Their results suggest that a HP can consume between 18 and 35 kWh daily to provide space heating and domestic hot water, with powers eventually surpassing 3 kW. In contrast, during summer, the energy consumption for space cooling and domestic hot water decreases to around 10 kWh, but the power remains near 2.7 kW. Transport electrification at the residential level mainly comprises electric vehicles. The average battery capacity for EVs is around 35 kWh in Europe, but some vehicles can reach up to 90 kWh

[9]. The power of the residential EV chargers is usually 11 kW; however, faster chargers' power is 22 kW [10]. Nevertheless, unlike the HPs, EVs can be charged using public infrastructure, but the usage and availability of public charging points largely depend on the country or region. For example, in the US, 80 % of EVs are charged at home [11], while only 46 % had private chargers at home in the Netherlands [7].

Literature provides numerous studies on the effect of the energy transition on electric networks, as detailed in Chapter 2. For example, [12] simulated Dutch residential apartment buildings with PV systems and HPs as loads in a CIGRE distribution network, demonstrating that, during summer, the power injection due to the PV can increase the voltage near 1.5 p.u., while, during winter, the voltage can drop below 0.9 p.u. Similarly, [10] studied the combined effect of HPs and EV chargers in German low-voltage distribution networks for different penetration levels using PowerFactory, concluding that the German infrastructure might not be prepared to supply the extra demand required for residential heating and private transport electrification.

Those scenarios are a reality already in many power systems worldwide, creating technical and, therefore, economic challenges, as infrastructure costs would constitute the most significant part of energy expenditures in the future [13]. At the European Union level, the gross domestic product (GDP) share for the energy transition is near 1 % annually from 2015 to 2050 [14]. In the Netherlands, the distribution system operator Stedin has to reinforce numerous distribution stations and thousands of transformers, requiring approximately €1.8 billion in additional equity in the coming years [15]. In addition, the tariffs for congestion management fees could increase to compensate for the introduction of renewables and the additional demand caused by heating and transport electrification, urging complementary solutions to face the challenges of the energy transition.

5.2.1. Evaluation of Ancillary Services in Low-Voltage Distribution Networks

System operators have to propose and realize solutions to ensure power delivery, despite a constantly changing network due to the energy transition. Typically, those solutions involve reinforcing the grid, which is limited by the heavy financial burdens placed on governments by energy infrastructure deployments [16], the accuracy of former network planning models [16] and a shortage in the available qualified workforce could postpone such projects [17]. Given the challenges the energy transition causes to system operators in terms of infrastructure reinforcement, some authors have recommended different approaches. Reducing energy consumption (degrowth) was proposed by [18]. Based on two case studies in Spain and Greece, it was concluded that the strategy would not lead to considerable reductions in energy consumption. Creating new energy markets would have more realistic results [19], requiring still the inclusion of energy storage, handling of the variability in the final energy costs caused by the stochastic behaviour of DRES and evaluating the impact of high-voltage lines [16].

Ancillary services provide a collaboration framework between the system operators, generators, consumers and prosumers to ensure the operation of transmission or distribution systems [20]. Most current ancillary services in the Netherlands are at the high-voltage level [21]. However, if one considers the nature of the need for such ser-

vices, it becomes apparent that the challenges, once limited to transmission networks, are repeating in the distribution networks. Classifying the ancillary services in congestion management, voltage control, and frequency regulation or balancing reserves [22] allows a correlation between the objective of each group to the different challenges created by the energy transition. Including EV chargers and heat pumps in the distribution grid can considerably increase the power demand, depending on the penetration levels, thus creating congestion and leading to undervoltages, especially during winter. On the contrary, distributed renewable energy sources inject more power into the grid than can be consumed locally during summer, increasing the voltage and urging voltage regulation mechanisms in DRES-rich networks. Frequency regulation, nonetheless, is unlikely in distribution networks, as it would require a significant load or generation change in a short time, and individually, the prosumers cannot cause such power swings. These reasons lead recent literature to suggest that ancillary services are also attractive at the distribution level.

A detailed correlation between the specific ancillary services and different assets considered for the energy transition, such as DRES, battery energy storage systems (BESS), EVs and HPs, was provided in Chapter 2. For the residential level, the ancillary services suggested are congestion management, voltage control, demand response, direct load control, peak-shaving, and power curtailment. A four-step approach to provide flexibility to DSOs through congestion management is studied in [23]. The proposed method includes acquiring voltage and current measurements on the transformer, feeders, and connection points with the prosumers to calculate the active and reactive powers throughout the network. This data is then used to forecast the aggregated demand on the transformer, allowing an informed decision-making process and finishing with an interface for DSOs so they can request external stakeholders for flexibility. Other works suggest using the free capacity of microgrids [24] or multi-carrier energy hubs [25] within the network or using energy storage [26] or EVs [27] to dispatch power when needed. These approaches have in common a complex prediction-based control and the need for external assets, either storage systems or full microgrids, which are unlikely to be found in residential low-voltage distribution networks.

Voltage control using reactive power compensation in inverters is not allowed by the IEEE Standard 1547-2018 [28]. Instead, the technical standard indicates that the DSO are responsible for ensuring the voltage remains within the limits. In this sense, deploying such a service would require a technical framework. Demand response and direct load control aim to switch the load to meet the network requirements. Demand response is typically scheduled based on the predicted needs of the grid, whereas direct load control is performed in real-time based on the current needs of the grid [29]. The participation of small consumers and dispatchable DRES was proposed in [30] for low-voltage distribution networks, showing an improvement in the grid voltage and congestion. Still, demand response and direct load control would require robust communication with the DSO.

Peak-shaving is a well-known service in the literature that aims to reduce demand using local storage systems directly. Literature provides many examples of its deployment at the residential level. For instance, [31] used a PV-BESS system to reduce the demand peaks by up to 98 %, decreasing the yearly consumption by 15 % and the PV exports to the

grid by 75 %. In [32], a 5 kW PV system was coupled with an 8 kWh BESS to provide peak-shaving to residential loads, reducing the demand by 47 %. Similar results were obtained by [33] and [34], demonstrating the solution's maturity. Similarly, power curtailment is commonly used in generation plants, and, recently, some local governments such as the United Kingdom (ENA EREC G100) [2] and Germany (EEG2012 70%) [6], have provided DSOs to enforce it at the low-voltage distribution network, which means the ancillary service is already part of the energy market. Peak-shaving and power curtailment have in common that they can follow either fixed or dynamic setpoints defined by the DSO at the connection point; the prosumer can manage the internal energy flow locally, thus reducing data privacy vulnerabilities and the complexity of the communication infrastructure required.

Based on the previous analysis, this Chapter focuses on peak-shaving and power curtailment, as they have already been implemented in some energy markets. Many inverters already have power limitation functionalities, enabling peak-shaving. For power curtailment, the datasheets of five of the biggest residential inverter brands were examined to determine their function capacities and limitations. It was investigated whether power curtailment was possible, the curtailment range, and the type of curtailment control. Static control is a fixed power injection limit, after which the inverter would curtail the generation. Dynamic control allows communication with the DSO to define the maximum allowed power the grid can receive at any moment. Table 5.1 shows that all surveyed brands can perform power curtailment in the whole generation range, from 0 to 100 %. However, dynamic control was not that common. Only SolarEdge inverters allow communications with the DSO to change the injection limit. The remaining brands require the user to define a fixed threshold. One interesting exception is Enphase, which, albeit not having communication functionalities, allows the user to set a setpoint profile for the curtailment, allowing a more flexible approach than a single value.

Table 5.1: Power curtailment capabilities in inverter brands.

Brand	Power curtailment	Range	Control	Ref
Enphase	Enabled	0-100	Static (profile)	[35]
Growatt	Enabled	0-100	Static	[36]
SMA	Enabled	0-100	Static	[37]
SolarEdge	Enabled	0-100	Static/Dynamic	[38]
Victron	Enabled	0-100	Static	[39]

5.3. Additional Technical and Financial Mathematical Descriptions

It was indicated that BESS and PV systems would degrade differently when providing peak-shaving and power curtailment, respectively, than when the ancillary services are not provided. Thus, it is necessary to elaborate on their degradation models. Models available in the literature were used to quantify the degradation of the BESS and the PV

converter, as developing degradation models for the components is outside the scope of this thesis. For the latter, a switching control strategy is presented that would allow a boost converter to curtail the power. In addition, a model for the PV module is presented to describe the voltage and current as functions of the irradiance, as the model presented in Chapter 3 only accounts for the power output MPPT conditions, which is insufficient to estimate the degradation in the converter. It is assumed that the HP and the thermal energy storage system's operation is as designed and no additional degradation will occur when providing ancillary services.

5.3.1. BATTERY DEGRADATION MODEL

Energy storage plays a major role in providing flexibility to the distribution networks. The review presented in Chapter 2 evaluated different energy storage systems based on their suitability to provide one or more ancillary services to support grids with high RES penetration. From an energy perspective, BESSs were chosen as the most versatile technology thanks to its fast response, energy and power densities, and decreasing prices. However, it was also recommended to study the degradation changes when providing ancillary services, as they might affect their profitability. Similar to generation technologies, the profitability of energy storage systems can also be evaluated using a levelized cost. The levelized cost of storage (LCoS) is the ratio of cost vs. energy supplied; therefore, for a business opportunity using a BESS to be attractive, the earnings should be above the LCoS. In [40], the reduction of income due to degradation for different applications was studied. A detailed review of the costs related to PV and BESS is provided in [41] and used to calculate the LCoS for different yearly cycling conditions. The economic opportunities for second-life electric vehicles BESS in the day-ahead dispatch market in California were studied in [42], concluding that frequent cycling patterns to provide ancillary services accelerate the BESS degradation.

Battery degradation can be split into calendar and cyclic ageing modes. Calendar ageing is always present and is mainly driven by the formation of the solid electrolyte interphase (SEI) layer due to unwanted side reactions [43]. Calendar ageing can be accelerated by keeping the BESS idle with high SoC values and high ambient temperature [43]–[45]. Cyclic ageing is caused by increased SEI formation due to particle cracking [46] as well as lithium plating [47]. There are three common categories of battery degradation models. Physics-based models mathematically describe the electrochemical mechanisms [48], requiring high computational power. Empirical models fit functions using large experimental datasets (e.g., using equivalent circuits or machine learning methods) [49]. In between, semi-empirical models fit a known equation over measured degradation data to obtain a model [50]. This Chapter focuses on the latter. In [51], the authors derive a semi-empirical model for LFP/Gr cells, using the Arrhenius equation to model cyclic ageing and considering temperature, C-rate, and energy throughput. Calendar ageing is not included, and the influence of the depth-of-discharge (DoD) is neglected because LFP has a low dependency on DoD [52]. In [53], the authors derive a similar model for NMC-LMO/Gr cells, including calendar and cyclic ageing. In this model, temperature, SoC, DoD, C-rate, and energy throughput are included, but the influence of SoC on cyclic ageing is overlooked (this is the model used in this thesis). In [45], the influence of middle SoC was added to the cyclic model, but the influence of temperature

Table 5.2: Parameters for the empirical degradation model [53]

Parameter	c_1 [-]	c_2 [A^{-1}]	c_3 [-]	c_4 [-]	c_5 [$A/s^{0.5}$]
Value	0.0008	0.39	1.035	50	1.721×10^{-4}

was omitted.

As mentioned, the literature presents multiple methods to estimate BESS degradation depending on the available data. In this Section, a control-oriented semi-empirical model is used [53], [54]. The model aggregates the degradation mechanisms (e.g., SEI layer growth, particle cracking, and active material loss) into the calendar ageing

$$i_{\text{cal}} = c_5 . e^{-\frac{24\,\text{kJ}}{RT}} . \sqrt{t}\,, \tag{5.1}$$

and cyclic ageing

$$i_{\text{cycle}} = \frac{c_1 . c_3}{c_4} . e^{c_2 . |i|} . (1 - SoC) . |i|\,, \tag{5.2}$$

resulting in the total current loss

$$i_{\text{loss}} = i_{\text{cycle}} + i_{\text{cal}}\,, \tag{5.3}$$

with the charge Q behaviour being

$$Q_{t+1} = Q_t - \frac{\Delta t}{3600} . i_{\text{loss}}\,, \tag{5.4}$$

where c_i are empirical parameters coming from curve fitting (see Table 5.2), R is the gas constant and T is the temperature.

5.3.2. POWER CURTAILMENT SWITCHING CONTROL

To investigate the cost implications of power curtailment, a PV array connected to a boost converter to supply power to a DC bus within a PV inverter was studied, as shown in Figure 5.1. In typical operation conditions, the switching pattern in the converter would ensure maximum power transfer; however, the power available could surpass the load, and the excess has to be injected into the grid, which could cause overvoltages. For that reason, given a signal, the converter would change from maximum power point tracker (MPPT) to curtailment mode. Changing the operation point has two effects. On the PV side, decreasing the power requires decreasing either the current or the voltage; nevertheless, they are mutually dependent; thus, changing the power output would change the voltage for the PV module, i.e., at the converter's input. On the converter side, a change in power is made by changing the duty cycle of the switch, therefore changing the time the switch and diode operate, as well as their currents. Although some components on the AC side, such as the DC link capacitor, are also affected by operating outside MPPT conditions, this Chapter focuses on the boost converter.

PV MODEL

Photo-voltaic modules are well-studied in the literature. The model proposed by [55] was used for this thesis, as it considers the effects of temperature and irradiance for the

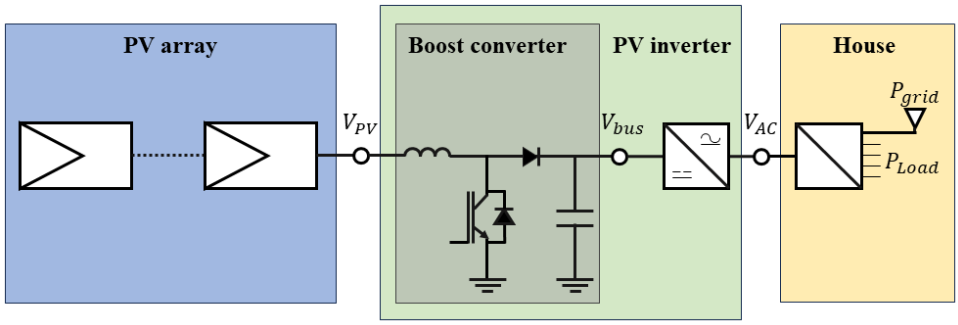

Figure 5.1: Diagram of the considered system (PV array, inverter and house loads).

current calculations. The model describes the current as a function of the voltage V_{PV}, the irradiance G, and the temperature T given by

$$I_{\mathrm{PV}}(V_{\mathrm{PV}}, G, T) = I_L(G, T) - I_0 \exp\left[\frac{q\,(V_{\mathrm{PV}} + I_{\mathrm{PV}} R_s)}{n\,k_{\mathrm{B}}\,T} - 1\right], \tag{5.5}$$

with

$$\begin{aligned}
I_L(G, T) &= I_{L_{T_1}}(G)\,[1 + K_0\,(T - T_1)]\,, \\
I_{L_{T_1}}(G) &= \frac{G\,I_{\mathrm{SC}_{T_1}}}{G_{\mathrm{ref}}}\,, \\
K_0 &= \frac{I_{\mathrm{SC}_{T_2}} - I_{\mathrm{SC}_{T_1}}}{T_2 - T_1} \\
I_0 &= I_{0_{(T_1)}} \left(\frac{T}{T_1}\right)^{\frac{3}{n}} \exp\left[\frac{-qV_g}{n\,k}\left(\frac{1}{T} - \frac{1}{T_1}\right)\right], \\
I_{0_{(T_1)}} &= \frac{I_{\mathrm{SC}_{T_1}}}{\exp\left(\dfrac{qV_{\mathrm{OC}_{T_1}}}{n\,k\,T_1} - 1\right)}\,, \\
R_S &= -\frac{\mathrm{d}V_{\mathrm{PV}}}{\mathrm{d}I_{V_{\mathrm{OC}}}} - \frac{1}{X_V} \\
X_V &= I_{0_{(T_1)}} \left(\frac{q}{n\,k\,T_1}\right) \exp\left(\frac{qV_{\mathrm{OC}_{T_1}}}{n\,k\,T_1}\right)
\end{aligned} \tag{5.6}$$

where $I_{\mathrm{SC}_{T_1}}$ and $V_{\mathrm{OC}_{T_1}}$ are the short circuit current and open circuit voltage at the reference temperature T_1 (in this case 25 °C), respectively. The remaining constants are the elementary charge q, the ideality factor n, the Boltzmann's constant k_{B}, the voltage temperature coefficient β, the reference irradiance G_{ref} (in this case 1000 W/m^2), and the band gap V_g. The manufacturer's datasheet provides these parameters.

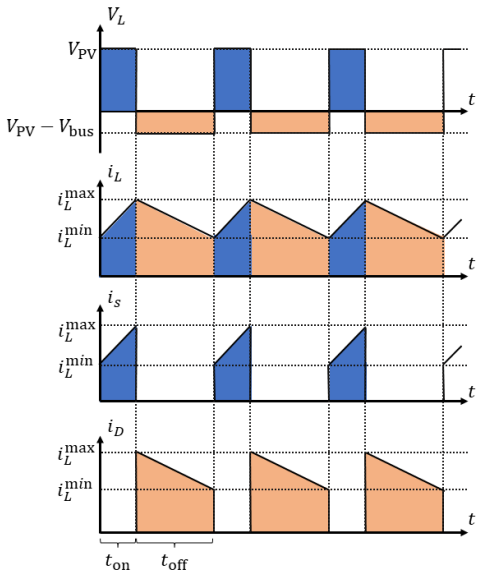

Figure 5.2: Behaviour of the a) inductor voltage V_L, b) inductor current i_L, c) switch current I_S and d) diode current I_D in continuous conduction mode.

Boost Converter

The degradation of any power electronics component depends on its utilization. For this reason, expressions for the currents on the critical components of the converter are needed. This Section focuses on the effects on the switch when power curtailment puts voltage constraintment at the DC link and assumes continuous conduction mode on a boost converter. The switching causes a voltage change in the inductor to reverse its polarity. When the switch conducts, the current flows through it. Otherwise, the current flows through the diode to the load (see Figure 5.2).

The switch duty cycle D determines the power obtained from the PV array and transferred to the load. As the bus has a constant voltage V_{bus} and a current i_o, the analysis should focus on the current level. For the inductor, the average current $\bar{i}_L$ is

$$\bar{i}_L = \frac{V_{\text{bus}} i_o}{V_{\text{PV}}}, \tag{5.7}$$

limited by

$$\begin{cases} i_{\max} = \bar{i}_L + \dfrac{\Delta i_L}{2} = \dfrac{V_{\text{bus}} i_o}{V_{\text{PV}}} + \dfrac{V_{\text{PV}} D}{2 f_s L} \\ i_{\min} = \bar{i}_L - \dfrac{\Delta i_L}{2} = \dfrac{V_{\text{bus}} i_o}{V_{\text{PV}}} - \dfrac{V_{\text{PV}} D}{2 f_s L} \end{cases} \tag{5.8}$$

Similarly, for the switch, the average current is

$$\bar{i}_S = \frac{D\,(i_{\max} + i_{\min})}{2} = \frac{V_{\text{bus}}\, i_o D}{V_{\text{PV}}}. \tag{5.9}$$

while the RMS current is

$$\begin{aligned} i_{S,\text{RMS}} &= \sqrt{f_s \int_0^{t_{\text{on}}} \left[\frac{(i_{\max} - i_{\min})\, t}{t_{\text{on}}} + i_{\min} \right]^2 dt} \\ &= \sqrt{D\left[\left(\frac{V_{\text{bus}}\, i_o}{V_{\text{PV}}} \right)^2 + \frac{1}{3} \left(\frac{V_{\text{PV}} D}{2 f_s L} \right)^2 \right]} \end{aligned}. \tag{5.10}$$

SWITCHING CONTROL

The operation of the converter will be governed by permitted power injection into the grid due to the imbalance between the load and the PV generation. In this thesis, the maximum permitted power to be injected in the grid at any time will be called *curtailment threshold* $P_{\text{grid}}^{\min}$ (the convention considered for P_{grid} is positive when power is demanded from the grid). If no curtailment is needed, the duty cycle will ensure maximum power point (MPP) conditions. However, when the power imbalance surpasses the curtailment threshold, the control will reduce the power extracted from the PV system by changing the duty cycle. At any moment, the time the switch is activated t_{on} is given by

$$t_{\text{on}}\left(P_{\text{grid}}\right) = \frac{V_{\text{bus}} - V_{\text{PV}}\left(P_{\text{grid}}\right)}{f_s V_{\text{bus}}}, \tag{5.11}$$

where V_{bus} is the voltage at the DC bus, V_{PV} is the voltage from the PV array and f_s is the switching frequency.

One can either increase or decrease the maximum power point voltage to reduce the power extracted from a PV module, as shown in the characteristic I-V and P-V curves in Figure 5.3. On the one hand, increasing the voltage would allow a wider curtailment range as the duty cycle is improved, given the inverse proportionality between V_{PV} and D, with a fixed V_{bus}. However, controlling the power in that range might be more complex due to the steep power decline when increasing the voltage above the MPP point [56]. On the other hand, reducing the power by reducing the voltage allows smoother control but reduces the curtailment range as the duty cycle increases. Nevertheless, the curtailment is unlikely to reach 100 %. Normally, the load demands power from the PV system, and the DSO sets the curtailment threshold at the grid connection point. Thus, this Section considers the left side of the maximum power point to control the curtailment.

5.3.3. CONVERTER POWER LOSSES MODEL

Although many modern solar inverters can curtail power, the effect of operation outside the maximum power point to follow curtail orders still has to be investigated. If the power electronics converter (PEC) continuously operates outside its nominal conditions, i.e., MPP, its reliability might be affected, leading to a different lifetime [57]. Some authors have studied the reliability of solar converters under non-standard conditions

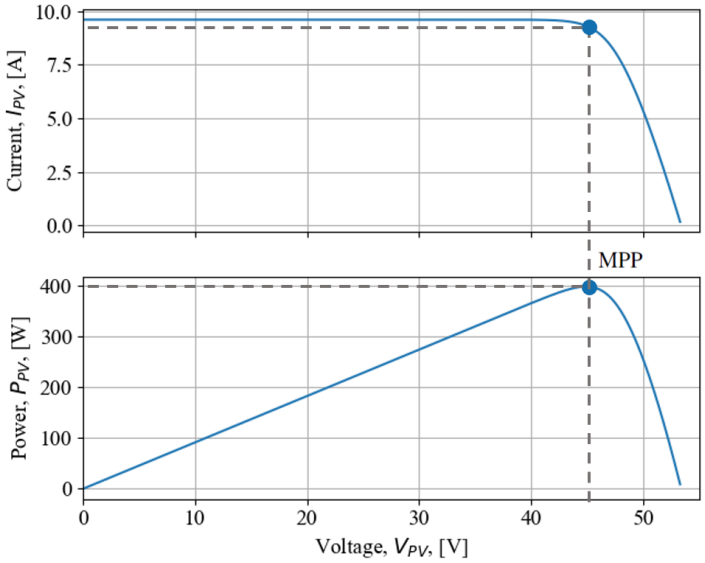

Figure 5.3: I-V and P-V curves for the PV module considered in standard test conditions.

to assess their effect on converter degradation. For example, [58] studied the reliability changes in solar inverters for sun-tracking PV systems, demonstrating that given the increased power the inverter has to handle, the total failure rate also increases. The impact of reactive power injection was studied in [59] and [60], evaluating the economic impact of the converter's lifetime reduction. All studies used the mission profile method. This way, there is a risk that enforced curtailment would affect the financial forecast not only on the energy lost but also would accelerate the inverter degradation, ultimately requiring an early replacement.

For this work, we used the mission profile method, as it allows a more straightforward evaluation of different power profiles associated with different power curtailment levels [61]. This Section focuses on the switch degradation. Following the method proposed by [62]; first, the average and RMS currents in the switch must be determined, as (5.9) and (5.10) respectively. For this Section, the switches are considered to be IGBTs. Their conduction and switching losses per switching cycle are, respectively,

$$P_c(t) = V_s|\bar{i}| + R_{\mathrm{CE}} i_{\mathrm{RMS}}^2 \tag{5.12}$$

and

$$P_s = \frac{f_s E_s |V_s|}{V_{\mathrm{nom}}} \tag{5.13}$$

where V_s and V_{nom} are the instantaneous voltage and nominal voltage for test conditions, respectively, and R_{CE} is the collector-emitter resistance. The turn-on energy loss is given by

Table 5.3: Parameters used in Bayerer's lifetime model.

Symbol	Parameter	Value	Unit
	IGBT model: STGB5H60DF		
A	IGBT technology factor	9.34×10^{14}	-
β_1	-	-4.416	-
β_2	-	1285	-
β_3	-	-0.463	-
β_4	-	-0.716	-
β_5	-	-0.761	-
β_6	-	-0.5	-
I	Current per bond foot	10	A
V	Voltage class	6	-
d	Bond wire diameter	450	μm

$$E_s = a_T + b_T|\tilde{i}| + c_T i_{\text{RMS}}^2 \tag{5.14}$$

where a_T, b_T, and c_T are dynamic characteristic parameters that can be obtained from the datasheet. This way, the total power losses are

$$P_{T,s} = P_c + P_s\,. \tag{5.15}$$

The junction temperature can be calculated as a function of the total power losses and the ambient temperature T_{amb} using

$$T_S = P_T Z_{j-c} + T_{\text{amb}}\,. \tag{5.16}$$

The thermal impedance between the junction and the case, Z_{j-c}, can be calculated by the Foster method as

$$Z_{j-c} = \sum_{i=1}^{n}\left(\lim_{t\to\infty} R_i\left[1-\exp\left(\frac{-t}{\tau_i}\right)\right]\right) \tag{5.17}$$

Where R_i and τ_i are the equivalent thermal resistances provided by the manufacturer.

Following the recommendations in [63], the Bayerer method was used to estimate the end of life of the switches. The thermal cycles to failure are given by

$$\mathrm{N}_f = A\Delta T_j^{\beta_1}\exp\left(\frac{\beta_2}{T_j^{\min}}\right) t_{\text{on}}^{\beta_3} I_b^{\beta_4} V^{\beta_5} d^{\beta_6}\,, \tag{5.18}$$

where ΔT_j is the $j-th$ thermal cycle, $T_j^{\min}$ is the minimum junction temperature (in kelvin) at the $j-th$ thermal cycle, t_{on} is the on-time, I_b is the current per band wire, V is the voltage, d is the diameter of the bonding wire, and A and β_i are constants given by the method, shown in Table 5.3.

A method for cycle counting is required to determine the combinations of ΔT_j and $T_j^{\min}$ for each cycle to failure N_f. Rainflow counting is often used in this context [64], allowing the user to estimate the accumulated damage D caused per cycle to failure as

$$D = \sum_{j=1}^{m} \frac{n_j}{\mathrm{N}_{f,j}}, \tag{5.19}$$

where n_j is the total number of thermal cycles with the conditions in (5.18).

5.3.4. Levelized Cost Estimations

Most users' main incentive for acquiring a PV system is to reduce energy costs [65]. Such savings are often determined by comparing the PV system's levelized cost of energy against the price of the energy purchased from the grid. The lower the PV system LCoE, the bigger the revenue. This way, the LCoE is a function of the total cost and energy generation of the system during a period of n, given by

$$\mathrm{LCoE} = \frac{\mathrm{CAPEX} + \sum_{i=1}^{n} \left[\frac{\mathrm{OPEX}_i}{(1+r)^i} \right]}{\sum_{i=1}^{n} E_i} \tag{5.20}$$

5

where the CAPEX is the capital expense of the project, i.e., the up-front cost of the system, the OPEX are the project's operational expenditures, and r is the discount rate. Given their size, residential PV systems rarely have operational costs beyond component replacement, mostly due to external factors (e.g., weather or manufacturing defects). Therefore, the inverter replacements are considered as operational costs due to the shortening in the converter's life caused by the curtailment (it was assumed that the inverters could not be repaired if the converter failed). Also, a linear PV generation decrease of 20 % in 25 years was used to estimate the yearly energy production E_i in (5.20).

Similarly, energy storage devices have a levelized cost metric, based on the amount of energy stored that is then delivered, called levelized cost of storage, given by

$$\mathrm{LCoS} = \frac{\mathrm{CAPEX} + \sum_{i=1}^{n} \left[\frac{\mathrm{OPEX}_i}{(1+r)^i} \right]}{\sum_{i=1}^{n} E_i^{\mathrm{out}}}. \tag{5.21}$$

In this case, the storage system becomes profitable if the energy cost exceeds the storage cost. Nevertheless, unlike PV systems, the system's lifetime n depends on its usage, as explained in Section 5.3.1. For this reason, estimating the LCoS accuracy before the investment relies on the power profile, the degradation model used and the capacity loss considered as the end-of-life of the battery, which is normally 80 %. Therefore, the LCoS highly depends on the application, as shown in Section 5.5.

5.4. Business Model Canvas

This Chapter focuses on two groups of residential prosumers: those with a PV system and those with a PV system and a HP. It was assumed that EVs would be connected to public charging points controlled by the DSO; thus, they are excluded. The models presented in Chapter 3 were used to create a representative yearly power imbalance profile between the PV generation and the house power demand, both with and without the

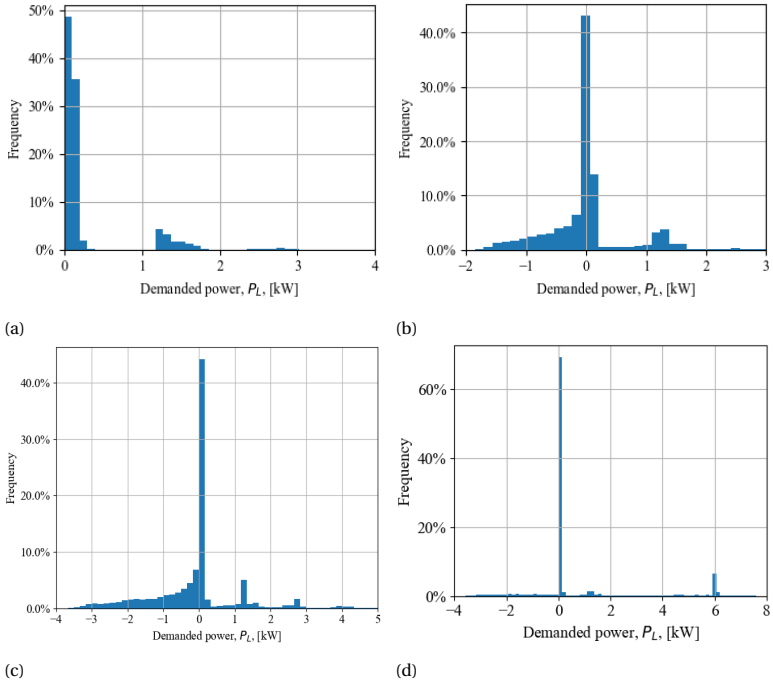

Figure 5.4: Power demanded from the grid with (a) no PV or HP, (b) a 2 kW PV, (c) a 4 kW PV and a 6 kW HP, and (d) a 4 kW PV a 6 kW HP and a 200 kWh TESS.

heat pump. To simulate the demand behaviour of a house, a synthetic load profile was created based on the probability function 3.70. Then, irradiance data from the Royal Netherlands Meteorological Institute (KNMI) was used to create a power profile for the PV generation for the case studies presented in Section 5.5. This way, the power exchanged with the grid, called from now on *power imbalance*, was determined by combining the PV generation and load profiles. Figure 5.4 shows a histogram of the power imbalance, which better represents the frequency at which different powers are demanded or returned to the grid throughout the year. Figure 5.4a shows the power distribution for the base load, Figure 5.4b for a prosumer with a 2 kW PV system, Figure 5.4c for a prosumer with a 4 kW PV and 6 kW HP, and Figure 5.4d for a prosumer with a 4 kW PV, a 6 kW HP and a 200 kWh TESS. Power consumed from the grid is represented as a positive power imbalance, whereas negative power imbalances are power injected back into the grid.

Figure 5.4 illustrate why DRES and HP create challenges for DSOs and their peak-shaving and power curtailment opportunities. The base case shows that, typically, the grid expects powers below 0.5 kW from households, separated into groups spread based on the power used by different high-power appliances (e.g., the microwave, kettle, or induction kitchen) which, in very infrequent cases, they can reach 4 kW when several of such appliances are used simultaneously. Adding a PV system reduces the probability of high power being demanded as the maximum power is below 3 kW. However, the effect

is visible mainly in the lower power range, as the probability of powers between 0 and 0.5 kW is reduced drastically. However, a considerable amount of power is injected into the grid, in ranges between 1.8 kW with lower probabilities and near 0 kW with higher probabilities. Adding the heat pump would require a bigger PV system to compensate for the increased energy consumption, leading to a higher maximum injected power and keeping the probability behaviour of the case with only the PV. Small groups created by high-power appliances still characterize the demand, which has increased to maximum powers near 6 kW. Adding a TESS requires a higher energy consumption, as the HP needs to charge the TESS. This higher use frequency of the HP, summed to the higher temperatures required, reduced its COP, increasing the electrical power consumed by the heat pump, as explained in Section 3.3.6.

The low probability of high power injection into the grid would suggest that power curtailment below a specific threshold would not considerably affect the prosumers' revenue due to feed-in. Nonetheless, fixing a curtailment threshold to limit the power injection into the grid would greatly benefit DSOs. Such a limit would allow more controlled power injections into the grid, providing more certainty for design scenarios. Similarly, the discrete demand groups are a promising scenario for peak-shaving, as the higher the power, the lower the occurrence probability. Thus, the BESS can be sized based on demand limits to avoid affecting the grid. Note that the base case has most of the demand below 2 kW, and the probability of powers above that threshold is almost neglectable in the case without HP, making it less attractive. On the other hand, the cases with HP have low-probability demand groups above 2 kW, which are more promising for peak-shaving. Still, peak-shaving would be a more complex business case, as it requires prosumers to purchase BESSs, increasing their costs and urging a more generous compensation to at least reach the balance point.

Establishing the power imbalance behaviours would provide insight into the business opportunities for the four scenarios. Consequently, analyzing the actors involved allows one to create a business model that provides value for prosumers and the DSOs by enabling peak-shaving and power curtailment. Following the approach proposed in [66] to simplify the canvas analysis, it was divided into three sections: value proposition, value creation and delivery and value capture. The first includes the value proposition, customer relationships and segments; the second includes resources, activities, partners and channels; and the last includes the cost structure and revenue streams. The resulting business model canvas is shown in Figure 5.5.

Value proposition

The general *value proposition* of the business model is to reduce LV distribution infrastructure reinforcement costs for DSOs due to the energy transition by enabling peak-shaving and power curtailment participation at the residential level. Naturally, to create a business, the prosumers should also benefit from it. Therefore, determining the cost associated with premature infrastructure reinforcement would allow DSOs to set a maximum budget to compensate the prosumers who provide those ancillary services. Once DSOs set the boundaries for power exchange (maximum allowed injection for power curtailment and maximum power demand for peak-shaving), they will be communicated to the prosumers. Thus, *customer relationships* are from DSOs to the prosumers through the utility providers. The setpoints prosumers must follow to support the grid can be

static, i.e., fixed limits for power exchange, or dynamic, based on the network status or predicted status at any particular point. Each ancillary service would have its own *customer segment*, as both have different hardware requirements. On the one hand, the power curtailment segment includes prosumers with solar systems, whose inverters can receive and execute power curtailment setpoints, which most commercially available solar inverters can do. On the other hand, the peak-shaving segment requires prosumers with short power peaks in their consumption profile. Heat pumps are characterized by having such behaviour [8]; thus, prosumers with HP meet this requirement, as normal residential loads are not as frequent nor have such high power demand. However, peak-shaving would require prosumers to acquire a BESS with an energy management system capable of receiving peak-shaving signals to charge and discharge the batteries accordingly, as they would unlikely have one already.

VALUE CREATION AND DELIVERY

The *resources* required to implement an ancillary service can be categorized into technical and regulatory. Technical requirements include the technology and infrastructure (including software and hardware, e.g., communication protocols and cybersecurity). Regulatory requirements refer to the legal and policy frameworks. For this reason, DSOs need *partners* throughout the energy supply chain, with different *activities*. The DSOs should determine the maximum they would pay for the ancillary services, based on the network modifications (reinforcement and operation) required by the energy transition. The estimations should be presented to policymakers and regulatory authorities, enabling the legal framework to be updated based on the market's results and changes. Utility companies should facilitate communication between the DSO and the prosumers, which would also require a part of the compensation. Finally, prosumers should evaluate whether providing ancillary services to the DSO would be more profitable than the current tariffs, risking less cooperative schemes in the future.Based on its surveys, [66] recommends newsletters and websites as the most accepted communication *channels* for energy business models.

VALUE CAPTURE

The value proposition is based on a collaborative approach; thus, the *cost structure* is divided among the different partners. From a CAPEX perspective, it relies on the prosumers, as they require a specific system to participate in the ancillary service market (PV alone for power curtailment and PV+BESS for peak-shaving). On the other hand, DSOs and energy utility companies would require lower initial investments, as the business model's value is precisely the reduction or absence of infrastructure reinforcement. Their investment would rely on the communication infrastructure, which could be purchased or subcontracted, in which case, part of those costs are transferred to the OPEX. From the OPEX perspective, the prosumers do not have any additional costs as they currently do, aside from penalties for not complying with the ancillary service contract. DSOs and utility companies, however, do have operational expenses, as they are to compensate the prosumers for the usage of their assets to support the grid. In this sense, there would be profit if the compensation costs were below the projected grid infrastructure costs. For the DSO, the *revenue* would come from the difference between the infrastructure reinforcement costs and the compensation for providing ancillary services to

the prosumers and utility companies. For prosumers, peak-shaving and power curtailment would have different revenue structures. The former requires them to purchase a BESS and use it to keep their demanded power below a threshold set by the DSO; thus, they should be compensated for the purchase and availability of the storage unit. Power curtailment is more straightforward, as the compensation should equal or exceed the earnings lost due to energy curtailment under a feed-in tariff. DSOs would profit as intermediaries between the DSOs and prosumer

5.4.1. Business Model Canvas Analysis

Power curtailment presents the most straightforward implementation; the technology is available, and minimum infrastructure is required for static conditions. This enables different compensation schemes, such as a fixed amount to ensure the limit, based on the curtailed energy, or both. If a feed-in tariff is considered, there would be no cost difference for either the prosumer or the DSO to pay the curtailed energy the same price as if the energy had been injected into the grid. The difference would be from a resilience perspective, as the energy is no longer injected, thus avoiding the challenges associated with DRES penetration. Using fixed amounts would be attractive for prosumers only if the compensation is equal to or exceeds the revenue not received due to curtailment, and it might be challenging for DSOs to define a value that would fit all prosumers.

Peak-shaving has a more complex scenario. First, the prosumer must purchase a BESS to support the grid. In markets such as the Dutch, where there are no noticeable changes between hourly residential tariffs and small prosumers cannot participate in the day-ahead or intraday markets [21], the revenue comes from the reduced purchased energy. Therefore, the compensation for providing peak-shaving should be at least equal to the cost associated with the degradation of the battery, as energy arbitrage at this scale is unlikely to be profitable enough to cover the purchase of the BESS.

Dynamic tariffs would be a more flexible approach for both ancillary services, giving DSOs more control over the power flows. However, its deployment is more challenging. The DSOs would need full observability over the system, information on the location of the customer within the network, and the capability of sending them information in real-time. Likewise, the customers should follow the DSO setpoints, requiring a more complex and robust communication infrastructure and regulatory framework. Either way, dialogue is required among all the actors to understand the opportunities and risks involved in peak-shaving and power curtailment markets. Most of the framework exists as it applies to other actors in the energy supply chain. Thus, the fastest solution would be to estimate fixed power thresholds for each ancillary service and compensate prosumers who meet these targets, provided they were not met before. In the case of power curtailment, the easiest compensation would be based on the amount of energy curtailed. The fastest implementation route for peak-shaving would be a fixed amount for storage availability. Then, the main challenge for DSOs would be to set the peak-shaving and power curtailment thresholds that allow them to minimize the infrastructure reinforcement. Once this framework is established, the operation includes a regular evaluation of the distribution network to assess the effectiveness of the used setpoints.

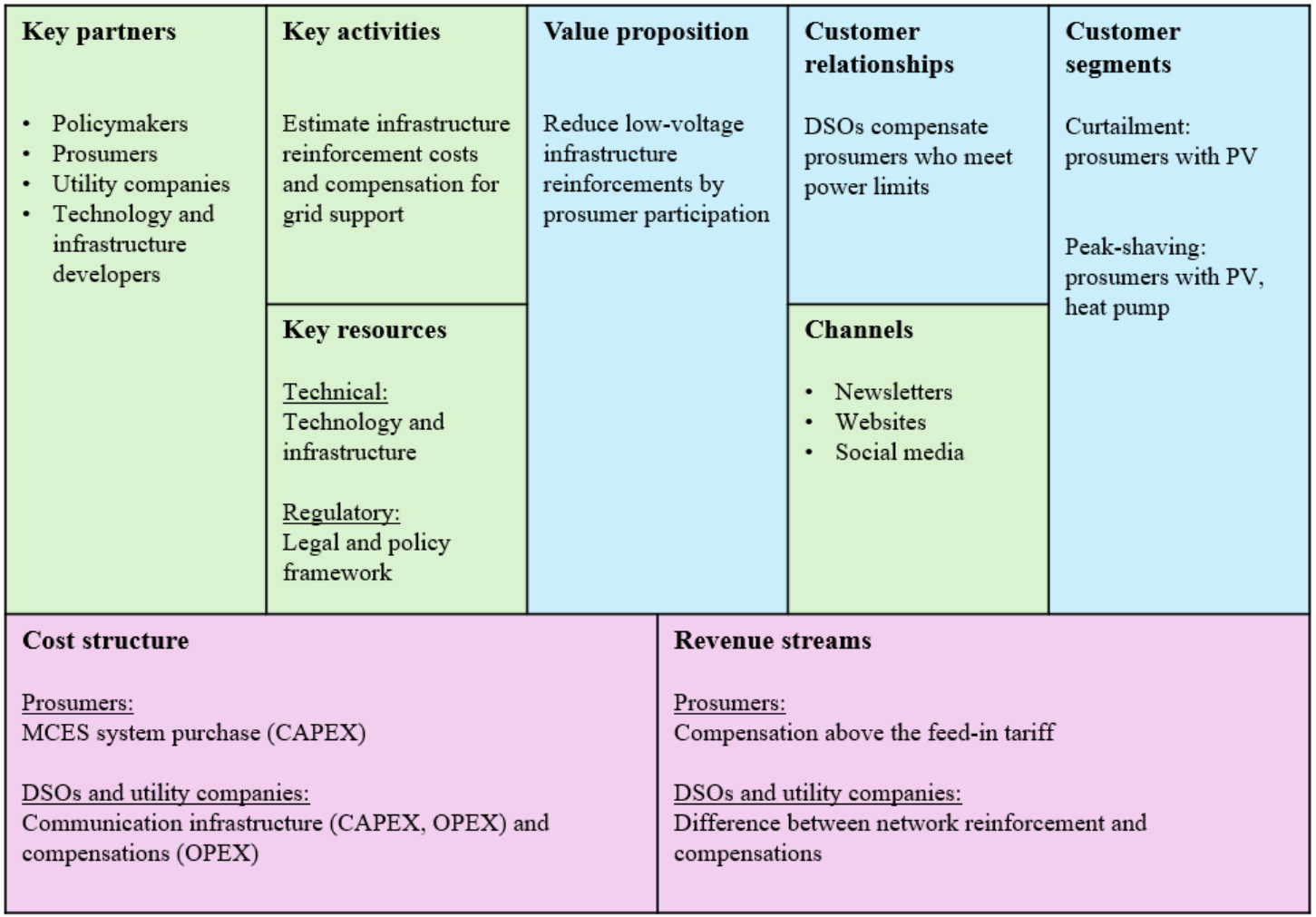

Figure 5.5: Business model canvass

5.5. Case Study Analysis

The two prosumer segments considered for this Chapter are those with only a PV installed and those with a PV and an HP installed. This is because, on the one hand, the current market conditions do not incentivize the usage of electric or thermal energy storage. On the other hand, policymakers have incentivized the deployment of PV and HP, which have been widely adopted. However, it was demonstrated in Chapter 2 that energy storage systems are key in the energy transition, providing flexibility in the distribution networks through ancillary services. As the aim of this work is to provide insight into short-term solutions, the analysis in Section 5.2.1 determined that peak-shaving and power curtailment present a higher potential for fast implementation than other ancillary services, which can be implemented in mid- or long term.

Peak-shaving and power curtailment have similar working principles from a power perspective. Both aim to reduce the power exchanged between the prosumer and the grid; peak shaving reduces the demand, whereas power curtailment reduces the injection. One could notice that a prosumer with only a PV system can already provide power curtailment. However, peak-shaving requires an energy storage system. In this case, a lithium-ion battery was selected. Chapter 2 also mentioned that the combination of a PV and a BESS is preferred for residential tariffs, as participating in the wholesale market is not possible, and normally, the profits earned by energy arbitrage using only a BESS at the residential level are not enough to justify the purchase given the low price and high purchase price for small residential BESS [67]. This Chapter considers three case studies for each ancillary service, as shown in Table 5.4. A BESS system is not considered for power curtailment for two reasons. One, the market segment is prosumers with installed PV systems, which are already causing challenges to the distribution system operators. Two, the peaks produced in households without high power loads, such as HPs or EVs, deem it unlikely to have demand peaks high or frequently enough to be shaved.

Table 5.4: Components considered for each case study.

Case	PV	BESS	HP	TESS
Peak-shaving				
Base load	2 kW	10 kWh/2.56 kW	-	-
Base load and HP	4 kW	20 kWh/5.12 kW	6 kW	-
Base load, HP and TESS	4 kW	20 kWh/5.12 kW	6 kW	200 kWh
Power curtailment				
Base load	2 kW	-	-	-
Base load and HP	4 kW	-	6 kW	-
Base load, HP and TESS	4 kW	-	6 kW	200 kWh

5.5.1. Peak-Shaving Results with the Base Load

In this case, the EMS will dispatch energy from the BESS when the power demanded from the grid is above the peak-shaving threshold, considering only the house loads. Figure 5.6 shows the amount of energy stored in the BESS before its SOH (set at 80 %),

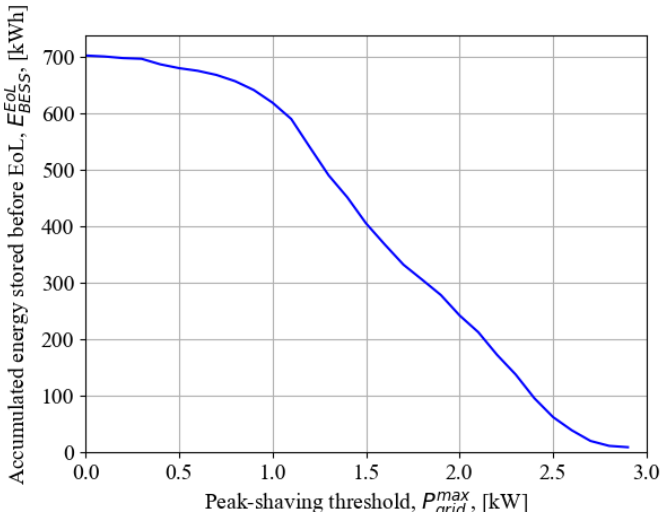

Figure 5.6: Accumulated energy in the BESS before EoL.

suggesting that lower thresholds reduce the amount of energy stored during the life of the BESS. This can be explained by comparing the distribution of BESS power at a particular SoC. Figure 5.7 provides the distribution of the starting SoC of the BESS for every dispatch point. As can be seen, the power range the BESS dispatches is reduced by increasing the peak-shaving threshold, keeping the SoC of the BESS close to its maximum allowed (90 % in this case). The correlation with Figure 5.4b is clear, as the discharge points (positive BESS power) seem to centre near 0, 1.5 and 2.5 kW in the power imbalance. As the peak-shaving threshold increases, the points near 0 kW in the power imbalance stop showing, and the points near 1.5 kW and 2.5 kW in the power imbalance displace towards BESS powers closer to 0 kW. For example, in Figure 5.7a, there are two clear clusters of BESS power, 0 kW and 1.5 kW, coincident with Figure 5.4b, as the peak-shaving threshold is 0. In Figure 5.7b, there is still, albeit minor, a cluster in 0 kW, but the cluster that was near 1.5 kW in Figure 5.7a is now near 1 kW, as the peak-shaving threshold is now 0.5 kW; thus, the relative power between the threshold and the imbalance cluster is now 1 kW instead of 1.5 kW. The cluster near 2.5 kW in the power imbalance became more visible in higher peak-shaving thresholds because the frequency of these powers is around two orders of magnitude lower than the peak centred at 0 kW and one order of magnitude lower than the peak centred at 1.5 kW. Therefore, when the peak-shaving threshold increases, the BESS no longer covers lower power imbalance points, thus increasing the relative frequency of the higher imbalance powers. Also, the BESS might not have enough energy always to comply with low peak-shaving thresholds, as shown in Figure 5.8.

Figure 5.6 shows a decrease in energy accumulated in the BESS before its EoL. This behaviour is because the frequency of powers above the threshold decreases the higher the threshold (see Figure 5.4b), which, added to a smaller difference between the power

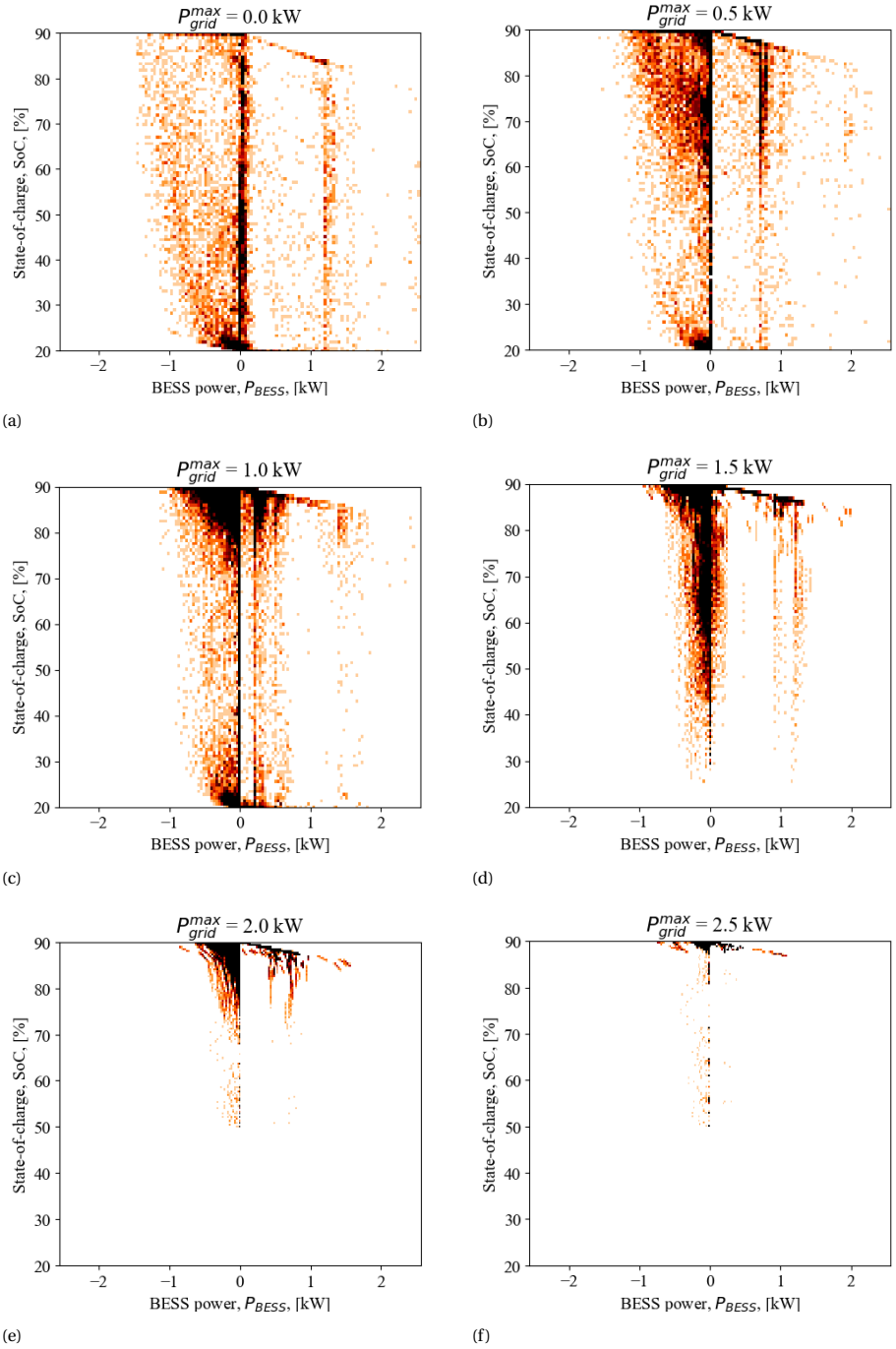

Figure 5.7: Distribution of the starting SoC and power for the BESS for different peak-shaving thresholds.

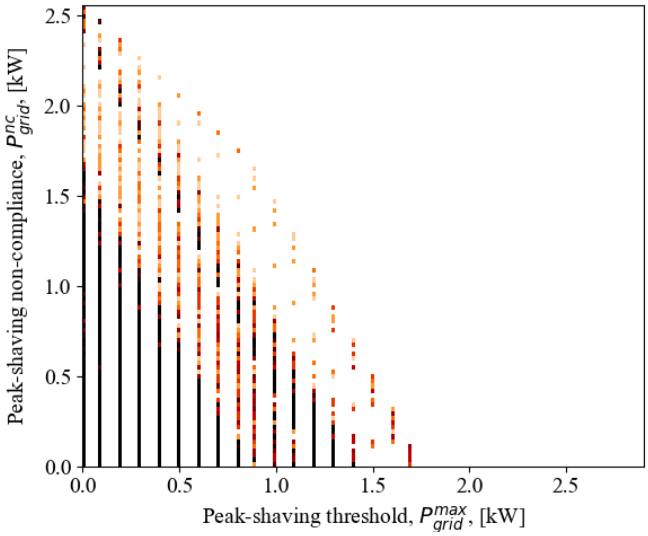

Figure 5.8: Power demanded from the grid above the peak-shaving threshold.

imbalance peaks and the threshold, keeps the BESS in higher SoCs, as shown in Figure 5.7. This way, the main degradation mechanism of the BESS is due to calendar ageing instead of cycling, thus degrading the BESS without using it. In lower thresholds, the BESS has to deliver more power; thus, the DoD is higher, and the BESS degrades faster, reducing its lifetime as shown in Figure 5.9. This is reflected in the levelized cost of storage presented in Figure 5.10. Considering an investment of €6 500, the LCoS increases exponentially, from 9.25 €/kWh to 693.65 €/kWh. The zoom in the figure provides the LCoS for peak-shaving thresholds below 1.5 kW. The LCoS slowly increases from 9.25 €/kWh at the zero-consumption scenario to 10.12 €/kWh at a threshold of 1 kW, increasing exponentially afterwards. In this case, as most of the power consumption is below 1 kW, setting the threshold above this number would result in an underused battery, increasing the levelized cost of storage as less energy is provided by the battery.

Similarly, Figure 5.7 also provides insight into the role of the BESS sizing, both in capacity and power, with respect the the peak-shaving threshold. In this case, the 10 kWh/2.56 kW seems undersized for peak-shaving thresholds near 0 kW, where the extensive usage of the BESS, both in number of cycles and DoD, would accelerate its ageing, suggesting that higher capacity would allow a less deep cycling. Similarly, the inverter capacity seems insufficient to cover the highest, albeit less frequent, peaks. The opposite effect is shown in more permissive thresholds, where the BESS seem oversized. Other case scenarios would probably show different results regarding the expected end-of-life of the battery and its LCoS; but similar to the analysis on the power curtailment case, the behaviour is expected to be similar. This would allow designers to determine the inflexion points for different cases and propose thresholds based on the prosumer's load

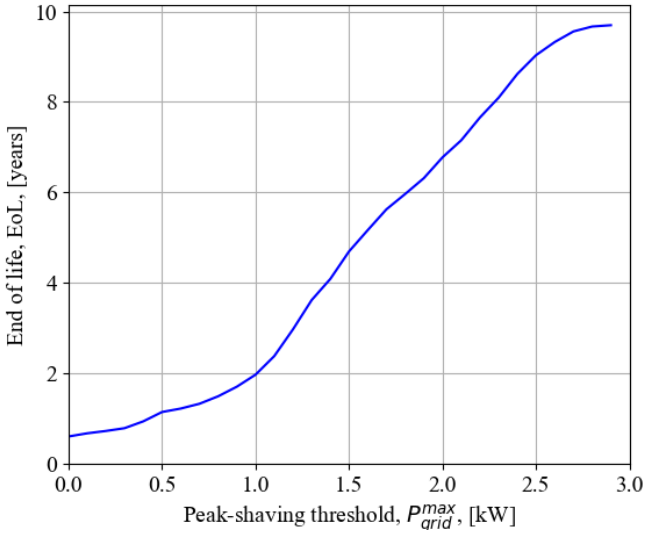

Figure 5.9: BESS expected end of life as a function of the peak shaving threshold.

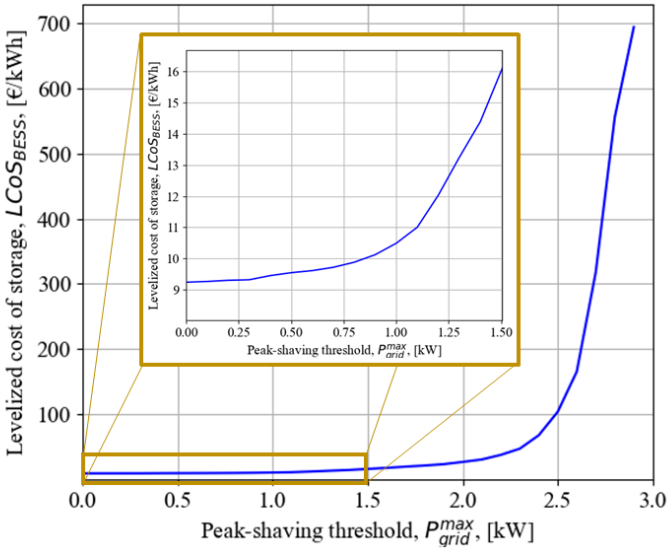

Figure 5.10: LCoS as a function of the peak shaving threshold.

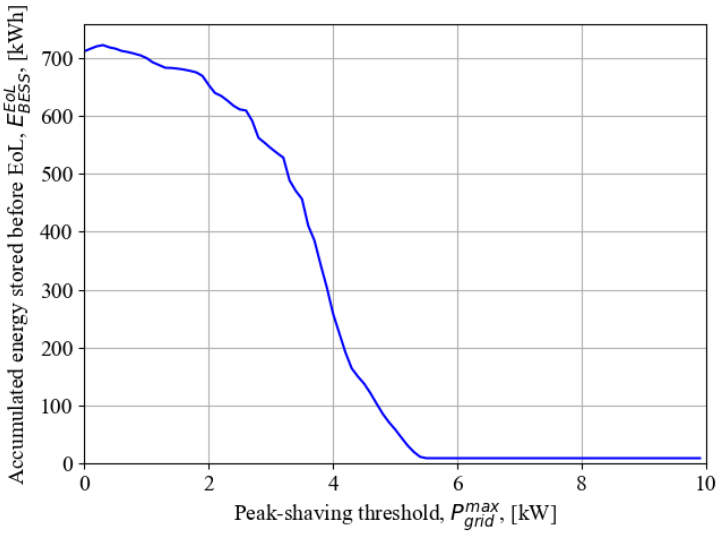

Figure 5.11: Accumulated energy in the BESS before EoL using the HP.

profile characteristics.

5.5.2. PEAK-SHAVING RESULTS WITH A HEAT PUMP

Adding a heat pump to the base load did not drastically change the imbalance distribution compared to the base load with a PV system. Comparing Figures 5.4b and 5.4c show the demand clusters near 1.5 kW and 2.5 kW remain after adding the heat pump to the base load. Additionally, the new cluster near 4 kW is associated with the HP power. This similitude is also reflected in the behaviour of the energy before the EoL of the battery as a function of the peak-shaving threshold (Figure 5.11) and the distribution of BESS power and its state-of-charge (Figure 5.12).

On the other hand, the compliance with the peak-shaving threshold differs from the case scenario presented in Section 5.5.1. Adding the heat pump includes sudden high-power peaks that might exceed the battery's capacity in terms of power or energy; therefore, ensuring a grid exchange below the peak-shaving threshold becomes more challenging, as shown in Figure 5.13. Likewise, the end-of-life of the BESS and its LCoS increase dramatically after the compliance power that can be ensured for this case scenario, around 3 kW, as shown in Figures 5.14 and 5.15.

5.5.3. PEAK-SHAVING RESULTS WITH A HEAT PUMP AND THERMAL STORAGE

This case considers, in addition to the heat pump added in Section 5.5.2, an underground water tank thermal energy storage system. As demonstrated in Chapter 3, adding a TESS increases the usage of the heat pump, reducing also its average COP. However, it also allows the prosumer to provide thermal power when energy prices are high without

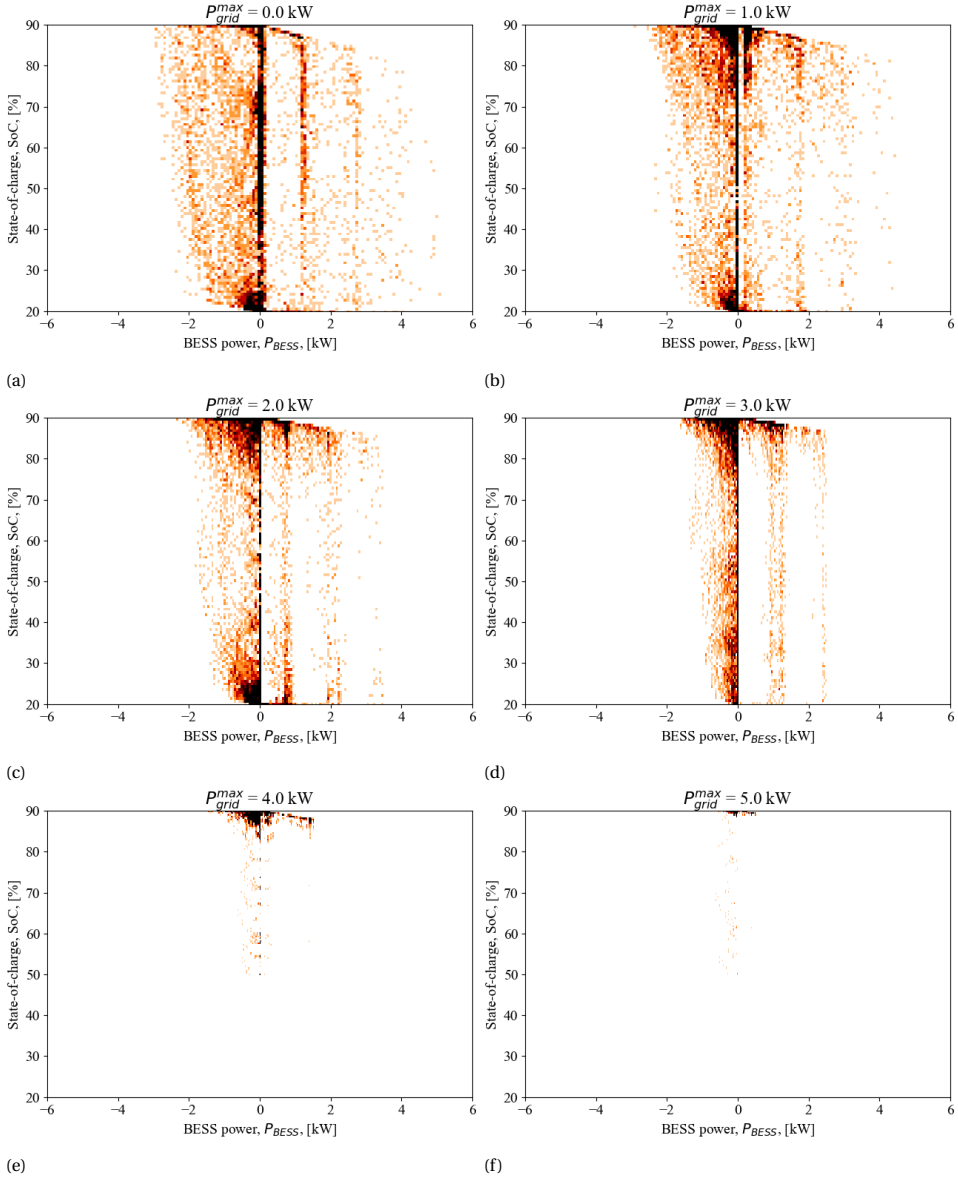

Figure 5.12: Distribution of the starting SoC and power for the BESS for different peak-shaving thresholds, using the HP.

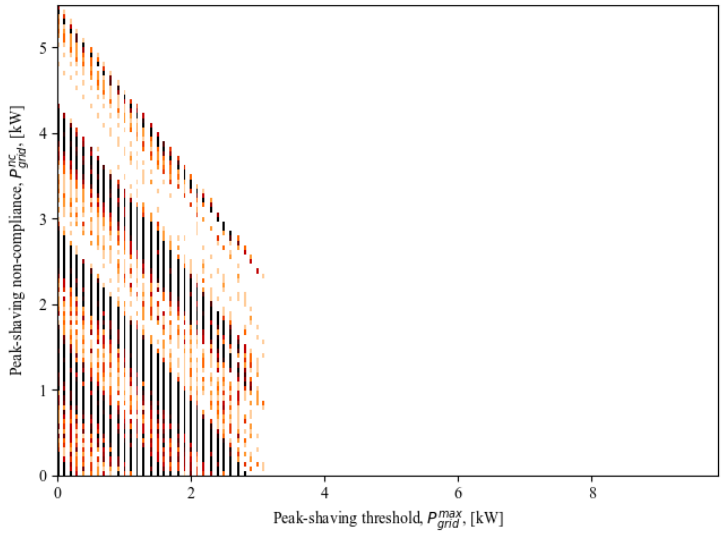

Figure 5.13: Power demanded from the grid above the peak-shaving threshold using the HP.

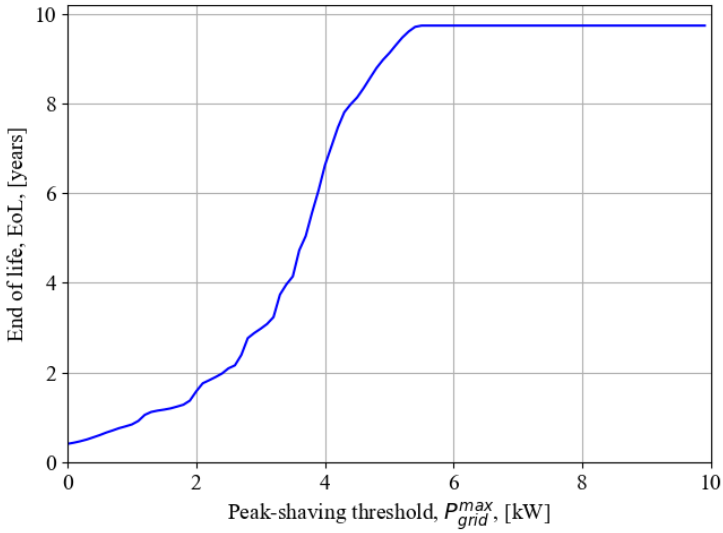

Figure 5.14: BESS expected end of life as a function of the peak shaving threshold using the HP.

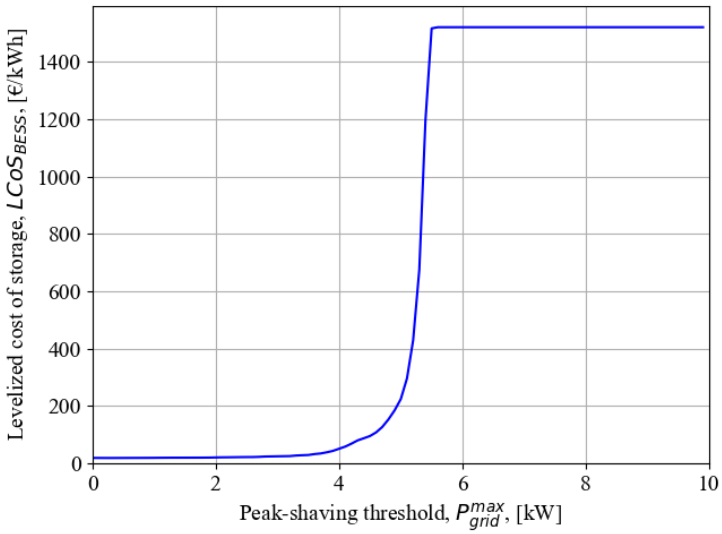

Figure 5.15: LCoS as a function of the peak shaving threshold using the HP.

using the heat pump, or using the heat pump when prices are negative without heating the house if it is not required. Figure 5.16 shows that the accumulated energy before the end-of-life of the battery remains somewhat constant over 650 kWh until the peak-shaving threshold reaches 6 kW.

Similar to the cases in Sections 5.5.1 and 5.5.2, the drop in energy stored before the EoL is explained by the load distribution shown in Figure 5.4d, where the majority of the demand has low power, except for demands near 6 kW. The demand near that power represents the heat pump charging the TESS at its maximum power. After that point, the demand is so infrequent that the BESS activity is neglectable. Figure 5.17 confirms this statement, as the clusters around 1.5 kW, 4.5 kW and 6 kW are dominant, with very low activities above 6 kW. This lower activity is also shown in Figure 5.18, where 6 kW is the compliance limit; after that point, the BESS can ensure the peak-shaving threshold. The reduced use of the battery increases dramatically its expected end-of-life and levelized cost of storage (see Figures 5.19 and 5.20). As the BESS is less cycled, the calendar ageing mechanism becomes dominant over the cyclic.

5.5.4. Power Curtailment Results with the Base Load

The curtailment algorithm was evaluated for thresholds between 2 kW and 0 kW based on the power imbalance presented in Figure 5.4b. Figure 5.21 shows the accumulated energy of the system by the source during 25 years, considering a linear degradation in the PV modules. As expected, due to the lower frequency in higher power injections, the curtailed energy decreases notably after a threshold of around 1 kW. At this point, the revenue loss due to the curtailed generation increases the system's levelized energy cost, as shown in Figure 5.22, making the investment less profitable for the prosumer. Note that for thresholds higher than 1 kW, the revenue loss due to the curtailed energy

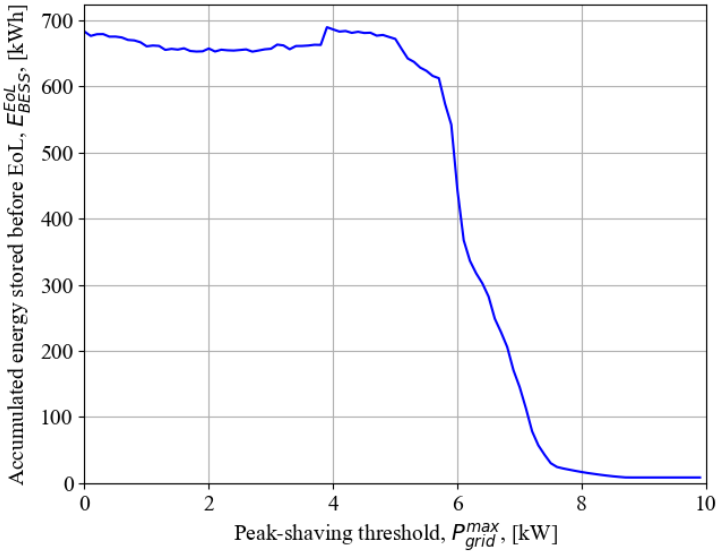

Figure 5.16: Accumulated energy in the BESS before EoL using the HP and the TESS.

did not significantly impact the overall LCoE. Considering an investment of €4000 and no operational costs for the PV system, the LCOE of the system increases exponentially from 0.0722 €/kWh when no curtailment is applied to 0.222 €/kWh when the EMS does not inject any power into the grid, considering a discount rate of 8 % and an inflation rate of 2 %. Given the above, PV system owners could support the network operators by curtailing the power to some degree without affecting considerably their return on investment.

For this case scenario, a PV system was sized to achieve a net-zero energy building; however, the results provide insight into how other case scenarios would behave. On the one hand, residential PV systems with yearly accumulated generation below the accumulated energy consumption still would likely inject power into the grid due to the irregular residential power profile and its mismatch with the PV power generation. On the other hand, oversized PV systems aimed to profit out of the feed-in tariff would be especially less profitable under power curtailment conditions, although one could argue that residential PV systems should not be oversized, as they are designed for self-consumption. The curtailment threshold where the LCoE starts increasing would also change based on the ratio of accumulated PV generation vs. accumulated energy consumption and the load pattern. Nevertheless, the general exponential behaviour will remain in residential case scenarios.

It was mentioned that operating the PV converter using a different operation mode might affect its lifetime. From (5.11), one can notice that the lower voltages resulting from different curtailment thresholds will decrease the duty cycle despite increasing the maximum current. This is reflected in lower currents flowing through the switch. Note that such lower currents will occur only when the converter is not operating in

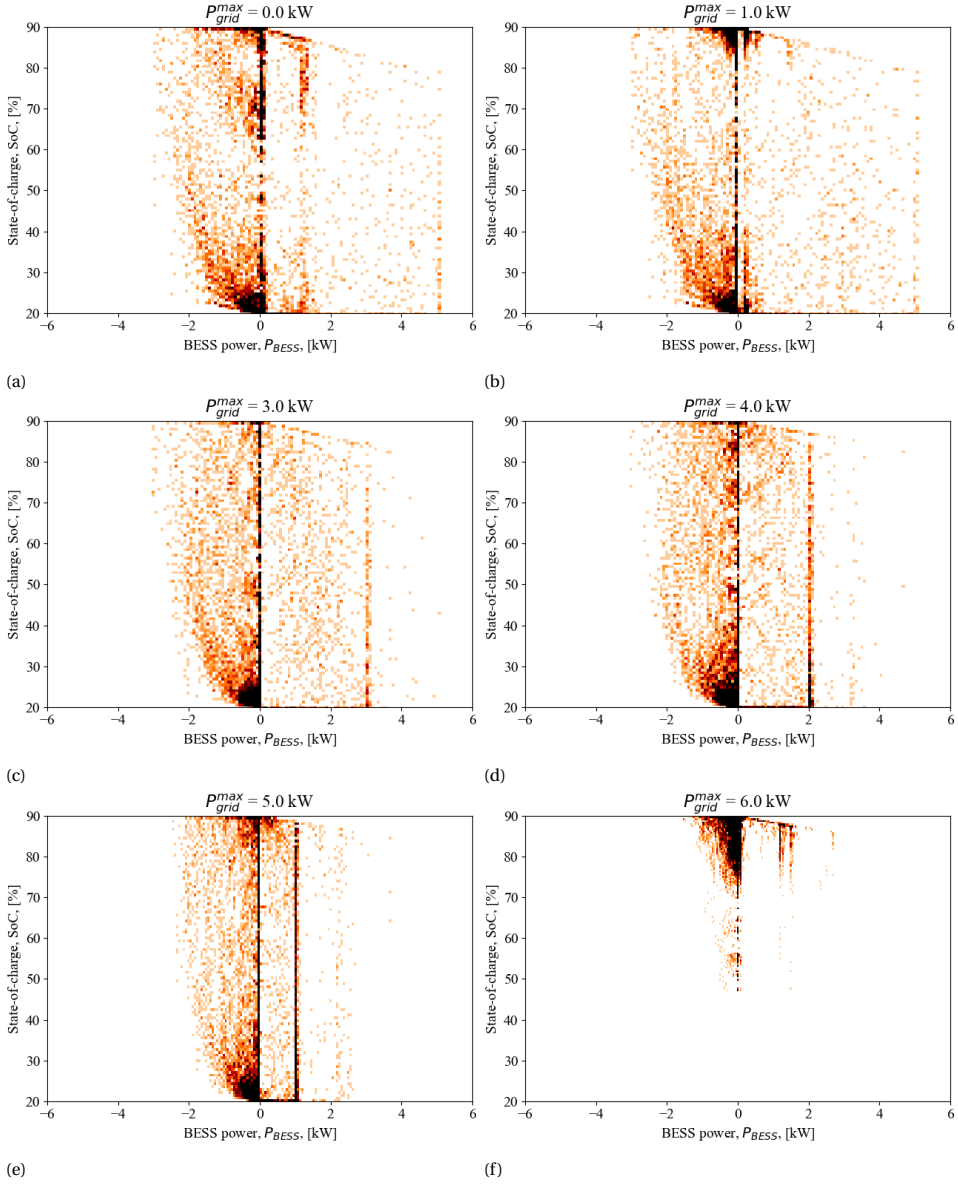

Figure 5.17: Distribution of the starting SoC and power for the BESS for different peak-shaving thresholds, using the HP and the TESS.

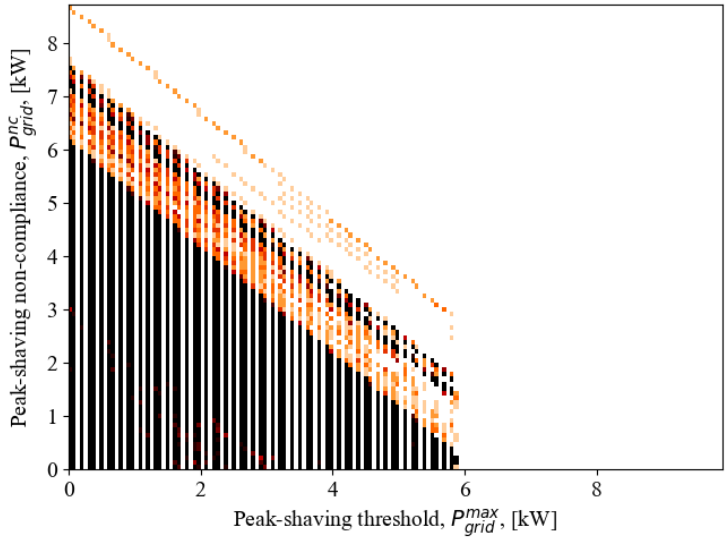

Figure 5.18: Power demanded from the grid above the peak-shaving threshold using the HP and the TESS.

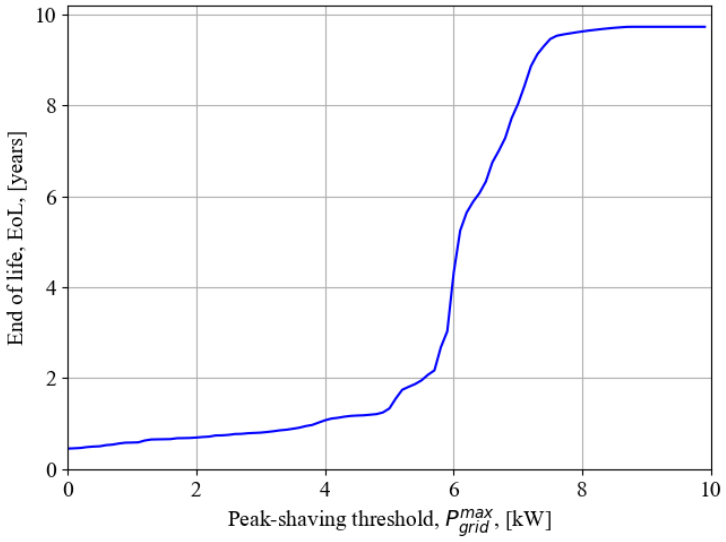

Figure 5.19: BESS expected end of life as a function of the peak shaving threshold using the HP and the TESS.

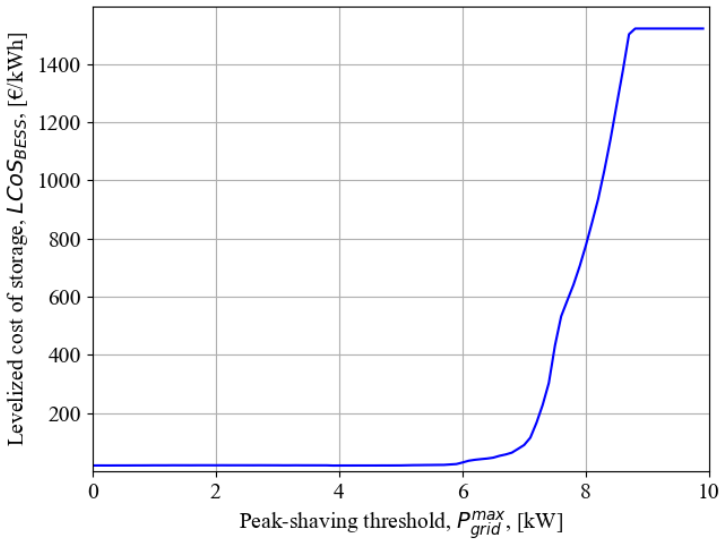

Figure 5.20: LCoS as a function of the peak shaving threshold using the HP and the TESS.

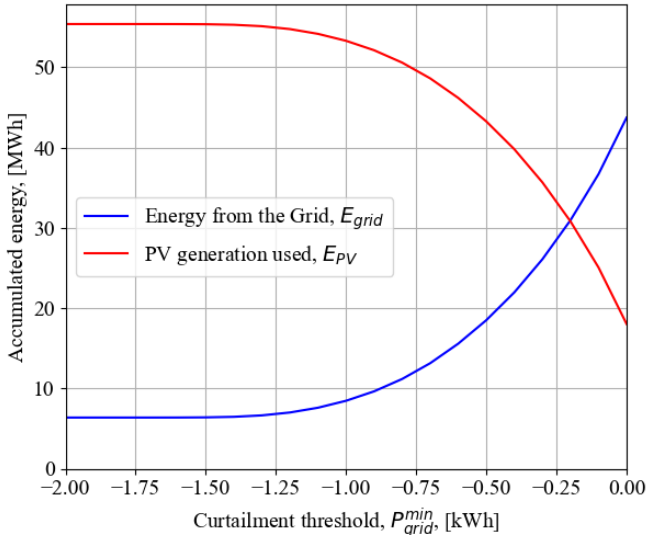

Figure 5.21: Accumulated energy from the PV and the grid based on the curtailment threshold.

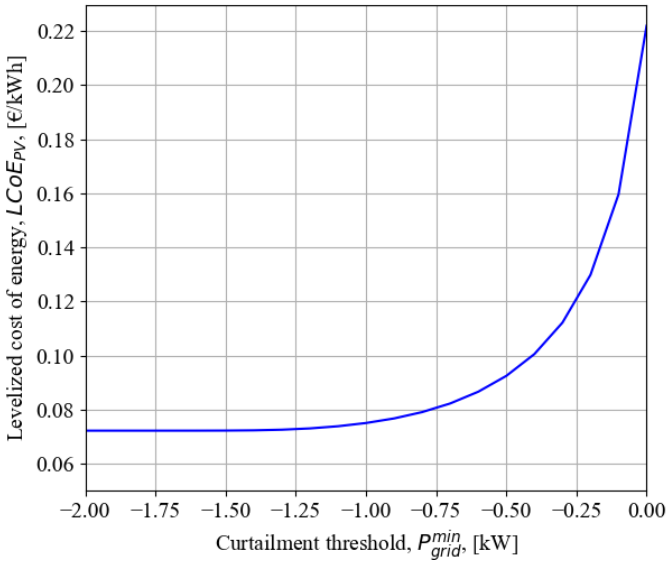

Figure 5.22: LCoE of the PV system based on the curtailment threshold.

MPPT mode but in curtailment. Thus, a sudden curtailment requirement will produce a deeper thermal cycle ΔT, since the junction temperature is proportional to the current, as per (5.12) - (5.16). For the simulation, the distribution of the power imbalance distribution without curtailment shown in Figure 5.4b, and the parameters are shown in Table 5.5 were used.

The previous effect is demonstrated in Figure 5.23, the current and mission profile for two days are shown, one in winter and one in summer. Curtailing in summer is more frequent; higher irradiance requires the converter to reduce more power output as the curtailment threshold moves towards a zero-injection scenario, reducing the voltage and increasing the ΔT. When this effect is studied for the full range of curtailment thresholds in the case scenario, it becomes apparent that curtailment thresholds closer to 0 will have more and deeper thermal cycles, as shown in Figure 5.23. This directly affects the component's lifetime, as shown in Figure 5.24.

Similarly, the converter's lifetime depends on its components. By assuming a direct proportionality between the converter and switch lifetime, the replacement year was estimated by normalising the replacement year to the case without curtailment shown in Section 5.5.4. Figure 5.24 suggests that actively curtailing the power will lead to early replacements for the current curtailment operation mode. This would drastically affect the forecasted revenue of the system, as inverters can account for up to a third of the total cost of a residential PV system. Note that this assumption is, in fact, optimistic, as the reliability of other components is not considered in this work, namely the diode and the capacitor, which would likely have similar thermal responses to the power curtailment.

Table 5.5: Parameters used in the simulation.

Symbol	Parameter	Value	Unit
	PV module		
V_{OC}	Open circuit voltage	53.4	V
I_{SC}	Short circuit current	9.60	A
V_{MPP}	MPP voltage	44.1	V
I_{MPP}	MPP current	9.08	A
β	Voltage temperature coefficient	-0.29	%/°C
V_g	Band gap	1.79×10^{-19}	J
n	Ideality factor	1.4	-
	Boost converter		
V_{bus}	Bus voltage	400	V
f_s	Switching frequency	20	kHz
L	Inductance	1.45	mH
	IGBT model: STGB5H60DF		
V_T	Terminal collector-emitter voltage	1.198	V
R_{CE}	Collector-emitter resistance	00856	Ω
a_T	-	0.0195	W-s
b_T	-	0.011	V-s
c_T	-	0.0005	Ω
V_{nom}	Testing nominal voltage	600	V
$R_{j\text{-}c,i}$	Junction-case thermal resistance	1.7	°C/W
$R_{c\text{-}h\text{-}a,i}$	Case-ambient thermal resistance	8	°C/W

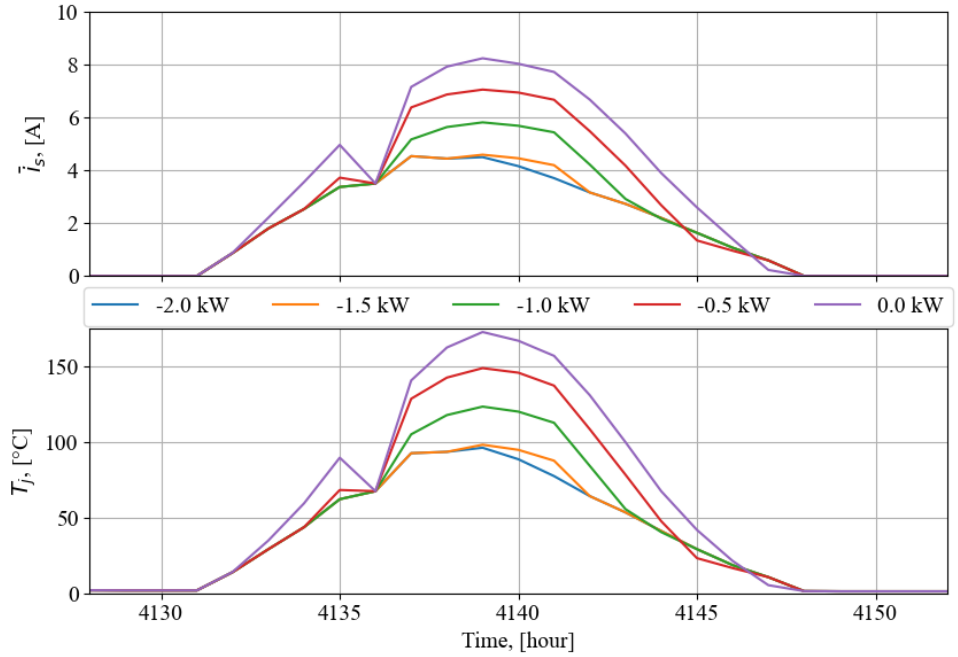

(a)

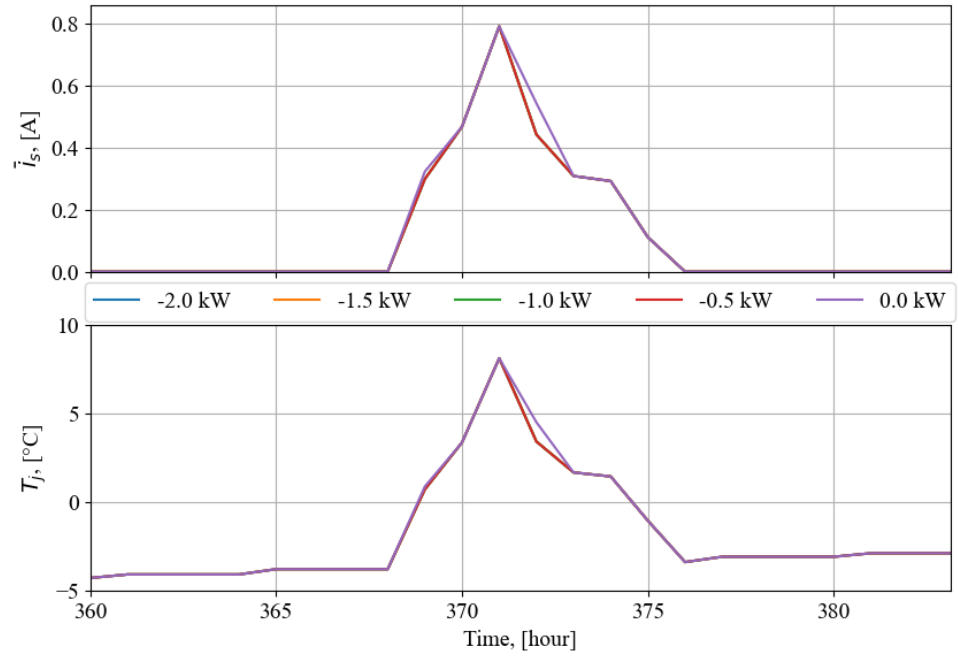

(b)

Figure 5.23: Representative behaviour of the average current and junction temperature during a) summer and b) winter for different curtailment thresholds.

5

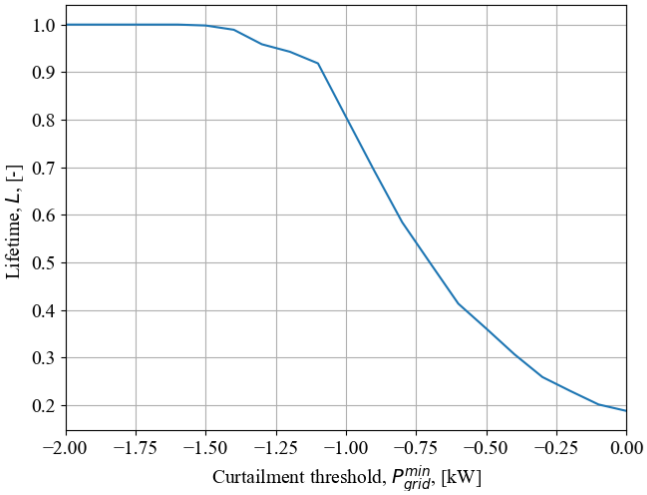

Figure 5.24: Normalized expected lifetime of the switch per curtailment threshold.

One can now analyse the changes in the LCoE, considering the estimated replacement dates for the different curtailment thresholds. The LCoE was estimated for each curtailment threshold using (5.20), with a period of 25 years, a discount rate of 8 %, and an initial investment of €4 000. For the inverter, it was considered a replacement cost of €1 250 (equipment and labour) and an expected base lifetime of 15 years [68]. Two cases for the LCoE are shown in Figure 5.25: one without considering the early replacement due to accelerated degradation caused by the power curtailment (taken as the base case) and one considering the replacement costs, demonstrating a clear increment in the LCoE when the replacement costs are considered. In this case scenario, the homogenous behaviour of curtailment thresholds above 1.15 kW is explained by the load distribution shown in Figure 5.4b. As can be seen, the power injected back to the grid has lower occurrences above 1.15 kW; therefore, the system's behaviour is expected to remain constant in that range, being the LCoE that considers the replacements equal to the base case. The demand increases for values closer to zero-injection; thus, the system has to curtail power more frequently the closer the threshold is to 0 kW. This directly impacts the switches, as the current and junction temperature increase, leading to an exponential increment in the LCoE to over 135 % of the base case, increasing from 0.244 €/kWh to 0.573 €/kWh. For these ranges, turning off the inverter completely could be an option, but a control strategy considering the degradation of the device would be required.

5.5.5. Power Curtailment Results with a Heat Pump

For this case, the PV system's power, investment and replacement costs were doubled to 4 kW, €8000 and €2500, respectively, to compensate for the additional energy consumption of the HP. The modules were arranged in two strings in parallel with five modules

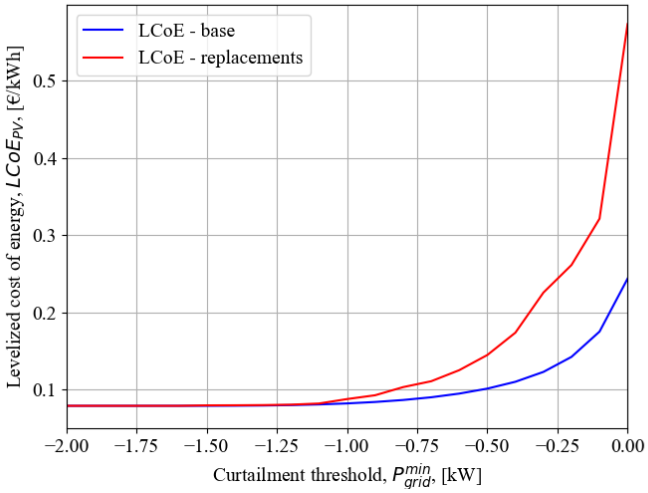

Figure 5.25: LCoE for different curtailment thresholds.

each. To avoid this extra current affecting the converter designed for the case scenario presented in Section 5.5.4, the case-ambient thermal resistance was adjusted to 2 °C/W. For the selected curtailment control method, the current through the switch increases when the power curtailment threshold is moved towards zero-injection, especially in summer, as shown in Figure 5.26.

The increased current through the switch in lower curtailment thresholds directly impacts its relative lifetime to the case without curtailment, as shown in Figure 5.27. The reduced lifetime increases the levelized cost of energy. Figure 5.28 provides the behaviour of the LCoE when the replacements are considered and not for the different curtailment thresholds. In this case, curtailing above 2.25 kW does not cause any difference between considering or not the replacements, after which the difference increases exponentially up to a difference of 170 % in the zero-injection condition, from 0.301 €/kWh to 0.514 €/kWh.

5.5.6. POWER CURTAILMENT RESULTS WITH A HEAT PUMP AND A TESS

Coupling the heat pump with the thermal energy storage system increases the total energy consumption, reducing the power injection into the grid, as shown in Figure 5.4d. Although the overall curtailed energy is reduced in comparison with Section 5.5.5, the thermal behaviour in the switch follows the same increasing trend when the limit gets closer to zero-injection, as shown in Figure 5.29. Nevertheless, reducing the power injected into the grid reduces the need for curtailment to meet the permitted grid injection limit, extending its relative expected life, as shown in Figure 5.30. Similarly, as the energy to be curtailed is reduced, the levelized cost of energy at the zero-injection condition does not increase as dramatically as in other cases. However, the proportion between the cases considering and not considering the replacement of the com-

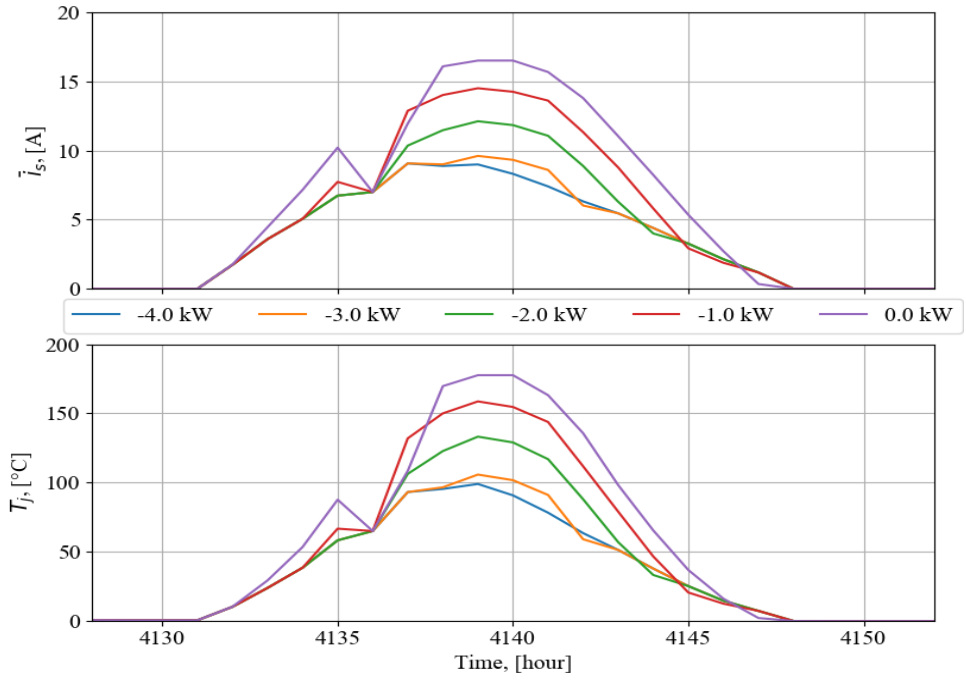

(a)

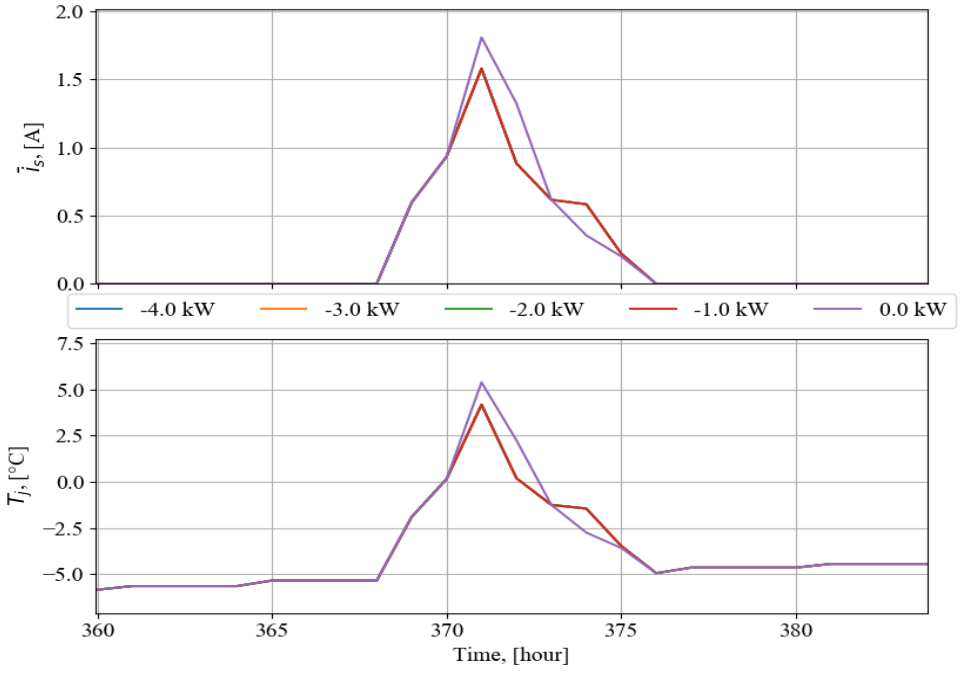

(b)

Figure 5.26: Representative behaviour of the average current and junction temperature during a) summer and b) winter for different curtailment thresholds, using the HP.

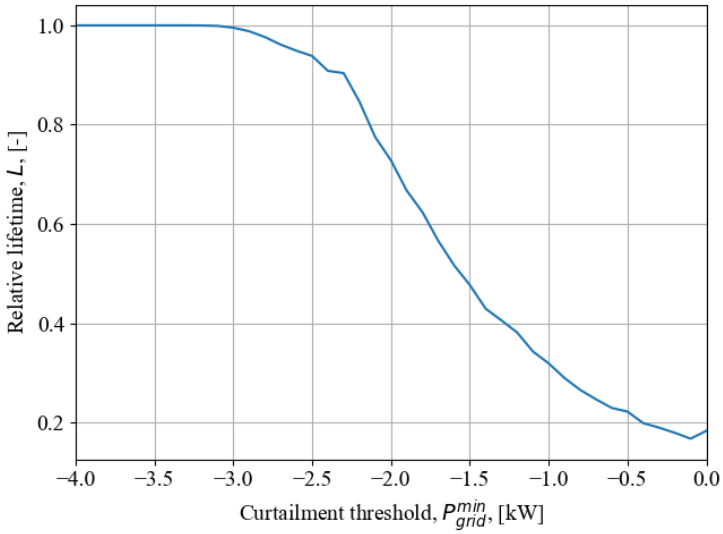

Figure 5.27: Normalized expected lifetime of the switch per curtailment threshold using the HP.

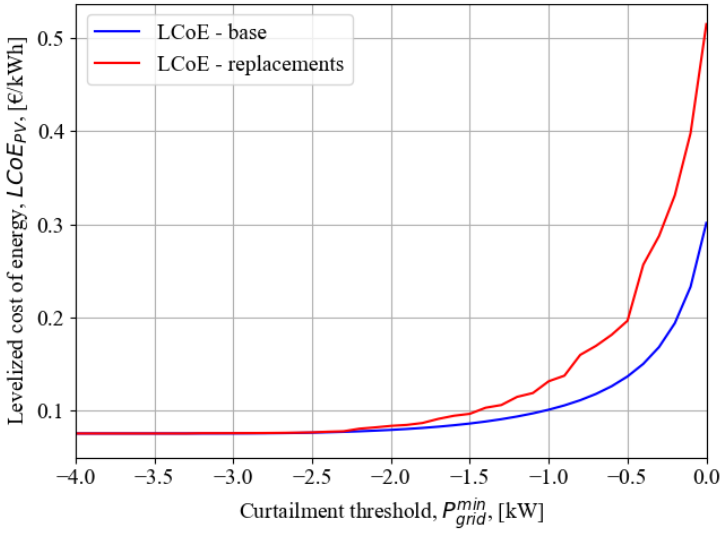

Figure 5.28: LCoE for different curtailment thresholds using the HP.

ponents is around 170 % in the zero-injection condition, varying from 0.1965 €/kWh to 0.336 €/kWh, as shown in Figure 5.31. Interestingly, the power curtailment threshold where the LCoE considering and not considering the replacement of the inverters remains around 2.25 kW, as the case with only the HP.

5.6. Discussion

5.6.1. Peak-Shaving Analysis

Three case scenarios were used to evaluate the residential prosumer's requirements to support the grid using peak-shaving. It was noted that the three cases had similar demand ranges with high occurrence frequencies, namely around 1.5 kW and 2.5 kW. Nevertheless, the cases with the heat pump had one additional cluster of around 4 kW, and the case with thermal storage had one very frequent demand cluster of around 6 kW. The common clusters (1.5 kW and 2.5 kW) are inherent from the base load and show that the PV system alone cannot ensure a decrease in the peak power demand from the grid due to a mismatch between generation and demand despite having a near net-zero building. The increased frequency in the base clusters, plus the new cluster near 4 kW, is associated with the heat pump working. This effect is more clear in the case with the TESS. Since the HP electric power is limited to 6 kW, this cluster represents the HP working at maximum capacity to charge the TESS due to its high temperature and low COP, as explained in Section 3.3.6. Identifying these clusters provides insight into how frequently high power peaks will be demanded from the grid, and the amount of energy required to reduce them below acceptable limits set by the DSO.

To realize peak-shaving as an alternative, two conditions should be met. On the one hand, the prosumers should, at least, recover their investment during the lifetime of the BESS. On the other hand, the DSO should be certain that the BESS will ensure the limit requested. From the prosumer perspective, Figures 5.6, 5.11 and 5.16 show that the slope at which the accumulated energy in the BESS before its end-of-life as a function of the peak-shaving threshold decreases depends on the distribution of the power demanded from the grid, as shown in Figure 5.4. For the base case and the case with only the heat pump, the accumulated energy before EoL decreases from 0 kW towards the highest power demanded because the demand has highest probabilities at lower powers and linearly decreases when the demand increases. However, the case with the TESS has a high occurrence cluster at 6 kW, and fairly constant occurrence frequencies below that power until reaching near 0 kW. This way, the accumulated energy before EoL remains somewhat constant until reaching 6 kW. Afterwards, the behaviour follows the trend present in the other two cases.

The inflexion point and slope of the accumulated energy before EoL are also present in the expected life and levelized cost of storage of the BESS. For the three cases, the end-of-life as a function of the peak-shaving threshold shows an opposite behaviour of the accumulated energy before EoL, which is expected (see Figures 5.9, 5.14 and 5.19). The increased activity of the BESS in lower peak-shaving thresholds accelerates the ageing of the battery, whereas higher peak-shaving thresholds require less frequent and deeper cycles as shown in Figures 5.7, 5.12 and 5.17, making the calendar ageing dominant, therefore extending the life of the battery. Similarly, the levelized cost of storage shows

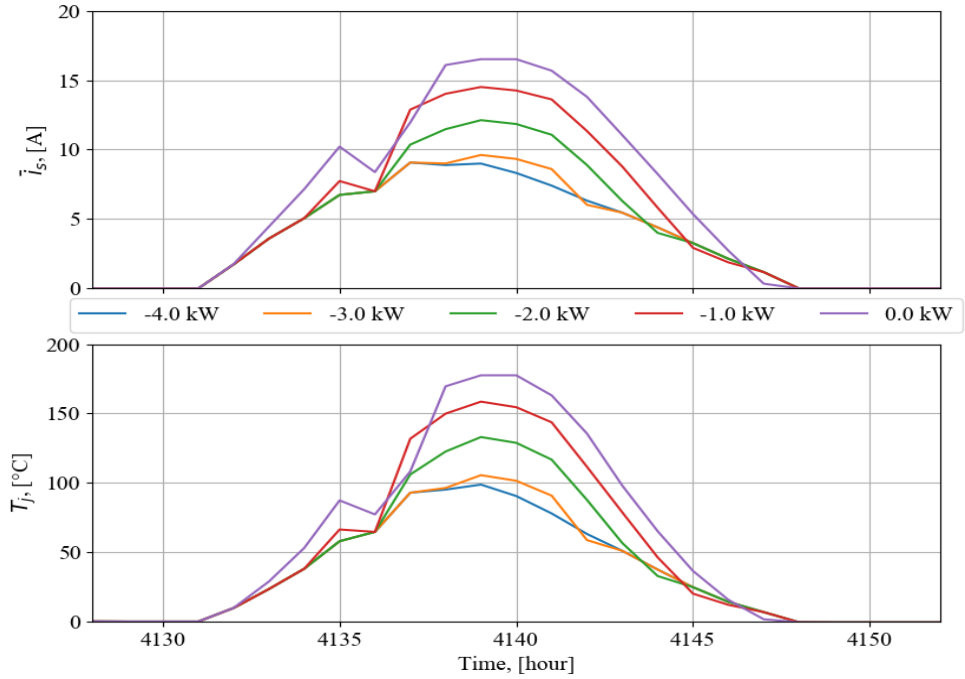

(a)

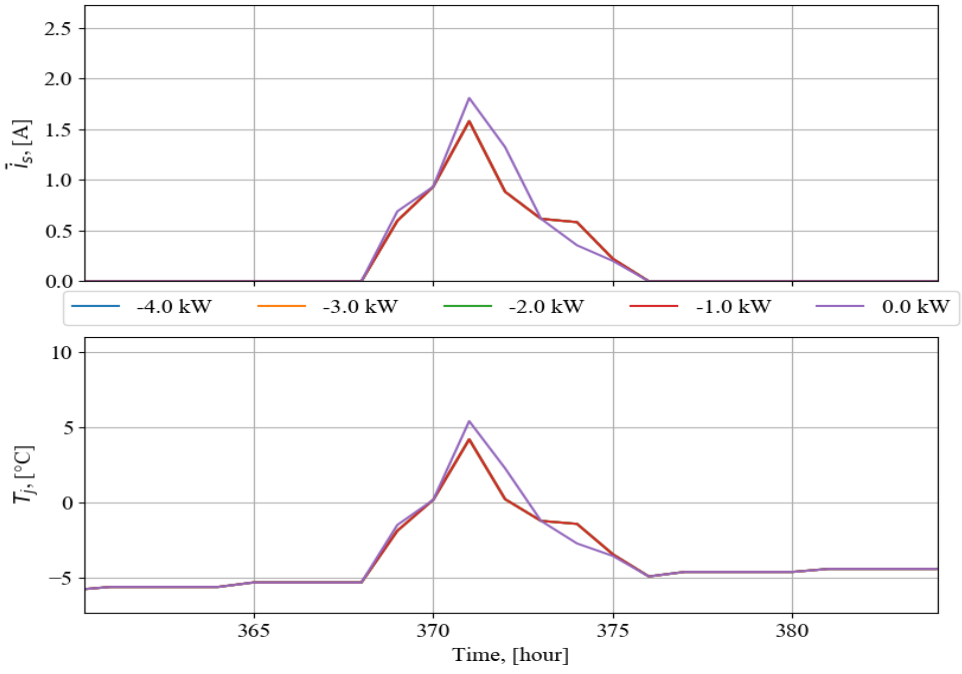

(b)

Figure 5.29: Representative behaviour of the average current and junction temperature during a) summer and b) winter for different curtailment thresholds, using the HP and the TESS.

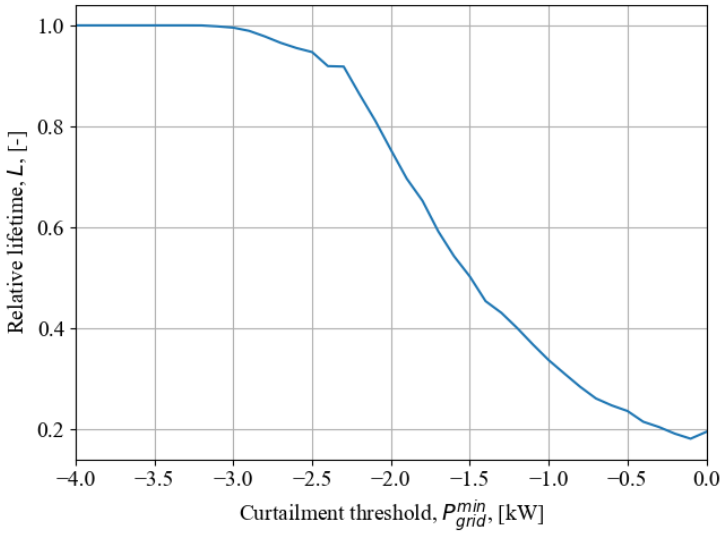

Figure 5.30: Normalized expected lifetime of the switch per curtailment threshold using the HP and the TESS.

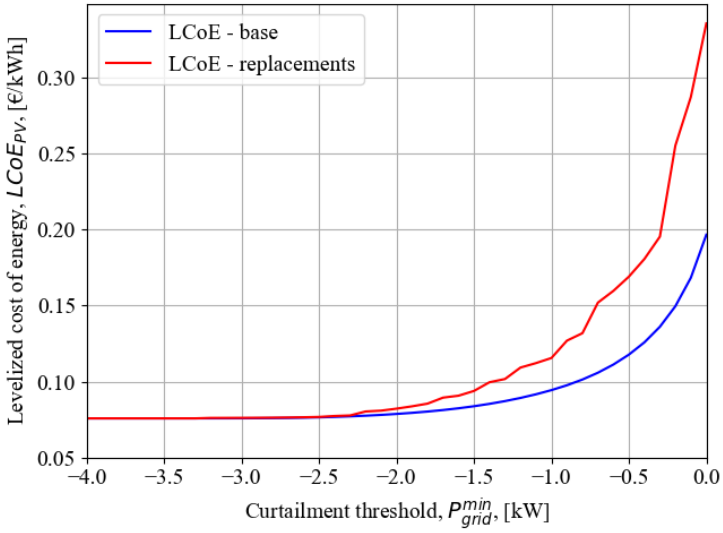

Figure 5.31: LCoE for different curtailment thresholds using the HP and the TESS.

lower values with higher amounts of energy accumulated before EoL. Interestingly, for the three cases, the LCoS has an inflexion point towards an exponential growth at the peak-shaving thresholds that cause EoL close to 2 years, or accumulated energy before EoL of around 90 % of the maximum value.

From the DSO perspective, non-compliance with the defined peak-shaving threshold was used as an indicator. Figures 5.8, 5.13 and 5.18 demonstrate that high the peak-shaving thresholds entail lower non-compliance frequency. In this case, no correlation was found among the three case studies; therefore, generalizing the compliance with the limit set by the DSO would require a deeper probabilistic analysis. In addition, the BESS can be sized for this application. Nevertheless, the BESS used for the cases with HP and TESS is already 20 kWh, which competes with the BESS of an EV. Assuming the prosumers own an EV and that the higher demand peaks would be when the inhabitants are in the house, a new case scenario can be built to evaluate the feasibility of using an EV instead of a BESS, as the capacity of the battery would be higher and the investment is not dedicated exclusively to the ancillary service, which might result in a more attractive case.

5.6.2. POWER CURTAILMENT ANALYSIS

The mismatch between generation and consumption results in power injection into the grid. Considering a feed-in tariff, the prosumers still perceive revenue for the injection; however, this injection is problematic for the DSO. It was discussed that it is to be expected that commercially available inverters can perform power curtailment, at least using a static threshold. Nevertheless, curtailing power reduces the revenue for the prosumer. In addition increasing the current to regulate the output power resulted in an increased temperature in the converter's switch, as shown in Figures 5.23, 5.26 and 5.29. Therefore, the power curtailment algorithm might decrease the expected lifetime, as shown in Figures 5.24, 5.27 and 5.30.

Reducing the lifetime of the converter entails early replacements, reducing the system LCoE. For the three case scenarios, the LCoE was around 0.0722 €/kWh before curtailment. However, after a specific curtailment threshold, the LCoE increases exponentially. Additionally, the LCoE is affected by the replacements. Figures 5.25, 5.28 and 5.31 show how neglecting the effect of curtailment in the life of the converter could cause deviations of up to 60 % in the LCoE. Still, the LCoE for considering and not considering the replacements differs at the curtailment threshold where the LCoE of the case considering the replacement starts its exponential growth. It was determined that, for the base case, the case with the HP and the case with the HP and the TESS, this divergence point was 1.15 kW, 2.25 kW and 2.25 kW, respectively, and the proportion of solar energy curtailed to not be injected back into the grid was 5.06 %, 6.41 % and 5.95 %, and the proportions of solar energy curtailed with respect to the total generation are 3.51 %, 4.90 % and 3.74 %, respectively. This way, it could be considered that, for similar case scenarios, the LCoE will increase considerably if more than 4 % of the total generation is curtailed, corresponding to around 6 % of the total energy injected into the grid.

5.7. Conclusions

This Chapter determined, based on the literature review provided in Chapter 2, what ancillary services can be implemented the fastest in the Dutch context, selecting peak-shaving and power curtailment. Then, models were presented to evaluate the degradation of the BESS and the solar converter when operating to provide such ancillary services. With this information, an actor analysis was performed to create a business model canvas to create value for prosumers and the DSOs based on providing such ancillary services. Two customer segments (with PV, and PV and HP), and three case scenarios (their base load, their base load with a HP and their base load with a TESS) were considered. It was determined that prosumers with PV systems could provide power curtailment without affecting their revenue if their compensation is similar to the energy tariff, as the residential market uses a feed-in scheme. Peak-shaving is only worth the investment in a BESS when the demand peaks are high and frequent enough so that, when many households in a low-voltage residential network have such load, the voltage in the lines reduces below voltage quality standards, so that the DSOs would be interested in reducing the demand. Such conditions are not typical in Dutch residential consumptions (excluding HPs or EVs). The DSO should estimate the power demand limit for peak-shaving, and the reinforcement costs associated with those power ranges to propose compensation to the prosumers. A static setpoint is preferred over a dynamic one for a fast implementation. Albeit less flexible, existing technologies would allow immediate adoption since market-ready inverters and EMSs allow curtailment already, and the regulatory frameworks would require minimum changes. Nevertheless, a dynamic setpoint would be more beneficial for DSOs as they could adjust their requirements based on the network state and the location of the prosumer.

In addition, this Chapter investigated, from a cost perspective, what conditions can make it attractive for individual prosumers to participate in a low-voltage ancillary service market, specifically for three case scenarios for peak-shaving and power curtailment. The market segment considered for peak-shaving included prosumers with PV and HP. Using a semi-empirical ageing model, degradation of the batteries was estimated for three case scenarios. The LCoS tend to increase when increasing the peak-shaving threshold, having a minimum value of 9 €/kWh for the base load case and a maximum value of 20 €/kWh for the case with HP, HP and TESS. The LCoS remains somewhat constant until a threshold that causes an EoL for the battery of 2 years. After that point, the LCoS increases exponentially when allowing higher power demands because the imbalance power has low frequencies in the high-demand region, leading to lower energy stored in the BESS and higher calendar degradation. However, from an owner's perspective, supporting the grid can be done at any threshold if the prosumer is compensated above the LCoS. Lower permitted power exchange limits, near zero-consumption, require more frequent battery usage, resulting in a faster degradation. Also, the three case scenarios often fail to meet the injection limit, urging higher PV and BESS capacities, ultimately leading to an oversized system, a different approach for the EMS, or using an EV instead of a BESS, due to its larger battery. Note that this analysis is done for a static peak-shaving threshold. In a dynamic threshold, DSOs would evaluate the network status and determine the acceptable power for each node to avoid congestion at a certain time. Chapter 6 studies the dynamics of integrating residential multi-carrier energy sys-

tems into the low-voltage distribution network.

Power curtailment ensured a predefined power exchange with the grid. There was no significant LCoE change in the case studies when less than 4 % of the total generation is curtailed. However, curtailing above that point, towards a zero-injection scenario, increased the LCoE exponentially from 0.0722 €/kWh up to 0.222 €/kWh for the base case, 0.514 €/kWh for the case with the HP, and 0.336 €/kWh for the case with the TESS. The Chapter also analyzed the degradation and cost effects enforced power curtailment has on the converter of a PV system in a residential case scenario. Considering a boost converter, it investigated the change in the lifetime of an IGBT switch as the component most likely to fail, thus urging a replacement of the inverter. From a degradation perspective, curtailment thresholds closer to 0 kW decreased the voltage on the converter's input. Lower input voltages required lower duty cycles and sudden changes to lower currents. Those sudden current changes resulted in more frequent and deep thermal cycles, increasing the probability of an early failure and reducing the expected component lifetime by up to 80 % in the zero-injection scenario. Then, assuming a correlation between the lifetime of the switch and the converter's (thus, the inverter), the levelized cost of energy due to curtailment will increase, suggested by the increased probability of early failure in the switch. However, enforcing curtailment without compensation can lead to unprofitable scenarios, as the prosumers would reduce the energy their system produces while accelerating the degradation of the components, with no gain.

BIBLIOGRAPHY

[1] *EN Standard 50160 - Voltage characteristics of electricity supplied by public electricity networks*. EN, 2010.

[2] "Technical requirements for customers' export and import limitation schemes", Energy Networks Association, Engineering Recommendation G100 Issue 2 2022 Amendment 2, Apr. 2023. [Online]. Available: https://www.energynetworks.org/assets/images/ENA_EREC_G100_Issue_2_Amendment_2_(2023).pdf.

[3] M. Stecca, L. R. Elizondo, T. B. Soeiro, P. Bauer, and P. Palensky, "A comprehensive review of the integration of battery energy storage systems into distribution networks", *IEEE Open Journal of the Industrial Electronics Society*, vol. 1, pp. 46–65, 1 2020, ISSN: 26441284. DOI: 10.1109/OJIES.2020.2981832.

[4] S. Karrari, M. Noe, and J. Geisbuesch, "High-speed flywheel energy storage system (fess) for voltage and frequency support in low voltage distribution networks", in *2018 IEEE 3rd International Conference on Intelligent Energy and Power Systems (IEPS)*, 2018, pp. 176–182. DOI: 10.1109/IEPS.2018.8559521.

[5] "2020-2050 Integraded Infrastructure Outlook", TenneT, Tech. Rep. II3050, Oct. 2023. [Online]. Available: https://tennet-drupal.s3.eu-central-1.amazonaws.com/default/2023-10/II3050_Eindrapport.pdf.

[6] "Export limitation", SolarEdge, Application Note Version 2.8, Mar. 2022. [Online]. Available: https://knowledge-center.solaredge.com/sites/kc/files/feed-in_limitation_application_note.pdf.

[7] B. Wolterman, T. Duurkoop, A. Haarhuis, M. Zweistra, E. Hiep, and M. van Biezen, "Laden van elektrische auto's in Nederland: Ervaringen en meningen van EV-rijders", Rijksdienst voor Ondernemend Nederland, Tech. Rep., 2023. [Online]. Available: https://elaad.nl/wp-content/uploads/downloads/Nationaal-Laadonderzoek-2023-Rapport.pdf.

[8] N. Damianakis, G. C. R. Mouli, and P. Bauer, "Risk-averse estimation of electric heat pump power consumption", in *2023 IEEE 17th International Conference on Compatibility, Power Electronics and Power Engineering (CPE-POWERENG)*, 2023, pp. 1–6. DOI: 10.1109/CPE-POWERENG58103.2023.10227424.

[9] "Global EV Outlook 2023: Trends in electric light-duty vehicles", IEA, Tech. Rep., 2023. [Online]. Available: https://www.iea.org/reports/global-ev-outlook-2023/trends-in-electric-light-duty-vehicles.

[10] P. Fakhrooeian, V. Pitz, and B. Scheppat, "Systematic evaluation of possible maximum loads caused by electric vehicle charging and heat pumps and their effects on common structures of german low-voltage grids", *World Electric Vehicle Journal*, vol. 15, no. 2, 2024, ISSN: 2032-6653. DOI: 10.3390/wevj15020049. [Online]. Available: https://www.mdpi.com/2032-6653/15/2/49.

[11] "Charging at home", Department of Energy, Tech. Rep., 2020. [Online]. Available: https://www.energy.gov/eere/electricvehicles/charging-home.

[12] J. Alpízar-Castillo, L. Ramírez-Elizondo, and P. Bauer, "The effect of non-coordinated heating electrification alternatives on a low-voltage distribution network with high pv penetration", in *2023 IEEE 27th International Conference on Compatibility, Power Electronics, and Power Engineering (CPE-POWERENG)*, Jun. 2023.

[13] D. Bogdanov, M. Ram, A. Aghahosseini, *et al.*, "Low-cost renewable electricity as the key driver of the global energy transition towards sustainability", *Energy*, vol. 227, p. 120 467, 2021, ISSN: 0360-5442. DOI: https://doi.org/10.1016/j.energy.2021.120467.

[14] P. D'Aprile, H. Engel, G. van Gendt, *et al.*, "Net-zero europe decarbonization pathways and socioeconomic implications", McKinsey Company, Tech. Rep., 2020. [Online]. Available: https://www.mckinsey.com/~/media/mckinsey/business%20functions/sustainability/our%20insights/how%20the%20european%20union%20could%20achieve%20net%20zero%20emissions%20at%20net%20zero%20cost/net-zero-europe-vf.pdf.

[15] "Integraleinfrastructuurverkenning2030-2050", Netbeheer Nederland, Tech. Rep., Oct. 2023. [Online]. Available: https://tennet-drupal.s3.eu-central-1.amazonaws.com/default/2023-10/II3050_Eindrapport.pdf.

[16] E. Hache and A. Palle, "Renewable energy source integration into power networks, research trends and policy implications: A bibliometric and research actors survey analysis", *Energy Policy*, vol. 124, pp. 23–35, 2019. DOI: 10.1016/j.enpol.2018.09.036.

[17] W. Bai, L. Zhang, S. Lu, J. Ren, and Z. Zhou, "Sustainable energy transition in southeast asia: Energy status analysis, comprehensive evaluation and influential factor identification", *Energy*, vol. 284, p. 128 670, 2023, ISSN: 0360-5442. DOI: https://doi.org/10.1016/j.energy.2023.128670.

[18] M. Tsagkari, J. Roca, and G. Kallis, ""from local island energy to degrowth? exploring democracy, self-sufficiency, and renewable energy production in greece and spain"", *Energy Research Social Science*, vol. 81, p. 102 288, 2021, ISSN: 2214-6296. DOI: https://doi.org/10.1016/j.erss.2021.102288.

[19] Y. Zhou and P. D. Lund, "Peer-to-peer energy sharing and trading of renewable energy in smart communities trading pricing models, decision-making and agent-based collaboration", *Renewable Energy*, vol. 207, pp. 177–193, 2023. DOI: 10.1016/j.renene.2023.02.125.

[20] "Directive 2009/72/ec of the european parliament and of the council of 13 july 2009 concerning common rules for the internal market in electricity and repealing directive 2003/54/ec", EUROPEAN PARLIAMENT, Tech. Rep., Jul. 2009. [Online]. Available: https://eur-lex.europa.eu/LexUriServ/LexUriServ.do?uri=OJ:L:2009:211:0055:0093:en:PDF.

[21] "Dutch ancillary services", TenneT, Tech. Rep. [Online]. Available: https://www.tennet.eu/markets/dutch-ancillary-services.

[22] G. C. Kryonidis, E. O. Kontis, T. A. Papadopoulos, *et al.*, "Ancillary services in active distribution networks: A review of technological trends from operational and online analysis perspective", *Renewable and Sustainable Energy Reviews*, vol. 147, Sep. 2021, ISSN: 18790690. DOI: 10.1016/j.rser.2021.111198.

[23] R. Fonteijn, P. H. Nguyen, J. Morren, and J. G. Slootweg, "Demonstrating a generic four-step approach for applying flexibility for congestion management in daily operation", *Sustainable Energy, Grids and Networks*, vol. 23, Sep. 2020, ISSN: 23524677. DOI: 10.1016/j.segan.2020.100378.

[24] M. Babagheibi, S. Jadid, and A. Kazemi, "An incentive-based robust flexibility market for congestion management of an active distribution system to use the free capacity of microgrids", *Applied Energy*, vol. 336, p. 120 832, 2023, ISSN: 0306-2619. DOI: https://doi.org/10.1016/j.apenergy.2023.120832.

[25] A. Hosseini, A. Mirzapour-Kamanaj, R. Kazemzadeh, K. Zare, and B. Mohammadi-Ivatloo, "Congestion management for coordinated electricity and gas grids in the presence of multi-energy hubs: A risk-based optimal scheduling", *Sustainable Energy, Grids and Networks*, vol. 36, p. 101 153, 2023, ISSN: 2352-4677. DOI: https://doi.org/10.1016/j.segan.2023.101153.

[26] F. H. Aghdam, M. W. Mudiyanselage, B. Mohammadi-Ivatloo, and M. Marzband, "Optimal scheduling of multi-energy type virtual energy storage system in reconfigurable distribution networks for congestion management", *Applied Energy*, vol. 333, p. 120 569, 2023, ISSN: 0306-2619. DOI: https://doi.org/10.1016/j.apenergy.2022.120569.

[27] F. Noori, M. Korani, V. Farrokhikia, and F. Faghihi, "Evaluating the impact of integrating cryogenic energy storage and electric vehicles on congestion management in reconfigurable distribution networks considering conditional value-at-risk index", *Energy Reports*, vol. 11, pp. 1979–1992, 2024, ISSN: 2352-4847. DOI: https://doi.org/10.1016/j.egyr.2024.01.035.

[28] *IEEE Standard 1547-2018 - For Interconnection and Interoperability of Distributed Energy Resources with Associated Electric Power Systems Interfaces*. IEEE, 2018, ISBN: 9781504446396.

[29] J. Alpízar-Castillo, L. Ramirez-Elizondo, and P. Bauer, "Assessing the role of energy storage in multiple energy carriers toward providing ancillary services: A review", *Energies*, vol. 16, no. 1, 2023, ISSN: 1996-1073. DOI: 10.3390/en16010379. [Online]. Available: https://www.mdpi.com/1996-1073/16/1/379.

[30] B. Canizes, V. Silveira, and Z. Vale, "Demand response and dispatchable generation as ancillary services to support the low voltage distribution network operation", *Energy Reports*, vol. 8, pp. 7–15, 2022, The 8th International Conference on Energy and Environment Research –"Developing the World in 2021 with Clean and Safe Energy", ISSN: 2352-4847. DOI: https://doi.org/10.1016/j.egyr.2022.01.040.

[31] C. Jankowiak, A. Zacharopoulos, C. Brandoni, P. Keatley, P. MacArtain, and N. Hewitt, "Assessing the benefits of decentralised residential batteries for load peak shaving", *Journal of Energy Storage*, vol. 32, Dec. 2020, ISSN: 2352152X. DOI: 10.1016/j.est.2020.101779.

[32] V. K. Teki, M. K. Maharana, and C. K. Panigrahi, "Study on home energy management system with battery storage for peak load shaving", *Materials Today: Proceedings*, vol. 39, pp. 1945–1949, 2021, 3rd International Conference on Solar Energy Photovoltaics, ISSN: 2214-7853. DOI: https://doi.org/10.1016/j.matpr.2020.08.377.

[33] Y. Zhou, H. Obeid, S. Laghrouche, M. Hilairet, and A. Djerdir, "A novel second-order sliding mode control of hybrid fuel cell/super capacitors power system considering the degradation of the fuel cell", *Energy Conversion and Management*, vol. 229, Feb. 2021, ISSN: 01968904. DOI: 10.1016/j.enconman.2020.113766.

[34] L. Chen, Q. Xu, Y. Yang, and J. Song, "Optimal energy management of smart building for peak shaving considering multi-energy flexibility measures", *Energy and Buildings*, vol. 241, p. 110 932, 2021, ISSN: 0378-7788. DOI: https://doi.org/10.1016/j.enbuild.2021.110932.

[35] "Pcs integration in enphase energy system", Enphase, TECHNICAL BRIEF – North America TEB-00049-2.0, Sep. 2023. [Online]. Available: https://enphase.com/download/pcs-integration-enphase-energy-system-tech-brief.

[36] "Growatt export limitation guide", Growatt, 2020. [Online]. Available: https://growatt.pl/wp-content/uploads/2020/01/Growatt-Export-Limitation-Guide.pdf.

[37] "Sma export control solution", SMA Solar Technology, Manufacturer's Declaration HK_ENA_EREC_G100_en_11, Apr. 2018. [Online]. Available: https://s3.amazonaws.com/ecodirect_docs/SMA/EDMM-US-10/SMA-EDMM-US-10-Export-Control-Solution-HK_ENA_EREC_G100_en_11.pdf.

[38] "Solaredge inverters, power control options", SolarEdge, Application Note Version 9, Mar. 2023. [Online]. Available: https://knowledge-center.solaredge.com/sites/kc/files/application_note_power_control_configuration.pdf.

[39] "Ess design and installation manual", Victron, Rev. 10, Sep. 2023. [Online]. Available: https://www.victronenergy.com/media/pg/Energy_Storage_System/en/configuration.html#UUID-42f56b22-76b3-0c69-57c2-3e54b2e0df4e.

[40] J. Layedra, M. Martínez, and P. Mercado, "Levelized cost of storage for lithium batteries, considering degradation and residual value", in *2021 IEEE URUCON*, 2021, pp. 127–131. DOI: 10.1109/URUCON53396.2021.9647345.

[41] T. Liu, Z. Yang, and Y. Duan, "Short- and long-duration cooperative energy storage system: Optimizing sizing and comparing rule-based strategies", *Energy*, vol. 281, p. 128 273, 2023, ISSN: 0360-5442. DOI: https://doi.org/10.1016/j.energy.2023.128273. [Online]. Available: https://www.sciencedirect.com/science/article/pii/S0360544223016675.

[42] H. Tang and S. Wang, "Life-cycle economic analysis of thermal energy storage, new and second-life batteries in buildings for providing multiple flexibility services in electricity markets", *Energy*, vol. 264, p. 126 270, 2023, ISSN: 0360-5442. DOI: https://doi.org/10.1016/j.energy.2022.126270.

[43] S. J. An, J. Li, C. Daniel, D. Mohanty, S. Nagpure, and D. L. Wood, "The state of understanding of the lithium-ion-battery graphite solid electrolyte interphase (SEI) and its relationship to formation cycling", *Carbon*, vol. 105, pp. 52–76, Aug. 2016, ISSN: 0008-6223. DOI: 10.1016/j.carbon.2016.04.008. (visited on 08/15/2023).

[44] J. Olmos, I. Gandiaga, A. Saez-de-Ibarra, X. Larrea, T. Nieva, and I. Aizpuru, "Modelling the cycling degradation of Li-ion batteries: Chemistry influenced stress factors", *Journal of Energy Storage*, vol. 40, p. 102 765, Aug. 2021, ISSN: 2352-152X. DOI: 10.1016/j.est.2021.102765. (visited on 09/11/2023).

[45] J. Schmalstieg, S. Käbitz, M. Ecker, and D. U. Sauer, "A holistic aging model for Li(NiMnCo)O2 based 18650 lithium-ion batteries", *Journal of Power Sources*, vol. 257, pp. 325–334, Jul. 2014, ISSN: 0378-7753. DOI: 10.1016/j.jpowsour.2014.02.012. (visited on 08/31/2023).

[46] W. Ai, B. Wu, and E. Martínez-Pañeda, "A coupled phase field formulation for modelling fatigue cracking in lithium-ion battery electrode particles", *Journal of Power Sources*, vol. 544, p. 231 805, Oct. 2022, ISSN: 0378-7753. DOI: 10.1016/j.jpowsour.2022.231805. (visited on 08/24/2023).

[47] X. Lin, K. Khosravinia, X. Hu, J. Li, and W. Lu, "Lithium Plating Mechanism, Detection, and Mitigation in Lithium-Ion Batteries", *Progress in Energy and Combustion Science*, vol. 87, p. 100 953, Nov. 2021, ISSN: 0360-1285. DOI: 10.1016/j.pecs.2021.100953. (visited on 08/28/2023).

[48] F. B. Planella, W. Ai, A. M. Boyce, *et al.*, "A continuum of physics-based lithium-ion battery models reviewed", *Progress in Energy*, vol. 4, no. 4, p. 042 003, Jul. 2022, ISSN: 2516-1083. DOI: 10.1088/2516-1083/ac7d31. (visited on 10/17/2023).

[49] F. von Bülow and T. Meisen, "A review on methods for state of health forecasting of lithium-ion batteries applicable in real-world operational conditions", *Journal of Energy Storage*, vol. 57, p. 105 978, Jan. 2023, ISSN: 2352-152X. DOI: 10.1016/j.est.2022.105978. (visited on 10/18/2023).

[50] W. Vermeer, G. R. Chandra Mouli, and P. Bauer, "A Comprehensive Review on the Characteristics and Modeling of Lithium-Ion Battery Aging", *IEEE Transactions on Transportation Electrification*, vol. 8, no. 2, pp. 2205–2232, Jun. 2022, ISSN: 2332-7782, 2372-2088. DOI: 10.1109/TTE.2021.3138357. (visited on 03/12/2024).

[51] J. Wang, P. Liu, J. Hicks-Garner, *et al.*, "Cycle-life model for graphite-LiFePO4 cells", *Journal of Power Sources*, vol. 196, no. 8, pp. 3942–3948, Apr. 2011, ISSN: 0378-7753. DOI: 10.1016/j.jpowsour.2010.11.134. (visited on 09/21/2023).

[52] J. Olmos, I. Gandiaga, A. Saez-de-Ibarra, X. Larrea, T. Nieva, and I. Aizpuru, "Modelling the cycling degradation of li-ion batteries: Chemistry influenced stress factors", *Journal of Energy Storage*, vol. 40, p. 102 765, 2021, ISSN: 2352-152X. DOI: https://doi.org/10.1016/j.est.2021.102765. [Online]. Available: https://www.sciencedirect.com/science/article/pii/S2352152X21004904.

[53] J. Wang, J. Purewal, P. Liu, *et al.*, "Degradation of lithium ion batteries employing graphite negatives and nickel–cobalt–manganese oxide + spinel manganese oxide positives: Part 1, aging mechanisms and life estimation", *Journal of Power Sources*, vol. 269, pp. 937–948, Dec. 2014, Empirical aging modelused by Wiljan, ISSN: 03787753. DOI: 10.1016/j.jpowsour.2014.07.030. [Online]. Available: https://linkinghub.elsevier.com/retrieve/pii/S037877531401074X.

[54] W. Vermeer, G. R. Chandra Mouli, and P. Bauer, "A comprehensive review on the characteristics and modeling of lithium-ion battery aging", *IEEE Transactions on Transportation Electrification*, vol. 8, no. 2, pp. 2205–2232, 2022. DOI: 10.1109/TTE.2021.3138357.

[55] J. Gow and C. Manning, "Development of a model for photovoltaic arrays suitable for use in simulation studies of solar energy conversion systems", in *1996 Sixth International Conference on Power Electronics and Variable Speed Drives (Conf. Publ. No. 429)*, 1996, pp. 69–74. DOI: 10.1049/cp:19960890.

[56] V. Paduani and N. Lu, "Implementation of a two-stage pv system testbed with power reserves for grid-support applications", in *2021 North American Power Symposium (NAPS)*, 2021, pp. 1–6. DOI: 10.1109/NAPS52732.2021.9654654.

[57] S. Nyamathulla, D. Chittathuru, and S. M. Muyeen, "An overview of multilevel inverters lifetime assessment for grid-connected solar photovoltaic applications", *Electronics*, vol. 12, no. 8, 2023, ISSN: 2079-9292. DOI: 10.3390/electronics12081944.

[58] A. Azizi, S. Peyghami, S. F. Zarei, and F. Blaabjerg, "The impact of sun tracking on the reliability of solar inverters", in *2022 International Power Electronics Conference (IPEC-Himeji 2022- ECCE Asia)*, 2022, pp. 1553–1559. DOI: 10.23919/IPEC-Himeji2022-ECCE53331.2022.9807153.

[59] S. S. Kshatri, D. S. N. M. Rao, P. C. Babu, D. G. Kumar, and N. V. Sireesha, "Reliability evaluation of pv inverter considering impact of reactive power injection", in *2022 IEEE 2nd International Conference on Sustainable Energy and Future Electric Transportation (SeFeT)*, 2022, pp. 1–5. DOI: 10.1109/SeFeT55524.2022.9909259.

[60] A. Anurag, Y. Yang, and F. Blaabjerg, "Impact of reactive power injection outside feed-in hours on the reliability of photovoltaic inverters", in *2015 IEEE 6th International Symposium on Power Electronics for Distributed Generation Systems (PEDG)*, 2015, pp. 1–8. DOI: 10.1109/PEDG.2015.7223032.

[61] M. Ahmadi, F. Kardan, A. Shekhar, and P. Bauer, "Reliability assessment of modular multilevel converters: A comparative study of mil and mission profile methods", in *International Conference on Integrated Power Electronics Systems CIPS 2024*, 2024.

[62] R. Bayerer, T. Herrmann, T. Licht, J. Lutz, and M. Feller, "Model for power cycling lifetime of igbt modules - various factors influencing lifetime", in *5th International Conference on Integrated Power Electronics Systems*, 2008, pp. 1–6.

[63] F. Kardan, A. Shekhar, and P. Bauer, "Quantitative comparison of the empirical lifetime models for power electronic devices in ev fast charging application", in *2023 11th International Conference on Power Electronics and ECCE Asia (ICPE 2023 - ECCE Asia)*, 2023, pp. 3239–3244. DOI: 10.23919/ICPE2023-ECCEAsia54778.2023.10213916.

[64] S. S. Kshatri, J. Dhillon, and S. Mishra, "Impact of solar irradiance and ambient temperature on pv inverter reliability considering geographical locations", *International Journal of Heat and Technology*, vol. 39, no. 1, pp. 292–298, 2021. DOI: 10.18280/ijht.390132.

[65] F. Penizzotto, R. Pringles, and F. Olsina, "Real options valuation of photovoltaic power investments in existing buildings", *Renewable and Sustainable Energy Reviews*, vol. 114, p. 109 308, 2019, ISSN: 1364-0321. DOI: https://doi.org/10.1016/j.rser.2019.109308.

[66] A. Teladia, E. van der Waal, J. Brouwer, and H. van der Windt, "From kilowatts to cents: Financial inclusion of citizens through dutch community energy business model configurations", *Energy Research Social Science*, vol. 106, p. 103 322, 2023, ISSN: 2214-6296. DOI: https://doi.org/10.1016/j.erss.2023.103322.

[67] J. Alpízar-Castillo, V. Vega-Garita, N. Narayan, and L. Ramirez-Elizondo, "Open-access model of a pv-bess system: Quantifying power and energy exchange for peak-shaving and self consumption applications", *Energies*, vol. 16, no. 14, 2023, ISSN: 1996-1073. DOI: 10.3390/en16145480. [Online]. Available: https://www.mdpi.com/1996-1073/16/14/5480.

[68] Bucher, Christof, Wandel, Jasmin, and Joss, David, "Life expectancy of pv inverters and optimizers in residential pv systems", in *WCPEC-8: EU PVSEC Proceedings*, 2022. DOI: 10.24451/arbor.18138.

6

AGGREGATED ENERGY MANAGEMENT SYSTEMS: OPTIMIZATION IN LOW-VOLTAGE RESIDENTIAL DISTRIBUTION NETWORKS

"There is nothing wrong with letting the people who love you help you"

Uncle Iroh, Avatar: The Last Airbender, Season 2, Episode 8, by Michael Dante DiMartino and Bryan Konietzko.

This Chapter is based on:

- **J. Alpízar-Castillo**, L. Ramírez-Elizondo and P. Bauer, "The Effect of Non-Coordinated Heating Electrification Alternatives on a Low-Voltage Distribution Network with High PV Penetration," 2023 IEEE 27th International Conference on Compatibility, Power Electronics, and Power Engineering (CPE-POWERENG), Tallinn, Estonia, 2023, pp. 1-6, doi: 10.1109/CPE-POWERENG58103.2023.10227394.
- M. Kitso, B. I. Priambodo, **J. Alpízar-Castillo**, L. Ramirez-Elizondo, and P. Bauer, "Coordination of Multiple BESS in a Low-Voltage Distribution Network Using a Leader-based and a Leaderless Control," *Submitted*.
- **J. Alpízar-Castillo**, L. Ramírez-Elizondo, A. van Voorden and P. Bauer, "Aggregation residential multi-carrier energy storage as voltage control provider in low-voltage distribution networks," *Submitted*.

6.1. INTRODUCTION

Policymakers have encouraged the inclusion of distributed renewable energy sources (DRES) at the household level as part of the energy transition toward decarbonization. The effects of DRES on the distribution networks have been investigated and documented, including stability issues, grid congestion, and power plants underused due to power curtailment [1]. For example, in New England [2], the circuits operate near their limits. Germany [3] and China [4] have been obliged to curtail renewable generation plants to address the congestion on the grid. Therefore, distribution system operators actively work to find alternatives to ensure stability on the network.

More recently, strategies to electrify transportation and heat have also been proposed. However, the technologies required to deploy such strategies also affect the grid, adding highly stochastic power demands to an already weather-dependent network, as mentioned in Chapter 2. To mention some, [5] and [6] demonstrated that including electric vehicle (EV) chargers in the low voltage (LV) grid, without an aggregated energy management strategy, can cause severe voltage drops, failing to comply the technical standard EN50160. On the other hand, the effect of heating electrification in the LV networks has not been deeply studied. Instead, most research focuses on providing ancillary services with heat pumps (HP), such as demand response and direct load control. For example, [7] concluded that demand response algorithms could avoid voltage drops caused by the high power loads caused by combining HP and EV. Similarly, [8] found that the impact of heat pumps on a low-voltage network is related to their distribution, causing voltage imbalances beyond the allowed limit.

Including energy storage systems on the grid could reduce the adverse effects mentioned above [9], [10]. The techno-economic study done by [11] demonstrated that installing BESS in the LV network can ensure voltage limits above 0.9 pu while representing only 77 % of the costs of upgrading the lines in the network to satisfy the voltage limit. The effect of coordinating strategically located BESS was studied by [12], demonstrating that the power and energy share between the BESS can address voltage issues in real-time while minimizing the size of the batteries and inverters. However, including BESS at the household level does not necessarily imply reducing the adverse effects on the grid as well [13]. Energy management systems (EMS) are configured to reduce the cost for the equipment owner since there are no direct benefits for providing ancillary services at this scale in many energy markets yet. Additionally, the EMS does not share data with neighbouring EMS; thus, multiple EMS in the same distribution network work in a non-coordinated fashion.

In addition, there is plenty of literature available about models used to maximize profit when participating in the energy market. As detailed in Chapter 2, this profit is either from energy arbitrage, or providing ancillary services (although some authors classify energy arbitrage as an ancillary service, as prices are set to incentivize certain consumption patterns to indirectly support the grid, they are classified separately in this work [14]). Participating in the existing ancillary services markets requires the prosumer to follow a set of rules, as detailed in [15], and is limited to medium and high voltage networks, with large-scale assets. However, there are no major market constraints to profit based on energy arbitrage, once the interconnection limit is defined, and it can be done at any voltage level. Particularly at residential low-voltage networks, most DSOs cannot

enforce power limitations on prosumers, either passively by setting a cap below the contracted power, or actively by sending signals in real-time for prosumers to adjust their power. For this reason, algorithms used to profit using residential assets (e.g., EVs or HPs) focus on this mechanism, considering day-ahead pricing [16].

A model predictive control strategy was used by [17] to control a residential PV-BESS (battery energy storage system) system, reducing energy costs up to 30 % compared to a mean nonlinear model predictive control. The same system architecture was approached using the long short-term memory algorithm by [18] to predict generation and consumption patterns, achieving good accuracy. More complex system architectures, forming multi-carrier systems, have also been studied. For example, in [16], a system including PV, solar collectors, BESS, EV, thermal energy storage (TESS) and heat pumps was optimized to minimize the cost of energy purchase and the ageing of the BESS, achieving a reduction of 20 % to 45 % when compared to state-of-the-art solutions, but highlighting the high computational cost. Similarly, the work in [19] used max-min game theory to control the power flow of a system comprised of a PV, a BESS, 30 EV chargers and a hydrogen fuel cell-electrolyzer installed in a five-floor office building to minimize the degradation of the BESS and the hydrogen system. The results surpassed EMSs using mixed-integer linear programming and heuristic methods in reducing the degradation between 12.64 % and 75.61 % for the BESS and 23.16 % and 82.81 % for the fuel cell, respectively.

The previous mechanisms can be done without causing major problems in the distribution grid if the number of participants is low enough. Nonetheless, in higher penetration levels (i.e., higher number of prosumers in the grid), they pose a risk to the network [20], [21]; thus, aggregation control is required [22]. Aggregation can be either set to support the local network where the assets are connected or the upstream network through the substation. For instance, [23] proved that aggregating assets in lower voltage networks can create load profiles at the substation, so that the aggregator can participate in the ancillary services market on behalf of all the individual members using the IEEE 33-node test network. This is particularly attractive for medium- and high-voltage operators, as the power and voltage problems at the substation can be addressed. Still, keeping the limits at the substation does not guarantee that power or voltage limitations in the conductors and nodes downstream are fulfilled.

To address this challenge, the literature offers some strategies used to coordinate the prosumers. Nonetheless, most studies have focused on proposing technical solutions, neglecting the existing regulatory framework. Mixed integer linear programming and heuristic methods are compared by [24] in the IEEE 13-node and 123-node networks to control BESS to minimize the effect of DRES in distribution networks. Using the mixed integer linear programming reduced the degradation of the BESS by 34 %. A two-stage distributionally robust optimization model is used by [25] to minimize the cost of energy storage investment and distribution network operation under extreme conditions for a PV-BESS system. The method was tested using the IEEE 33-node network and PV and loads from a distribution network in China, resulting in better PV accommodation capacity and resilience of the distribution network while minimizing costs, when compared to stochastic optimization and robust optimisation approaches. In [26], the same test network was used, used to minimize voltage variations when combining PV

and BESS, improving the maximum node offset by 4.4 %. The method proposed by [27] identifies and evaluates flexibility perimeters in radial distribution networks. Two case studies using the IEEE 123-node network with different voltage load areas demonstrating that increasing the number of areas decreases the flexibility volume required for voltage control.

A weighted multi-objective optimization to minimize power loss and voltage deviations in the lines, energy cost and PV energy curtailed was done in [28]. Their results suggest that adjusting the optimization weights can maintain the voltage within limits in a 15-node medium voltage distribution network in Yangzhou, China, with controlled PV, BESS and EVs. Likewise, [29] used a convex approximation of the exact nonlinear programming model to minimize the energy costs and power losses in the lines for a representative urban case using the IEEE 33-node network, and a rural case using a 27-node network. The results showed an improvement of around 1.5 % compared to continuous genetic algorithm, particle swarm optimization and parallel vortex search algorithm, but computation time was reduced up to one order of magnitude. As a response to the complexity of building the network model, a model-free controller was proposed in [30] to keep voltage variations in the 1 ± 0.05 pu range using PV and synchronous generator assets. The test in a medium voltage 21-node distribution network demonstrated correction times in the order of seconds.

Given the above, understanding how the EMS affects the energy exchange between the electric network and prosumers with multi-carrier energy systems is relevant for distribution system operators (DSOs). This way, it would be possible to quantify the effect of the deployments of electrical alternatives for heat and mobility at the residential level to prevent worsening the congestion in the grid; therefore, this Chapter:

1. proposes two control strategies for aggregated BESS that reaches consensus when voltage is regulated within the limits; thus, the algorithm is terminated as soon as voltage is regulated and not when all batteries agree on the same amount of power contribution to the system, and
2. asses the flexibility potential of a multi-carrier system, comprised of a PV, HP, BESS and TESS systems, in residential buildings, compared to a centralized PV-BESS system, for a low-voltage distribution network in the Netherlands,
3. analyzes the trade-off between economic cost and flexibility of a residential multi-carrier energy system for three different aggregation schemes, considering separated control for the prosumer and aggregator, and
4. compares the benefits for voltage support of residential aggregated single- and multi-carrier energy systems with a centralized battery storage system coupled with a PV.

6.2. SINGLE-CARRIER AGGREGATION

The mismatch between local generation and consumption leads to overvoltage when the supply is greater than the demand [31], [32]. This issue was studied in [33], demonstrating that uncontrolled distributed renewable energy sources (DRES) throughout low-voltage distribution networks compromise the voltage stability, especially further from

the connection with the substation. In those nodes, the power injection from the DRES into the grid increases the voltage, ultimately leading to reverse current flows. Chapter 2 demonstrated that battery energy storage systems (BESSs) are accepted by the literature as a solution to reduce the power injected into the grid, thus compensating for the power imbalance. Although the geographical proximity of the nodes would produce similar DRES generation profiles, the number of nodes in a residential network and the different load behaviours of users would require coordinated control for the BESSs to minimize the DRES affection on the grid.

The usage of energy storage to compensate for the effects of the energy transition has been widely studied in the literature from different perspectives. On the one hand, many researchers have focused on the optimal sizing and location of assets. For instance, [34] used H_2-norm and Kron reduction to simplify a modified version of the IEEE 39-bus system into 13-bus for optimal size and allocation of BESS for transient frequency support through virtual inertia using Matlab/Simulink, resulting in a 77.1 % reduction in the pressure on the generators. However, the inclusion of DRES includes disturbances and uncertainties which represent a challenge for the method. An optimal planning method was proposed by [35] to consider economic and reliability objectives, tested in the IEEE 34-node network. The results showed an enhanced capacity of absorb distributed PV generation; however, it was mentioned the existing market conditions create a challenge for enterprise investments in such kind of projects. Similarly, [36] examined the potential of BESS to mitigate transmission network congestion to increase the deployment of DRES projects in South Wales using the flow decomposition technique to determine the optimal sizes and locations. Using DIgSILENT PowerFactory 2024 to model the transmission network for 2024 and 2030, the results suggest that cost of deploying BESS sized and located using the method proposed is 38% to 63% of the cost of line reinforcement. Nevertheless, the cost-benefit analysis uses a simplified model focused on representative peak days, thus, a more complex market analysis is required.

Similar conclusions were obtained by [37] and [38]. The former studied the optimal placement of shared BSSS in urban energy communities considering economic, technical and environmental performances, resulting in an increase of self-sufficiency rates by up to 17.44% and reducing peak loads by up to 37.19% using a real case scenario of 191 buildings in Seoul, South Korea, but it lacked economic viability and negative net present values. The latter investigated the usage of small-scale BESS in energy intensive cities to maximize electricity self-sufficiency rate, while minimizing the grid import from the network and maximizing the net present value, achieving good results for the first two objectives, but failing to create an attractive business case. Despite the optimistic results of the previous works in technical terms, the actual implementation of this strategies face a number of roadblocks aside from the load and DRES generation uncertainty, including the need for a framework to allow DSOs own storage assets, attractive markets for aggregators investment and participation, and connection and physical space availability in the selected nodes.

On the other hand, other works focus on the optimal usage of available BESS units distributed throughout the network as response of the challenges optimal sizing and allocation face. A centralized control for multiple BESSs was implemented in [39], which required information on the voltage unbalance and state-of-charge (SOC) of the batter-

ies at every node. The control was tested in a radial distribution feeder with different starting SOC and phase conditions. Despite showing some success, the method showed some unfeasible solutions and slow response. Furthermore, its implementation requires a robust communication channel to control and monitor each storage device, making more complex network expansion projects. Although some works as [40] have shown good results in off-grid conditions, other works as [12] and [41] had similar challenges as [39] in grid-tied mode, confirming the unsuitability of centralized controllers for DRES-rich distribution networks.

In [42], a droop-based active power curtailment technique is implemented to prevent overvoltage in radial LV feeders. Real-time controllers were used for zonal control in [43], using multi-agents to communicate between zones. Fuzzy logic controllers are proposed in [44] to control the voltage at every bus. The work in [45] evaluated an adaptive control strategy for a PV-rich network, simulated in a real Australian medium-voltage feeder using smart meter data from the low-voltage network. A model predictive control approach using adaptive virtual impedance is detailed in [46]. However, recent literature has focused on using decentralized control to electric vehicles (EVs) charging stations [47]–[49]. In this context, decentralized control provides a robust approach to ensure the EV charge while minimizing the impact on the grid under high uncertainty conditions and without requiring complex communication infrastructure.

Distributed control is considered more efficient when it comes to the coordination of multiple static storage units. In distributed control, each storage unit of the system is considered an agent, and these agents communicate together. In [50], a method is implemented for secondary frequency response in a real distribution network. The work in [51] used distributed control to provide frequency regulation in low-inertial power systems with high penetration of DRES. In [52], a non-linear state of charge balancing strategy is proposed for voltage regulation. The consensus algorithm is used in [53] as part of a hierarchical framework to manage DRES for frequency control and in [54] to control the frequency and voltage at the point of common coupling of multiple BESSs. Similarly, [55] proposed an algorithm to balance the SOC using distributed estimators for the average desired power and units' SOC. In [56], distributed control was used to synchronize flexibility providers within a network using BESSs. One common point found in most of the literature was that the control algorithms aimed to agree on the power value the batteries supply; thus, all batteries should contribute the same. This way, voltage regulation was achieved; however, batteries are not operating efficiently as they absorb or produce more power than needed [51], [52].

Based on the literature review, it was found that many works focus on optimal sizing and placing of energy storage systems instead of using available resources; however, most DSOs cannot own energy strage assets due to regulation limitations. Also, most of the business models proposed suggest a single owner of all storage assets in the network, instead of considering storage assets owned by individual prosumers who could collaborate with the DSO. Likewise, most of the aggregation strategies found focus on medium and high voltage networks, nevertheless, low-voltage networks are particularly critical for the energy transition, as they do not have ancillary services providers to support the DSO, and the demand increase caused by the heating electrification and electric mobility can potentially cause major voltage challenges. Finally, the existing aggregation

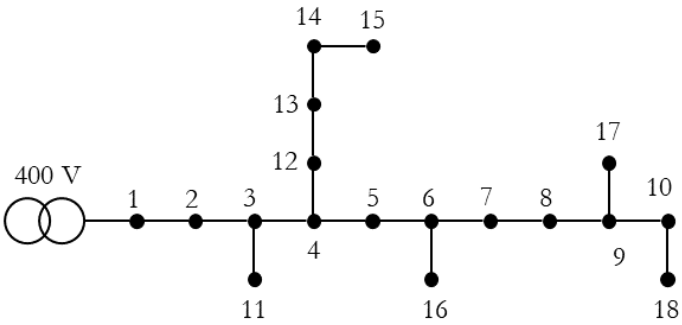

Figure 6.1: 18-node CIGRE LV test distribution network.

strategies require full observability of all the assets, which in real implementations would require complex communication infrastructure.

This section proposes two distributed control strategies using the consensus algorithm for BESS in a low-voltage distribution network to provide voltage regulation services without requiring all the storage units in the system to collaborate equally. The first strategy, detailed in Section 6.2.2 uses a leader-follower approach for the agents' power dispatch. The second, presented in Section 6.2.4, is a leaderless strategy where the agents are only required to communicate with their immediate neighbours. The methods were tested in overvoltage and undervoltage conditions, different initial SOC conditions, and when not all the agents were available to participate.

The CIGRE LV Test Distribution Network was used as a test environment for the algorithms. It consists of eighteen buses as shown in Figure 6.1, where six PV units and six BESS are integrated. The location of BESS was chosen to be near the PV unit and loads and is presented in Table 6.1. The communication graph of the network is shown in Figure 6.2.

Table 6.1: Sizes considered for the PV and BESS per node.

Node	P_{PV} [kW]	P_{BESS} [kW]	E_{BESS} [kWh]
1	11	5.5	38
11	9	4	30
15	12	6	40
16	11	5.5	38
17	9.5	4.5	32
18	12	6	40

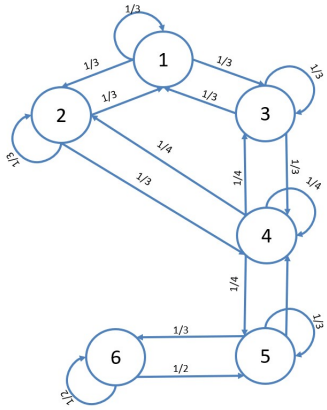

Figure 6.2: Communication graph of the BESS placed in the 18-node CIGRE LV network, following (6.2).

6.2.1. CONSENSUS ALGORITHM

In this Section, the BESSs coordination in a distributed manner can be analyzed as a multi-agent system (MAS). From a MAS perspective, BESSs are agents which can exchange information with their neighbours. This information exchange can be done either in a unidirectional or bidirectional way. Furthermore, the links in which the agents communicate can be represented in a graph. A graph comprises a set of vertices that represent the agents and a set of edges that represent the communication links in a MAS. A graph can be written in the form of $G = (V, E)$, where V indicates a set of vertices and E denotes a set of edges [57]. Furthermore, [57] describes that for a multi-agent system consisting of n agents, the corresponding graph will be in the form of $G = (V, E)$, where $V = 1, 2, 3, ..., n$ and $E \subseteq V \times V$. An edge represented as (i, j) $\in E$ means that agent j has a relationship with agent i (i.e., both agents have access to each other's information [57]). Besides, it also means that agent i is a neighbour of agent j.

To describe the number of neighbours that each agent has in a graph, a degree matrix $D(G)$ is used. A degree matrix is represented as a diagonal matrix with a size of $V \times V$ where V is the number of vertices in a graph (the agents). The degree matrix of a graph follows a general form below:

$$D(G) = \begin{bmatrix} d_{11} & 0 & \cdots & 0 \\ 0 & d_{22} & 0 & \vdots \\ \vdots & 0 & \ddots & 0 \\ 0 & \cdots & 0 & d_{ij} \end{bmatrix} \tag{6.1}$$

The values assigned to elements d_{ij}, where j=i, are the number of neighbours that agent i has. Besides the degree matrix, another important component in a graph is its adjacency matrix. The adjacency matrix of a graph, denoted in $A(G) = [a_{ij}]$ describes which agents are neighbours. Similar to a degree matrix, an adjacency matrix also has a size of $V \times V$.

In general, the following rules apply to the elements of the adjacency matrix (a_{ij}):

$$a_{ij} = a_{ji} = \begin{cases} 1, & \text{if agent i and j are connected and } i \neq j \\ 0, & \text{Otherwise} \end{cases} \tag{6.2}$$

The rule means that if agent i and agent j are neighbours, a value of 1 is assigned to element row i, column j as well as row j, column i in the matrix. The last important component of a graph is its Laplacian matrix. The general form of a Laplacian matrix is given by

$$L(G) = D(G) - A(G)\,. \tag{6.3}$$

A consensus algorithm aims to reach a state consensus among the agents. When consensus is reached, the state difference between neighbouring agents is zero. In the context of power sharing of multiple BESSs, the consensus is reached when all BESSs have the same utilization factor (i.e., the ratio between the injected or discharged power to a BESS' rated power). This means the power burden will be shared proportionately among the BESSs according to their rated power. To reach a consensus, each agent applies

$$\dot{x}_i(t) = \sum_{j \in N_i} a_{ij} \left[x_j(t) - x_i(t) \right] \tag{6.4}$$

which guarantees convergence to a collective decision through the interaction of nearby agents [58]. The equation implies that at $t \to \infty$, the value of $x_i(t) = x^* = c$ where x^* denotes a final value and c denotes a constant. Moreover, if the communication network is a balanced graph (the vertices have a similar number of edges), average consensus will be reached where the final value is the average of all initial states at time instance t as written in

$$x^* = \frac{\sum_i x_i}{n} \tag{6.5}$$

Since this work focuses on the calculation performed by each agent in every iteration, the discrete form of (6.4) is used, which is given by

$$x_i(k+1) = x_i(k) + \epsilon \sum_{j \in N_i} a_{ij} [x_j(k) - x_i(k)] \tag{6.6}$$

In (6.6), k indicates the k^{th} iteration, the parameter ϵ indicates the consensus step size, and a_{ij} is the element of the adjacency matrix, which indicates the communication link between agent i and agent j. If there is a connection between agent i and agent j, then $a_{ij} = 1$. Otherwise, a_{ij} is zero.
By applying the consensus algorithm in (6.4) to a graph, the global dynamics of the system is given by

$$\dot{x} = -Lx \tag{6.7}$$

Examples of global dynamics when using consensus algorithm explained in the form of (6.7) have been discussed in prior works such as [59] and [60]; thus, they are omitted in this work.

6.2.2. LEADER-FOLLOWER AGGREGATION

The control strategy developed for coordinating multiple BESSs combines local and distributed control. The distributed control is based on the consensus algorithm, as it reaches an agreement on a certain decision by the agents towards a goal. In this case, the goal is to keep the voltage in the nodes within a desired range. The lines that connect the buses are used as communication links that share the information between the neighbouring agents, (i.e. the BESS), to achieve a consensus when the voltage magnitude of one or more buses is violated. Each of these buses and BESS has an initial state, and a utilization factor is allocated to each BESS. The utilization factor determines how much power each BESS contributes to the voltage regulation. The consensus algorithm updates the utilization factors until the voltage magnitude does not surpass the limit points, ensuring that all BESS contribute the necessary amount of power for achieving voltage regulation.

To initialize the consensus algorithm, a *leader* utilization factor is defined (U_{leader}), which is updated until the voltage regulation of the system is achieved. This utilization factor is considered as a leader because it performs as a reference for the utilization factors of the other *followers* batteries (U_{i}) [12]. To achieve the voltage regulation of the LV distribution network by using the consensus algorithm, the leader utilization factor (U_{leader}) represent the battery connected to the leader bus. It can be the bus with the highest voltage if the higher voltage limit is violated, or the bus with the lowest voltage if the lower limit is violated. The leader utilization factor is updated until the voltage is regulated within limits, and the other utilization factors follow that value. Their value is determined by communication with the neighbouring agents.

The consensus algorithm uses voltage limits so that if the voltage exceeds the upper limit, the battery charges and if the voltage falls below the lower limit, the battery discharges. More specifically, if the voltage of the leader bus exceeds the upper limit (case 1: overvoltage), the utilization factor increases, whereas if the voltage of the leader bus falls below the lower voltage limit (case 2: undervoltage), the utilization factor decreases. In all other cases, when the voltage of the buses does not exceed any limits, the utilization factors are zero, and the batteries do not contribute to the system. This way the leader utilization factor is

$$U_{\text{leader}}(t) = \begin{cases} U_{\text{leader}}(t-t_{\text{s}}) + G_{\text{ov}}\,[V_{\text{n}}(t) - 1.05] & V_{\text{n}}(t) > 1.05 \\ 0 & 0.95 < V_{\text{n}}(t) < 1.05 \\ U_{\text{leader}}(t-t_{\text{s}}) + G_{\text{un}}\,[V_{\text{n}}(t) - 0.95] & V_{n}(t) < 0.95 \end{cases}, \tag{6.8}$$

where, t_{s} is the sampling time, V_n is the node voltage in p.u., and $G_{\text{ov}}, G_{\text{un}}$ are gains that control the speed of overvoltage and undervoltage regulation.

The battery connected to the leader bus will be the first to be informed about any

changes in the utilization factor. The other batteries will be informed about changes in their utilization factor according to

$$U_{\mathrm{i}}(t) = \sum_{j=1}^{n} C_{\mathrm{ij}}(t)\, U_{\mathrm{i}}(t - t_s)\,, \tag{6.9}$$

with

$$C_{\mathrm{ij}}(t) = \frac{A_{\mathrm{ij}}(t - t_{\mathrm{s}})}{\sum_{j=1}^{n} A_{\mathrm{ij}}(t - t_{\mathrm{s}})}, \tag{6.10}$$

where A is the adjacency matrix.

Following the proposed control scheme, all batteries contribute to the grid, despite their limitations and capabilities. Thus, the available capacity of each BESS is not affecting the power contribution from them. In Figure 6.3 the flowchart of the proposed control is presented. Each BESS's power contributes from its utilization factor multiplied by its nominal power ($P_{\mathrm{nom,i}}$). This way, each BESS provides the necessary power based on

$$P_{\mathrm{ref,i}} = P_{\mathrm{nom,i}} \times U_{\mathrm{i}}\,. \tag{6.11}$$

6.2.3. RESULTS ANALYSIS

To demonstrate the algorithm's functionality, its performance was evaluated using two starting SOC conditions. First, the same SOC was considered for all the BESSs have the same SOC. Then, different SOCs were considered for the BESSs. Both cases were compared against the base case without control, as shown in Figure 6.4. The voltage in buses 15, 17, and 18 exceeds the upper limit of 1.05 p.u. between 15:00 and 19:00, causing problems with network stability. Furthermore, between 21:00 and 23:00, the voltage on buses 15 and 18 exceeds the lower limit of 0.95 p.u. These limit violations occur since during the period between 15:00 and 19:00, when PV unit production is higher than demand, a large amount of power is inserted into the grid, causing an overvoltage, and during the period between 21:00 and 23:00, when PV unit production is low and demand is high, an undervoltage problem occurs. Thus, by integrating the BESS and implementing the developed control, these limit violations should be mitigated.

The voltage of the buses after implementing the proposed control strategy with all the BESSs having the same starting SOC can be seen in Figure 6.5, so the voltage magnitudes of the buses that had exceeded the limits are now restored into values within the limits. Figure 6.6 depicts the utilization factors used during the coordination control. They determine how much power each BESS should absorb or provide to the network to achieve voltage restoration within limits. When overvoltage occurs, the utilization factor of each BESS becomes positive; the higher the voltage violation on a bus, the higher the utilization factor of the BESS connected to that bus, and as a result, a more significant amount of power must be absorbed from the batteries. When undervoltage occurs, the utilization factors are negative, and the batteries must provide power to the network.

The SOC of the batteries is shown in Figure 6.7. When the utilization factors are equal to zero, the batteries do not contribute to the network, and the SOC remains constant; when the utilization factors are positive, the batteries charge and the SOC increases until

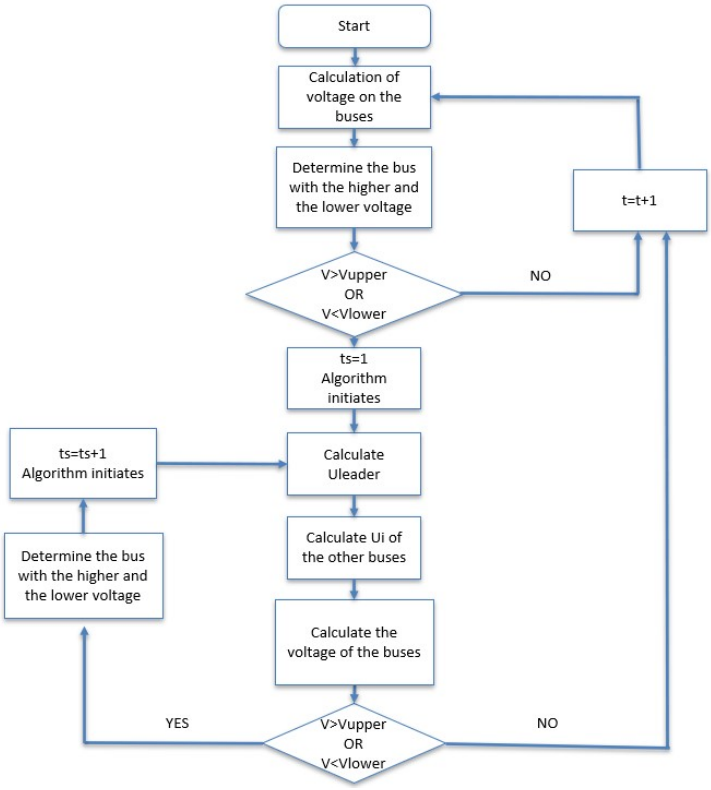

Figure 6.3: Leader-follower coordination strategy algorithm.

voltage restoration is achieved. When there is undervoltage, and the utilization factors are negative, the batteries discharge to keep the voltage within limits, and the SOC begins to decrease. In this case, since the undervoltage is for a very short period (30 min) and the amount of power needed from the battery is smaller than during the overvoltage problem, the decrease of the SOC is very small compared to the increase during the overvoltage.

In real-case scenarios, not all the BESS would have the same SOC. In some cases, one or more might not even be available. For this reason, it was also investigated the operation of the control strategy when one BESS is unavailable. In this case, the SOC of BESS 4 is set at 65 %; however, at 18:00, the SOC of the battery has reached the limit of 80 % (see Figure 6.8). The developed coordination control distributes the power required from BESS 4 equally to the neighbouring batteries, ensuring voltage stability. Even though one of the batteries is not available for use, the voltage magnitude of the buses is kept within the limits, as can be observed in Figure 6.9. A small peak is observed when the battery is disconnected, but the control strategy manages to regulate the voltage and mitigate this transient voltage change.

When BESS 4 is unavailable, the utilization factors of its neighbouring batteries (BESS 2,

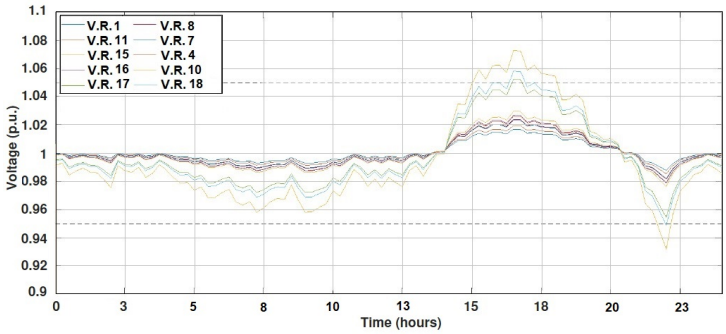

Figure 6.4: Voltage magnitude of buses with no control implemented.

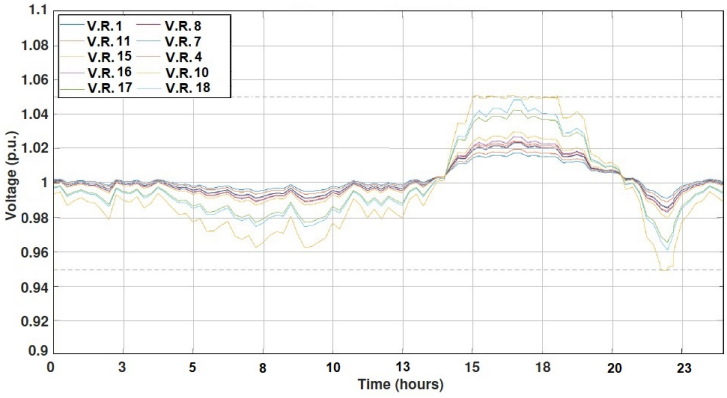

Figure 6.5: Voltage magnitude of buses using leader-follower coordination strategy.

BESS 3 and BESS 5) increase compared to the original values, as shown in Figure 6.10a. More specifically, the utilization factor of BESS 4 is 0.12, and it needs to be divided into three neighbouring BESS. As a result, the neighbouring batteries cover the required power that BESS 4 cannot store. At the highest point, BESS 2 increased from 0.13 to 0.17, BESS 3 increased from 0.16 to 0.2, and BESS 5 increased from 0.08 to 0.12. Figure 6.10b shows the power contribution of BESS 4 under normal operation when no limit of SOC is violated compared to this case where the limit of SOC is violated. When the SOC reaches 80 %, the battery is disconnected until it becomes available again.

To compare the results of the decentralized control strategy with the proposed leader-follower control strategy, the same mismatch profile is used; thus, the voltage magnitude of the buses with no control implemented is the same as in Figure 6.4. Under decentralized control, each battery is controlled locally, so the amount of power required is determined by the voltage magnitude on the bus to which the battery is connected. Figure 6.11 depicts the voltage after decentralized control is implemented. Although the voltage is regulated within acceptable limits, multiple fluctuations can be observed, affecting power quality. It can be noticed that the voltage fluctuations are higher when

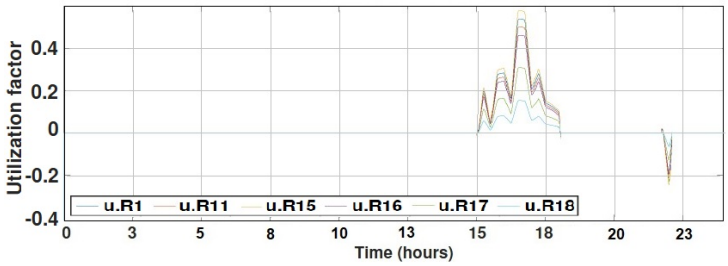

Figure 6.6: Utilization factors of BESS using leader-follower coordination strategy.

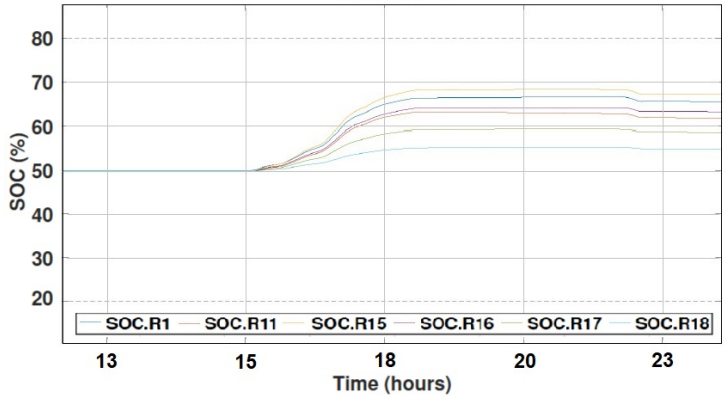

Figure 6.7: SOC of BESS using leader-follower coordination strategy.

the overvoltage is higher. This can also be explained as the droop control often has poor transient performance. In the case of the coordination control strategy, the voltage behaviour did not include frequent sudden changes around the limit point.

Furthermore, not all batteries help with voltage regulation. In this study, only BESS 3 (Bus 15) and BESS 6 (Bus 18) contribute, while the rest are not operating as the voltage on their buses does not surpass any limit. Thus, only the battery connected to a bus that exceeds the limits contributes, necessitating a larger capacity than the coordinated control strategy. This is depicted in Figure 6.12. It can be noticed that the power provided by BESS 3 is always higher with decentralized control. Moreover, all the frequent changes in the voltage magnitude can be observed in the power contribution of the battery. The frequent changes in the voltage affect the power contribution due to the poor performance of the droop control. These frequent changes in the battery's power output reduce its lifetime, making the decentralized control strategy less appropriate [61].

Finally, if one of the batteries used in voltage regulation reaches a SOC limit or is unavailable due to maintenance, the other batteries cannot provide the necessary power, and the voltage cannot be restored to acceptable levels. This is depicted in Figure 6.13, where BESS 3 is unavailable around 18:00. The voltage is not regulated and exceeds the

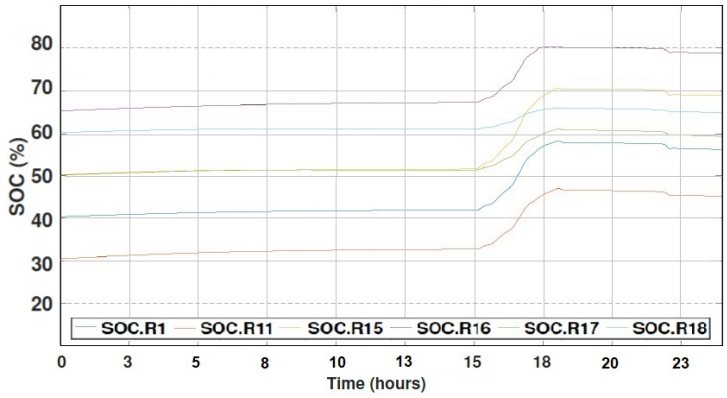

Figure 6.8: SOC profile of BESS using leader-follower coordination strategy - varying initial SOC.

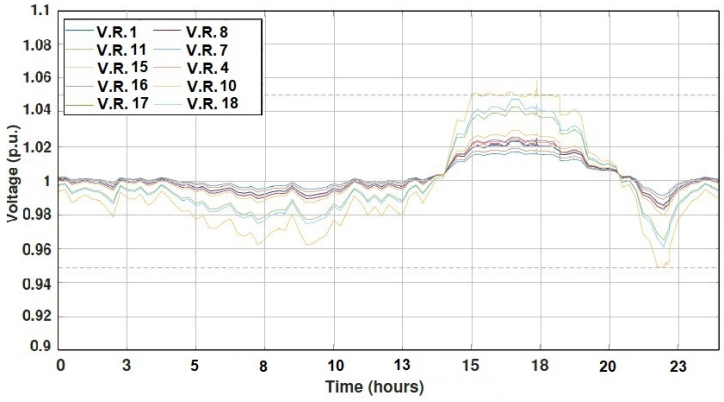

Figure 6.9: Voltage magnitude of buses using leader-follower coordination strategy - varying initial SOC.

limit. When the coordination control strategy was used, this was avoided.

6.2.4. LEADERLESS AGGREGATION

The second method uses the consensus algorithm without assigning a leader to coordinate the batteries spread out in the network. This method applies three steps to maintain voltage in the network: local utilization factor calculation, consensus utilization factor calculation, and final utilization factor calculation.

In the first step, local utilization factors U_i are calculated for every bus, based on their voltage V_i as

$$U_\mathrm{i}(t) = \begin{cases} 0, & (t=0) \\ U_\mathrm{i}(t-1) + U_{\mathrm{add,i}}(t) & \\ 0.5U_\mathrm{i}(t-1), & V_\mathrm{low} < V_\mathrm{i}(t) < V_\mathrm{high} \end{cases}, \tag{6.12}$$

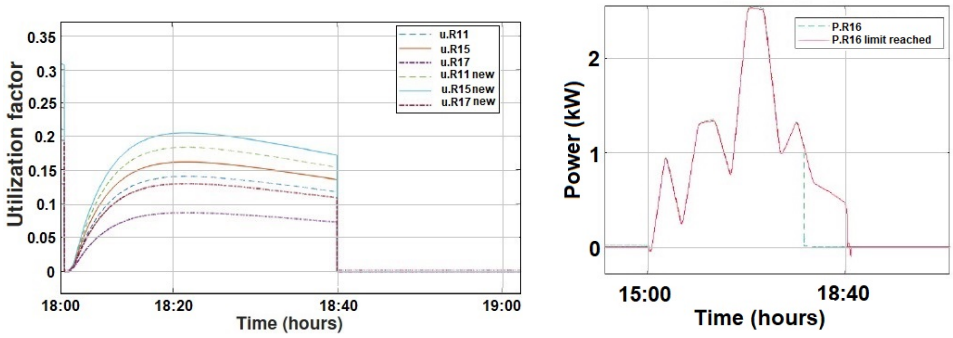

(a) (b)

Figure 6.10: (a) Utilization factor changes between normal operation and with a BESS unavailable. (b) Power contributed by BESS 4 under normal operation compared to when BESS 4 becomes unavailable.

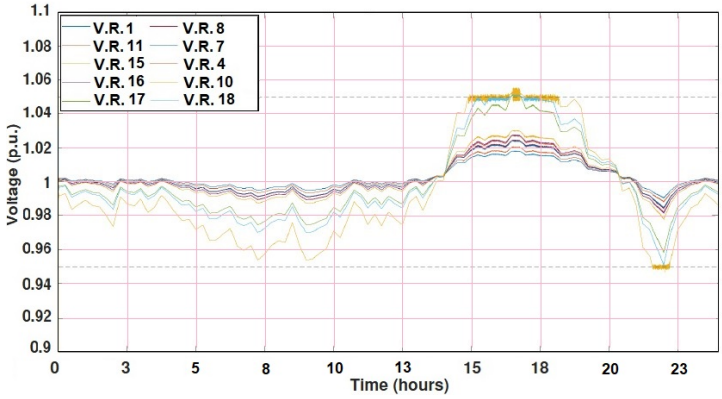

Figure 6.11: Voltage magnitude of buses using decentralized control.

where V_{high} and V_{low} are the upper and lower reset limits, respectively. Note that the utilization factor is halved every calculation step if the measured bus voltage is within a predefined reset limit, resulting in virtually zero utilization factor at steady state. Furthermore, (6.12) can be expanded as

$$U_{\text{add,i}}(t) = \begin{cases} G_{\text{ov}}\left[V_{\text{i}}(t) - 1.05\right], & V_{\text{i}}(t) > 1.05 \\ 0, & 0.95 \leq V_{\text{i}}(t) \leq 1.05 \\ G_{\text{un}}\left[V_{\text{i}}(t) - 0.95\right], & V_{\text{i}}(t) < 0.95 \end{cases}, \tag{6.13}$$

which represents the added or subtracted utilization factor at each timestep. The equation implies no addition or subtraction to the utilization factor if the measured bus voltage is within 0.95 and 1.05 p.u. Once the local utilization factor is calculated for every bus, the control step moves on to sharing the utilization factors among the batteries using the consensus algorithm.

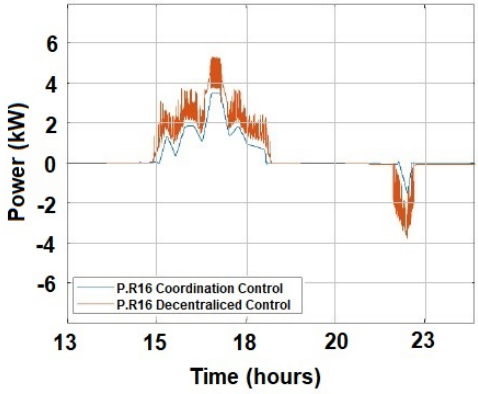

Figure 6.12: Power contribution of BESS 3 with coordinated control (blue) vs decentralized control strategy (orange).

The local utilization factors shared among the batteries are called the consensus utilization factor. This shared utilization factor is denoted by $U_{\text{cons,i}}(t)$ and is calculated with

$$U_{\text{cons,i}}(t) = U_{\text{i}}(t) + \epsilon \sum_{\text{j}\in \text{N}_{\text{i}}} a_{\text{ij}}[U_{\text{j}}(t) - U_{\text{i}}(t)]\,. \tag{6.14}$$

The estimated consensus utilization factor, $U_{\text{cons,i}}(t)$, at every time step t is the local utilization factor, $U_{\text{i}}(t)$, added by the sum of differences between the utilization factor at bus i and at its neighbour bus, j$\in N_i$, where N_i is a set of busses that are adjacent to bus i. The term a_{ij} represents the communication link between buses i and j. If buses i and j are linked, then $a_{\text{ij}} = 1$, otherwise $a_{\text{ij}} = 0$. The parameter ϵ represents the consensus step size, which determines how fast the consensus utilization factor is calculated for every iteration. Under a steady state, the consensus utilization factor for all buses will have the same value. Once the consensus utilization factor is found, a final modification to the utilization factor is performed to control battery SOC.

The BESSs spread across the LV network may not always have the correct amount of charge to absorb or release energy to perform voltage support. Some causes are the varying initial SOCs, unpredictable weather in different buses, and load variations. These variations affect voltage support readiness among the batteries. An SOC controller that follows (6.15) is implemented to keep the BESSs within a set SOC limit.

$$U_{\text{f,i}}(t) = \begin{cases} \frac{P_{\text{n,i}}}{P_{\text{nom,i}}}, & SOC_{\text{i}}(t) < SOC_{\text{lim,C}} \text{ and } 0 < P_{\text{n,i}} \leq P_{\text{pos}} \\ \frac{P_{\text{n,i}}}{P_{\text{nom,i}}}, & SOC_{\text{i}}(t) > SOC_{\text{lim,D}} \text{ and } P_{\text{neg}} \leq P_{\text{n,i}} < 0 \\ U_{\text{cons,i}}, & \text{otherwise} \end{cases} \tag{6.15}$$

By doing so, the BESSs will always be ready to support the network in preventing undervoltage and overvoltage conditions. The SOC controller in (6.15) works locally and

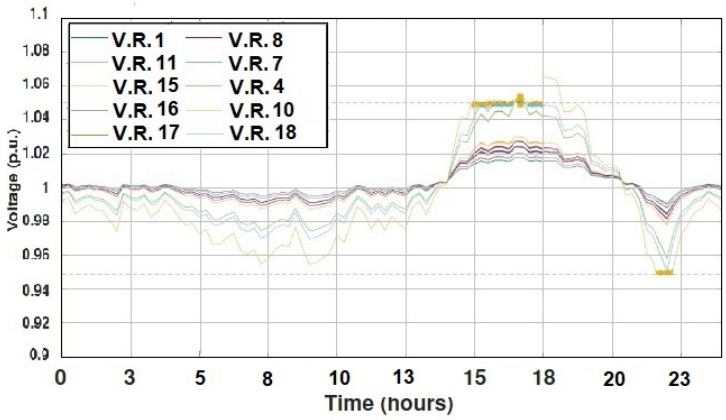

Figure 6.13: Voltage magnitude of buses using decentralized control when BESS 4 becomes unavailable.

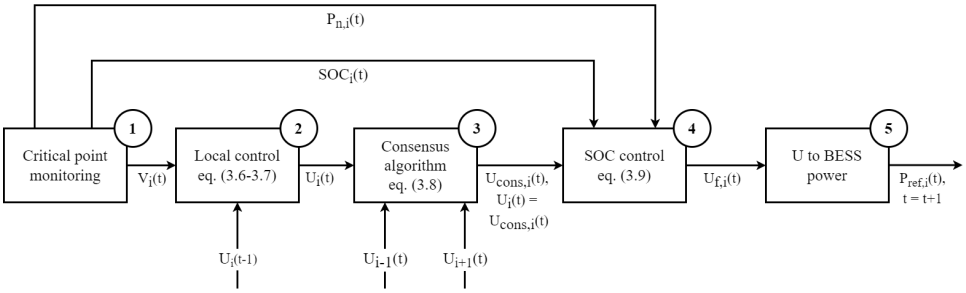

Figure 6.14: Calculation of the utilization factors in the leaderless approach. The positive utilization factor represents charging, while the negative one represents discharging.

takes on the SOC of a BESS, $SOC_{\mathrm{i}}(t)$, as well as the net power between PV and load at bus i ($P_{\mathrm{n,i}} = P_{\mathrm{PV}} - P_{\mathrm{Load}}$) as its input.

If a BESS has an SOC that is less than a specified charge limit, $SOC_{\mathrm{lim,C}}$, and the net power is between zero and a positive limit, P_{pos}, the BESS is charged by the net power $P_{\mathrm{n,i}}$. A similar rule is applied if the BESS has an SOC that exceeds the charge limit, $SOC_{\mathrm{lim,D}}$, and the net power is between zero and a negative limit, P_{neg}. However, the battery is discharged in this case to compensate for the power deficit in the bus. When none of these conditions are met, the BESS will keep its consensus utilization factor from the consensus controller as its reference. The main goal of (6.15) is to keep the BESSs SOC between $SOC_{\mathrm{lim,D}}$ and $SOC_{\mathrm{lim,C}}$ as much as possible, where $0 < SOC_{\mathrm{lim,D}} < SOC_{\mathrm{lim,C}}$. The final utilization factor, $U_{\mathrm{f,i}}(t)$, is multiplied by the BESS rated power to become its reference power according to

$$P_{\mathrm{ref,i}}(t) = P_{\mathrm{nom,i}} \times U_{\mathrm{f,i}}(t)\,. \tag{6.16}$$

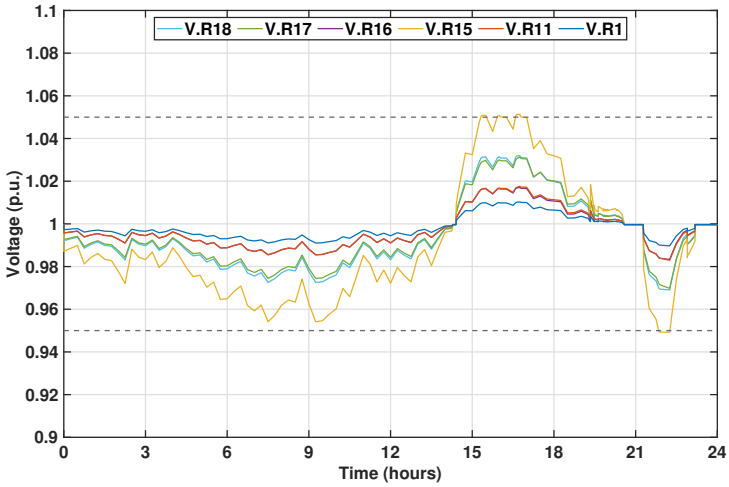

Figure 6.15: Voltage magnitude of buses using leaderless coordination method. All bus voltages are kept within limits of 0.95 and 1.05 p.u.

6.2.5. RESULTS ANALYSIS

To evaluate the behaviour of the second coordination method, voltage profiles of the buses, utilization factors, and SOC profiles of the batteries can be observed. Generally, this second coordination method can also prevent bus voltage from exceeding the limits while keeping battery SOC close to uniform throughout the simulation process. The voltage magnitudes can be kept within the limits, as seen in Figure 6.15. A slight violation can be observed for both overvoltage and undervoltage mitigation; however, the deviation is relatively small at 0.01 p.u. with respect to the predefined limit.

Similar to the leader-follower algorithm, the utilization factors also increase to a positive value when there is overvoltage and decrease to a negative value during undervoltage, as seen in Figure 6.16. The utilization factors of all batteries are the same during overvoltage (16:00 to 20:00) or undervoltage periods (22:00 to 23:00); thus, the batteries contribute proportionally to their rated power. Meanwhile, around 21:00, for example, the non-zero utilization factors represent the charging or discharging of batteries outside the over/undervoltage period to balance their SOC. This SOC balancing action is an additional rule on top of the consensus algorithm to ensure uniform voltage mitigation readiness for all batteries.

The utilization factors are also reflected in the battery powers as they are similar in profiles. One highlight is that the power profiles for all batteries are different when the utilization factors are uniform. In contrast, the power profiles are uniform when the batteries have different utilization factors. This behaviour is due to the variation in the batteries' nominal power. As indicated earlier in (6.11), the reference charging/discharging power is determined by the utilization factor and nominal power; therefore, uniform utilization factors do not guarantee similar reference powers.

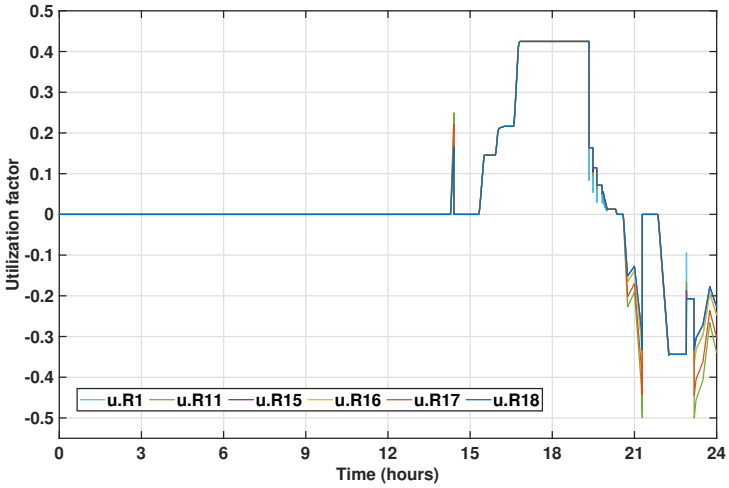

Figure 6.16: Utilization factors of BESS using leaderless coordination method. A positive utilization factor represents charging while a negative utilization factor represents discharging.

6.2.6. DISCUSSION

This section highlights the key difference between the leader-follower and leaderless control strategies discussed in this work. Three aspects are highlighted, namely, voltage, utilization factors, and SOC of the batteries. Bus voltages in both the leader-follower and leaderless strategies are kept within the predefined limit, albeit with small differences in the voltage of the non-critical buses. Using the leaderless method, the voltage of the non-critical buses is kept at levels that are further away from the predefined limit compared to the leader-follower method, as shown in Figures 6.9 and 6.15. This is due to the shared utilization factor. As the leaderless method aims to distribute the required contribution to ensure the limit, instead of depending on the leader, it minimizes the under and over-usage of the individual agents. Therefore, the overall SOC of the different agents in the network is more uniform and can react to sudden load or availability changes. The leader-follower method can charge or discharge one single agent at the point that it becomes unavailable under extreme conditions. If that happens, the compensation required is distributed among the neighbouring agents.

In addition, the utilization factor in the leader-follower method is immediately reset after the overgeneration or overdemand has receded. Meanwhile, the utilization factor stays in the leaderless method until a reset signal is given. The delayed reset prevents voltage fluctuations following an immediate power reset. Besides the resetting behaviour, the utilization factor in the leader-follower method is not uniform during voltage control action (see Figure 6.6), implying that the batteries do not contribute based on their rated capacity ($U_\mathrm{i} = P_\mathrm{ref,i}/P_\mathrm{nom,i}$). On the other hand, the leaderless method drives the utilization factor to a uniform during voltage control, indicating each battery contributing in proportion to its rated power. If their rated powers are the same, then the power each battery contributes is also the same.

Regarding battery SOC, the leaderless method offers more uniform SOC values across

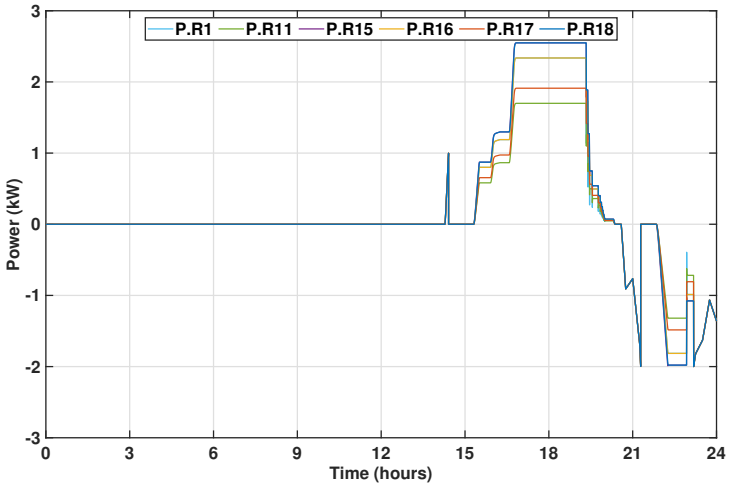

Figure 6.17: Power profiles of BESS using leaderless coordination method. The profile mimics the utilization factors profile shown in Figure 6.16.

all batteries than the leader-follower method. As explained in Section 6.2.4, the proposed leaderless method has an additional SOC control, which ensures uniform voltage mitigation readiness for all batteries. Moreover, the leaderless approach does not require every node to have full observability of the system but only on its neighbouring nodes, reducing communication congestion and data privacy boundaries. Those features provide a more robust voltage control.

Implementing these strategies, however, might be challenging from a data privacy perspective. For the leader-follower, an aggregator must measure the status of all devices and provide the leader signal to the agents. The leaderless, despite not requiring direct communication among all agents at a given time, it still requires sharing the SoC with an aggregator, which might be undesired for some users. Similarly, given the nature of the control strategy, i.e., the consensus algorithm, including other storage elements would be challenging. As there should be consensus on the utilization factor per energy storage asset per node, either a correlation or a priority must be determined between them. Thus, the methods might not be as suitable for multi-carrier systems as they are for single-carrier.

6.3. MULTI-CARRIER AGGREGATION

Section 6.2 provided two powerful strategies to aggregate BESS in distribution networks, however, there are some gaps found that still need to be addressed. On the one hand, aggregators are assumed to have full observability and control over the assets, potentially causing privacy challenges for residential prosumers who would own assets connected to the network. On the other hand, the control is still either consumer-centred or DSO-centred, instead of relating one to another. In addition, most works on the literature depend on test networks with a small number of connections (either DRES and BESS

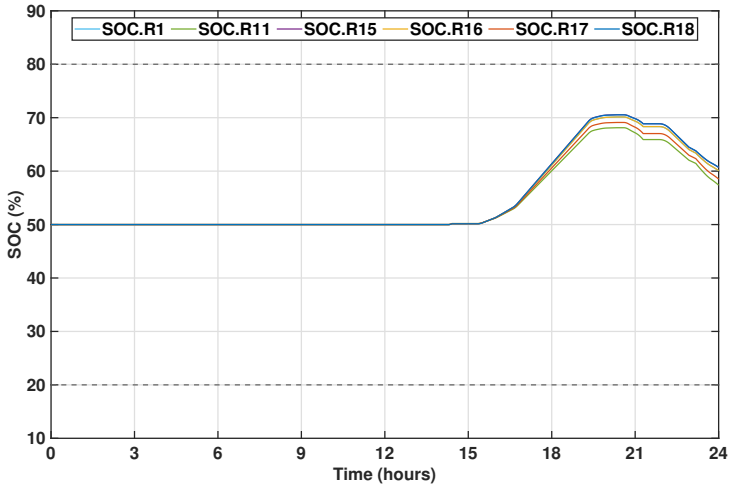

Figure 6.18: SOC profile of BESS using leaderless coordination method.

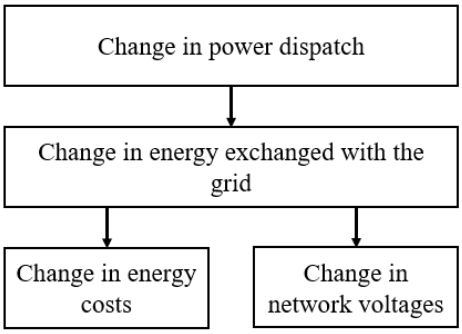

Figure 6.19: Causality sequence considered for the analysis.

assets, or loads) for case scenarios, instead of using data from existing distribution networks. To fill those research gaps, this Section considered independent controllers for the DSO and the prosumers, to understand the changes in energy cost for prosumers and voltages in the low-voltage network. These changes were obtained through an analysis on the grid exchange behaviour caused by the change in internal power dispatch at the household level was done for different single- and multi-carrier system architectures, demonstrated using a 301-node, 114-houses low-voltage distribution network from the Netherlands. The analysis done in this Section follows the flow presented in Figure 6.19.

6.3.1. DISTRIBUTION NETWORKS

A model of a low-voltage distribution network is required to evaluate the aggregation strategy. In this case, a voltage-based model was used, since residential loads are unlikely to cause major frequency shifts. The network's topology is then represented as an

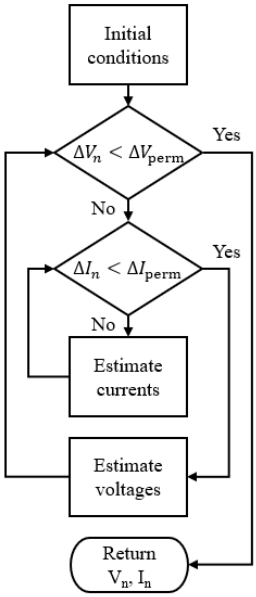

Figure 6.20: Flow diagram used to estimate the nodes' voltage and current.

admittance matrix A, the voltages at every node as a vector V_n, and the impedances and currents between two interconnected nodes are Z and I, respectively. This power-flow problem is solved using an iterative method, following

$$V_n(k+1) = A\,V_n(k) - Z(k)\;I(k) + B\,V_0(k)\,, \tag{6.17}$$

where V_0 is the voltage inputs at the substations and B is a matrix indicating to which nodes they are connected. Note that during the iteration process, it is assumed that the values for the impedances, currents and feeder voltage are constants, as the iterative process is done every time step k. The current estimation has a similar approach, following

$$I(k+1) = A^{\mathrm{T}}\,I(k) + I_n(k)\,, \tag{6.18}$$

where I_n is a vector with the current at every node. The current, however, is also a function of the voltage, as

$$I_n(k) = \frac{S_n(k)}{V_n(k)} \tag{6.19}$$

where S_n is the apparent power at every node [24]. Figure 6.20 shows the method used to solve the network's power-flow.

6.3.2. MULTI-CARRIER ENERGY SYSTEM

Some buildings in the network were coupled with one or more devices to create different scenarios, as described in Section 6.3.5. This gradual inclusion of devices provides information on the individual effect at the network level. The more complex system couples all the considered devices into a multi-carrier energy system (MCES) comprised of a PV, a battery energy storage system, a heat pump and an underground thermal energy storage system. The models for each device are detailed in Chapter 3, and a summary of the models is provided in Table 6.2. For the Li-ion battery, we followed the semi-empirical degradation model proposed in [62] to account for calendar and cycling ageing, as recommended in Section 4.6. The thermal energy storage is an underground, well-mixed water tank with separated charge and discharge coils. The heat loss to the environment of both the TESS and the house was modelled following the methods proposed in [63]. The distribution of the thermal power in the house is done using a water system that can use the TESS and the HP individually or simultaneously. The HP is used to charge the tank.

The PV systems used per house are sized to reach as close as possible to a net-zero energy building, using 400 W modules, with an area A_{PV} of 2 m^2, efficiency at standard test conditions η_{STC} of 18.4 %, temperature coefficient β of -0.3 %/°C. The BESS charge and discharge efficiencies are set at 94.3 %, with a maximum permitted power of $\pm$10 kW and a capacity of 10 kWh. The TESS is assumed to be filled with 4 m^3 of water, and the heat exchangers have an efficiency η_{TESS} and η_{HP} of 80 % with a mass flow of $\dot{m}_f$ of 0.22 m^3/s through the heating circuit. The supply temperature of the network T_{sup} is 50 °C. The details of the thermal losses can be found in Chapter 3.

6.3.3. LOCAL EMS CONTROL

Chapter 4 provided an in-depth analysis of EMS strategies for multi-carrier energy systems. Since the goal of this chapter is to study the flexibility oportunities for residential multi-carrier systems, the computational cost becomes relevant. For that reason, the heuristic EMS strategy proposed in Section 4.5 is used. The general policy π_k for each timestep k is then comprised of the individual policies per device j and objective i, resulting in

$$\pi_k = [\delta^T, \delta^\lambda, \delta^P]\,. \tag{6.20}$$

Table 6.2: Equations used to model the components of the MCES.

Parameter	Symbol	Equation	
PV generation	$P_{\text{PV}}(k)$	$\text{A}_{\text{PV}} G(k) \eta_{\text{STC}} \left(1 - \beta \left[T_{\text{PV}}(k-1) - T_{\text{ref}}\right]\right)$	(6.21)
BESS energy	$E_{\text{BESS}}(k)$	$= \begin{cases} E_{\text{BESS}}(k-1) + \eta^{\text{c}}_{\text{BESS}} P_{\text{BESS}}(k-1)\,\Delta t - E^{\text{SD}}(k-1) & \forall\, P_{\text{BESS}}(k-1) < 0 \\ E_{\text{BESS}}(k-1) + \dfrac{P_{\text{BESS}}(k-1)}{\eta^{\text{d}}_{\text{BESS}}}\Delta t - E^{\text{SD}}(k-1) & \forall\, P_{\text{BESS}}(k-1) > 0 \end{cases}$	(6.22)
TESS power	$\dot{Q}_{\text{TESS}}(k)$	$= \eta_{\text{TESS}} \dot{m}_f c_f \left[T_{\text{sup}} - T_{\text{TESS}}(k-1)\right]$	(6.23)
TESS temperature	$T_{\text{TESS}}(k)$	$= \text{T}_{\text{TESS}}(k-1) + \dfrac{\Delta t \left[\eta^{c}_{\text{TESS}} \dot{Q}^{\text{TESS}}_{\text{HP}}(k-1) - \dfrac{\dot{Q}_{\text{TESS}}(k-1)}{\eta^{d}_{\text{TESS}}} + \dot{Q}^{\text{SD}}(k-1)\right]}{m\,c}$	(6.24)
HP COP	$\text{COP}(k)$	$= 7.90471\text{e}^{-0.024\left[T_{\text{ret}}(k-1) - T_{\text{amb}}(k-1)\right]}$	(6.25)
HP thermal power	$\dot{Q}_{\text{HP}}(k)$	$= \eta_{\text{HP}} \dot{m}_f c_f \left[T_{\text{sup}} - T_{\text{ret}}(k-1)\right]$	(6.26)
Thermal demand	$\dot{Q}_D(k)$	$= \left(\sum_{i=1}^{n} U_i A_i + c_a \rho_a q_v + c_a \rho_a q_i\right) \left[T_{\text{in}}(k-1) - T_{\text{out}}(k-1)\right]$	(6.27)
Indoor temperature	$T_{\text{in}}(k)$	$= \text{T}_{\text{in}}(k-1) + \dfrac{\Delta t \left[\dot{Q}_{\text{TESS}}(k-1) + \dot{Q}_{\text{HP}}(k-1) - \dot{Q}_D(k-1)\right]}{\sum_{i=1}^{n} m_i c_i}$	(6.28)
Return temperature	$T_{\text{ret}}(k)$	$= \text{T}_{\text{ret}}(k-1) + \dfrac{\dot{Q}_{\text{TESS}}(k-1) + \dot{Q}_{\text{HP}}(k-1) - \dot{Q}_D(k-1)}{\dot{m}_f c_f}$	(6.29)

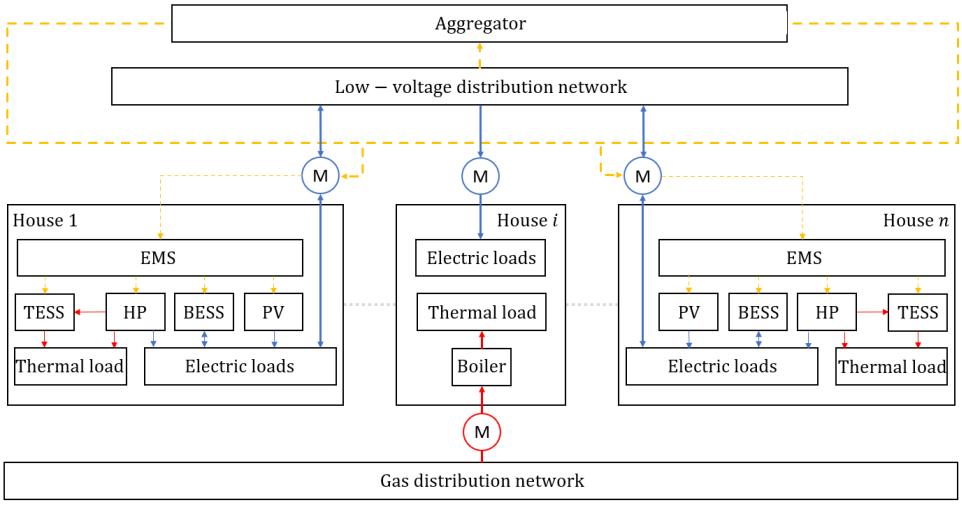

Figure 6.21: Control scheme representing the interactions between the aggregator, the low-voltage distribution network, the consumers and the prosumers (the yellow lines represent communication flow, the blue lines electric power flow, and the red lines thermal power flow).

6

6.3.4. AGGREGATION CONTROL

It is expected that increasing the number of assets in the grid leads to congestion, in particular, if they use the same EMS, which follows the energy price. For this reason, an aggregator was implemented, so that the effect on the network is minimized. Unlike most aggregators in the literature that are assumed to have full observability over the assets at each node, the proposed aggregator only has information up the meter, i.e., can only measure the current and power a particular node exchanges with the grid, and the voltage at every node in the network. This way, the aggregator would provide a setpoint power to each prosumer, and the local EMS would handle the power allocation to fulfil such a setpoint (see Figure 6.21). Consumers (i.e., households without flexibility assets) are excluded from the setpoint assignment. These conditions, of course, create challenges for the control strategy in terms of asset controllability, but in the view of the authors, provide a more realistic approach in terms of short-term implementation and data privacy management.

Since the aggregator has no visibility on what are the states of the assets behind the meter, it is assumed that the power exchanged with the grid at any point k is the optimal value found by the local EMS. Based on this assumption, it is proposed to find the power setpoints P^* for every prosumer while minimizing the change between the measured power and the actual setpoint. This way, the optimization problem is formulated as

$$\min_{P_i^*} \quad \sum_{i \in N} \left(P_i^* - P_i\right)^2 \tag{6.30}$$

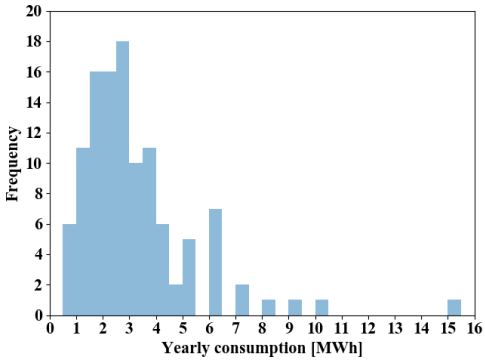

Figure 6.22: Distribution of the yearly consumption per household in the network.

$$s.t. \quad P_i^* = P_i, \forall\, i \in N_c, \tag{6.31a}$$

$$P_i^* = 0, \forall\, i \in N_d. \tag{6.31b}$$

$$V_{\min} \leq V_i \leq V_{\max}, \forall\, i \in N, \tag{6.31c}$$

where, i is the node number, the set N contains all the nodes in the network, N_c is the subset with the nodes where a consumer is connected to the grid, and N_d the subset with the distribution nodes where no loads are connected. The capacity of the conductors was not included in the constraints as it was not observed to cause problems. Note that, as shown in Section 6.3.1, the process to calculate V_i is iterative, which might interfere with the optimization process. For that reason, it is proposed to use an approximation for the worst voltage in the grid (worst defined as the node whose voltage is further from 1 p.u. either towards consumption or injection) as a function of the average exchanged power with the grid per node $\hat{V}(\overline{P}_{\text{Grid}})$, as detailed in Section 6.3.6. This way (6.31c) is replaced for

$$V_{\min} \leq \hat{V}(\overline{P}_{\text{Grid}}) \leq V_{\max}, \forall\, i \in N. \tag{6.32}$$

6.3.5. SCENARIOS DESCRIPTION

This Section aims to demonstrate the effect of different energy transition scenarios on a low-voltage residential network. The network used is a 301-node network with 114 houses (with known yearly consumptions), provided by the Dutch DSO Stedin. The yearly consumption of the 114 houses ranged from 500 kWh to 15000 kWh, with an average close to 3000 kWh. The distribution of energy consumption is shown in Figure 6.22. As heating consumption was not provided, the houses were classified according to their consumption as a 55 m^2 apartment, a 120 m^2 apartment and a 240 m^2 house for consumptions between 0-1000 kWh, 1000-4000 kWh and above 4000 kWh, respectively.

For each scenario, four penetration percentages were evaluated (20 %, 40 %, 60 % and 80 %) during a week during winter and during summer. Five different random sets

Table 6.3: Scenario description.

Scenario	Architecture	EMS objective
0: Base case	-	-
1: RES inclusion	PV	-
2: Heat electrification	PV + HP	Thermal comfort
3: Single-carrier non-aggregated storage	PV + HP + BESS	Thermal comfort + minimize costs
4: Single-carrier aggregated storage	PV + HP + BESS	Thermal comfort + grid support
5: Multi-carrier non-aggregated storage	PV + HP + BESS + TESS	Thermal comfort + minimize costs
6: Multi-carrier aggregated storage	PV + HP + BESS + TESS	Thermal comfort + grid support
7: Multi-carrier semi-aggregated storage	PV + HP + BESS + TESS	Thermal comfort + minimize costs + grid support
8: Centralized Storage[1]	PV + BESS	Grid support

[1]The centralized storage is considered to compensate for scenarios 1 and 2.

of nodes to locate the systems in the network were considered for each penetration level to better represent a real case where the DSOs cannot control where new prosumers would install their systems. These sets were maintained for all the scenarios so that they could be compared.

Seven energy transition scenarios are evaluated. A *base case* is defined as a reference, considering only the existing electric loads and gas heating. Then, the *RES inclusion* was considered in the form of PV systems sized for near-net-zero houses. *Heating electrification* through heat pumps is added to eliminate the dependency on gas boilers in the selected nodes. Battery storage systems were added to create a *single-carrier non-aggregated storage* system, as these batteries are not communicating with each other, and a *single-carrier aggregated storage* system where an aggregator sends setpoints to the prosumers, who would follow them if possible. A *multi-carrier non-aggregated storage* scenario was then created by adding thermal energy storage to the previous scenario. With this architecture, two more scenarios were constructed, a *multi-carrier aggregated storage* system, where an aggregator directs the power to be exchanged with the grid at any point, and a *multi-carrier semi-aggregated storage* system, where the aggregator suggests a power setpoint, but the local EMS can decide to follow it or not, based on its own strategy. Table 6.3 summarises the scenarios and the variables considered for each.

Different metrics were used to compare scenarios 1 to 7 from the grid perspective and from the household perspective. For the former, the voltage outside the 1 ± 0.05 p.u. ($V_{0.95}$ and $V_{1.05}$) and 1 ± 0.1 p.u. ($V_{0.90}$ and $V_{1.10}$) ranges per node was the selected metric. At the household level, for each selected house it was compared the change in the energy exchange (ΔE_G^{in} for consumption and ΔE_G^{out} for injection). Similarly, the change in the cost of electricity (ΔC_E), total energy including electricity and gas ($\Delta C_{E,g}$), the PV energy curtailed (ΔE_{PV}), the total energy consumed by the heat pump (ΔE_{HP}), the energy stored ($\Delta E_{\text{BESS}}^{\text{in}}$) and degradation ($\Delta C_{\text{BESS}}$) of the battery, the thermal energy used by the heat pump to charge the TESS ($\Delta E_{\text{PV}}^{\text{TESS}}$) and the thermal energy used by the TESS to heat the house (ΔQ_{TESS}). As each penetration level has multiple cases, the range between the minimum and maximum value among those cases per metric was provided.

Scenario 8 will be analyzed only from the DSO perspective. This is because it is intended to compensate for the prosumer's behaviour without interacting with them for scenarios 1 and 2. This way, we only consider the voltage outside the 1 ± 0.05 p.u. ($V_{0.95}$ and $V_{1.05}$) and 1 ± 0.1 p.u. ($V_{0.90}$ and $V_{1.10}$) ranges per node. However, the location and sizing of the BESS (energy and power) and PV must be determined. To define the node

where the centralised system will be connected, the network will be analysed for each case per penetration to determine the most critical node, defined as the node with higher accumulated voltage deviations outside the permitted range, calculated by

$$\Sigma_{V,i} = \left[\sum_{k=0}^{T} V_{\min} - \underline{V}_i(k)\right] + \left[\sum_{k=1}^{T} \overline{V}_i(k) - V_{\max}\right], \forall\, \underline{V}_i(k) < V_{\min}, \overline{V}_i(k) > V_{\max}, i \in N. \quad (6.33)$$

Once the node is defined, a BESS and PV system was placed on that node to evaluate whether a centralized system can ensure voltage compliance with EN50160.

6.3.6. VOLTAGE ESTIMATION RESULTS

The iterative nature of the power flow solution method, using the node voltages in the network as constraints, might lead to high computational costs or, ultimately, unfeasibilities. For that reason, the unaggregated scenarios were evaluated to find an alternative to estimate the network behaviour. Each scenario was simulated for a 100 % penetration level and then plotted the minimum and maximum voltages in the network against the average grid power per node $\overline{P}_{\text{Grid}}$. As shown in as shown in Figures 6.23a, 6.23c, 6.23e and 6.23g, two polynomial correlation became evident for all scenarios. On the one hand, for the positive average grid powers (consumption), the worst voltage in the network is the minimum (shown in red), whereas the best voltage is the maximum (shown in blue). On the other hand, when the average grid power is negative (injection), the correlation is reversed; i.e., the worst voltage is the maximum, and the best is the minimum. This behaviour is consistent with previous studies in power systems where small incremental changes in power in the network resulted in quasi-lineal voltage behaviour [64].

Interestingly, the best and worst voltage points, despite reversing at $\overline{P}_{\text{Grid}} = 0$, complement each other. Using a second-order polynomial regression, the worst voltage curve $\hat{V}$ was estimated as a function of the average grid power with very high accuracy (black line). The experiment was then repeated for 20 different combinations of node samplings and penetration levels per scenario (see Figure 6.25 for details on the sampling distribution) during summer and winter without extrapolating the average grid power ranges per case, as shown in Figures 6.23b, 6.23d, 6.23f and 6.23h. As can be seen, there is a strong correlation between the average grid power and the worst voltage in the network, which is then confirmed plotting the yearly curves per scenario together in Figure 6.24. The resulting approximation of the worst voltage on the grid that is used for (6.32) is

$$\hat{V}(\overline{P}_{\text{Grid}}) = -0.00083106\,\overline{P}^2_{\text{Grid}} - 0.03378\,\overline{P}_{\text{Grid}} + 0.9997 \quad (6.34)$$

6.3.7. RESULTS ANALYSIS

The analysis was carried out for a representative week during winter and summer, as the technical standard EN50160 requires that the voltage remain within ±0.1 p.u. during 95 % of the week. Knowing that the location of the node where the system should be placed leads to different results on the network, five random samples per penetration percentage were created, uniformly distributed throughout the network, as shown

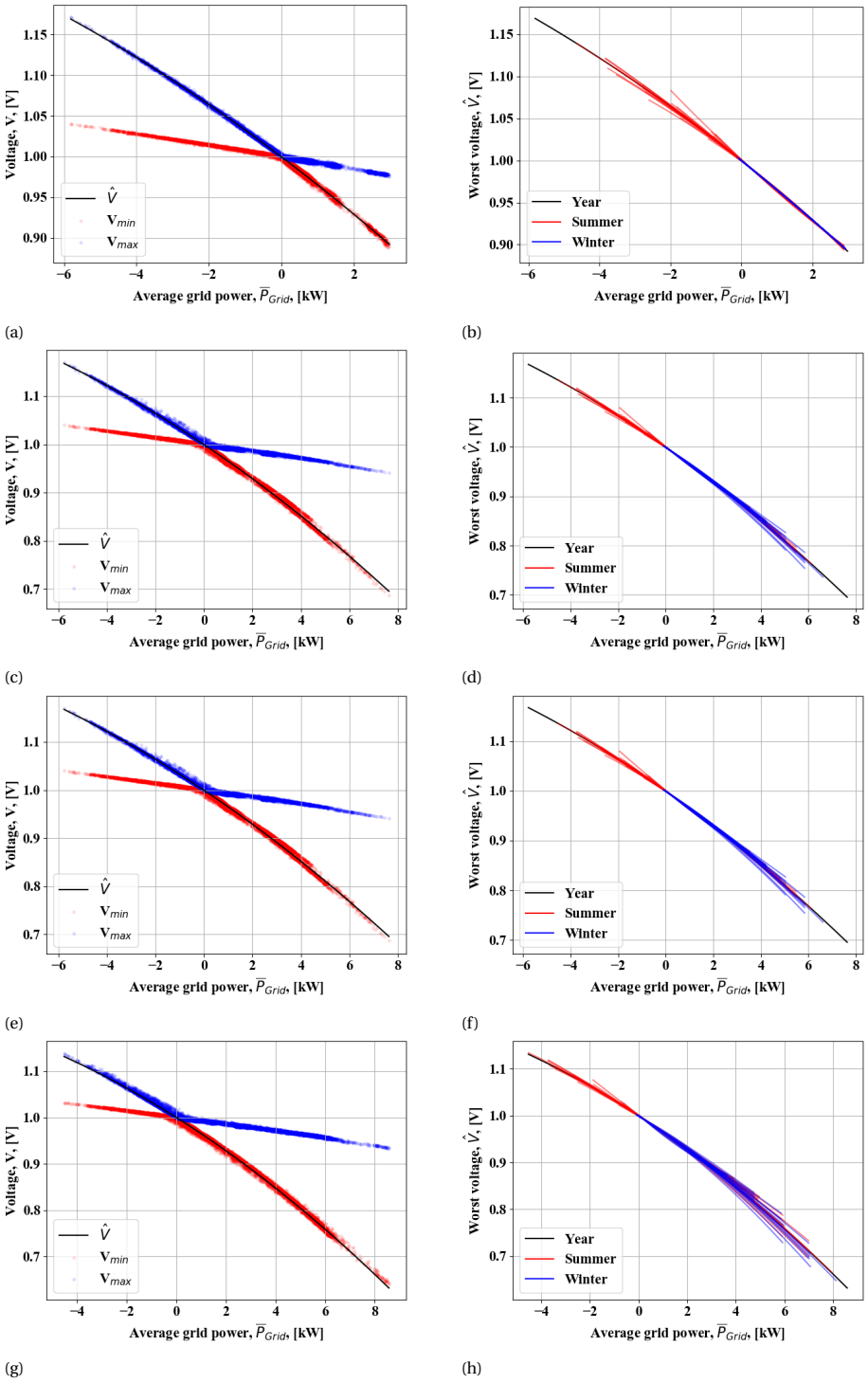

Figure 6.23: Relationship between the average power and the minimum and maximum voltage in the network (a, c, e, g), and results for all scenarios and penetration levels during winter, summer and yearly (100 % penetration) (b, d, f, h) for scenarios 1, 2, 3 and 5 respectively.

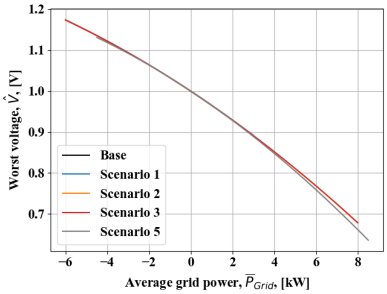

Figure 6.24: Comparison of the yearly correlations between the worst voltage on the network and the average grid power for scenarios 0, 1, 2, 3 and 5.

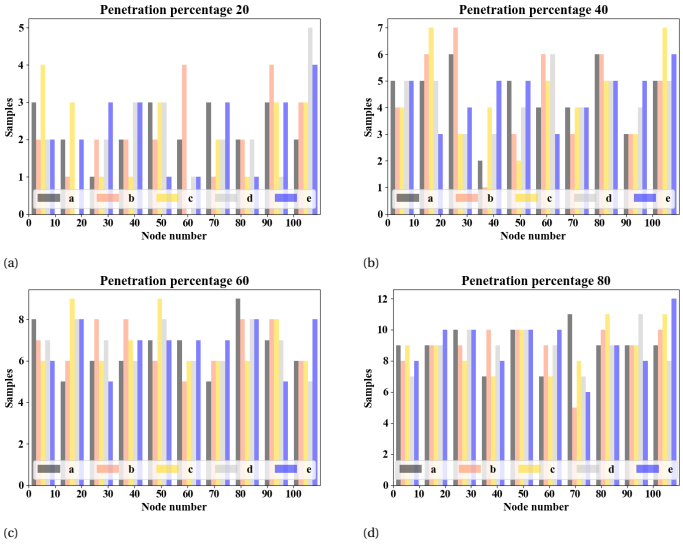

Figure 6.25: Distribution of nodes selected per case, per penetration percentage.

in Figure 6.25. The network was simulated, including the corresponding system architecture per scenario in the selected nodes. A summary of the results is shown in Tables 6.4 and 6.5.

Table 6.4: Result ranges per season for different penetration levels (20 % - 40 %).

		0 %	20 %							40 %						
			1	2	3	4	5	6	7	1	2	3	4	5	6	7
Winter	$V_{0.95}$ [%]	3.263	3.263	3.56-3.66	3.53-3.66	3.31-3.59	5.46-8.90	3.20-3.46	3.94-8.07	3.26	6.75-7.99	6.70-7.95	3.24-3.57	24.07-25.26	3.14-3.41	22.64-24.17
	$V_{1.05}$ [%]	0	0	0	0	0	0	0	0	0	0	0	0	0	0	0
	$V_{0.90}$ [%]	0.020	0.020	0.107-0.130	0.100-0.127	0.001978-0.1360	0.235-0.298	0.00346-0.0870	0.213-0.290	0.020	0.338-0.367	0.331-0.360	0.0593-0.1276	2.98-4.47	0.0400-0.0727	1.145-2.42
	$V_{1.10}$ [%]	0	0	0	0	0	0	0	0	0	0	0	0	0	0	0
	ΔC_E [%]	*Ref*	-(5.48-6.84)	19.09-281	15.80-281.1	30.44-459.6	34.62-831	34.78-675.01	45.23-1026	-(5.35-6.71)	19.09-323	15.80-322.9	39.52-855.5	34.62-955	29.31-1041	45.23-1147
	$\Delta C_{E,g}$ [%]	*Ref*	-(5.48-6.84)	-(60.17-78.56)	-(61.27-78.56)	-(53.51-71.04)	-(45.09-65.41)	-(55.28-73.84)	-(33.81-59.03)	-(5.35-6.71)	-(60.17-78.85)	-(61.27-78.85)	-(40.33-76.73)	-(44.92-65.67)	-(42.36-73.80)	-(33.51-59.58)
	$\Delta E_{\mathbf{G}}^{\mathbf{in}}$ [%]	*Ref*	-(4.01-4.94)	59.84-665.1	25.7-665.1	80.57-1624	151.3-3295	76.05-1660	158.97-3676	-(4.08-4.96)	59.84-745.9	25.7-745.9	44.65-1807	151.3-3696	33.43-2685	158.81-4123
	$\Delta E_{\mathbf{G}}^{\mathbf{out}}$ [%]	-	*Ref*	-(5.53-13.8)	-(13.3)-105.2	683-61468	784.5-40768	598.8-55767	831.0-69643	*Ref*	-(5.39-18.5)	-(18.5)-77.5	321-54609	784.5-40768	338.1-45882	820.9-69643
	$\Delta E_{\mathbf{PV}}$ [%]	-	*Ref*	0	0	-(53.30-75.90)	0	-(60.39-74.21)	-(61.57-75.74)	*Ref*	0	0	-(62.10-77.45)	0	-(62.56-77.35)	-(61.89-75.74)
	$\Delta E_{\mathbf{HP}}$ [%]	-	-	*Ref*	0	-(4.19-21.06)	102.3-313.2	(-49.06)-101.14	102.3-313.2	-	*Ref*	0	-(2.50-21.08)	102.3-313.2	(-51.71)-151.44	102.3-313.2
	$\Delta E_{\mathbf{BESS}}^{\mathbf{in}}$ [%]	-	-	-	*Ref*	(-1.674)-102.9	(-5.52)-0	10.99-96.43	61.86-89.74	-	-	*Ref*	30.18-125.4	(-5.52)-0	(-7.08)-167.34	61.34-89.97
	$\Delta C_{\mathbf{BESS}}$ [%]	-	-	-	*Ref*	-(0.312-1.773)	0-0.240	-(0.610-1.691)	-(0.981-1.442)	-	-	*Ref*	(-2.05)-0.0814	0-0.240	-(-2.83)-0.1769	-(0.973-1.454)
	$\Delta E_{\mathbf{HP}}^{\mathbf{TESS}}$ [%]	-	-	-	-	-	*Ref*	-(21.05-97.37)	0	-	-	-	-	*Ref*	-(34.87-97.37)	0
	$\Delta Q_{\mathbf{TESS}}$ [%]	-	-	-	-	-	*Ref*	(-68.22)-8.33	0	-	-	-	-	*Ref*	(-68.22)-24.30	0
Summer	$V_{0.95}$ [%]	3.258	3.11-3.17	3.17-3.24	3.17-3.24	3.10-3.36	3.89-5.21	3.10-3.41	3.36-4.22	2.85-2.94	3.05-3.14	3.05-3.14	2.94-3.16	10.50-11.28	3.06-3.34	8.66-9.52
	$V_{1.05}$ [%]	0	0	0	0	0	0	0	0	0-0.55	0-0.44	0-0.44	0-0.235	0-0.0712	0	0
	$V_{0.90}$ [%]	0.020	0.0044	0.10-0.12	0.10-0.12	0.00692-0.050	0.295-0.392	0.00593-0.0731	0.1978-0.220	0.0044	0.21-0.23	0.21-0.23	0.00742-0.0494	1.165-1.929	0.0249-0.131	0.673-0.918
	$V_{1.10}$ [%]	0	0	0	0	0	0	0	0	0	0	0	0	0	0	0
	ΔC_E [%]	*Ref*	-(165.0-242.9)	-(49.0-180.8)	-(49.0-180.8)	-(51.25-182.8)	(-149.7)-394.6	(-267.4)-814.0	(-51.14)-636.2	-(164.8-242.9)	-(49.0-180.8)	-(49.0-180.8)	(-251.8)-18.86	(-148.9)-473.6	(-33.69)-1151	(-71.77)-762.3
	$\Delta C_{E,g}$ [%]	*Ref*	-(165.0-242.9)	-(93.21-136.5)	-(93.21-136.6)	-(88.73-111.0)	-(34.09-125.7)	(-132.5)-13.86	-(1.906-71.75)	-(164.8-242.9	-(93.21-137.2)	-(93.21-137.3)	-(58.19-118.52)	-(34.09-125.7)	(-70.94)-42.02	-(1.590-81.83)
	$\Delta E_{\mathbf{G}}^{\mathbf{in}}$ [%]	*Ref*	-(30.57-39.64)	(-31.0)-107.3	(-31.1)-107.3	3.03-943.67	32.81-1971	20.71-1988	56.14-2188	-(30.57-39.81)	(-31.0)-107.3	(-31.1)-107.3	(-17.73)-981.8	32.81-1971	(-13.43)-1861	25.78-2187
	$\Delta E_{\mathbf{G}}^{\mathbf{out}}$ [%]	-	*Ref*	-(3.32-9.03)	-(3.32-9.03)	(-40.34)-359.3	(-15.51)-277.2	(-67.85)-284.6	(-55.66)-325.9	*Ref*	-(3.30-9.52)	-(3.30-9.52)	(-44.00)-406.5	(-14.83)-291.9	(-79.95)-340.5	(-55.20)-345.9
	$\Delta E_{\mathbf{PV}}$ [%]	-	*Ref*	0	0	-(40.63-80.01)	0	-(8.95-56.62)	(-44.11-50.65)	*Ref*	0	0	-(30.24-52.98)	0	-(9.00-64.39)	-(44.14-50.69)
	$\Delta E_{\mathbf{HP}}$ [%]	-	-	*Ref*	0	(-1.631)-1	477.0-941.1	288.9-272.1	477.0-941.1	-	*Ref*	0	(-2.47)-0	477.0-941.1	131.3-737.3	477.0-941.1
	$\Delta E_{\mathbf{BESS}}^{\mathbf{in}}$ [%]	-	-	-	*Ref*	37.47-62.12	(-1.631)-0	42.73-102.9	32.08-55.89	-	-	*Ref*	37.98-63.52	(-1.631)-0	29.69-97.04	31.76-51.23
	$\Delta C_{\mathbf{BESS}}$ [%]	-	-	-	*Ref*	-(0.545-1.020)	0-0.0611	-(0.661-1.770)	-(0.461-0.900)	-	-	*Ref*	-(0.558-1.008)	0-0.0611	-(0.431-1.621)	-(0.453-0.789)
	$\Delta E_{\mathbf{HP}}^{\mathbf{TESS}}$ [%]	-	-	-	-	-	*Ref*	-(5.21-48.60)	0	-	-	-	-	*Ref*	-(13.95-59.56)	0
	$\Delta Q_{\mathbf{TESS}}$ [%]	-	-	-	-	-	*Ref*	(-1.612)-6.45	0	-	-	-	-	*Ref*	0-6.45	0

Table 6.5: Result ranges per season for different penetration levels (60 % - 80 %).

		0 %	60 %							80 %						
			1	2	3	4	5	6	7	1	2	3	4	5	6	7
Winter	$V_{0.95}$ [%]	3.263	3.26	12.84-13.53	12.81-13.50	3.94-4.74	27.26-28.18	3.47-3.85	26.58-27.37	3.26	14.44-14.47	14.38-14.41	5.05-5.62	27.26-28.33	4.18-4.30	26.87-27.15
	$V_{1.05}$ [%]	0	0	0	0	0-0.0465	0-0.0934	0-0.0618	0-0.207	0	0	0	0.229-0.426	0.890-1.212	0.309-0.586	1.580-2.34
	$V_{0.90}$ [%]	0.020	0.020	1.14-1.83	1.13-1.86	0.1622-0.1834	14.89-15.73	0.0524-0.0999	11.62-12.57	0.020	4.45-4.88	4.44-4.88	0.269-0.302	22.32-22.72	0.1305-0.1869	21.52-22.01
	$V_{1.10}$ [%]	0	0	0	0	0	0	0	0	0	0	0	0	0	0	0
	ΔC_E [%]	*Ref*	-(5.40-6.84)	10.76-323	5.18-322	55.57-835.2	21.22-954.9	29.35-614	33.27-1183	-(5.35-6.84)	10.76-307.76	5.18-308	39.26-805.4	21.22-910.2	30.02-788.9	45.23-1169
	$\Delta C_{E,g}$ [%]	*Ref*	-(5.40-6.84)	-(52.68-78.85)	-(55.06-78.56)	-(40.01-74.64)	-(44.64-65.67)	-(55.28-73.84)	-(32.43-62.51)	-(5.35-6.84)	-(52.68-78.66)	-(55.06-78.66)	-(40.81-77.98)	-(44.60-65.96)	-(44.52-73.10)	-(33.03-62.37)
	$\Delta E_{\mathbf{G}}^{\mathbf{in}}$ [%]	*Ref*	-(3.92-4.87)	41.52-745.9	35.52-746	70.61-1591	99.71-3696	33.99-1460	107.6-4102	-(3.92-4.96)	41.52-737.1	35.52-737	43.85-1686	99.71-3653	34.09-1978	107.6-4079
	$\Delta E_{\mathbf{G}}^{\mathbf{out}}$ [%]	-	*Ref*	-(5.40-18.50)	(-18.5)-77.51	297.0-31107	458.96-40768	(-39.26)-34987	326.3-69643	*Ref*	-(4.98-19.96)	(-20.0)-105.2	(-34.95)-53026	458.96-40768	(-38.37)-43960	326.3-53454
	$\Delta E_{\mathbf{PV}}$ [%]	-	*Ref*	0	0	-(61.86-77.58)	0	-(60.42-81.35)	-(61.89-75.74)	*Ref*	0	0	-(53.22-77.72)	0	-(54.16-77.47)	-(59.9-75.74)
	$\Delta E_{\mathbf{HP}}$ [%]	-	-	*Ref*	0	-(2.36-21.08)	102.28-313.22	(-52.06)-99.39	102.3-313.2	-	*Ref*	0	-(2.32-24.07)	102.28-313.22	(-54.42)-59.96	102.3-313.2
	$\Delta E_{\mathbf{BESS}}^{\mathbf{in}}$ [%]	-	-	-	*Ref*	(-4.05)-149.1	(-5.52)-0	(-7.45)-173.2	61.76-90.50	-	-	*Ref*	(-20.12)-145.7	(-9.58)-0	(-10.37)-164.0	61.76-89.98
	$\Delta C_{\mathbf{BESS}}$ [%]	-	-	-	*Ref*	(-2.42)-0.1226	0-0.240	(-2.98)-0.1828	-(0.983-1.453)	-	-	*Ref*	(-2.40)-0.419	0-0.264	(-2.83)-0.233	-(0.989-1.454)
	$\Delta E_{\mathbf{HP}}^{\mathbf{TESS}}$ [%]	-	-	-	-	-	*Ref*	(-48.72-97.90)	0	-	-	-	-	*Ref*	-(61.23-97.90)	0
	$\Delta Q_{\mathbf{TESS}}$ [%]	-	-	-	-	-	*Ref*	(-69.07)-34.58	0	-	-	-	-	*Ref*	(-69.07)-31.78	0
Summer	$V_{0.95}$ [%]	3.258	2.83-2.84	3.37-3.53	3.33-3.53	2.73-2.92	13.39-13.74	3.60-3.89	12.62-12.74	2.82-2.83	4.04-4.12	4.04-4.12	2.68-2.95	15.22-15.57	4.29-4.42	14.22-14.39
	$V_{1.05}$ [%]	0	2.40-3.18	2.03-2.69	2.03-2.69	1.170-2.39	0.466-1.406	0.0168-0.555	0.0420-1.191	5.40-6.16	4.79-5.54	4.79-5.54	5.03-5.75	3.971-4.556	1.412-1.645	3.10-3.47
	$V_{0.90}$ [%]	0.020	0.0044	0.31-0.33	0.31-0.33	0.0178-0.0534	5.33-5.88	0.0623-0.1315	3.31-3.80	0.0044	0.42-0.47	0.42-0.47	0.0588-0.0751	8.80-9.06	0.1696-0.265	6.80-7.17
	$V_{1.10}$ [%]	0	0	0	0	0	0	0	0	0.023-0.314	0.01-0.26	0.01-0.26	0-0.0895	0-0.0351	0	0
	ΔC_E [%]	*Ref*	-(158.6-257.5)	-(49.02-204.3)	-(49.02-204.3)	-(719.0)-158.7	(-176.7)-473.6	(-219.6)-949.5	(-39.88)-706.6	-(158.6-257.5)	-(49.02-204.3)	-(49.02-204.3)	(-723.7)-180.7	(-176.7)-473.6	(-342.0)-514.9	(-72.30)-766.4
	$\Delta C_{E,g}$ [%]	*Ref*	-(158.6-257.5)	-(93.21-158.5)	-(93.21-160.5)	-(38.89-180.8)	-(34.09-149.4)	(-115.6)-8.92	-(1.906-71.75)	-(158.6-257.5)	-(93.21-158.5)	-(93.21-160.5)	-(37.23-181.6)	-(34.09-149.4)	-(154.6-0.475)	-(1.619-82.17)
	$\Delta E_{\mathbf{G}}^{\mathbf{in}}$ [%]	*Ref*	-(30.6-39.8)	-(34.8)-107.3	-(36.63)-107.3	-(20.04)-973.87	6.83-2049	(-12.77)-1543	61.66-2277	-(30.6-39.6)	-(34.8)-107.3	-(36.63)-107.3	3.14-1011	6.83-1971	9.40-1809	25.71-2188
	$\Delta E_{\mathbf{G}}^{\mathbf{out}}$ [%]	-	*Ref*	-(3.00-9.52)	-(3.00-9.52)	(-51.20)-446.2	(-15.80)-291.9	(-89.01)-323.1	(-56.82)-344.4	*Ref*	-(3.00-9.57)	-(3.00-9.57)	(-47.30)-462.0	(-15.51)-289.8	(-86.1)-373.4	(-56.51)-344.4
	$\Delta E_{\mathbf{PV}}$ [%]	-	*Ref*	0	0	-(28.23-55.12)	0	-(8.31-82.67)	-(43.64-50.69)	*Ref*	0	0	-(26.06-57.84)	0	-(8.31-79.61)	-(44.24-50.69)
	$\Delta E_{\mathbf{HP}}$ [%]	-	-	*Ref*	0	(-5.43)-0	477.0-941.1	128.0-716.7	477.0-941.1	-	*Ref*	0	(-5.64)-0.1621	477.0-941.1	151.89-638.0	477.0-941.1
	$\Delta E_{\mathbf{BESS}}^{\mathbf{in}}$ [%]	-	-	-	*Ref*	35.57-67.53	(-1.631)-0	24.43-111.3	32.09-53.49	-	-	*Ref*	35.12-67.00	(-1.631)-0	35.95-115.2	31.80-52.73
	$\Delta C_{\mathbf{BESS}}$ [%]	-	-	-	*Ref*	-(0.511-1.095)	0-0.611	-(0.363-1.882)	-(0.456-0.831)	-	-	*Ref*	-(0.500-1.082)	0-0.611	-(0.545-1.941)	-(0.455-0.843)
	$\Delta E_{\mathbf{HP}}^{\mathbf{TESS}}$ [%]	-	-	-	-	-	*Ref*	-(15.38-70.94)	0	-	-	-	-	*Ref*	-(20.47-69.36)	0
	$\Delta Q_{\mathbf{TESS}}$ [%]	-	-	-	-	-	*Ref*	0-6.45	0	-	-	-	-	*Ref*	(-1.613)-9.68	0

Starting with the voltage results shown in Tables 6.4 and 6.5, on the one hand, it can be noted that the inclusion of PV systems does not result in overvoltages beyond the regulation. Considering that the PV systems for scenario 1 and onwards were sized for a near-net-zero building using the base case as referece, the penetration required to surpass the 1.05 p.u. limit defined in the EN50160 standard is around 80 % during summer. The low production during winter makes the power injection effect in the grid barely noticeable. On the other hand, it can be noticed that the inclusion of heat pumps does have a negative impact on the grid. Penetration around 40 % causes non-compliance with the 0.95 p.u. limit. Figure 6.26 shows how the energy consumed from the grid changes for a typical week in winter and summer for scenarios 1, 2 and 5. Adding the PV alone reduces the overall consumption as expected; however, the inclusion of heat pumps in scenario 2 and then thermal storage in scenario 5 resulted in energy consumption up to two orders of magnitude greater than the base case, as the heating comes only from electricity. There is also a decay in the change in energy consumption proportional to the yearly consumption, but the PV can only compensate for prosumers with consumptions above 2 MWh/year during summer in scenarios 2 and 3. The reasons are discussed in Section 6.3.8.

From a cost perspective, however, the PV and the heat pump are complimentary, which can be seen in the reduction of energy export E_G^{out} into the grid in scenario 2 when compared with scenario 1. Despite the consumption of the heat pump increasing considerably the energy consumption from the grid E_G^{in} (see Figure 6.26), therefore the electricity cost C_E, especially during winter, thanks to the dynamic pricing and solar generation, the overall energy cost $C_{E,g}$ (electricity plus gas) decreases for all houses, as shown in Figure 6.27. Particularly during winter, Figures 6.27c and 6.27e show that for the different types of houses (studio, apartment and detached), the change in energy cost has different slopes when adding the heat pump in scenarios 2 and 5, opposite to the smooth slope observed in the change in electricity cost. During summer, the distinction between house types is less abrupt for the change in energy cost and has the same pattern as the change in electricity cost, as can be observed in Figures 6.27d and 6.27f.

Adding a battery did not make a significant change in almost any metric, as shown in Tables 6.4 and 6.5. Comparing scenarios 2 and 3 shows a small decrease in the purchase of energy from the grid and a relatively higher increase in energy export during winter. This is explained by the nominal difference between the import and export of energy during winter. Due to the low irradiance during winter, the export to the grid is very low, so a small increase in the consumption from the BESS during the low-price timeframes, to then inject it into the grid during the high-price timeframes creates a significant relative change in the energy exports of several orders of magnitude, particularly in scenario 5 (see Figure 6.28e). This phenomenon is not as predominant in summer, as the generation exceeds the consumption during most cases, so the role of the BESS is neglectable for scenarios 2 and 3 (see Figures 6.28a and 6.28c). For scenario 5, the more frequent activity of the BESS resulted in higher energy injections, as shown in Figure 6.28f.

Unlike the other components, the effects of the TESS are more notorious throughout the metrics shown in Tables 6.4 and 6.5. The increased energy consumption by the heat pumps to charge the TESS is reflected in the spike of both the change in energy con-

sumption (see Figures 6.26e and 6.26f) and voltages below 0.95 p.u. from scenarios 1-3 to 5, causing non-compliances even in penetrations below 20 %. Nevertheless, the flexibility in the sources of thermal energy resulted in an increased energy export directly from the PV during the high-price timeframes, reducing the usage of the BESS (lower $E^{\text{in}}_{\text{BESS}}$ and therefore its degradation ΔC_{BESS}) in scenario 5. The effect of adding a thermal storage system on energy costs is also not an improvement when compared with scenarios 2 and 3. Despite outperforming scenario 1 during winter, scenario 5 is the least economically attractive during summer (see Figure 6.27).

The role of the aggregator had significant changes in the metrics. From the network perspective, when the prosumers follow the setpoint provided by the aggregator always (scenarios 4 and 6), the voltage in the network remains within the ±0.05 p.u. during 95 % of the time for penetrations up to 80 % in scenario 6, and 60 % in scenario 4, and very rarely below 0.9 p.u. (maximum 0.302 % of the time in scenario 4 and maximum 0.1869 % of the time in scenario 6). This is accomplished by drastic changes in the internal power dispatch from the EMS. Comparing scenarios 3 and 4 shows a noticeable decrease in the usage of the heat pump. Similarly, the amount of energy consumed decreased considerably when comparing scenarios 6 and 5. To minimize the injection of energy, the BESS was used more often –thus degraded–, mostly from energy purchased from the grid as the PV curtailment increased, and less energy was used to charge the TESS $E^{\text{TESS}}_{\text{HP}}$, reducing its availability for thermal power dispatch Q_{TESS}.

For most of the households, this reduction in consumption was translated into a reduction of costs, particularly in winter, by the mere fact that less energy was purchased. Nonetheless, this reduction also led to lower indoor temperatures, as shown in Figure 6.29, particularly during winter. When the setpoint was not enforced in scenario 7 (semi-aggregated), small differences are noticed with scenario 5 (no aggregation), most notably on the usage of the BESS, charged from the grid, and the curtailment of PV generation. Interestingly, Figure 6.29 also shows that scenarios 2 and 3 tend to have lower temperatures than the others without an aggregator. This is due to the operation strategy for the heat pump; it is not used in high-price timeframes that might coincide with higher setpoint temperatures, and in low-price timeframes (during the night), the setpoint is lower. This way, the TESS provides flexibility to the heat generation so that the indoor temperature remains higher without considerably changing the energy cost.

Provided that there is a benefit in the MCES for both the prosumer and the DSO, the minimum compensation each prosumer would require to make it profitable to support the DSO (scenario 6) was estimated, using scenario 2 (PV+HP) as a reference. This is based on Chapter 3 recommendation. To define the capital expenses of the MCES per house, it was used 1.15 €/W for the PV (sized per house) with a minimum value of €2500, €6500 for the heat pump, €10000 for the BESS and €25000 for the underground TESS and run scenarios 2 and 6 for one year considering a 100 % penetration to estimate their revenue. The revenue considers the profit earned by the normal operation of the system under the existing market conditions for each scenario compared to the base scenario.

For the support scenarios to be attractive to prosumers, they should be, at least, as profitable as the case without supporting the grid. In this case, scenario 2 was selected as the reference, based on a fully-electrified heating condition. Figure 6.30 shows the minimum requirements for scenarios 4 and 6 to have the same return on investment

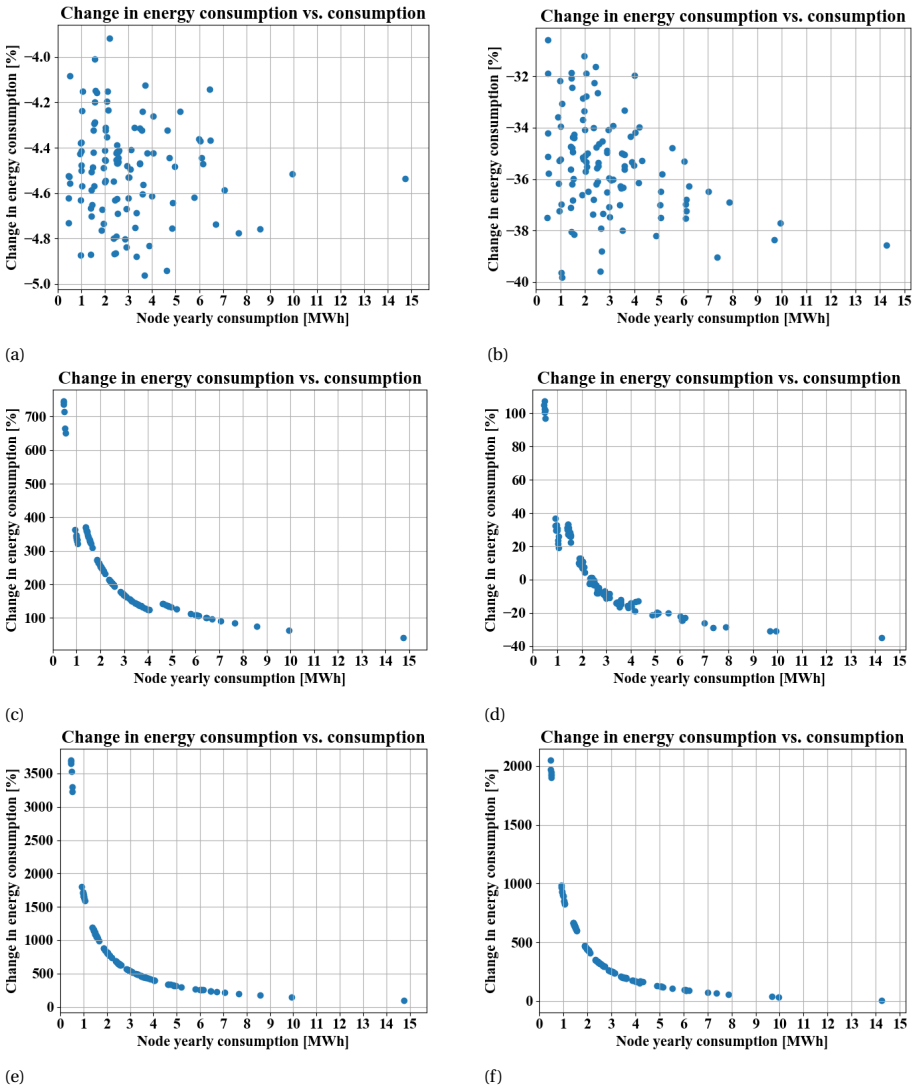

Figure 6.26: Distribution of the change in energy consumed from the grid per household for scenarios 1,2 and 5 during a week in winter (a),(c),(e) and summer (b),(d),(f), respectively.

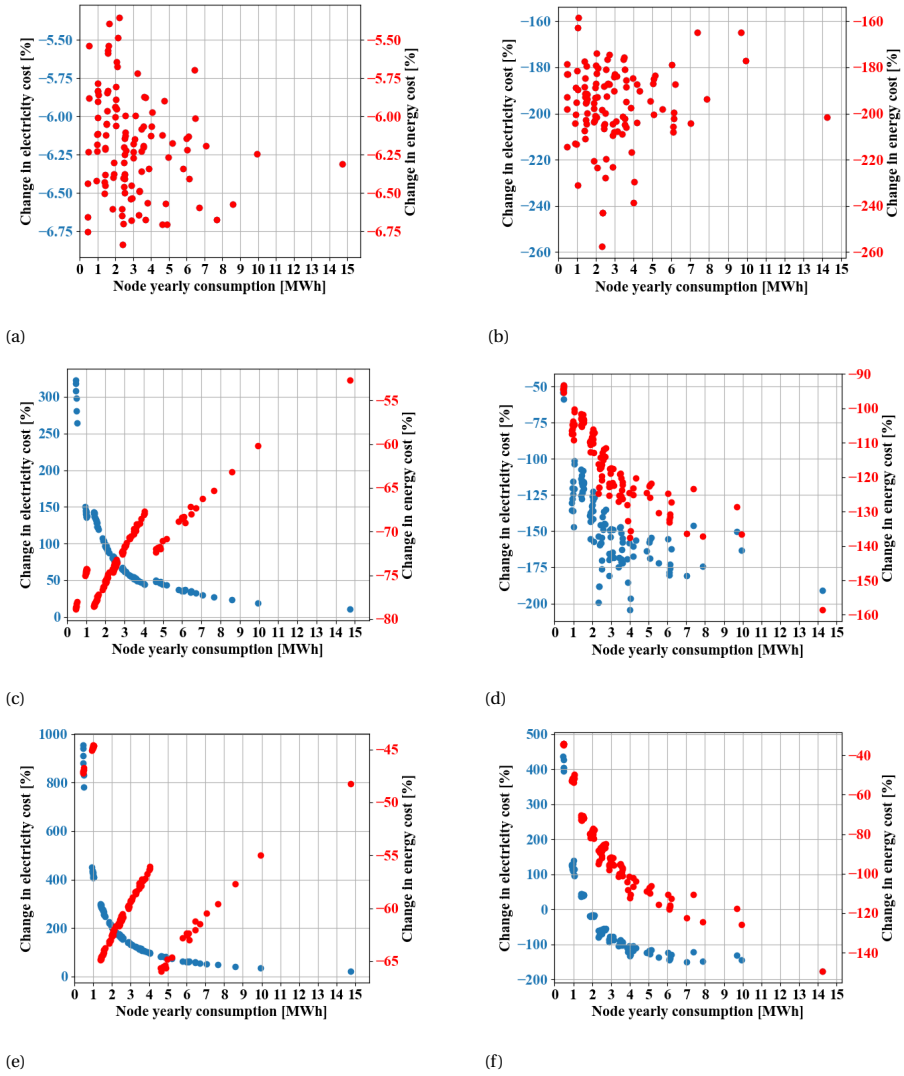

Figure 6.27: Distribution of the change in energy cost from the grid per household for scenarios 1,2 and 5 during a week in winter (a),(c),(e) and summer (b),(d),(f), respectively.

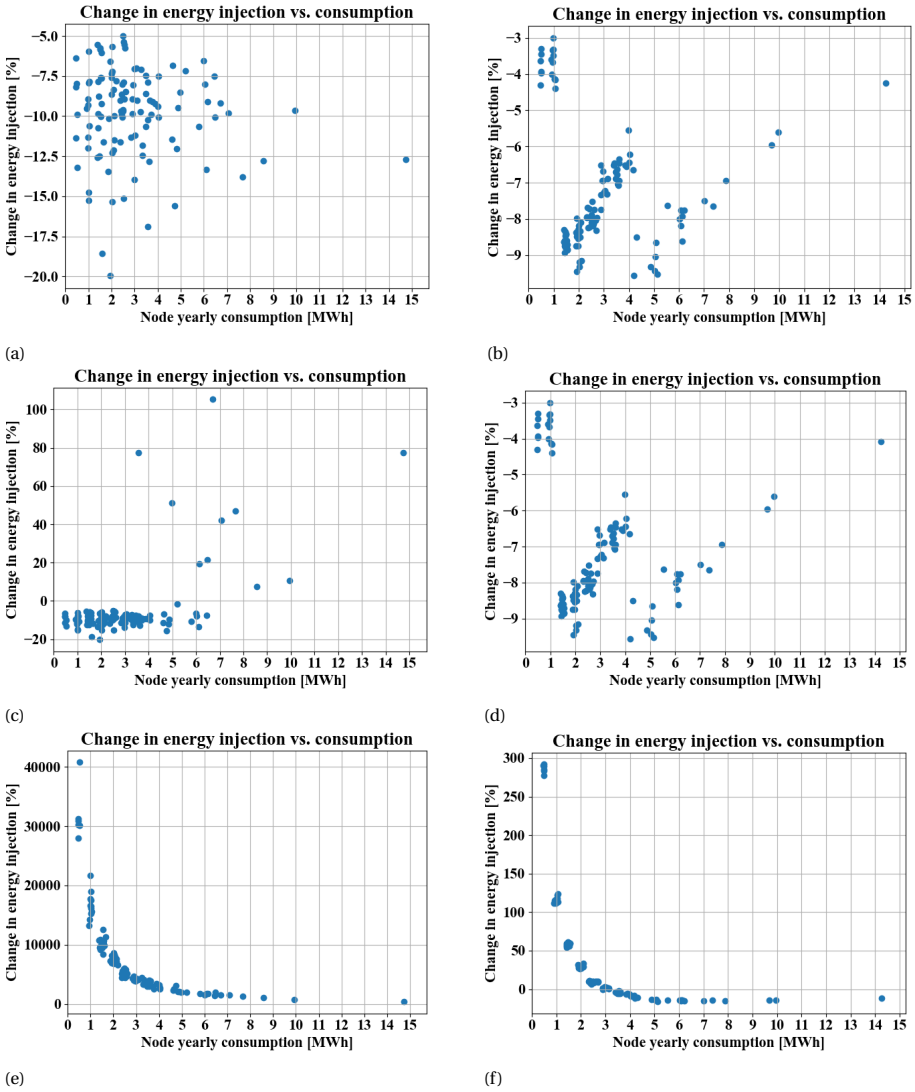

Figure 6.28: Distribution of the change in energy injected to the grid per household for scenarios 2, 3 and 5 during a week in winter (a),(c),(e) and summer (b),(d),(f), respectively.

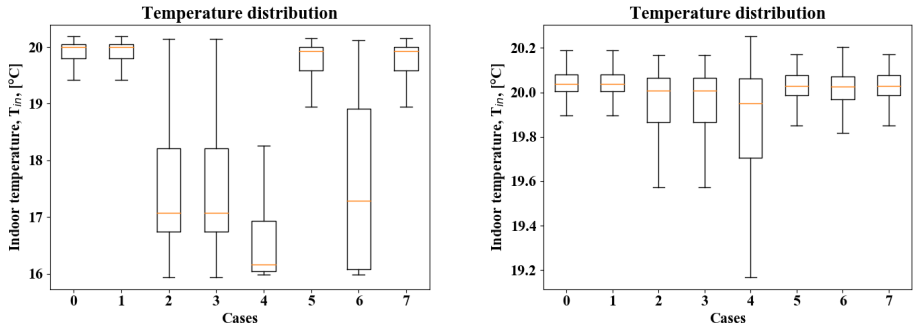

(a) (b)

Figure 6.29: Indoor temperature distribution in the houses during (a) winter, and (b) summer for each scenario.

(ROI) as scenario 2. Scenarios 4 and 6 had similar changes in energy cost (see Tables 6.4 and 6.5), however, the capital expenses for scenario 4 are considerably lower due to the high cost of the TESS. Figure 6.30a shows that the average energy cost is higher than the monthly compensation required for scenario 4 to have the same ROI as scenario 2, and Figure 6.30b shows, per household, the difference between the cost and the required compensation. Figure 6.30c compares the compensation required per household for scenario 6, so that the ROI is the same as scenario 2. The results indicate that the compensation and costs behave fairly similar, and the compensation is mostly greater until consumption is around 7 MWh/year, where the energy cost is higher than the compensation required. Then, Figure 6.30d shows the difference per household.

Following (6.33), the accummulated voltage incompliance per node was calculated for each case, grouped per penetration level, during winter and summer. Figure 6.31 shows the results. For scenario 1, the penetration do not greately affect the incompliance during winter because there is little generation, and the incompliances are due to the base congestion in the grid (see Figure 6.31a). During summer, however, increasing the penetration does increase the incompliance due to energy injection, as indicated in Table 6.5 (see Figure 6.31b). The summer incompliance for scenario 2 is fairly similar to scenario 1, as the higher temperatures require lower usage of the heat pumps (see Figure 6.31d), but during winter, the incompliances increase considerably, and proportionally to the penetration, due to the energy used by the heat pumps, as mentioned in Tables 6.4 and 6.5 (see Figure 6.31c). For three of the four cases (winter and summer in scenario 1, and summer in scenario 2), the most critical node was 270. For winter in scenario 2, the most critical node was 238, but node 270 still remained critical. For this reason, node 270 was chosen to place the centralized system.

Initially, a 1 MWh/1MW BESS system coupled with a 200 kW PV system is considered. However, it was insufficient for penetrations above 60 %. Thus, the capacity of the BESS was increased to 2 MWh for the 60 % penetration and to 10 MWh for the 80 % penetration. No improvements were observed above those values. Similarly, increasing the PV system did not show any major benefit as, during winter, the generation is almost neglectable in comparison with the demanded power, and during summer, most of the generation above that threshold was curtailed to avoid overvoltages. Table 6.6

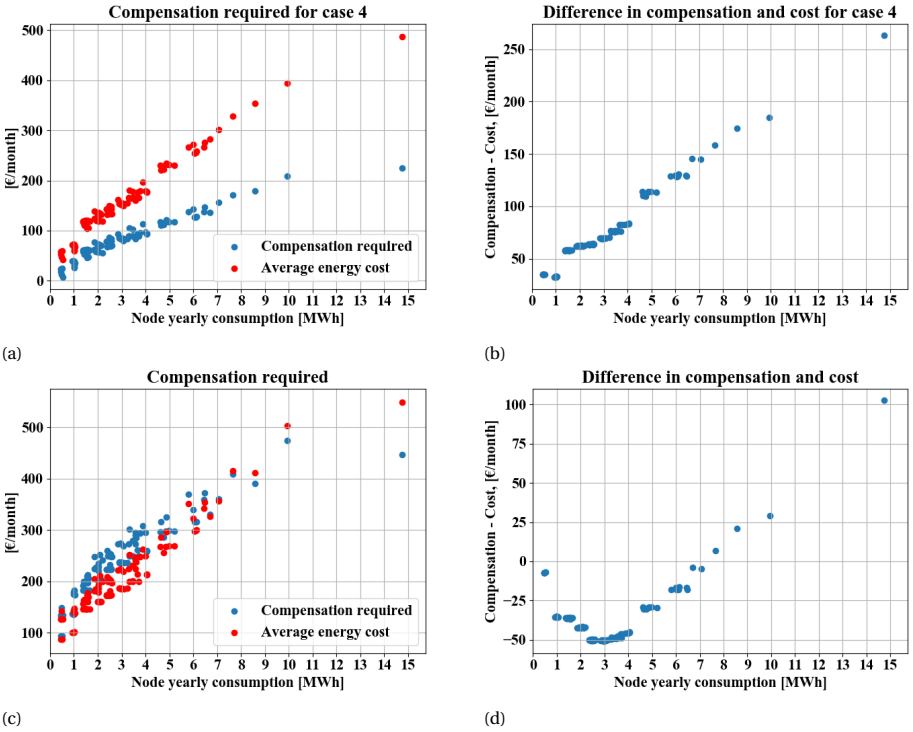

Figure 6.30: Investment comparison of scenario 2 with scenarios 4 and 6, considering (a), (c) the required monthly compensation to ensure the ROIs for both scenarios are the same and (b), (d) the difference between the required compensation and the average monthly energy cost, respectively.

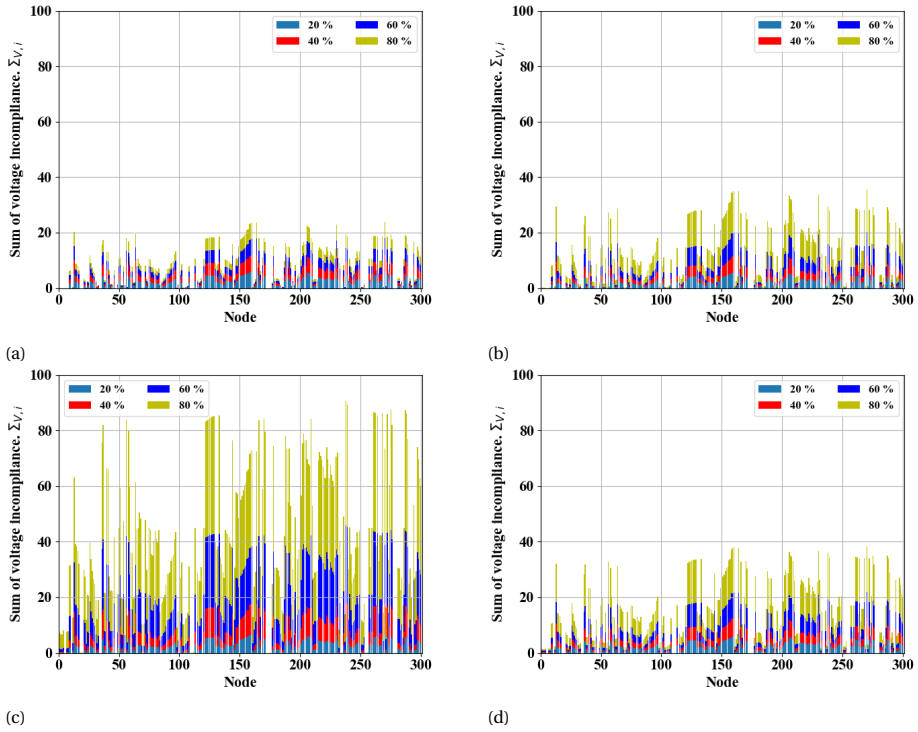

Figure 6.31: Accumulated voltage incompliance per node for scenarios 1 and 2 during (a), (c) winter and (b), (d) summer, respectively.

Table 6.6: BESS and PV system sizes per penetration level of PV+HP for case 8.

Penetration	BESS	PV
20 %	1 MWh, 1 MW	200 kW
40 %	1 MWh, 1 MW	200 kW
60 %	2 MWh, 1 MW	200 kW
80 %	10 MWh, 1 MW	200 kW

Table 6.7: Result ranges per season for different penetration levels of PV+HP for case 8.

Penetration [%]	Winter				Summer			
	$V_{0.95}$ [%]	$V_{1.05}$ [%]	$V_{0.90}$ [%]	$V_{1.1}$ [%]	$V_{0.95}$ [%]	$V_{1.05}$ [%]	$V_{0.90}$ [%]	$V_{1.1}$ [%]
20	0.1898-1.150	0	0-0.0717	0	0.200-0.236	0	0	0
40	4.18-5.28	0	0.240-0.267	0	0.259-0.402	0.00005-0.438	0	0
60	8.87-9.25	0.0005	0.621-1.156	0	0.475-0.617	1.981-2.59	0-0.0252	0
80	10.96-11.18	0.007-0.01	1.902-2.08	0	6.87-6.92	4.71-5.45	0.293-0.311	0.0089-0.257

lists the sizes considered per penetration level for the assets, and Table 6.7 summarizes the voltage results per penetration level per season. During summer, the network does not require external assistance to comply with the voltage limits (see Table 6.5. Still, the BESS is capable of improving the network behaviour for penetrations up to 60 %. At 80 %, the BESS can compensate for the overvoltages by consuming power from the grid, at the cost of increasing the undervoltages. In winter, however, the central system cannot ensure compliance with EN50160. Despite the worse node being compensated, other nodes remained with little or no change before and after including the centralized storage, as shown in Figre 6.32, and the BESS have to consume almost all the energy used to compensate the grid from the grid itself, as the PV generation is almost neglectable in comparison with the energy required to compensate for the grid.

6.3.8. DISCUSSION

After presenting the results in Section 6.3.7, the following correlations became notorious, leading to consequences both for the prosumer and the DSO. In both cases, changing the

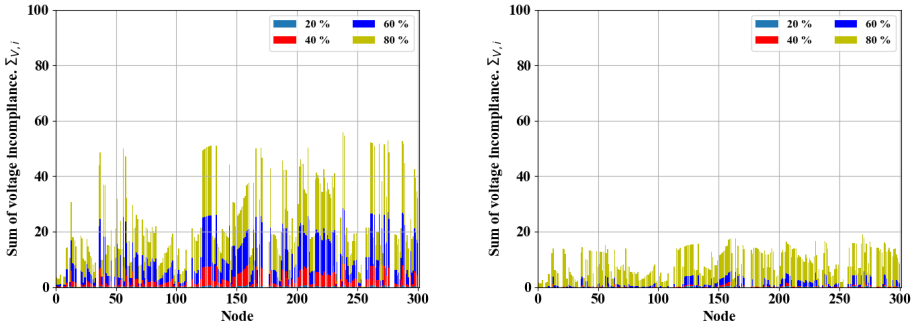

(a) (b)

Figure 6.32: Accumulated voltage incompliance per node for scenarios 8 during (a) winter and (b) summer.

system architecture would result in different power dispatches. Removing the gas boiler naturally would transfer all the thermal load to the electrical network through the heat pumps, however, adding storage devices might shift or shave the consumption peaks. In this work, every house was assumed to have the same EMS strategy. Even though each house has different electric and thermal load conditions, the day-ahead prices for all are the same. Particularly for scenarios 2-5 and 7, which are very heavily dependent on prices to minimize the cost for the prosumer, an unconscious synchronization of peaks is to be expected. The effect is consistent with the results in [20], where the local EMSs react to the changes in energy price simultaneously, consuming or injecting energy accordingly. As a result, the prosumers would use controllable high-power appliances, such as the BESS or the HP, during low-price periods, creating congestion. This phenomenon increases with the penetration, as shown in Tables 6.4 and 6.5, where the voltages for scenarios 2, 3, 5 and 7 consistently drop in the absence of an aggregated control.

The same logic can be applied in reverse order if an aggregator has observability over the network's voltages and powers. In that case, the aggregator can define a power setpoint to minimize those violations. As shown in scenario 6, when the setpoint defined by the aggregator is enforced, there is a clear drop in undervoltages, consistent with [33]. Nevertheless, the prosumers require flexible loads and energy sources to be able to meet the setpoint. In this sense, both the BESS and the TESS play a key role. On the one hand, the BESS can store or dispatch electric power, either to supply the local demand or to directly support the grid. Similarly, the thermal storage could provide thermal power in a restrictive event when the heat pump would contribute to high congestion. Both effects are shown in our simulations, but cannot be generalized. Instead, the results suggest that this would depend on the load conditions. From an electrical point of view, in some cases, the load would match with the PV generation, and the electrical storage is less critical, leading to different patterns of energy supplied by the BESS, as shown in Tables 6.4 and 6.5. For the thermal storage, smaller spaces, characterized by lower electric and thermal demand, benefit from the thermal storage, as the thermal demand can be met with the TESS, whereas bigger houses have larger thermal demands and would require a larger TESS to reduce their dependency on the heat pump.

From a cost perspective, the more devices comprise the system, the higher the revenue is required to justify the system acquisition. The change in cost presented in Section 6.3.7 demonstrated that, in fact, more complex systems do not guarantee lower relative costs compared to the base scenario. During summer, only a PV system (scenario 1) results in the most profitable since the higher temperatures require lower usage of the thermal elements (i.e., heat pump and TESS). During winter, combining the PV with a heat pump is the most profitable architecture, as it eliminates the dependence on gas for heating. Adding storage elements like BESS or TESS did not demonstrate any economic benefit for either of the three aggregation scenarios given the current market mechanism (day-ahead pricing considering feed-in tariff and no compensation for supporting the grid) and would require higher investments, making them unattractive for prosumers, despite their benefits for the DSO. However, previous works suggest that new markets could make such investments attractive [65], [66], as mentioned in Chapter 5. In this sense, Figure 6.30 shows that given compensation, the ROI of scenarios 4 and 6 can be

Table 6.8: Maximum penetration ranges per scenario without violating voltage limits.

Scenario	Winter [%]	Summer [%]
1: RES inclusion	>80	>80
2: Heat electrification	20-40	>80
3: Single-carrier non-aggregated storage	20-40	>80
4: Single-carrier aggregated storage	60-80	>80 %
5: Multi-carrier non-aggregated storage	0-20	0-20
6: Multi-carrier aggregated storage	>80	>80
7: Multi-carrier semi-aggregated storage	0-20	20-40
8: Centralized Storage[1]	20-40	60-80

reduced to the ROI of scenario 2. Scenario 4 might be an interesting business case, as the compensation prosumers require is below the overall energy cost (see Figure 6.30a). However, scenario 6 might not be attractive to DSOs, as the compensation would go beyond the energy costs for low- to mid-consumption prosumers (see Figure 6.30c). Instead, additional schemes can be considered. For example, providing not a total but a partial compensation to the prosumer below the energy cost or involving governmental institutions to provide subsidies in this kind of investment under the condition of collaboration with the DSO.

DSOs are required to ensure voltage conditions on the grid, as stated in EN50160. Each scenario requries different levels of involvement from the DSOs to ensure the voltage conditions, based on the penetration percentage, as shown in Table 6.8. On the one hand, it is not expected that the penetration increases linearly with time, but instead saturates at some point, from where the increase in the penetration is slower. That being said, knowing that the approach allows a later deployment of reinforcement reduces the time pressure to commission the project; the higher the penetration, the more time the DSO would have to come up with the best approach, including execution time. On the other hand, the fact that the grid can withhold larger penetrations, without changes, would also imply that the reinforcement required is smaller (to ensure minimum compliance), gaining more value from the same system, either before or after reinforcement. As can be seen, the aggregated scenarios (4 and 6) result in more reliable systems, whereas the cases without aggregation require reinforcements on the grid more urgently.

jou

Using a centralized PV+BESS system (scenario 8) could not outperform single- nor multi-carrier aggregated storage. The results of the centralized system to compensate for the inclusion of PV and heat pumps in households shown in Table 6.7 demonstrate a single unit can support the network in low penetrations. owever, penetrations above 60 % during winter and 80 % during summer show incompliance with EN50160. The reason is the distribution of power throughout the radial grid. If there are loads in branches whose nodes are far from both the substation and the centralized system, their voltage drops will not be compensated effectively, as they would in a distributed case, such as scenarios 4 and 6. In addition, the storage capacity required for a centralized system largely exceeds the sum of the household storage units. For instance, for a penetration of 40 %, a system of 1 MWh is required for the centralized system, compared

to 28 systems of 10 kWh used in scenarios 4 and 6 (280 kWh in total). Yet, the grid shows better behaviour with the aggregated storage during winter, as shown in Table 6.4, where the voltage is below 0.95 p.u. during up to 3.57 % of the time with the aggregated single-carrier storage and 3.46 % with the aggregated multi-carrier storage, compared to the 5.28 % with the central system. For higher penetrations, the central system cannot satisfy EN50160, regardless of the capacity of the battery, as some nodes saw almost no change before (see Figure 6.31) and after (see Figure 6.32) including the central BESS.

Also, it is worth mentioning the physical capacity of the distribution system. Normally, the cabling towards the end of the distribution systems is thiner than close to the substation. This is due to the traditional, uni-directional, power flow considered for the design of those systems in the past. Thus, placing a centralized system in nodes far from the substation might require reinforcement regardless, as the cables cannot transport the current needed to compensate the voltage drop, making the centralized solution unsuitable.

6.4. CONCLUSIONS

Section 6.2 presented two approaches to coordinate distributed BESS in low-voltage distribution networks for voltage control using the consensus algorithm. Both strategies were tested using the 18-node CIGRE network. The leader-follower and the leaderless methods maintained the voltage within the set limits of ±0.05 p.u. However, the leader-follower approach was less robust than the leaderless when one of the storage agents became unavailable. Conversely, the leaderless approach does not require full observability of the network and instead relies on distributing the utilization factor for all the assets, which leads to an even usage of the agents, making it more robust to unavailability conditions. Despite promising, this strategy faced two main challenges: the data distribution and the adaptability to include other storage elements.

Given that limitation, Section 6.3 provided a different approach, using only meter information to estimate the state of the network and suggest setpoints to the prosumers. Two aggregated and four non-aggregated scenarios were analysed, considering both single- and multi-carrier energy storage systems, evaluated in a real low-voltage distribution network in the Netherlands. Considering different penetration levels and random samplings, insight was provided from both the prosumer and the DSO perspectives. On the one hand, it was demonstrated that a more complex system architecture does not guarantee higher revenue for prosumers in the existing residential energy market. Adding BESS or TESS resulted in energy cost savings between 45-66 % and 34-149 % in winter and summer, respectively, compared with a base case without any addition. Nevertheless, a PV+HP system results in savings between 55-79 % and 93-161 % during winter and summer, respectively. When considering the prosumer yearly consumption, lower consumption prosumers have worse ROIs and require compensations beyond their actual energy cost to make a profit from a multi-carrier energy storage system.

On the other hand, including PV systems sized for near-net-zero buildings did not violate the minimum voltage regulations of the standard EN50160 for penetrations below 80 %. Nevertheless, including heat pumps causes the voltage to be below 0.95 p.u. up to 8 % of the week in winter for penetrations above 40 %. Adding a BESS did not show any major benefit for the prosumer or the DSO. Including the TESS, despite being

convenient for the prosumer to keep higher indoor temperatures without major energy cost changes, does increase energy purchase considerably, up to three times the case with only the heat pump, leading to voltage non-compliances for penetrations as low as 20 %. Multi-carrier aggregation provided a significant benefit for the DSO, but only in the cases where the prosumer must always follow the setpoint. In such conditions, the network was able to accommodate over 80 % penetration with voltages below 0.95 p.u. only 4.3 % the time. Single-carrier aggregation (only batteries) provided satisfactory voltage behaviours (voltage below 0.95 p.u. during 5.62 % of the time in winter) at the cost of lower indoor temperatures and higher curtailments on the prosumer side. Finally, a centralized battery storage system could compensate only for low penetration levels, but due to the nature of a radial network, only outperforming the aggregated units for penetrations below 20 %, where the overall violations to EN50160 were almost zero. Above that penetration level, both aggregated storage architectures (single- and multi-carrier) resulted in a more stable voltage, with less than half of the total amount of storage capacity. In addition, the current limitations of the cabling around the node where the centralized system is required might be a bottleneck, as the cabling might not withstand the current, urging a grid reinforcement to accommodate the centralized system within the distribution network, thus resulting in a less attractive solution.

BIBLIOGRAPHY

[1] B. B. Adetokun, J. O. Ojo, and C. M. Muriithi, "Reactive power-voltage-based voltage instability sensitivity indices for power grid with increasing renewable energy penetration", *IEEE Access*, vol. 8, pp. 85 401–85 410, 2020. DOI: 10.1109/ACCESS.2020.2992194.

[2] X. He, H. Geng, R. Li, and B. Pal, "Transient stability analysis and enhancement of renewable energy conversion system during lvrt", in *2020 IEEE Power Energy Society General Meeting (PESGM)*, 2020, pp. 1–1. DOI: 10.1109/PESGM41954.2020.9282122.

[3] H. Schermeyer, C. Vergara, and W. Fichtner, "Renewable energy curtailment: A case study on today's and tomorrow's congestion management", *Energy Policy*, vol. 112, pp. 427–436, 2018, ISSN: 0301-4215. DOI: https://doi.org/10.1016/j.enpol.2017.10.037. [Online]. Available: https://www.sciencedirect.com/science/article/pii/S0301421517307115.

[4] T. Zhang, S. Liu, W. Qiu, *et al.*, "Kpi-based real-time situational awareness for power systems with a high proportion of renewable energy sources", *CSEE Journal of Power and Energy Systems*, vol. 8, no. 4, pp. 1060–1073, 2022. DOI: 10.17775/CSEEJPES.2020.01530.

[5] F. Pilo, G. Pisano, S. Ruggeri, *et al.*, "Impact of electrical vehicle residential charging stations on the quality of the low voltage network supply", in *2022 20th International Conference on Harmonics Quality of Power (ICHQP)*, 2022, pp. 1–6. DOI: 10.1109/ICHQP53011.2022.9808715.

[6] F. Gunes and M. A. Zehir, "Development of a vehicle-to-grid (v2g) energy management system to mitigate local operational challenges in low voltage distribution networks with photovoltaics", in *2022 4th Global Power, Energy and Communication Conference (GPECOM)*, 2022, pp. 389–394. DOI: 10.1109/GPECOM55404.2022.9815823.

[7] I. Diaz de Cerio Mendaza, I. G. Szczesny, J. R. Pillai, and B. Bak-Jensen, "Demand response control in low voltage grids for technical and commercial aggregation services", *IEEE Transactions on Smart Grid*, vol. 7, no. 6, pp. 2771–2780, 2016. DOI: 10.1109/TSG.2015.2465837.

[8] Y. Li and P. A. Crossley, "Monte carlo study on impact of electric vehicles and heat pumps on lv feeder voltages", in *12th IET International Conference on Developments in Power System Protection (DPSP 2014)*, 2014, pp. 1–6. DOI: 10.1049/cp.2014.0095.

[9] L. Xing, Y. Mishra, Y.-C. Tian, *et al.*, "Distributed voltage regulation for low-voltage and high-pv-penetration networks with battery energy storage systems subject to communication delay", *IEEE Transactions on Control Systems Technology*, vol. 30, no. 1, pp. 426–433, 2022. DOI: 10.1109/TCST.2021.3061651.

[10] M. Geraedts, J. Alpízar-Castillo, L. Ramírez-Elizondo, and P. Bauer, "Optimal sizing of a community level thermal energy storage system", in *2022 IEEE 21st Mediterranean Electrotechnical Conference (MELECON)*, 2022, pp. 52–57. DOI: 10.1109/MELECON53508.2022.9842945.

[11] M. R. Brubæk and M. Korpås, "A norwegian case study on battery storage as alternative to grid reinforcement", in *2021 IEEE Madrid PowerTech*, 2021, pp. 1–6. DOI: 10.1109/PowerTech46648.2021.9495054.

[12] L. Wang, D. H. Liang, A. F. Crossland, P. C. Taylor, D. Jones, and N. S. Wade, "Coordination of multiple energy storage units in a low-voltage distribution network", *IEEE Transactions on Smart Grid*, vol. 6, no. 6, pp. 2906–2918, 2015. DOI: 10.1109/TSG.2015.2452579.

[13] N. Karthikeyan, B. R. Pokhrel, J. R. Pillai, and B. Bak-Jensen, "Utilization of battery storage for flexible power management in active distribution networks", in *2018 IEEE Power Energy Society General Meeting (PESGM)*, Aug. 2018, pp. 1–5. DOI: 10.1109/PESGM.2018.8586215.

[14] J. Alpízar-Castillo, L. Ramirez-Elizondo, and P. Bauer, "Assessing the role of energy storage in multiple energy carriers toward providing ancillary services: A review", *Energies*, vol. 16, no. 1, 2023, ISSN: 1996-1073. DOI: 10.3390/en16010379. [Online]. Available: https://www.mdpi.com/1996-1073/16/1/379.

[15] T. Freire-Barceló, F. Martín-Martínez, and Á. Sánchez-Miralles, "A literature review of explicit demand flexibility providing energy services", *Electric Power Systems Research*, vol. 209, p. 107 953, 2022, ISSN: 0378-7796. DOI: https://doi.org/10.1016/j.epsr.2022.107953. [Online]. Available: https://www.sciencedirect.com/science/article/pii/S0378779622001833.

[16] D. Slaifstein, J. Alpízar-Castillo, A. M. Agudin, L. Ramírez-Elizondo, G. R. C. Mouli, and P. Bauer, "Aging-aware battery operation for multicarrier energy systems", in *IECON 2023- 49th Annual Conference of the IEEE Industrial Electronics Society*, 2023, pp. 1–8. DOI: 10.1109/IECON51785.2023.10312455. [Online]. Available: https://ieeexplore.ieee.org/document/10312455.

[17] Y. Li, D. M. Vilathgamuwa, D. E. Quevedo, C. F. Lee, and C. Zou, "Ensemble nonlinear model predictive control for residential solar battery energy management", *IEEE Transactions on Control Systems Technology*, vol. 31, no. 5, pp. 2188–2200, 2023. DOI: 10.1109/TCST.2023.3291540.

[18] M. M. Alam, M. H. Rahman, H. Nurcahyanto, and Y. M. Jang, "Energy management by scheduling ess with active demand response in low voltage grid", in *2020 International Conference on Information and Communication Technology Convergence (ICTC)*, 2020, pp. 683–686. DOI: 10.1109/ICTC49870.2020.9289284.

[19] W. Zou, J. Li, Q. Yang, and Z. Duan, "An improved max-min game theory control of fuel cell and battery hybrid energy system against system uncertainty", *IEEE Journal of Emerging and Selected Topics in Power Electronics*, vol. 11, no. 1, pp. 78–87, 2023. DOI: 10.1109/JESTPE.2022.3168374.

[20] D. Azuatalam, A. C. Chapman, and G. Verbič, "Probabilistic assessment of impact of flexible loads under network tariffs in low-voltage distribution networks", *Journal of Modern Power Systems and Clean Energy*, vol. 9, no. 4, pp. 951–962, 2021. DOI: 10.35833/MPCE.2019.000136.

[21] M. Ahmed, A. Ganeshan, A. M. Amani, *et al.*, "Effects of household battery systems on lv residential feeder voltage management", *IEEE Transactions on Power Delivery*, vol. 37, no. 6, pp. 5325–5336, 2022. DOI: 10.1109/TPWRD.2022.3176099.

[22] S. P. Menci, B. Herndler, F. Kupzog, M. Zweistra, R. Steegh, and M. Willems, "Scalability and replicability analysis of grid management services in low voltage networks in local flexibility markets: An interflex analysis", in *2021 IEEE Madrid PowerTech*, 2021, pp. 1–6. DOI: 10.1109/PowerTech46648.2021.9495061.

[23] S. Ramírez-López, G. Gutiérrez-Alcaraz, M. Gough, M. S. Javadi, G. J. Osório, and J. P. S. Catalão, "Bi-level approach for flexibility provision by prosumers in distribution networks", *IEEE Transactions on Industry Applications*, vol. 60, no. 2, pp. 2491–2500, 2024. DOI: 10.1109/TIA.2023.3330683.

[24] T. Gangwar, N. P. Padhy, and P. Jena, "Energy management approach to battery energy storage in unbalanced distribution networks", *IEEE Transactions on Industry Applications*, vol. 60, no. 1, pp. 1345–1356, 2024. DOI: 10.1109/TIA.2023.3321030.

[25] K. Cao, Y. Liu, and C. Wang, "A distributionally robust optimal allocation method of energy storage for resilience enhancement of distribution network", in *2023 IEEE International Conference on Energy Technologies for Future Grids (ETFG)*, 2023, pp. 1–6. DOI: 10.1109/ETFG55873.2023.10407791.

[26] D. Jia, S. Wang, T. Kang, and H. Yu, "An optimal control strategy for lv distribution network with pv and energy storage units", in *2022 7th International Conference on Power and Renewable Energy (ICPRE)*, 2022, pp. 1145–1150. DOI: 10.1109/ICPRE55555.2022.9960574.

[27] G. M. Casolino and A. Losi, "Flexibility aggregation perimeter for ancillary services in radial distribution systems", *IEEE Access*, vol. 11, pp. 35 945–35 953, 2023. DOI: 10.1109/ACCESS.2023.3265197.

[28] W. Li, X. Dou, Y. Shen, and W. Hu, "Voltage optimal strategy for low-voltage distribution network considering model missing", in *2021 IEEE Sustainable Power and Energy Conference (iSPEC)*, 2021, pp. 2709–2713. DOI: 10.1109/iSPEC53008.2021.9736062.

[29] V. M. Garrido-Arévalo, W. Gil-González, O. D. Montoya, L. F. Grisales-Noreña, and J. C. Hernández, "Optimal dispatch of ders and battery-based ess in distribution grids while considering reactive power capabilities and uncertainties: A second-order cone programming formulation", *IEEE Access*, vol. 12, pp. 48 497–48 510, 2024. DOI: 10.1109/ACCESS.2024.3382940.

[30] K. Hatipoglu and M. Olama, "A new distributed model-free control strategy to diminish distribution system voltage violations", in *2021 IEEE Power Energy Society General Meeting (PESGM)*, 2021, pp. 1–5. DOI: 10.1109/PESGM46819.2021.9638141.

[31] S. Balasubramanian and P. Balachandra, "Effectiveness of demand response in achieving supply-demand matching in a renewables dominated electricity system: A modelling approach", *Renewable and Sustainable Energy Reviews*, vol. 147, p. 111 245, 2021, ISSN: 1364-0321. DOI: https://doi.org/10.1016/j.rser.2021.111245. [Online]. Available: https://www.sciencedirect.com/science/article/pii/S1364032121005323.

[32] S. Mertens, "Design of wind and solar energy supply, to match energy demand", *Cleaner Engineering and Technology*, vol. 6, p. 100 402, 2022, ISSN: 2666-7908. DOI: https://doi.org/10.1016/j.clet.2022.100402. [Online]. Available: https://www.sciencedirect.com/science/article/pii/S2666790822000076.

[33] J. Alpízar-Castillo, L. Ramírez-Elizondo, and P. Bauer, "The effect of non-coordinated heating electrification alternatives on a low-voltage distribution network with high pv penetration", in *2023 IEEE 17th International Conference on Compatibility, Power Electronics and Power Engineering (CPE-POWERENG)*, 2023, pp. 1–6. DOI: 10.1109/CPE-POWERENG58103.2023.10227394. [Online]. Available: https://ieeexplore.ieee.org/document/10227394.

[34] N. Zhu, P. Hu, C. Jiang, Y. Yu, and D. Jiang, "Comparative analysis and optimal allocation of virtual inertia from grid-forming and grid-following controlled esss", *IET Renewable Power Generation*, vol. 18, no. 14, pp. 2416–2429, 2024. DOI: https://doi.org/10.1049/rpg2.13085. [Online]. Available: https://ietresearch.onlinelibrary.wiley.com/doi/abs/10.1049/rpg2.13085.

[35] L. Xie, Y. Xiang, X. Xu, *et al.*, "Optimal planning of energy storage in distribution feeders considering economy and reliability", *Energy Technology*, vol. 12, no. 7, p. 2 400 200, 2024. DOI: https://doi.org/10.1002/ente.202400200. [Online]. Available: https://onlinelibrary.wiley.com/doi/abs/10.1002/ente.202400200.

[36] M. Shafiekhani and M. Qadrdan, "Addressing electricity transmission network congestions using battery energy storage systems – a case study of great britain", *Applied Energy*, vol. 384, p. 125 418, 2025, ISSN: 0306-2619. DOI: https://doi.org/10.1016/j.apenergy.2025.125418. [Online]. Available: https://www.sciencedirect.com/science/article/pii/S0306261925001485.

[37] J. An and T. Hong, "Multi-objective optimization for optimal placement of shared battery energy storage systems in urban energy communities", *Sustainable Cities and Society*, vol. 120, p. 106 178, 2025, ISSN: 2210-6707. DOI: https://doi.org/10.1016/j.scs.2025.106178. [Online]. Available: https://www.sciencedirect.com/science/article/pii/S2210670725000563.

[38] J. An and T. Hong, "Optimizing battery energy storage system placement in energy intensive cities for sustainable urban development considering multiple objectives", *Sustainable Cities and Society*, vol. 118, p. 106 036, 2025, ISSN: 2210-6707. DOI: https://doi.org/10.1016/j.scs.2024.106036. [Online]. Available: https://www.sciencedirect.com/science/article/pii/S2210670724008588.

[39] A. M. Nour, A. A. Helal, M. M. El-Saadawi, and A. Y. Hatata, "A control scheme for voltage unbalance mitigation in distribution network with rooftop pv systems based on distributed batteries", *International Journal of Electrical Power & Energy Systems*, vol. 124, p. 106 375, 2021, ISSN: 0142-0615. DOI: https://doi.org/10.1016/j.ijepes.2020.106375. [Online]. Available: https://www.sciencedirect.com/science/article/pii/S014206152031293X.

[40] C. Samende, S. M. Bhagavathy, and M. McCulloch, "Power loss minimization of off-grid solar dc nano-grids-part i: Centralized control algorithm", *IEEE Transactions on Smart Grid*, vol. 12, no. 6, pp. 4715–4725, 2021. DOI: 10.1109/TSG.2021.3108236.

[41] R. H. Byrne, T. A. Nguyen, D. A. Copp, B. R. Chalamala, and I. Gyuk, "Energy management and optimization methods for grid energy storage systems", *IEEE Access*, vol. 6, pp. 13 231–13 260, 2018. DOI: 10.1109/ACCESS.2017.2741578.

[42] R. Tonkoski, L. A. C. Lopes, and T. H. M. El-Fouly, "Coordinated active power curtailment of grid connected pv inverters for overvoltage prevention", *IEEE Transactions on Sustainable Energy*, vol. 2, no. 2, pp. 139–147, 2011. DOI: 10.1109/TSTE.2010.2098483.

[43] M. Bahramipanah, D. Torregrossa, R. Cherkaoui, and M. Paolone, "A decentralized adaptive model-based real-time control for active distribution networks using battery energy storage systems", *IEEE Transactions on Smart Grid*, vol. 9, no. 4, pp. 3406–3418, 2018. DOI: 10.1109/TSG.2016.2631569.

[44] A. M. M. Nour, A. A. Helal, M. M. El-Saadawi, and A. Y. Hatata, "Voltage imbalance mitigation in an active distribution network using decentralized current control", *Protection and Control of Modern Power Systems*, vol. 8, no. 1, 2023. DOI: 10.1186/s41601-023-00293-y. [Online]. Available: https://www.scopus.com/inward/record.uri?eid=2-s2.0-85159853260&doi=10.1186%2fs41601-023-00293-y&partnerID=40&md5=4e407f2865a69334c1dd0d7c09424350.

[45] A. T. Procopiou, K. Petrou, L. F. Ochoa, T. Langstaff, and J. Theunissen, "Adaptive decentralized control of residential storage in pv-rich mv–lv networks", *IEEE Transactions on Power Systems*, vol. 34, no. 3, pp. 2378–2389, 2019. DOI: 10.1109/TPWRS.2018.2889843.

[46] M. H. Khan, S. A. Zulkifli, N. Tutkun, and A. Burgio, "Adaptive virtual impedance control with mpc's cost function for dg inverters in a microgrid with mismatched feeder impedances for future energy communities", *Sustainability*, vol. 16, no. 2, 2024, ISSN: 2071-1050. DOI: 10.3390/su16020525. [Online]. Available: https://www.mdpi.com/2071-1050/16/2/525.

[47] L. Wang, A. Dubey, A. H. Gebremedhin, A. K. Srivastava, and N. Schulz, "Mpc-based decentralized voltage control in power distribution systems with ev and pv coordination", *IEEE Transactions on Smart Grid*, vol. 13, no. 4, pp. 2908–2919, 2022. DOI: 10.1109/TSG.2022.3156115.

[48] J. Then, A. P. Agalgaonkar, and K. M. Muttaqi, "Coordinated charging of spatially distributed electric vehicles for mitigating voltage rise and voltage unbalance in modern distribution networks", *IEEE Transactions on Industry Applications*, vol. 59, no. 4, pp. 5149–5157, 2023. DOI: 10.1109/TIA.2023.3273186.

[49] H. Yu, C. Xu, W. Wang, G. Geng, and Q. Jiang, "Communication-free distributed charging control for electric vehicle group", *IEEE Transactions on Smart Grid*, pp. 1–1, 2023. DOI: 10.1109/TSG.2023.3324731.

[50] T. Anderson, M. Muralidharan, P. Srivastava, *et al.*, "Frequency regulation with heterogeneous energy resources: A realization using distributed control", *IEEE Transactions on Smart Grid*, vol. 12, no. 5, pp. 4126–4136, 2021. DOI: 10.1109/TSG.2021.3071778.

[51] T. Zhao, A. Parisio, and J. V. Milanović, "Location-dependent distributed control of battery energy storage systems for fast frequency response", *International Journal of Electrical Power & Energy Systems*, vol. 125, p. 106 493, 2021, ISSN: 0142-0615. DOI: https://doi.org/10.1016/j.ijepes.2020.106493. [Online]. Available: https://www.sciencedirect.com/science/article/pii/S0142061520311078.

[52] T. Morstyn, A. V. Savkin, B. Hredzak, and V. G. Agelidis, "Multi-agent sliding mode control for state of charge balancing between battery energy storage systems distributed in a dc microgrid", *IEEE Transactions on Smart Grid*, vol. 9, no. 5, pp. 4735–4743, 2018. DOI: 10.1109/TSG.2017.2668767.

[53] S. Xia, S. Bu, C. Wan, X. Lu, K. W. Chan, and B. Zhou, "A fully distributed hierarchical control framework for coordinated operation of ders in active distribution power networks", *IEEE Transactions on Power Systems*, vol. 34, no. 6, pp. 5184–5197, 2019. DOI: 10.1109/TPWRS.2018.2870153.

[54] D. H. Nguyen and J. Khazaei, "Unified distributed control of battery storage with various primary control in power systems", *IEEE Transactions on Sustainable Energy*, vol. 12, no. 4, pp. 2332–2341, 2021. DOI: 10.1109/TSTE.2021.3091976.

[55] T. Meng, Z. Lin, Y. Wan, and Y. A. Shamash, "State-of-charge balancing for battery energy storage systems in dc microgrids by distributed adaptive power distribution", *IEEE Control Systems Letters*, vol. 6, pp. 512–517, 2022. DOI: 10.1109/LCSYS.2021.3082103.

[56] J. Engels, B. Claessens, and G. Deconinck, "Grid-constrained distributed optimization for frequency control with low-voltage flexibility", *IEEE Transactions on Smart Grid*, vol. 11, no. 1, pp. 612–622, 2020. DOI: 10.1109/TSG.2019.2926956.

[57] A. Amirkhani and A. H. Barshooi, "Consensus in multi-agent systems: A review", *Artificial Intelligence Review*, vol. 55, no. 5, pp. 3897–3935, 2022, ISSN: 1573-7462. DOI: 10.1007/s10462-021-10097-x. [Online]. Available: https://doi.org/10.1007/s10462-021-10097-x.

[58] R. Olfati-Saber, J. A. Fax, and R. M. Murray, "Consensus and cooperation in networked multi-agent systems", *Proceedings of the IEEE*, vol. 95, no. 1, pp. 215–233, 2007, ISSN: 1558-2256. DOI: 10.1109/JPROC.2006.887293.

[59] M. Zeraati, M. E. Hamedani Golshan, and J. M. Guerrero, "Distributed control of battery energy storage systems for voltage regulation in distribution networks with high pv penetration", *IEEE Transactions on Smart Grid*, vol. 9, no. 4, pp. 3582–3593, 2018. DOI: 10.1109/TSG.2016.2636217.

[60] Y. Wang, K. T. Tan, X. Y. Peng, and P. L. So, "Coordinated control of distributed energy-storage systems for voltage regulation in distribution networks", *IEEE Transactions on Power Delivery*, vol. 31, no. 3, pp. 1132–1141, 2016, ISSN: 1937-4208. DOI: 10.1109/TPWRD.2015.2462723.

[61] S. Gantenbein, M. Schönleber, M. Weiss, and E. Ivers-Tiffée, "Capacity fade in lithium-ion batteries and cyclic aging over various state-of-charge ranges", *Sustainability*, vol. 11, no. 23, 2019, ISSN: 2071-1050. DOI: 10.3390/su11236697. [Online]. Available: https://www.mdpi.com/2071-1050/11/23/6697.

[62] J. Wang, J. Purewal, P. Liu, *et al.*, "Degradation of lithium ion batteries employing graphite negatives and nickel–cobalt–manganese oxide + spinel manganese oxide positives: Part 1, aging mechanisms and life estimation", *Journal of Power Sources*, vol. 269, pp. 937–948, Dec. 2014, Empirical aging modelused by Wiljan, ISSN: 03787753. DOI: 10.1016/j.jpowsour.2014.07.030. [Online]. Available: https://linkinghub.elsevier.com/retrieve/pii/S037877531401074X.

[63] J. Alpízar-Castillo, L. M. Ramírez-Elizondo, and P. Bauer, "Modelling and evaluating different multi-carrier energy system configurations for a dutch house", *Applied Energy*, vol. 364, p. 123 197, 2024, ISSN: 0306-2619. DOI: https://doi.org/10.1016/j.apenergy.2024.123197.

[64] S. Bolognani and S. Zampieri, "On the existence and linear approximation of the power flow solution in power distribution networks", *IEEE Transactions on Power Systems*, vol. 31, no. 1, pp. 163–172, Jan. 2016, ISSN: 1558-0679. DOI: 10.1109/TPWRS.2015.2395452.

[65] J. Alpízar-Castillo, L. Ramírez-Elizondo, and P. Bauer, "Addressing premature reinforcement of low-voltage distribution infrastructure with peak-shaving and power curtailment: A business model", in *2024 20th International Conference on the European Energy Market (EEM)*, 2024, pp. 1–6. DOI: 10.1109/EEM60825.2024.10608931.

[66] J. Alpízar-Castillo, K. Linders, D. Slaifstein, L. Ramírez-Elizondo, and P. Bauer, "Economic opportunities of power curtailment and peak shaving on residential pv-bess systems", in *2024 20th International Conference on the European Energy Market (EEM)*, 2024, pp. 1–6. DOI: 10.1109/EEM60825.2024.10608921.

7

Conclusion and Future Work

"A heart's a heavy burden"

Sophie, Howl's Moving Castle, by Hayao Miyazaki.

This thesis investigated the possibilities for residential prosumers to support the low-voltage distribution grid through multi-carrier energy storage systems. Through an extensive literature review on ancillary servies provided at other voltage levels, the most suitable for the residential distribution systems were identified (Chapter 2). Then, analytical models for the components (Chapter 3) and EMS strategies (Chapter 4) were provided to test the technical feasibility of such strategies. A business study was done to then evaluate the market conditions to make an economically attractive scenario for prosumers to participate (Chapter 5). Finally, a test for different aggregation conditions and system architectures quantified their impact on a real low-voltage distribution network in the Netherlads (Chapter 6). this Section summarizes the conclusions per chapter, associating them to the research questions proposed in Chapter 1.

7.1. CONCLUDING REMARKS

The main conclusions that answer the proposed research questions are as follows.

Q1. *Which is the behaviour of different energy storage devices when coupled together, as a multi-carrier energy storage system, to supply electric and thermal load requirements at the household level?*

The electric and thermal loads respond at different timescales. Space heating has considerable thermal inertia that avoids sudden temperature changes, whereas electric loads require immediate power. Chapter 3 demonstrated the combined behaviour of electric and thermal systems. Higher thermal storage capacities reduce the dependency on electrical heat generation devices, such as heat pumps, at moments that might be inconvenient due to grid limits or unfavourable prices. when the heat pump is activated during such conditions, the electric storage can compensate partially for the electric power request, depending on the energy available and the power capacity of the inverter. It was noted that large sizes of TESS tend to saturate in the amount of thermal energy they can receive, as it responds to the thermal demand, similar to their electric counterparts. If the TESS is overdimensioned, the thermal energy it stores throughout the year reaches a maximum, compensating for the thermal demand and the thermal losses of the TESS. Likewise, the energy stored in the BESS also saturates, as there is no need for extra energy. However, if the TESS is sized according to the thermal demand, the energy stored in the battery varies based on the size of the external energy source; in the case of Chapter 3, the size of the PVT system.

From the analysis done in Chapter 4 it became apparent that different optimization strategies would result in different behaviours in the coupled system. For instance, minimizing the cost would activate the heat pump during low-price periods either to charge the thermal storage or to provide thermal power while also using the BESS to purchase energy when it is cheaper to be used later when it is more expensive, reducing the correlation, but instead synchronizing the energy storage systems. This way, it can be concluded that there is a correlation between the usage of storage systems, which depends on the EMS objective.

Q2 *What are the advantages multi-carrier energy storage systems have over single-carrier energy storage systems when aggregated, considering the cost/benefit of providing simultaneous ancillary services to the electrical network?*

The electrification of heat has created challenges for both prosumers and distribution system operators. On the one hand, prosumers must replace their gas-based heaters with alternative sources, such as heat pumps, PVT systems or solar collectors. On the other hand, the increased electric power demand required to generate thermal power increases the risks in the already congested networks. Prosumers can use renewable energy sources, normally PV systems, coupled with batteries to compensate for the additional consumption. Nevertheless, the energy and power capacities of the batteries cannot always compensate for the additional demand or generation. The extensive literature review in Chapter 2 provided case scenarios where it was demonstrated that including thermal storage reduces the congestion since they can provide thermal power in congestion periods and be charged in the availability of DRES generation or less congested timeframes.

The value of aggregated energy storage was proved in Chapter 6. Normally, aggregation strategies require observability and controllability of the storage assets by the aggergator. However, it was proved that, even when the the aggregator does not directly controls the assets, it is possible to coordinate the prosumers' EMS together with the aggregator to provide support. Single-carrier energy storage requires less complex aggregation strategies to support the grid, and are also more profitable for prosumers, but are less robust. Adding thermal storage to create a multi-carrier energy storage system resulted in the most robust solution for voltage strability in low-voltage distribution networks thanks to the multiple sources of thermal and electric power to meet the local demand in case the grid is contested. Nevertheless, such systems are more expensive and do not provide a more profitable scenario than single-carrier energy storage systems, thus, multi-carrier systems are deemed less attractive for business cases and new ancillary services markets at the residential level.

Chapter 6 also demonstrated that single-carrier centralized storage is not capable of ensuring voltage stability in radial distribution networks with relatively high penetration of heat pumps during winter. This was attributed to the nature of the power flow. Placing the centralized storage can correct the voltage in the nearby nodes; nevertheless, nodes in other branches, or far from the centralized systems, have little to no influence by the centralized storage, urging for aggregated solutions.

Q3 *How to determine the optimal combination of ancillary services a multi-carrier energy storage system can provide, which satisfies the local demand at the household level while minimizing the adverse effects on the grid and the environment when aggregated at the community level, and maximizing the advantage for the prosumer?*

The main challenges the distribution system operators face in low-voltage residential distribution networks are voltage-related. The aggregation of multi-carrier energy storage distributed in the network can compensate for the voltage deviations in the absence of balancing reserves using active power control, as the stan-

dard IEEE 1547 does not allow reactive power compensation for voltage support. In this sense, there are two conditions: overvoltages and undervoltages. Chapter 2 evaluated different ancillary services to address such challenges. Overvoltages are caused by the injection of power into the grid. Such injection can be minimized by either consuming the power locally, storing it or curtailing it.

Consumption and storage are not always options, as they depend on the loads, either base loads or additional ones, such as a heat pump and the state of charge of the electric energy storage systems available, such as stationary batteries or electric vehicles. This way, Chapter 5 provided insight into how much power the system can curtail without affecting the profit for the prosumer, including the degradation of the switches of the solar converter that curtails the generation. It was demonstrated that the ageing of the BESS and the potential early failure of the power electronics pose the major challenge to create a realistic business model. Still, considering simplified degradation models, it was possible

Because of the low-power nature of the assets per prosumer, the individual effect is unlikely to cause significant differences in the overall network. Nevertheless, the accumulated effect of systems negatively contributing to the network can lead to severe voltage deviations. For this reason, a local energy management system should consider the local impact the system has on the grid, while maximizing its performance. Chapter 4 compared three different EMS strategies: rule-based, genetic algorithm and heuristic. For real-time, the genetic algorithm resulted optimal in terms of adaptability for different system architectures, cost and thermal comfort. However, including short-term predictions increases the complexity of the solution space, resulting in less optimal control decisions and high computational cost. The heuristic method provided a good balance between adaptability, performance and computational cost, which was later used to simulate a low-voltage distribution network. Despite $CO_{2,eq}$ were considered as objective, it was demonstrated that, as the only emmiting source is the grid, minimizing the grid purchase minimises the equivalent emmissions in households.

In Chapter 6, different aggregation strategies were proposed to compensate for the voltage fluctuations. The results showed that it is relatively simple to ensure voltage stability if no additional objectives are considered. However, combining other objectives like thermal comfort of energy price require more complex strategies. For single-carrier energy storage systems, such as BESS, it is possible to reduce cost while following a power setpoint, at the cost of the thermal comfort. However, when thermal energy is added, thermal comfort can be guaranteed without a significant change in energy cost. Notably, if all EMS use the same price signal, the assets would congest the network during low-price period, resulting in dynamic pricing being a counteproductive mechanism for voltage control.

7.2. FUTURE WORK

This thesis provided a holistic study of residential multi-carrier energy systems as flexibility providers, in the form of voltage control, in low-voltage distribution networks. The results and conclusions obtained can be complemented by future research in the topics

listed below.

- This work focused on residential buildings comprised of individual houses, or few apartments. With the growth trends and needs, many cities will have, instead, larger skyrise buildings with many apartments, without much space for PV (given the limited roof area) or thermal storage (due to its low energy density). Those cases should be investigated in more detail, using the models proposed in this work, but considering a different business case.

- It was concluded that using BESS is, given the current residential energy market conditions, the most suitable energy storage device. However, its energy and power capacity have to be overdimentioned to support the grid. Including controlled EV charging infrastructure in the LV residential distribution networks could result in a double-win scenario. On the one hand, transportation electrification is holistically included within the residential energy system. On the other hand, including EVs could eventually reduce the need for stationary BESS. The current residential energy market is, arguably, unattractive for prosumers to support the grid using energy storage devices. In fact, it was demonstrated that the dynamic pricing scheme is counterproductive to keep the grid stable, as the EMSs would uninentionally synchronize to purchase energy during low-price periods. Therefore, the existing energy markets should be reevaluated for the energy transition, as the traditional approaches are no longer suitable.

- Any business case that implies using energy system to support the grid requries a comprehensive knowledge on the degradation of the asset during this type of operation. Therefore, studies in the degradation of the components when providing ancillary services, for instance, capacity degradation on the BESS, or early failure in the power electronics.

EPILOGUE

Conservation of energy and mass is the basis of classical mechanics. Yet, it requires a fundamental assumption, the system must be closed. If one sees the universe as a closed system, then the law is always true (given the current understanding of the universe, of course). But what happens when a system with a more reasonable scale, let's say, the low-voltage distribution networks? Until not too long ago, one could assume them as closed systems. The energy flowed from the generation plants through the high-voltage transmission and medium-voltage distribution lines to the substation that fed the circuit. The energy that flowed through the substation matched the loads and distribution losses without any external interference, the infrastructure withheld the power, and there was balance.

Now with the energy transition, the scenery changes. External energy flows from the once unidirectional houses into the grid, disturbing the status quo of the distribution system operators. What is more, heat generation arrives as a new load in the energy balance, altering the now not-so-closed distribution system. Nevertheless, the natural order requires balance, and the question that arises is how? The electric network infrastructure, the container that ensured the validity of the closed system assumption, can no longer support the new dynamics of the system and requires external influence. This influence can, of course, come from the system operator, in the form of reinforcement. Is this the optimal usage of resources tho? This thesis proved that, in fact, a solution to the problem can emerge from the problem itself, the sources of change, in a more efficient manner in terms of resources and energy. If the new-born prosumers have (multi-carrier) storage with an aggregated dynamic, a technical win-win condition emerges during the steady-state: their monthly bills are reduced, and the grid requires less, if any, reinforcement. The transient, despite potentially fast, is, as foreseeable, more convoluted. The prosumers require an external influence to add energy storage. Again, it is a matter of balance, in this case, no longer technical but economic. Possible? Absolutely. Probable? To be determined in further work.

Does this conservation also apply to "human-created forms" of matter and energy? The Phillips machine proved that money, if seen as mass, is conserved and redistributed within a closed system (the economy), but external energy is required to ensure the machine works. Where does this energy come from? The obvious answer is *us*. Less obvious is the energy flow in the background. Much has, is, and will be said about the sources of energy humans require to keep moving. From a larger point of view, many could argue that the conservation of energy applies: people gain energy by eating and sleeping, and release energy while doing tasks. Even from there, one can wonder, is there a balance?

Interestingly, this can be claimed untrue from different perspectives that are complimentary by convention. In some eyes, if the output remains within the system, the energy is transformed; otherwise, it is considered energy loss to the (not close anymore) environment. In other eyes, the energy dedicated to oneself is kept in the system, while

the remainder is lost to the environment. A Venn diagram could explain how the energy flows from one reservoir to the other, but even so, is there really a balance? Is one's input energy always enough to ensure the output energy required to execute one's tasks? Many times, like this thesis itself as an example, the answer decides to ignore the first law of thermodynamics, while following the second. The question remains, where does this "dark" energy come from? Is it, aside from eating and sleeping (if applicable), from others? From the environment itself? Do we have an internal source of energy that, for the sake of keeping the natural order of things, uses an imaginary fuel to generate the shortage of energy required to ensure equilibrium? The answer could very well be either all of the above or neither. The result is, therefore, an observable but not necessarily controllable system whose resilience can be evaluated through a stability analysis before or after failure, in the hope that the information is enough for an observer to create a Sankey diagram to (dis)prove the conservation of energy.

ACKNOWLEDGEMENTS

Would I had been as thorough with this section as with the rest of the thesis, it would had probably presented an accurate view of all the motivation and support I received from many people. For this purpose, words alone cannot make justice, as many times I did not earned it. To every one of you I am deeply grateful.

A

PROPOSITIONS

A

Propositions

accompanying the dissertation

RESIDENTIAL MULTI-CARRIER ENERGY STORAGE SYSTEMS AS POTENTIAL FLEXIBILITY PROVIDERS IN LOW-VOLTAGE NETWORKS

A NEW PLAYER HAS JOINED THE GAME

by

Joel Jesus ALPIZAR CASTILLO

1. It is a misconception that maximizing heat electrification and the installed RES capacity alone will minimize the GHG emissions; carelessly doing so will lead to disorganized decisions and actions that might, ultimately, be counterproductive *(this thesis, Chapter 2)*.
2. Curtailing the PV generation can reduce the lifetime of a solar inverter *(this thesis, Chapter 5)*.
3. The exising scheme of dynamic-pricing tariffs in non-controlled residential markets are detrimental for the existing electric infrastructure *(this thesis, Chapter 6)*.
4. Any system, regardless of its nature or aim, requires a certain degree of flexibility.
5. Science is a baroque representation of nature, whereas engineering is minimalistic.
6. Written words are condemned to be forgotten if nobody talks about them.
7. Compensation must always go beyond the economic cost of a task, thus considering emotional, social or physical costs, for instance.
8. Rich countries depend more on the poor ones than the latter are aware of and more than the first would admit.
9. Defining an intention as good or bad is not a deterministic process, yet, there are many irrational assumptions widely accepted to assume it.
10. Academic research has become a pyramid-scheme content-creation business. Authors (content creators) have to pay to publish, editors and reviewers (content moderators) provide their experience and time for free, and researchers (content consumers) have to pay to access the research results.

These propositions are regarded as opposable and defendable, and have been approved as such by the promotor Prof. dr. ir. P. Bauer and copromotor Dr. ir. L. M. Ramirez Elizondo.

B

Abbreviations

Table B.1: Abbreviations used in this manuscript.

AC	**A**laternate **C**urrent
BESS	**B**attery **E**nergy **S**torage **S**ystem
BM	**B**ucket **M**odel
CHP	**C**ombined **H**eat and **P**ower
$CO_{2,eq}$	Carbo Dioxide (equivalent)
COP	**C**oefficient **O**f **P**erformance
DC	**D**irect **C**urrent
DG	**D**istributed **G**enerator/**Generation**
DoD	**D**epth-of-**D**ischarge
EoL	**E**nd-**o**f-**L**ife
GA	**G**enetic **A**lgorithm
DRES	**D**istributed **R**enewable **E**nergy **S**ystem
DSO	**D**istribution **S**ystem **O**perator
ECM	**E**quivalent **C**ircuit **M**odel
EMS	**E**nergy **M**anagement **S**ystem
ESS	**E**nergy **S**torage **S**ystem
EV	**E**lectric **V**ehicle
EVA	**E**thylene **V**inyl **A**cetate
G2V	**G**rid-**to**-**V**ehicle
GDP	**G**ross **D**omestic **P**roduct
HEMS	**H**ome **E**nergy **M**anagement **S**ystems
HFC	**H**ydrogen **F**uel **C**ell
HP	**H**eat **P**ump
HV	**H**igh-**V**oltage
HVAC	**H**eating, **V**entilation, and **A**ir **C**onditioning
LCoE	**L**evelized **C**ost **o**f **E**nergy
LCoS	**L**evelized **C**ost **o**f **S**torage
LFP	Lithium iron phosphate
Li-ion	**Li**thium-**ion**
LMO	**L**ithium-ion **M**anganese **O**xide
LV	**L**ow-**V**oltage
MCES	**M**ulti-**C**arrier **E**nergy **S**ystem
MCESS	**M**ulti-**C**arrier **E**nergy **S**torage **S**ystem
MPC	**M**odel **P**redictive **C**ontrol
MPP	**M**aximum **P**ower **P**oint
MPPT	**M**aximum **P**ower **P**oint **T**racking
MV	**M**edium-**V**oltage
NCA	Lithium **N**ickel **A**luminium **C**obalt
NMC	Lithium **M**ickel **M**anganese **C**obalt
OCV	**O**pen **C**ircuit **V**oltage
OPEX	**Op**erational **Ex**penditures
PEC	**P**ower **E**lectronics **C**onverter
PSH	**P**umped **S**torage **H**ydro
PV	**P**hoto-**V**oltaic (system)

PVT	**P**hoto-**V**oltaic **T**hermal (system)
RB	**R**ule **B**ased
RES	**R**enewable **E**nergy **S**ystem
RMS	**R**oot **M**ean **S**quare
ROI	**R**eturn **o**n **I**nvestment
SEI	**S**olid **E**lectrolyte **I**nterphase
SC	**S**olar **C**ollector
SoC	**S**tate-**o**f-**C**harge
ST	**S**olar **T**hermal
STC	**S**tandard **T**est **C**onditions
TES	**T**hermal **E**nergy **S**torage
TESS	**T**hermal **E**nergy **S**torage **S**ystem
TSO	**T**ransmission **S**ystem **O**perator
V2G	**V**ehicle-**to**-**G**rid

C

VARIABLES AND CONSTANTS

Table C.1: Variables and constants used in this thesis.

Symbol	Variable	Units	Definition
α	Thermal diffussivity	-	-
α_0	Soil thermal absorbtivity	-	Table 3.5
α_{glass}	(PVT) glass thermal diffussivity	-	Table 3.6
α_{PV}	(PVT) Si layer thermal diffussivity	-	Table 3.6
α_{s}	Soil thermal diffussivity	-	Table 3.5
β	Comfort factor	-	Table 4.1
β_{PV}	PV temperature coefficient	-	Table 3.6
β_1	(Bayerer) factor	-	Table 5.3
β_2	(Bayerer) factor	-	Table 5.3
β_3	(Bayerer) factor	-	Table 5.3
β_4	(Bayerer) factor	-	Table 5.3
β_5	(Bayerer) factor	-	Table 5.3
β_6	(Bayerer) factor	-	Table 5.3
$\gamma_{n_{\text{EV}}}$	EV availability	-	(4.58)
ΔR	Thermal radiation	W/m^2	(3.25)
ΔT	Thermal cycle	°C	-
δ	Control power policy	-	-
δ^{λ}	Energy purchase policy	-	-
$\delta^{\lambda}_{\text{HP}}$	Heat pump energy purchase policy	-	(4.24)
$\delta^{\lambda}_{\text{TESS}}$	TESS discharge energy purchase policy	-	(4.25)
$\delta^{\lambda}_{\text{HP}\rightarrow\text{TESS}}$	TESS charge energy purchase policy	-	(4.26)
$\delta^{HP}_{\text{HP}\rightarrow\text{TESS}}$	Simultaneous heating constraint	-	(4.27)
$\delta^{\text{SoC}}_{\text{HP}\rightarrow\text{TESS}}$	TESS SoC charge constraint	-	(4.28)

$\delta_{\text{TESS}}^{\text{SoC}}$	TESS SoC discharge constraint	-	(4.29)
δ^{P}	Electric power policy	-	-
δ^{T}	Thermal comfort policy	-	-
$\delta_{\text{HP}}^{\text{T}}$	Heat pump thermal comfort policy	-	(4.22)
$\delta_{\text{TESS}}^{\text{T}}$	TESS thermal comfort policy	-	(4.23)
ϵ	(Concensus algorithm) step size	-	-
ε	Emmissivity	-	-
$\varepsilon_{\text{glass}}$	PVT glass layer emmissivity	-	Table 3.6
ε_{PV}	PVT Si layer emmissivity	-	Table 3.6
ε_{s}	Soil emmissivity	-	Table 3.5
ε_{SoC}	Deviation of the EV SoC upon departure time	-	(4.61)
η	Efficiency	-	-
η_c	(BESS) Coulombic efficiency	-	-
η_c^{TESS}	TESS charging efficiency	-	Table 3.5
η_d^{TESS}	TESS discharging efficiency	-	Table 3.5
$\eta_{\text{PV}}^{\text{STC}}$	PV STC efficiency	-	-
η_{PV}	PV efficiency	-	(3.57)
η_{SC}	Solar collector efficiency	-	(4.1)
η_{T}	Heat exchanger efficiency	-	Table 3.6
$\theta_{a,t}$	Asset parameter vector	-	-
θ_{CO_2}	CO_2 cost balance weight	-	Table 4.1
θ_{E}	Energy cost balance weight	-	Table 4.1
θ_{T}	Thermal cost balance weight	-	Table 4.1
λ_{buy}	Grid energy purchase cost	€/kWh	-
λ	(Electrical) (thermal) power cost	€/kW	-
λ_{BESS}	BESS power cost	€/kW	Table 4.1
λ_G	Grid power cost	€/kW	-
λ_{sell}	Grid energy sell cost	€/kWh	-
π_k	General control policy	-	(4.34)
ρ	Density	kg/m^3	-
ρ_a	(PVT) Absorber density	kg/m^3	Table 3.6
ρ_a	Air density	kg/m^3	Table 3.3
ρ_f	Water density	kg/m^3	Table 3.5
ρ_{glass}	(PVT) Glass density	kg/m^3	Table 3.6
ρ_s	Soil density	kg/m^3	Table 3.5
$\Sigma_{v,i}$	(Distribution network) accumulated node voltage deviation	V	(6.33)
τ	Transmittance	-	-
τ_{glass}	(PVT) glass transmittance	-	Table 3.6
A	Area	m^2	-
A	Adjacency matrix	-	-
A	Admitance matrix	-	-
A	(Bayerer) technology factor	-	Table 5.3

$A_{\Delta y}$	TESS side (discrete differential) area	m^2	-
A_{a}	(PVT) absorber area	m^2	Table 3.6
A_{bottom}	TESS bottom area	m^2	Table 3.5
A_{es}	Exposed (household) area	m^2	Table 3.3
A_{glass}	(PVT) glass area	m^2	Table 3.6
A_{PV}	(PVT) PV (Si layer) area	m^2	Table 3.6
A_{sides}	TESS sides area	m^2	Table 3.5
A_t^{cross}	(PVT) tube's cross area	m^2	Table 3.6
A_{top}	TESS top area	m^2	Table 3.5
A_{SC}	Solar collector area	m^2	Table 4.1
A_u	(Household) unit leak area	in^2/ft^4	Table 3.3
$a_{i,j}$	(Adjacency matrix) element	-	(6.2)
$a_{OCV,sa}$	Voltage model parameter	V	-
a_T	(Switch) dynamic characteristic parameter	J	-
B	(Distribution system) substation matrix	-	-
$b_{OCV,sa}$	Voltage model parameter	V	-
b_T	(Switch) dynamic characteristic parameter	J/A	-
C	Storage capacity	kWh	-
C_{BESS}	BESS capacity	kWh	Table 4.1
$C_{\mathrm{CO_2}}$	CO_2 cost	-	Table 4.1
C_{E}	Energy cost	-	Table 4.1
C_{grid}	Net grid cost	-	(4.38)
$C_{i,j}$	Concensus matrix	-	(6.10)
C_{loss}	Battery degradation cost	-	(4.40)
$C_{1,sa}$	(ECM) pole capacitive element	F	-
C_S	(Household) stack coefficient	$cfm^2/(in^4{}^\circ F)$	Table 3.3
C_{T}	Thermal cost	-	Table 4.1
C_{TESS}	TESS capacity	kWh	(3.17)
C_w	(Household) wind coefficient	$cfm^2/(in^4 mph^2)$	Table 3.3
CI	Carbon intensity	kg_{CO_2}/kWh	-
CI_G	(Grid) carbon intensity	kg_{CO_2}/kWh	Table 4.1
c	Specific heat capacity	$J/(kg{}^\circ C)$	-
c_1	BESS empirical degradation parameter	-	Table 4.7
c_2	BESS empirical degradation parameter	A^{-1}	Table 4.7
c_3	BESS empirical degradation parameter	-	Table 4.7
c_4	BESS empirical degradation parameter	-	Table 4.7

c_5	BESS empirical degradation parameter	$A/s^{0.5}$	Table 4.7
c_a	(PVT) absorber specific heat capacity	J/(kg°C)	Table 3.6
c_a	Air specific heat capacity	J/(kg°C)	Table 3.3
c_{glass}	(PVT) glass heat capacity	J/(kg°C)	-
c_f	(TESS) fluid specific heat capacity	J/(kg°C)	Table 3.5
c_f	(PVT) fluid specific heat capacity	J/(kg°C)	Table 3.6
c_{PV}	(PVT) PV (Si layer) heat capacity	J/(kg°C)	-
c_s	Soil specific heat capacity	J/(kg°C)	Table 3.5
c_{styro}	Styrofoam specific heat capacity	J/(kg°C)	Table 3.5
c_T	(Switch) dynamic characteristic parameter	J/A^2	-
CAPEX	Capital expenses	€	-
COP	HP coefficient of performance	-	(3.60)
D	Accumulated damage	-	(5.19)
D	Degree matrix	-	(6.1)
D	Duty cycle	-	-
D_H	Hydraulic diameter	m	-
d	(Bayerer) bond wire diameter	μm	Table 5.3
d	Depth for the reference temperature	m	Table 3.5
$d_{i,j}$	(Degree matrix) element	-	-
E	Electric energy	kWh	-
E^{out}	Electric energy delivered	kWh	-
E_s	(Converter) turn-on energy loss	kWh	(5.14)
E_{BESS}	BESS energy	kWh	(3.73)
E_{EV}	EV energy	kWh	-
f	Frequency	Hz	-
f_s	(Converter) switching frequency	Hz	-
G	Solar irradiance	kW/m^2	-
G_{ov}	(Concensus algorithm) overvoltage control gain	-	-
G_{ref}	Reference solar irradiance	kW/m^2	-
G_{un}	(Concensus algorithm) undervoltage control gain	-	-
h	Heat transfer coefficient	$W/(m^2°C)$	(3.27)
h^{con}	Conduction heat transfer coefficient	$W/(m^2°C)$	(3.5)
h^{conv}	Convection heat transfer coefficient	$W/(m^2°C)$	(3.28)
h^{conv}_{glass}	Ambient-glass (PVT) convection heat transfer coefficient	$W/(m^2°C)$	-
$h^{conv}_{glass\text{-}PV}$	Glass-(PVT) PV (Si layer) convection heat transfer coefficient	$W/(m^2°C)$	(3.53)

h^{r}	Radiative heat transfer coefficient	W/(m^2°C)	(3.29)
$h^{\mathrm{r}}_{\mathrm{glass}}$	Ambient-glass (PVT) radiative heat transfer coefficient	W/(m^2°C)	-
$h^{\mathrm{r}}_{\mathrm{glass\text{-}PV}}$	Glass-(PVT) PV (Si layer) radiative heat transfer coefficient	W/(m^2°C)	(3.54)
$h_{\mathrm{a\text{-}f}}$	Fluid-thermal absorber heat transfer coefficient	W/(m^2°C)	(3.55)
I	(Bayerer) current per bond	A	Table 5.3
I	Current between nodes in a distribution network	A	(6.18)
I_0	(PV module) diode saturation current	A	(5.6)
$I_{0_{T_1}}$	(PV module) diode saturation current at reference temperature	A	(5.6)
$I_{L_{T_1}}$	(PV module) photo-induced current at reference temperature	A	(5.6)
I_n	(Distribution network) node current	A	(6.19)
I_{PV}	PV module current	A	(5.5)
I_{SC}	(PV module) short-circuit current	A	-
$I_{\mathrm{SC}_{T_1}}$	(PV module) short-circuit current at reference temperature	A	-
$I_{\mathrm{SC}_{T_2}}$	(PV module) short-circuit current at reference temperature	A	-
i	Current	A	-
$\bar{i}$	Average current	A	-
i_0	(Converter) bus current	A	-
$i_{\mathrm{cal},sa,t}$	Calendar aging current	A	(4.55)
$i_{\mathrm{cycle},sa,t}$	Cyclic aging current	A	(4.54)
i_L	(Converter) inductor current	A	-
$\bar{i}_L$	(Boost converter) average inductor current	A	(5.7)
i_{loss}	Loss current	A	(4.56)
i_{max}	(Converter) maximum inductor current	A	-
i_{min}	(Converter) minimum inductor current	A	-
$i_{R_1,sa,t}$	Pole current	A	-
i_{RMS}	RMS current	A	-
i_S	(Converter) switch current	A	-
$\bar{i}_S$	(Converter) average switch current	A	(5.9)
$i_{S,\mathrm{RMS}}$	(Converter) RMS switch current	A	(5.10)
$i_{sa,t}$	Current passing through a cell	A	(4.49)
K_0	(PV) temperature coefficient	A/°C	(5.6)
k	Thermal conductivity	W/(m-°C)	-

C

k_a	Air conductivity	W/(m-°C)	Table 3.6
k_B	Boltzmann's constant	J/K	-
k_{EVA}	(PVT) EVA layer conductivity	W/(m-°C)	Table 3.6
k_f	(PVT) fluid conductivity	W/(m-°C)	Table 3.6
k_{ins}	(PVT) insulation table conductivity	W/(m-°C)	Table 3.6
k_{PV}	(PVT) Si layer conductivity	W/(m-°C)	Table 3.6
k_s	Soil conductivity	W/(m-°C)	Table 3.5
k_{styro}	(TESS) styrofoam conductivity	W/(m-°C)	Table 3.5
L	(Converter) inductance	H	-
L	Laplacian matrix	-	(6.3)
L	(Layer) thickness	m	-
L_a	(PVT) Absorber thickness	m	Table 3.6
L_{air}	(PVT) Air gap thickness	m	Table 3.6
L_{EVA}	(PVT) PV EVA thickness	m	Table 3.6
L_{glass}	(PVT) Glass thickness	m	Table 3.6
L_{ins}	(PVT) Insulation thickness	m	Table 3.6
$L_{PV,\ glass}$	(PVT) PV glass thickness	m	Table 3.6
L_{TESS}	TESS wall thickness	m	Table 3.5
L_{ted}	(PVT) PV tedlar thickness	m	Table 3.6
LCoE	Levelized cost of energy	€/kWh	(5.20)
LCoS	Levelized cost of storage	€/kWh	(5.21)
m	Mass	kg	-
m_a	(PVT) absorber mass	kg	-
m_{glass}	(PVT) glass mass	kg	-
m_{PV}	(PVT) PV (Si layer) mass	kg	-
m_{tank}	(PVT) tank mass	kg	-
$\dot{m}_{TESS}$	TESS mass	kg	Table 3.6
$\dot{m}$	Mass flow	kg/s	-
$\dot{m}_f$	Thermla network mass flow	kg/s	Table 3.6
N	Number of tubes in a PVT module	-	-
N_c	(Distribution network) nodes with a consumer connected	-	-
N_d	(Distribution network) nodes without a consumer connected	-	-
N_{br}	Number of bedrooms	-	Table 3.3
N_{EV}	Number of EVs	-	-
N_f	(Bayerer) thermal cycles to failure	-	(5.18)
$N_{p,sa}$	Number cells in parallel within the BESS	-	-
$N_{s,sa}$	Number cells in series within the BESS	-	-
n	(PV) ideality factor	-	-
n	Number of states	-	-
n_j	Number of thermal cycles per cycling condition	-	-

$OCV_{sa,t}$	Cell open circuit voltage	V	(4.50)
OPEX	Operating expenses	€	-
P	Electric power	kW	-
$P^*_{a,t}$	Optimal power decision	kW	-
$\overline{P}^*_{a,t}$	Optimal power decision upper limit	kW	-
$\underline{P}^*_{a,t}$	Optimal power decision lower limit	kW	-
P^*	Electric power setpoint from the DSO	kW	-
P_{BESS}	BESS power	kW	-
P^{δ}_{BESS}	BESS power policy	kW	(4.32)
$P^{\text{max}}_{\text{BESS}}$	BESS converter power limit	kW	(4.15)
$\overline{P}^{\text{perm}}_{\text{BESS}}$	Maximum power the BESS can exchange based on its SoC	kW	(4.15)
$\underline{P}^{\text{perm}}_{\text{BESS}}$	Minimum power the BESS can exchange based on its SoC	kW	(4.16)
$\overline{P}^{\text{set}}_{\text{BESS}}$	BESS maximum power constraint	kW	(4.30)
$\underline{P}^{\text{set}}_{\text{BESS}}$	BESS minimum power constraint	kW	(4.31)
P_{c}	PEC power	kW	-
P_c	(Switch) conduction power losses	kW	(5.12)
$P_{\text{drive},n_{\text{EV}}}$	EV power used for driving	-	
P_{EV}	EV power	kW	-
P_{G}	Grid power	kW	(3.74)
P_{grid}	Grid power	kW	
$\bar{P}_{\text{grid}}$	(Distribution network) average grid power	kW	
P^+_{grid}	Purchased grid power	kW	-
P^-_{grid}	Sold grid power	kW	
P_{HP}	HP (electric) power	kW	(3.61)
P^e_{HP}	HP electric power	kW	-
P^{th}_{HP}	HP thermal power	kW	(4.43)
$P_{\text{HP}\rightarrow\text{TESS}}$	HP (electric) power used to charge the TESS	kW	-
P_i	(Distribution network) node power	kW	-
P^*_i	(Distribution network) setpoint node power	kW	-
P_{L}	(Electric) load power	kW	(3.70)
P^e_{load}	Electric load power	kW	-
P^{th}_{load}	Thermal load power	kW	-
$P_{n_{\text{EV}},t}$	EV charge power	kW	-
P_{PV}	PV power	kW	(3.72)
$P_{n,i}$	Node net power exchange with the grid	kW	-
$P_{\text{nom,i}}$	BESS agent nominal power	kW	-

C

P_{PV}^{δ}	PV power policy	kW	(4.33)
$P_{\text{PV}}^{\text{av}}$	PV available power	kW	-
$P_{\text{PV}}^{\text{peak}}$	PV peak power	kW	
P_{PVT}	PVT (electric) power	kW	-
P_{ref}	(Concensus algorithm) BESS agent reference power	kW	(6.11)
P_s	(Switch) switching power losses	kW	(5.12)
P_{ST}	Solar collector thermal power	kW	(4.44)
$P_{T,s}$	(Switch) total power losses	kW	(5.15)
P_{TESS}	TESS thermal power	kW	-
$P_{tot,n_{\text{EV}},t}$	Total EV power	kW	(5.15)
Pr	Prandtl number	-	-
p_{SoCDep}	Penalty SoC deviations upon EV departure	-	(4.39)
Q	Thermal energy	kWh	-
$Q_{sa,t}$	Cell capacity	Ah	-
Q_{TESS}	TESS energy	kWh	(3.16)
q	Elementary charge	C	-
q	Air flow	ft^3/min	-
q_i	Infiltration air flow	ft^3/min	(3.10)
q_v	Ventilation air flow	ft^3/min	(3.8)
$\dot{Q}$	Thermal power	kW	-
$\dot{Q}_{\text{B}}$	Boiler power	kW	-
$\dot{Q}_{\text{D}}$	Total thermal demand	kW	(3.11)
$\dot{Q}_{\text{HP}}$	HP (thermal) power	kW	(3.62)
$\dot{Q}_i$	Infiltration losses	kW	(3.9)
$\dot{Q}_{\text{L}}$	(Thermal) load power	kW	(3.6)
$\dot{Q}_{\text{PVT}}$	PVT (thermal) power	kW	-
$\dot{Q}_{\text{PVT, mod}}$	PVT module (thermal) power	kW	(3.58)
$\dot{Q}_{\text{SC}}$	Solar collector (thermal) power	kW	-
$\dot{Q}^{\text{SD}}$	TESS self discharge	kW	(3.34)
$\dot{Q}_{\text{bottom}}^{\text{SD}}$	TESS self discharge through the bottom wall	kW	(3.37)
$\dot{Q}_{\text{sides}}^{\text{SD}}$	TESS self discharge through the side walls	kW	(3.36)
$\dot{Q}_{\text{top}}^{\text{SD}}$	TESS self discharge through the top wall	kW	(3.35)
$\dot{Q}_{\text{TESS}}$	TESS power	kW	(3.15)
$\dot{Q}_{\text{TESS}}^{c}$	TESS charging power	kW	(3.14)
$\dot{Q}_v$	Ventilation losses	kW	(3.7)
$R_{0,sa}$	(ECM) series resistive element	Ω	-
$R_{1,sa}$	(ECM) pole resistive element	Ω	-
R_{CE}	(Converter) collector-emmiter series resistance	Ω	-
R_s	(PV) series resistance	Ω	(5.6)

r	Discount rate	-	-
Re	Reynolds number	-	-
RH	Relative humidity	%	-
$S_{a,t}$	State vector	-	-
$\overline{S}_{a,t}$	State vector upper limit	-	-
$\underline{S}_{a,t}$	State vector lower limit	-	-
$S^M_{a,t}$	Transition function	-	-
S_n	(Distribution network) node aparent power	kVA	-
SoC	State-of-charge	%	-
$SoC_{sa,t}$	State-of-charge state	-	(4.48)
SoC_{BESS}	BESS state-of-charge	%	-
$SoC^{\text{max}}_{\text{BESS}}$	BESS maximum allowed SoC	%	Table 4.1
$SoC^{\text{min}}_{\text{BESS}}$	BESS minimum allowed SoC	%	Table 4.1
SoC_{dep}	Requested departure EV state-of-charge	%	-
SoC_{EV}	EV state-of-charge	%	-
SoC_{TESS}	TESS state-of-charge	%	(3.18)
T	Temperature	°C	-
T^{max}	(TESS) maximum temperature	°C	Table 3.5
T^{min}	(TESS) minimum temperature	°C	Table 3.5
T_{amb}	Ambient temperature	°C	-
T_{a}	(PVT) thermal absorber temperature	°C	(3.38)
T_e	Effective temperature	°C	(3.33)
T_{f}	(PVT) fluid temperature	°C	(3.38)
T^{in}_{f}	(PVT) inlet fluid temperature	°C	-
T_{glass}	Glass temperature	°C	(3.38)
T_{in}	Indoor temperature	°C	(3.4)
T^{min}_j	Minimum temperature during a thermal cycle	°C	-
T_{PV}	PV (Si layer) temperature	°C	(3.38)
T_{ref}	Reference temperature	°C	-
T_S	(Switch) junction temperature	°C	(5.16)
T_s	Soil temperature	°C	(3.23)
T_{set}	Setpoint temperature	°C	-
$T^{\text{day}}_{\text{set}}$	Setpoint temperature during day hours	°C	-
$T^{\text{night}}_{\text{set}}$	Setpoint temperature during night hours	°C	-
T_{sky}	Sky temperature	°C	(3.26)
T_{TESS}	TESS temperature	°C	(3.13)
t	Time	s	-
t_{on}	(Converter) switch conduction time	s	-

U	Total heat transfer coefficient	W/(m^2°C)	(3.5)
U	Utilization factor	-	-
$U_{\text{add},i}$	(Leaderless) change in utilization factor	-	(6.13)
$U_{\text{cons},i}$	(Leaderless) shared utilization factor	-	(6.14)
$U_{f,i}$	(Leaderless) BESS control utilization factor	-	(6.15)
U_i	(Leader-follower) utilization factor	-	(6.9)
U_i	(Leaderless) utilization factor	-	(6.12)
U_{leader}	Leader utilization factor	-	(6.8)
U_{TESS}	TESS total heat transfer coefficient	W/(m^2°C)	-
u_w	Wind speed	m/s	-
V	Volume	m^3	-
V	Voltage	V	-
V	Voltage class	V	Table 5.3
$\hat{V}$	(Distribution network) estimated worst performing node voltage	p.u.	(6.34)
V_0	Voltage at the substation	p.u.	-
V_f	(TESS) water volume	m^3	Table 3.5
V_{bus}	(Converter) bus voltage	V	-
V_g	Band gap	V	-
V_{high}	(Distribution network) maximum allowed node voltage	p.u.	-
V_{low}	(Distribution network) minimum allowed node voltage	p.u.	-
V_n	Node voltage voltage	p.u.	(6.17)
V_{max}	(Distribution network) maximum allowed node voltage	p.u.	-
V_{min}	(Distribution network) minimum allowed node voltage	p.u.	-
V_{nom}	(Converter) nominal voltage	V	-
V_{OC}	(PV module) open circuit voltage	V	-
$V_{\text{OC}_{T_1}}$	(PV module) open circuit voltage at reference temperature	V	-
V_{PV}	PV module voltage	V	-
V_s	(Converter) instantaneous voltage	V	-
V_{TESS}	TESS volume	m^3	Table 4.1
$\dot{V}$	Volumetric flow	m^3/s	-
$v_{sa,t}$	Voltage on the cell	V	(4.53)
W_{t+1}	Exogenous process that introduces new information after making a decision	-	-
w_{grid}	Grid cost weight	-	Table 4.8
w_{SoC}	SoC deviation cost weight	-	Table 4.8

w_{loss}	Battery degradation cost weight	-	Table 4.8
$X^{\pi}(.)$	Optimal policy	-	-
x	State	-	(6.6)
x^*	Final state	-	(6.5)
$\dot{x}$	Derivative of a state	-	(6.4)
y	Soil depth	m	-
y_0	Depth of the TESS top wall	m	Table 3.5
y_f	Depth of the TESS bottom wall	m	Table 3.5
Z	(Distribution network) impedance	Ω	
Z_{j-c}	(Switch) junction-case thermal impedance	°C/W	(5.17)

CURRICULUM VITÆ

Joel Jesus ALPIZAR CASTILLO

14-04-1995	Born in San José, Costa Rica.

EDUCATION

2021–2025	Ph.D. candidate in Multi-Carrier Energy Storage Systems Delft University of Technology
2019–2021	Master in Applied Science in Senior Business Management Complutense University of Madrid
2019–2021	Master in Business Administration in Project Management CEREM International Business School
2013–2018	Licenciate (Graduate) in Mechatronics Engineering Costa Rica Institute of Technology

WORK EXPERIENCE

2021–2025	Ph.D. candidate in Multi-Carrier Energy Storage Systems Delft University of Technology
2018–2021	Part-time Lecturer in Control Systems Fidélitas University, Costa Rica
2020–2021	Account Support Manager Hewlett Packard Enterprise, Costa Rica
2019–2021	Chair of the National Technical Committee on Smart Cities Technical Standards Institute of Costa Rica, Costa Rica
2018–2021	Chair of the National Technical Subcommittee on Photovoltaic Systems Technical Standards Institute of Costa Rica, Costa Rica
2018–2020	Consultant in Renewable Energy and Storage Purasol Vida Natural, Costa Rica
2018	Advanced Control Systems Internship Rijskuniversiteit Groningen & Ocean Grazer, The Netherlands
2014–2017	Research Assistant in Spectrophotometry Costa Rica Institute of Technology, Costa Rica

List of Publications

Included in this thesis

Journal Papers

1. **J. Alpízar-Castillo**, L. Ramirez-Elizondo, and P. Bauer, “Assessing the Role of Energy Storage in Multiple Energy Carriers toward Providing Ancillary Services: A Review,” Energies, vol. 16, no. 1, p. 379, 2022, doi: 10.3390/en16010379.

2. **J. Alpízar-Castillo**, V. Vega-Garita, N. Narayan, L. Ramirez-Elizondo, "Open-Access Model of a PV–BESS System: Quantifying Power and Energy Exchange for Peak-Shaving and Self Consumption Applications," Energies, vol. 16, no. 14, 2023, pp.5480, doi: 10.3390/en16145480

3. **J. Alpízar-Castillo**, L. Ramirez-Elizondo, and P. Bauer, “Modelling and Evaluating Different Multi-Carrier Energy System Configurations for a Dutch House,” Applied Energy, 364, 123197, 2024, doi: 10.1016/j.apenergy.2024.123197.

4. M. Kitso, B. I. Priambodo, **J. Alpízar-Castillo**, L. Ramirez-Elizondo, and P. Bauer, “Coordination of Multiple BESS in a Low-Voltage Distribution Network Using a Leader-based and a Leaderless Control,” Energies, vol. 18, no. 17, p. 4566, 2025, doi: 10.3390/en18174566.

5. **J. Alpízar-Castillo**, L. Ramirez-Elizondo, A. van Voorden, and P. Bauer, “Aggregated residential multi-carrier energy storage as voltage control provider in low-voltage distribution networks,” Journal of Energy Storage, 132(A), 117507, 2025, doi: 10.1016/j.est.2025.117507.

Conference Papers

1. **J. Alpízar-Castillo**, L. Ramírez-Elizondo and P. Bauer, "The Effect of Non-Coordinated Heating Electrification Alternatives on a Low-Voltage Distribution Network with High PV Penetration," 2023 IEEE 27th International Conference on Compatibility, Power Electronics, and Power Engineering (CPE-POWERENG), Tallinn, Estonia, 2023, pp. 1-6, doi: 10.1109/CPE-POWERENG58103.2023.10227394.

2. D. Slaifstein, **J. Alpízar-Castillo**, A. M. Agudin, L. Ramírez-Elizondo, G. R. C. Mouli and P. Bauer, "Aging-Aware Battery Operation for Multicarrier Energy Systems," IECON 2023- 49th Annual Conference of the IEEE Industrial Electronics Society, Singapore, Singapore, 2023, pp. 1-8, doi: 10.1109/IECON51785.2023.10312455.

3. **J. Alpízar-Castillo**, L. Ramírez-Elizondo and P. Bauer, "Addressing Premature Reinforcement of Low-Voltage Distribution Infrastructure with Peak-Shaving and Power Curtailment: a Business Model," International Conference on European Energy Markets (EEM), Istanbul, Türkiye, 2024, pp. 1-6, doi: 10.1109/EEM60825.2024.10608931.

4. **J. Alpízar-Castillo**, K. Linders, D. Slaifstein L. Ramírez-Elizondo and P. Bauer, "Economic Opportunities of Power Curtailment and Peak Shaving on Residential PV-BESS Systems," International Conference on European Energy Markets (EEM), Istanbul, Türkiye, 2024, pp. 1-6, doi: 10.1109/EEM60825.2024.10608921.

5. **J. Alpízar-Castillo**, C. Engström, L. Ramírez-Elizondo and P. Bauer, "Investigating the Effect of Power Curtailment on the Switch of a Solar Boost Converter Under Residential Loads," IEEE Power Electronics and Motion Control Conference (PEMC), Pilsen, Czech Republic, 2024, pp. 1-6, doi: 10.1109/PEMC61721.2024.10726347.

6. **J. Alpízar-Castillo**, A. Fu, L. Ramírez-Elizondo, M. Cvetkovic and P. Bauer, "Multi-Carrier Home Energy Management System Using Genetic Algorithms and Random Forest Regression Estimations," IEEE Energy Conversion Conference and Expo (ECCE USA), Phoenix, United States of America, 2024, pp. 1037-1044, doi: 10.1109/ECCE55643.2024.10861342.

OUTSIDE OF THIS THESIS

JOURNAL PAPERS

1. V. Vega-Garita, V. Alpizar-Gutierrez, **J. Alpízar-Castillo**, "A practical method for considering shading on photovoltaics systems energy yield," Energy Conversion and Management: X, vol. 20, 2023, pp. 100412, doi: 10.1016/j.ecmx.2023.100412.

2. J. D. Soto Zúñiga, and **J. Alpízar-Castillo**, "Impact of electric vehicles on residential condominiums". Revista Fidélitas, 4(2), 2023, doi: 10.46450/revistafidelitas.v4i2.69

3. T. Beijneveld, **J. Alpízar-Castillo**, L. Ramirez-Elizondo, "Photovoltaic Thermal System Design Including Aquifer Thermal Energy Storage in a Fifth Generation District Heating Network in Hilversum," Case Studies in Thermal Engineering, vol. 68, 2025, pp. 105854, doi: 10.1016/j.csite.2025.105854

4. J. de Wind, **J. Alpízar-Castillo**, L. Ramirez-Elizondo, "E-Cooling Effect on the Energy Markets: a Case Study in the Netherlands," Case Studies in Thermal Engineering, vol. 73, 2025, pp. 106469, doi: 10.1016/j.csite.2025.106469

5. **J. Alpízar-Castillo**, and L. Ramirez-Elizondo, "Analysis on the Insulation Improvements in Dutch Houses," Energies, vol. 18, no. 20, p. 5467, 2025, doi: 10.3390/en18205467.

CONFERENCE PAPERS

1. M. Geraedts, **J. Alpízar-Castillo**, L. Ramírez-Elizondo and P. Bauer, "Optimal Sizing of a Community Level Thermal Energy Storage System," 2022 IEEE 21st Mediterranean Electrotechnical Conference (MELECON), Palermo, Italy, 2022, pp. 52-57, doi: 10.1109/MELECON53508.2022.9842945.

2. S. J. Kouwenberg, **J. Alpízar-Castillo**, L. Ramírez-Elizondo and P. Bauer, "Insight into the Characterization of Sea-Salt Batteries," 2023 IEEE 27th International Conference on Compatibility, Power Electronics, and Power Engineering (CPE-POWERENG), Tallinn, Estonia, 2023, pp. 1-6, doi: 10.1109/CPE-POWERENG58103.2023.10227412.

3. J. L. Solís-Calvo, E. Guillén-Murillo and, **J. Alpízar-Castillo**, "Review of waste-to-energy generation technologies from urban solid waste in Costa Rica," Sustainable Engineering for a Diverse, Equitable, and Inclusive Future at the Service of Education, Research, and Industry for a Society 5.0, San José, Costa Rica, 2024, pp. 1-6, doi: 10.18687/LACCEI2024.1.1.1964.

4. M. Deutman, **J. Alpízar-Castillo**, L. Ramírez-Elizondo and P. Bauer, "Addressing Voltage Sag Contributions from an Optimally Sized Industrial Hybrid Power System in the Netherlands," IEEE Energy Conversion Conference and Expo (ECCE EU), Darmstadt, Germany, 2024, pp. 1-6, doi: 10.1109/ECCEEurope62508.2024.10752022.

ADVISED MSC THESES

1. M. Geraedts, "Modelling Hybrid Energy Networks A numerical approach to sustainable energy network design." Master's thesis in Physics, University of Amsterdam, Vrije Universiteit Amsterdam, Delft University of Technology and SWECO, 6 May 2022. Available online: https://scripties.uba.uva.nl/search?id=record_28865

2. M. de Eusebio-Cobo, "Optimal revenue strategies for hybrid power plants in the Dutch wholesale energy market." Master's thesis in Sustainable Energy Technologies, Delft University of Technology and TNO, 8 August 2022. Available online: https://repository.tudelft.nl/record/uuid:247a8e13-c07c-4358-8b53-31182e5c49a8

3. C. van der Veen, "Analysing Thermal Energy Storage in Residential Buildings: Towards Decarbonization of the Heating Sector." Master's thesis in Sustainable Energy Technologies, Delft University of Technology, 27 October 2022. Available online: https://repository.tudelft.nl/record/uuid:c1fca7b7-a7cb-4ddc-936e-239a8f0a6cb7

4. K. Arora, "Characterization of a Ventilated Latent Heating Unit Using LiCl as Working Fluid for Green House Applications." Master's thesis in Sustainable Energy Technologies, Delft University of Technology and Dr. Ten, 21 November 2022. Available online: https://repository.tudelft.nl/record/uuid:81b20921-86f1-4865-965f-fa09adecc893

5. S. J. Kouwenberg, "On the Behaviour of Sea-Salt Based Batteries." Master's thesis in Sustainable Energy Technologies, Delft University of Technology and Dr. Ten, 28 November 2022. Available online: https://repository.tudelft.nl/record/uuid:09933cbf-0548-45f0-a454-b006bea3f304

6. B. I. Priambodo, "Distributed Control of Battery Energy Storage Systems for Voltage Support in PV Rich Low-Voltage Distribution Network." Master's thesis in Sustainable Energy Technologies, Delft University of Technology, 23 August 2023. Available online: https://repository.tudelft.nl/record/uuid:4111c411-0eb4-40cc-9d30-56e30e4324f5

7. M. Deutman, "Addressing voltage sag contribution of an optimally sized Industrial Hybrid Power System Using a multi-objective sizing framework considering cost and CO2 emission." Master's thesis in Electrical Power Engineering, Delft University of Technology, 11 September 2023. Available online: https://repository.tudelft.nl/record/uuid:67428726-21d0-4ef7-83bf-fc26bde07ff7

8. T. Beijneveld, "Photovoltaic Thermal System Design Including Aquifer Thermal Energy Storage in a Fifth Generation District Heating Network in Hilversum." Master's thesis in Sustainable Energy Technologies, Delft University of Technology and Stedin, 6 September 2024. Available online: https://repository.tudelft.nl/record/uuid:5b7db8b5-fbca-4eb5-89f1-ddf53f7487a8

9. J. de Wind, "An In-Depth Analysis of residential ECooling Demand in the Netherlands A Quantitative, Physical, and Economic Perspective." Master's thesis in Sustainable Energy Technologies, Delft University of Technology and Eneco, 18 February 2025. Available online: https://repository.tudelft.nl/record/uuid:f18c9919-35aa-4ad6-9e76-57cf11907ebf

10. N. Lurie, "Optimization of remote islanded microgrids in sub-Saharan Africa by considering component degradation and the uncertainty of the electrical consumption." Master's thesis in Sustainable Energy Technologies and Electrical Power Engineering, Delft University of Technology, 22 September 2025. Available online: https://repository.tudelft.nl/record/uuid:23482eed-60f6-46f3-bf32-c4c856315e3f

CO-ADVISED MSC THESES

1. M. I. Cabral de Noronha e Menezes, "Energy Hubs' Contribution to Network Management." Master's thesis in Sustainable Energy Technologies, Delft University of Technology and Stedin, 25 August 2023. Available online: https://repository.tudelft.nl/record/uuid:ddee8ba5-2f45-42f0-a174-3e62ab1dcf51

2. T. Broekman, "Designing an optimized closed electrical distribution system for a multi-carrier energy hub on a mixed-use area in Hilversum" Master's thesis in Sustainable Energy Technologies and HET, 11 July 2025. Available online: https://repository.tudelft.nl/record/uuid:1a33ff9f-eb89-4a9a-9afa-92cd274012a3

3. V. Vats, "Towards Zero-Emission Energy Autarky: Techno-economic optimisation of multi-carrier energy system for residential neighbourhood in Hilversum." Master's thesis in Sustainable Energy Technologies and HET, 11 August 2025. Available online: https://repository.tudelft.nl/record/uuid:dbc7ef6d-0897-44e3-901a-3f18bec0802e

4. K. Budwilowitz, "Effect of transition to sustainable heat sources in greenhouses on the grid stress in a horticultural MV electricity grid." Master's thesis in Sustainable Energy Technologies and HET, 8 September 2025. Available online: https://repository.tudelft.nl/record/uuid:f418cd38-52b0-4888-8877-dd925b11b717

PRESENTATIONS AND OUTREACH

1. Won the most inspiring poster at the 360° Poster Event PowerWeb Institute (7 October 2021).

2. Invited to present on the effect of non-coordinated heating electrification alternatives on a low-voltage distribution network with high PV penetration at the FLEXINet project Workshop 4: Realizing Hybrid Storage in Delft, the Netherlands (18 October 2022).

3. Invited to present on the Multi-carrier coupling and system aggregation at the FLEXINet project Workshop 2: FlexBat meets FLEXINet: Adding intelligent flexibility to the distribution grid in Delft, the Netherlands (03 October 2023).

4. Invited to present on the Multi-carrier coupling and system aggregation at the FLEXINet Workshop: Het realiseren van hybride energieopslag in de wijk in Delft, the Netherlands (11 April 2024).

5. Invited to present on the Multi-carrier system aggregation at the e4battery community meeting in Delft, the Netherlands (20 February 2025).

6. Won the Urban Energy paper award of the Best Energy Paper 2024 from the Delft University of Technology (18 March 2025).

7. Invited to present on the Urban Energy Meetup: Unlocking flexibility through home and community batteries in Delft, the Netherlands (22 April 2025).


SKILLS
TRANSFORMER
PROTECTIONS
SUBSTATIONS
CABLING